Consortium

for

Small-Scale Modelling

Newsletter

April 2014 *No. 14*

Deutscher Wetterdienst

Ufficio Generale Spazio Aereo e Meteorologia

Instytucie Meteorogii i Gospodarki Wodnej

Agenzia Regionale per la Protezione Ambientale dell'Emilia Romagna Servizio Idro Meteo Clima

Centro Italiano Ricerche Aerospaziali

MeteoSwiss

ΕΘΝΙΚΗ ΜΕΤΕΩΡΟΛΟΓΙΚΗ ΥΠΗΡΕΣΙΑ

Administratia Nationala de Meteorologie

Federal Service for Hydrometeorology and Environmental Monitoring

Amt fur GeoInformationswesen der Bundeswehr

Agenzia Regionale per la Protezione Ambientale del Piemonte

www.cosmo-model.org

Editors: Cosmin Barbu (NMA); Massimo Milelli (ARPA-Piedmont); Ulrich Schattler (DWD);

Table of Contents

Editorial **1**

Michał Ziemiański 1

1 Working Group on Data Assimilation **3**

Experiencing 1D-Var+nudging technique in the COSMO model
V. Poli, T. Paccagnella, P. P. Alberoni, D. Cesari, P. Patruno 3

Performance comparison of two COSMO-I2 implementations
M. Giorcelli, N. Vela, M. Milelli, E. Oberto, C. Cassardo, M. Galli 13

2 Working Group on Physical Aspects: Upper Air **19**

First COSMO-E Experiments with the Stochastically Perturbed Parametrization Tendencies (SPPT) Scheme
D. Maurer, A. Walser, M. Arpagaus 19

Diagnosis of Turbulence Schema in Stable Atmospheric Conditions and Sensitivity Tests
I. Cerenzia, F. Tampieri, M. S. Tesini 28

3 Working Group on Physical Aspects: Soil and Surface **37**

Initial fields of snow cover characteristics preparation for COSMO-Ru
E. Kazakova, M. Chumakov, I. Rozinkina 37

Experiments in soil physics – case study
G. Duniec, A. Mazur 43

4 Working Group on Interpretation and Applications **54**

First results of simulations with COSMO-1_ITA and comparison of results with COSMO configurations at different resolutions
M. P. Manzi, P. Mercogliano, M. Milelli 54

Between forecasting and nowcasting strong convective events
J. Parfiniewicz 69

5 Working Group on Implementation and Reference Version **70**

COSMO in Single Precision
S. Rüdisühli, A. Walser, and O. Fuhrer 70

6 Working Group on Predictability and Ensemble Methods **88**

Ensemble forecasting for Sochi-2014 Olympics: the COSMO–based ensemble prediction systems
A. Montani, D. Alferov, E. Astakhova, C. Marsigli,T. Paccagnella 88

A sensitivity test to assess the impact of different soil moisture initializations on short range ensemble variability in COSMO model
R. Bonanno, N. Loglisci 95

COTEKINO Priority Project – Results of Sensitivity Tests
G. Duniec, A. Mazur 106

Appendix: List of COSMO Newsletters and Technical Reports 114

The previous COSMO General Meeting which took place in Sibiu, Romania, from 2 to 5 September 2013 gave an opportunity to review and discuss the recent developments within our consortium. You can find the meeting presentations at http://www.cosmo-model.org/content /consortium/generalMeetings/general2013/default.htm.

The COSMO Newsletter offers you a platform for providing more extensive information to the COSMO community on the problems you are tackling and results of your work. I would like to encourage you to make use of this opportunity and to thank all the contributors to the current and recent issues.

The current COSMO year started with important meeting of COSMO Directors which took place in Helsinki in September 2013. The Directors approved the COSMO Strategy which aims at harmonization of COSMO and ICON within time horizon of 2020 (see the document on http://www.cosmo-model.org/content/consortium/reports/cosmoStrategy_2013-11-15.priv.pdf) and approved new COSMO Agreement.

An important achievement of the current COSMO year was a release of new version 5.0 of the COSMO model, together with new INT2LM 2.0. The release unifies recent ART, CLM and NWP developments. This success was possible due to hard and dedicated work of the development teams and I would like to express my sincere appreciation to all involved. The new version already became a foundation for further developments and especially for an implementation of COSMO-ICON physics library. This current work is aimed at bringing recently developed tools to the COSMO model to further improve its results and is an important element of our Strategy.

During the current COSMO year we continue to work on a new edition of COSMO Science Plan. I would like to thank for all your contributions. The Science Plan becomes a very interesting and important document which will guide development of COSMO model up to year 2020.

To discuss a wide range of current COSMO activities we will meet for the next General Meeting in Eretria, Greece, from 8 to 11 September 2014. I wish every success in your work.

Michał Ziemiański
COSMO Scientific Project Manager

Figure 1: Participants of the 15th COSMO General Meeting in Sibiu

Experiencing 1D-Var+nudging technique in the COSMO model

Virginia Poli, Tiziana Paccagnella, Pier Paolo Alberoni, Davide Cesari and Paolo Patruno

ARPA Emilia-Romagna, Bologna, Italy

1 Introduction

At very high resolution the use of dense and highly frequent observations become crucial in assimilation systems. In the proposed variational approach the retrieval of temperature and humidity profiles from radar derived surface rain rate is performed firstly, employing two linearized parameterizations of large-scale condensation and convection originally developed for the ECMWF model. The obtained profiles are then used as "pseudo" observations into the nudging scheme of the high resolution COSMO model.
The aim of this work is to test if the developed framework outperforms the currently running latent heat nudging (LHN hereafter) scheme which was specifically designed for the assimilation of radar rain rates.
One of the main reason for investing in this type of scheme is the rapidly decrease of the positive impact of radar data when using the LHN as progressing into the forecast as documented in Stephan et al. [8]. As suggested in this paper, a possible cause for this lack of persistence is the weak coupling between the LHN temperature adjustments and the model dynamic. The LHN effectively acts only rescaling the temperature profiles with an adjustment in the humidity field which is not consistent with the cloud scheme prediction. 1D-Var algorithm is built instead on a physically based operator which reproduces all of the processes that take place in the cloud and then should be able to vertically re-distribute in a coherent way the heat released by the rain formation process.
To assess the quality of this approach full model integrations with and without the assimilation of the retrieved profiles are finally used to quantify the impact of rain rate assimilation in improving the forecasted precipitation events.

2 1D-Var theory

In variational data assimilation, the goal is to find the optimal model state, the analysis, $\mathbf{x}_a$, that simultaneously minimizes the distance to the observations, $\mathbf{y}_0$, and a background model state, $\mathbf{x}_b$, usually coming from a previous short-range forecast. When the background and observation errors are uncorrelated and have a Gaussian distribution, then the maximum likelihood estimator of the state vector, $\mathbf{x}$, is the minimum of the following cost function

$$J(\mathbf{x}) = \frac{1}{2}(\mathbf{x}-\mathbf{x}_b)^T\mathbf{B}^{-1}(\mathbf{x}-\mathbf{x}_b) + \frac{1}{2}(H(\mathbf{x})-\mathbf{y})^T\mathbf{R}^{-1}(H(\mathbf{x})-\mathbf{y}) \tag{1}$$

where H is the operator simulating the observed data from the model variable $\mathbf{x}$, $\mathbf{R}$ is the observation error matrix which includes measurement errors and representativeness errors, including errors in H, and $\mathbf{B}$ is the background error covariance matrix of the state $\mathbf{x}_b$. The superscripts -1 and T denote inverse and transpose matrices, respectively.

Under the hypothesis of linearity for the observation operator (i.e. $H(\mathbf{x}) = H(\mathbf{x}_b) + \mathbf{H}(\mathbf{x}-\mathbf{x}_b)$) the optimal analysed state can then be found by solving $\nabla J(\mathbf{x}) = 0$ where

$$\nabla J(\mathbf{x}) = \mathbf{B}^{-1}(\mathbf{x}-\mathbf{x}_b) + \mathbf{H}^T\mathbf{R}^{-1}(H(\mathbf{x})-\mathbf{y}) \tag{2}$$

which leads to the expression for the analysis

$$\mathbf{x}_a = \mathbf{x}_b + \mathbf{K}(\mathbf{y}-\mathbf{y}_b) \tag{3}$$

with $\mathbf{K} = \mathbf{A}\mathbf{H}^T\mathbf{R}^{-1}$ and $\mathbf{A} = (\mathbf{B^{-1}} + \mathbf{H}^T\mathbf{R}^{-1}\mathbf{H})^{-1}$; $\mathbf{K}$ is the Kalman gain matrix, and $\mathbf{A}$ is the analysis error covariance matrix.

If the analysis is performed independently for each atmospheric column at the location of the observed quantities, the variational technique is said to be one dimensional (1D-Var) and the dimension of $\mathbf{x}$ reduces to the number of model levels times the number of control variables, thereby simplifying the minimization process. In this study the model state $\mathbf{x}$ contains vertical profiles of temperature and specific humidity and surface

pressure (i.e. $\mathbf{x}_b = (T, q, P_s)$) derived from the regional non-hydrostatic forecast model COSMO. The observation vector $\mathbf{y}$ contains the surface rain rate estimation from the radar network and is therefore a scalar. H is the diagnostic moist process model which converts temperature and humidity increments into rain rate increments. Tangent-linear and adjoint versions of H are available in order to avoid the excessive computational cost of a minimization based on finite-difference Jacobians.
The moist physics parameterizations used in this work are an adapted version of codes initially developed at ECMWF for the assimilation of global-scale satellite rainy microwave radiances [1] and of radar rain rates over the U.S.A. [5, 6]. They consist of two linearized parameterization of large-scale condensation [10] and convection [4] whose sensitivity to input perturbations is more linear than that of [9] parameterization. This ensures a smoother behaviour of the minimization and avoids excessive increments that may cause convergence problems [1]. The simulated surface rain rate therefore comprises both convective (RR_{conv}) and large scale (RR_{strat}) contributions.

Large-scale precipitation, RR_{strat}, is diagnosed from the grid-mean amount of cloud condensate, q_c, as:

$$RR_{strat} = q_c c_0 \left[1 - \exp\left\{-\left(\frac{q_c}{q_c^{crit}}\right)^2\right\}\right] \tag{4}$$

where q_c^{crit} (set to 0.5 kg kg^{-1}) is the critical value of the in-cloud water content at which precipitation generation starts and c_0 is the conversion factor (equal to 4.167×10^{-4} s^{-1}).

Finally, the 1D-Var minimization core finds the solution $\mathbf{x}_a$ through the minimization of $J(\mathbf{x})$.

3 Experiments setup

To formulate the procedure in a computationally light way and to be sure that some hypotheses underlaying the variational assimilation are verified, some topics are examined in details.

Firstly the 1D-Var algorithm is not enclosed in the COSMO code. This means that to make use of it the assimilation cycle needs to be doubled. Fields from a first COSMO nudging cycle are extracted every 15 minutes to feed the 1D-Var scheme with vertical profiles to start minimization. Then retrieved profiles in output are nudged by repeating the first assimilation cycle. The major problem associated to this off-line application is that the retrieval of the analysed profiles of humidity and temperature are not updated during the 12 hours of the assimilation cycle. To overcome this difficulty and, hence, to mitigate the effect due to the use of old profiles, the assimilation cycle is divided into 4 interval defining a framework similar to the one of the Rapid Update Cycle (Figure 1).

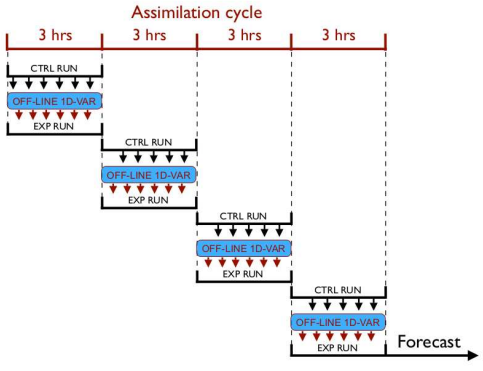

Figure 1: 1D-Var+nudging framework.

The second point of interest regards the data thinning.
The use of data with very high spatial and temporal resolution should guarantee improvements in the initial condition knowledge. Nevertheless, Liu and Rabier [3] showed how high density observations with correlated errors can produce a degradation of the analysis because of the potential spreading of error in correlated neighboring pixels. The most intuitive and commonly used thinning method is to reduce the amount of selected observations in predefined areas or at specified intervals [2]. Moreover, in our specific case the amount of data, coming from the italian network managed by the National Civil Protection Department, over the selected

domain is very large (57491 points every 15 minutes). The use of all the available observations generates AOFs so big to cause the killing of forecast runs by the system because of memory problems. As a first attempt, one observation every 5 grid points in both directions was taken, but, due to the poor results in forecasted precipitation fields the thinning procedure proposed by Lopez [7] has been chosen. As a result, only those points for which first guess and observed rain rates are greater than zero are used in the 1D-Var scheme.

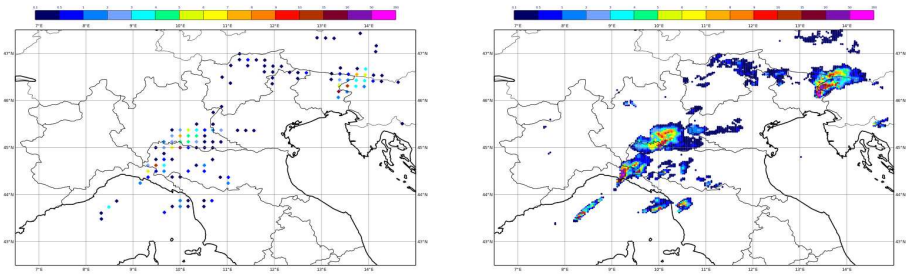

Figure 2: Regular data thinning (left) and suggested Lopez thinning (right) of precipitation field.

It is evident from Figure 2 how this two thinning methods are different in terms of number of points and structures in input to the 1D-Var minimization scheme.

The third topic is the bias correction.
The variational approach works in a statistically optimal way if observations and model errors are unbiased. Physics implemented in the forward operator, which is a simplified version of the cloud scheme implemented in the ECMWF forecast model, is different from the actual one implemented into the COSMO model. This means that, given a set of temperature and humidity profiles, precipitation fields generated by the cloud model diverge from those produced by the COSMO model. The differences between the linearized cloud model and COSMO have been compared by means of their diagnosed surface rain rate. In particular strong rain rates are not produced and the mean rainfall field is weak and diffuse (Figure 3) even taking note of the fact precipitation is not determined only by the "physical" balance of the total water contained in a 1D column but it also depends on dynamical driven processes.

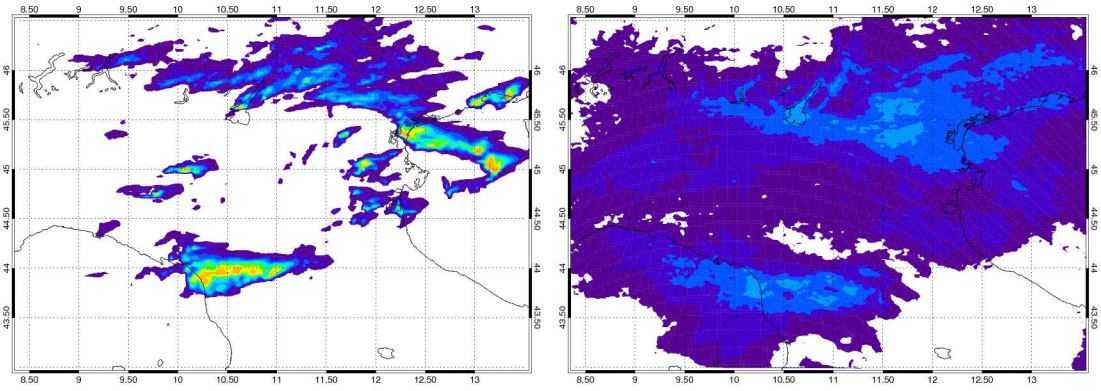

Figure 3: Mean surface rain rate for COSMO (left) and cloud (right) model calculated during the 12 hours assimilation cycle starting at 00 UTC of the 29^{th} of July 2010.

At first the bias correction was determined from the distribution of observed and simulated mean rainfall fields and it was applied to those observed precipitation rates for which there was an overestimation/underestimation compared to cloud model values. In this way the correction factor was evaluated a posteriori only for case studies. But, due to the difficulty in deducing this correction factor in a straightforward way not only for case studies, the idea was to change some parameters (such as convective cloud cover, autoconversion timescale of large cloud condensate to precipitation and autoconversion rate of convective cloud water to convective precipitation) trying to diminishing the spread effect observed in Figure 3 and to generate stronger rain rates. Mean rainfall fields following from different parameterizations are shown in Figure 4.

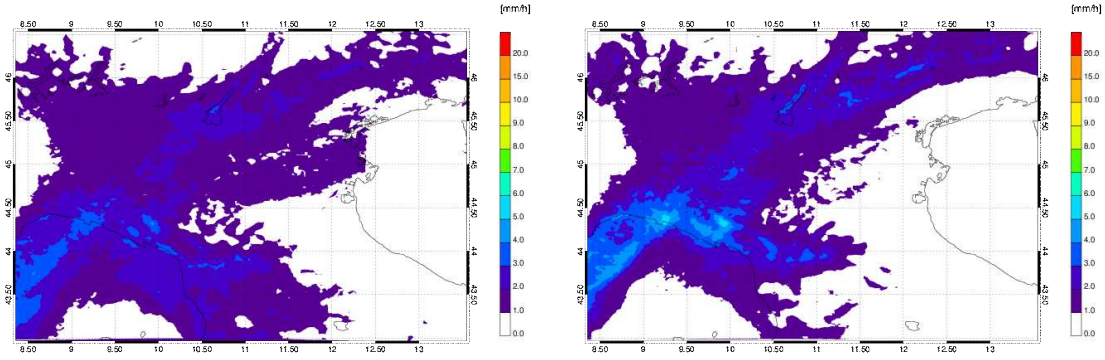

Figure 4: Mean rainfall fields obtained with the standard (left) and convective (right) parameterization. Data are from the 12 hours assimilation cycle starting at 00 UTC of the 26^{th} of September 2012

3 Case studies and results verification

To test the proposed methodology some case studies were chosen with two prerequisites to be fulfilled:

- presence of convective structures (short-lived and small-scale structures) in order to take advantage from 1 km resolution observations;
- high resolution COSMO model failure in forecasted precipitation in the operational configuration.

These requirements are demanding and limit the research of cases mainly in the summer season with a sharp restriction of the whole possible dataset.
For all of the three case studies presented, simulation runs consist of an assimilation and a forecast cycle both 12 hours long. A first verification is made by comparing qualitatively accumulated precipitation fields from the assimilation and the forecast cycle. The impact is assessed against the operational run, used as a control run, in which only conventional observations are assimilated through nudging scheme, and a run with LHN.

Then outcomes are verified quantitatively by means of the areal mean of accumulated precipitation over a selected domain. The area of verification, shaded in blue in Figure 5, is centered over the Northern Italy. Considered values are:

- 12 h accumulated precipitation in the assimilation cycle;
- hourly accumulated precipitation in the forecast cycle up to 12 hours.

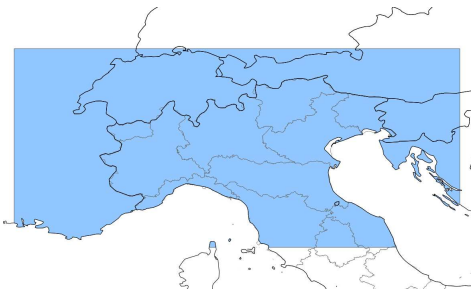

Figure 5: Selected domain used for the verification of results.

The first case study occurred during the Hymex Special Observation Period (SOP). The goal of the experiment is to resolve the underestimation of forecasted precipitation over Liguria and on the Apennines between Tuscany and Emilia-Romagna region. For this instance, the two different configurations of the 1D-Var are tested. Accumulated rainfall fields at the end of the assimilation cycle (Figure 6) display small modifications due to the change in parameterization parameters. Over the Alps the precipitation is a bit more widespread with an intensification of the convective core when radar observed profiles are assimilated. Over the Liguria region,

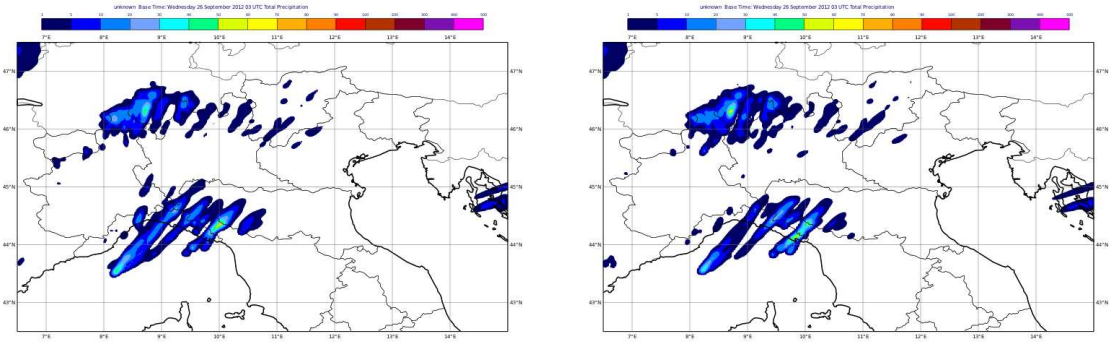

Figure 6: Accumulated rainfall fields over the assimilation cycle starting at 00 UTC of the 26^{th} of September 2012 obtained with the standard (left) and convective (right) 1D-Var configuration

an attenuation of precipitation can be recognized over the west structures, while there is an intensification in the east direction with the splitting in two parts of the convective nucleus.

Hence all of the runs are compared by means of accumulated precipitation fields.

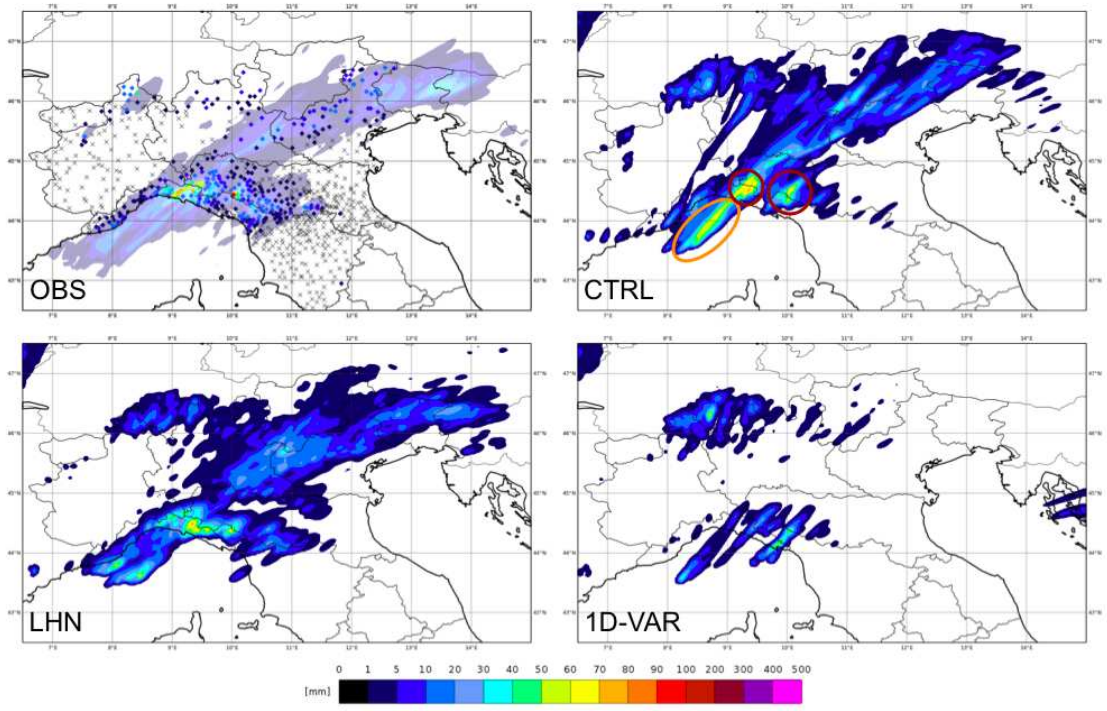

Figure 7: Accumulated rainfall fields at the end of the assimilation cycle for rain gauges and radar (top left), for control run (top right), for LHN run (bottom left) and for 1D-Var+nudging run (bottom right).

In the upper left panel of Figure 7 accumulated precipitation measured by rain gauges (diamonds) is displayed over the same field retrieved by the radar network (shaded area). These are observations that are used for the qualitative verification of output fields. Control run (upper right side) correctly predicts the pattern of precipitation field even if there is an overestimation over the Tyrrhenian sea (orange circle), and an underestimation over Apennines (red circles). LHN run (lower left panel) improves results decreasing precipitation over the sea, but does not reproduce highest rain rates over the Apennines. 1D-Var+nudging run (lower right panel), instead, predicts in a wrong way the rainfall fields with a general underestimation. The overestimation

over the Alps cannot be verified due to the lack of rain gauges and the probable blindness of radar in that region.

The comparison of accumulated rainfall over the forecast cycle does not show great differences among the 3 runs (Figure 8). All of the runs miss the precipitation over Liguria and over Apennines between Tuscany and Emilia-Romagna where an improvement of the forecasted fields are expected (pink circles). Instead, runs with the assimilation of radar observations better predict precipitation over Northeastern Italy where there was an overestimation in the control run.

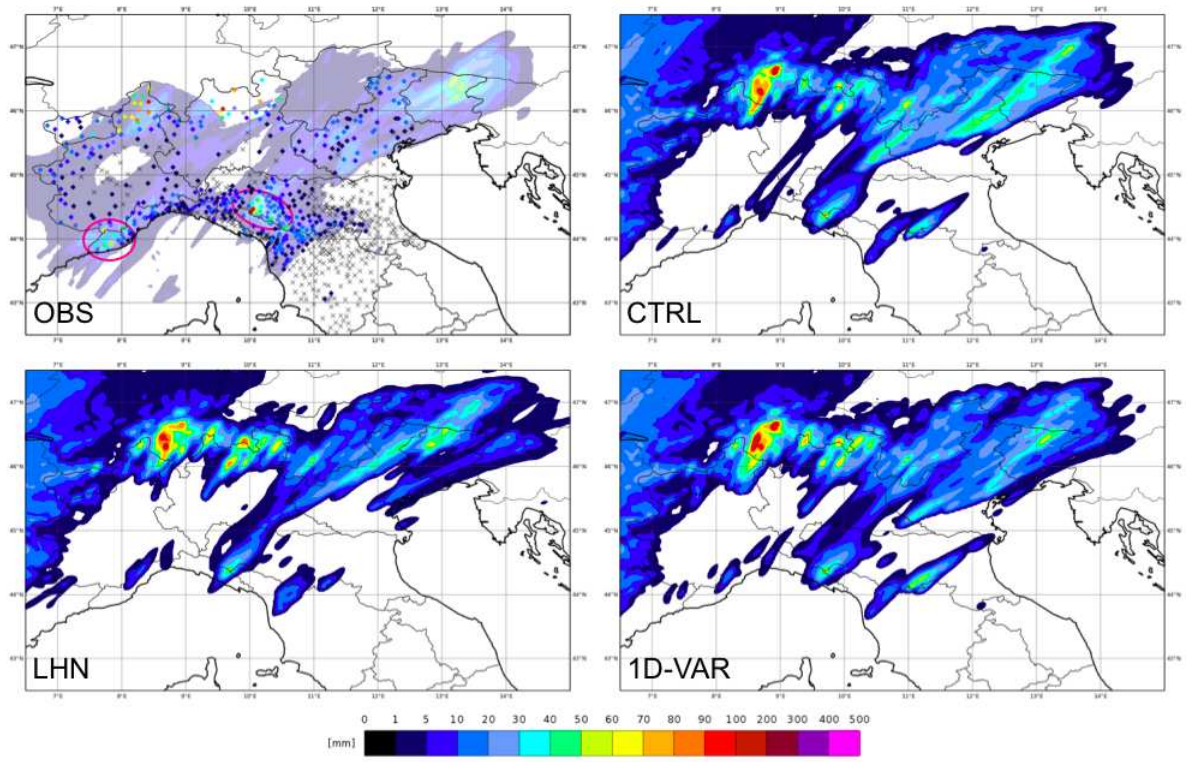

Figure 8: Accumulated rainfall fields at the end of forecast cycle for rain gauges and radar (top left), for control run (top right), for LHN run (bottom left) and for 1D-Var+nudging run (bottom right).

In the areal mean precipitation graph (Figure 9) all of the model runs start with a very low mean precipitation with respect to the observed one (blue line). The two different 1D-Var parameterizations (standard configuration in yellow, convective one in red) give quite the same results and have a positive trend towards observations. In the assimilation cycle (on the left) LHN (pink line) improves with respect to the control run. In the forecast cycle, control and LHN runs are slightly different and in the first three hours they are both better than 1D-Var+nudging run. 1D-var seems to go better between the 4^{th} and the 5^{th} hour. Behind this time all runs are slightly different. Observation information is substantially lost. At the end of forecast period, precipitation is clearly underestimated.

The second case study starts at the 00 UTC of 21^{th} of July 2012. Rainfall patterns both during assimilation and forecast are quite the same. The greatest difference is in the amount of precipitation. During the assimilation cycle (Figure 10) the control run overestimates all of the field, the overestimate of LHN is localized only over Northeastern Italy while, as settled before, 1D-Var presents a general underestimation. In the forecast (Figure 11) all of the runs miss the precipitation in the areas evidenced by red circles. Control and LHN runs display a very strong convective core not observed (pink circle), while over the same area 1D-Var+nudging run is completely dry. Surprisingly 1D-Var+nudging run gives more intense precipitation with respect to the other integrations.

The chart of Figure 12 shows very low precipitation values. In this case the best estimates are from 1D-Var+nudging run, while for the other runs there is a common overestimation. In the first hours the forecast runs are too wet with respect to the observations and they have a similar trend which does not fit the observed one.

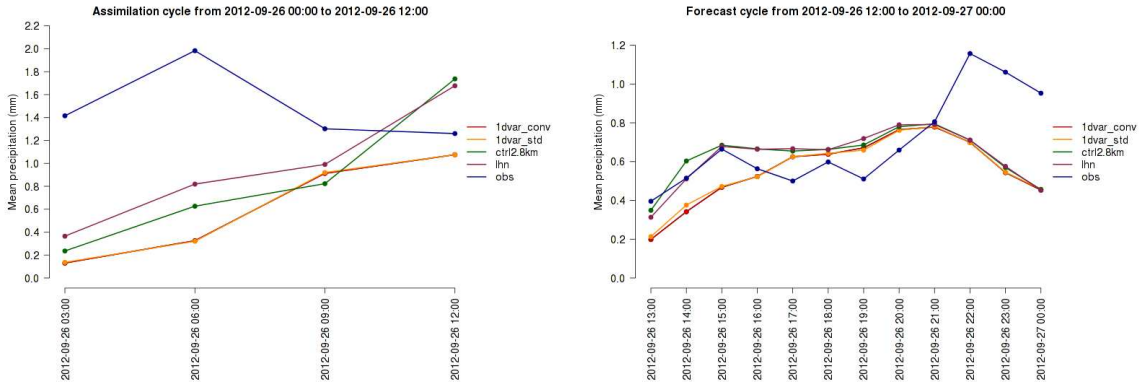

Figure 9: Areal mean precipitation in function of time for the assimilation (left) and forecast (right) cycle for the different runs against observation (blue line) for the 26^{th} of September 2012 case study.

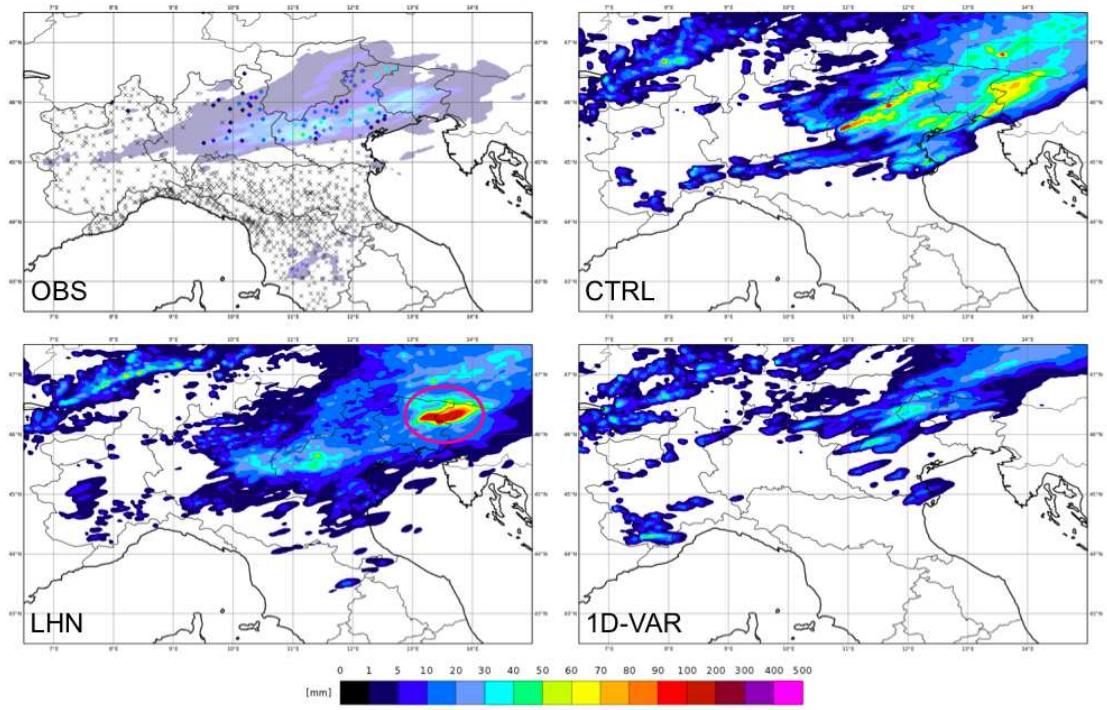

Figure 10: Accumulated rainfall fields at the end of the assimilation cycle for rain gauges and radar (top left), for control run (top right), for LHN run (bottom left) and for 1D-Var+nudging run (bottom right).

For the last case study only quantitative results are presented due to the small differences in forecasted patterns (Figure 13). From the quantitative point of view, in the assimilation cycle what can be recognized is that LHN and control runs have the same trend of observations even if the overestimation of the LHN is greater than the one of the control run. The 1D-Var+nudging run performs better in the first 9 hours and then maintains its tendency by underestimating precipitation over the last hours. In the forecast cycle, as expected, the run starting from the 1D-Var+nudging analysis starts dryer than the others, which are too wet. All of the three forecasts lose the peak in the observed precipitation at 18 UTC. However, as seen before and as a common result, can be observed that in the forecast cycle the influence of assimilated observations is completely loss after few hours. Moreover, tendencies of forecasted precipitation are not able to follow the great changes in the observations.

From these case studies, it was expected that assimilation of 1D-Var derived profiles should trigger some instability and should produce greater amount of precipitation mainly because only points where first guess and observations are greater than zero. Due to the small changes in the forecasted rainfall fields, and due to a

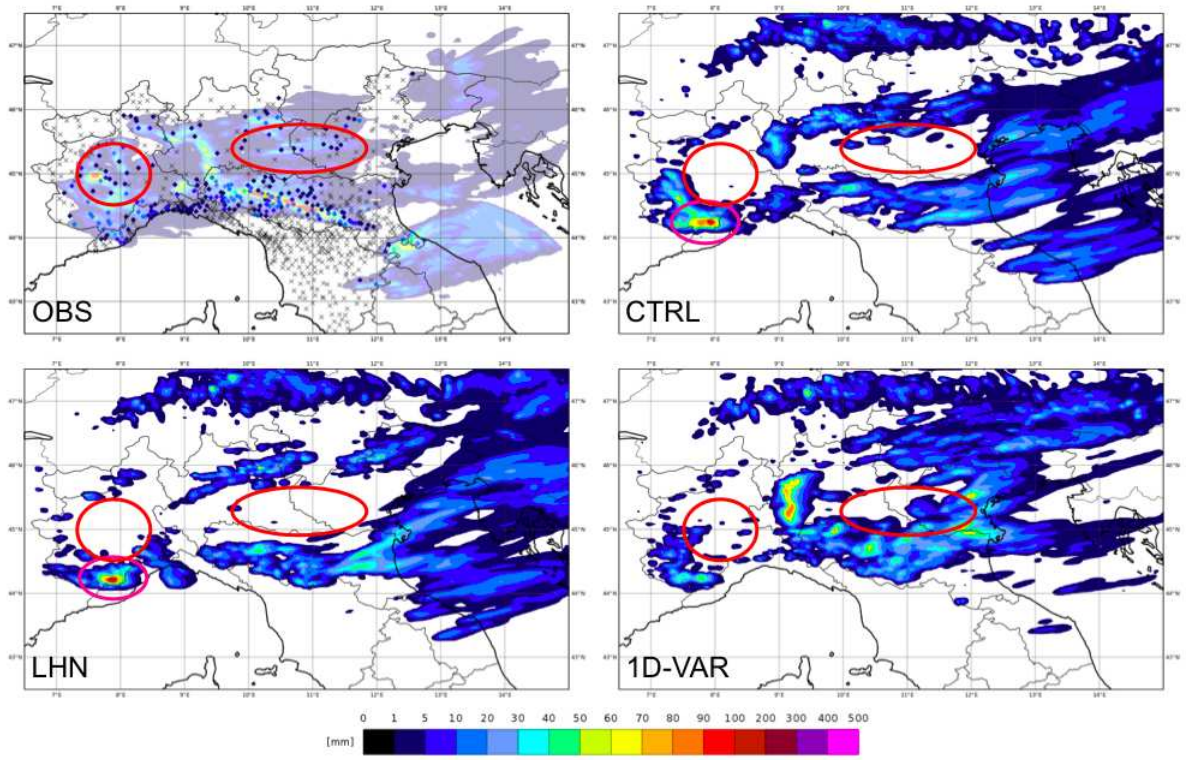

Figure 11: Accumulated rainfall fields at the end of forecast cycle for rain gauges and radar (top left), for control run (top right), for LHN run (bottom left) and for 1D-Var+nudging run (bottom right).

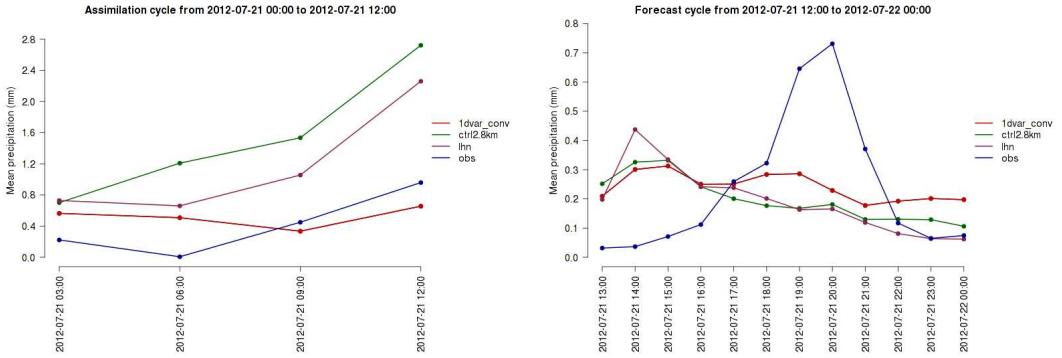

Figure 12: Areal mean precipitation in function of time for the assimilation (left) and forecast (right) cycle for the different runs against observation (blue line) for the 21^{th} of July 2012 case study.

general drying effect associated to the assimilation of 1D-Var retrieved profiles, a backward analysis starting from the 1D-Var algorithm was performed.
First investigation is made examining all of the profiles that come out from the 1D-Var scheme. Statistically the 70% of inputs converges providing temperature and humidity profiles to be nudged in COSMO. For the rest of the profiles the minimization of the cost function fails and points are discarded. A more detailed analysis is made over this sample. A direct comparison between observed radar rain rates and 1D-Var derived rain rates (Figure 14) shows how the minimization fails for the most part of points for which precipitation is moderate/heavy. Hence the information coming from points which should mainly contribute in producing rainfall is completely lost. The change of 1D-Var configuration is capable to increase the number of points associated to higher precipitation, but the strongest convective core structures are to a large extent lacking.

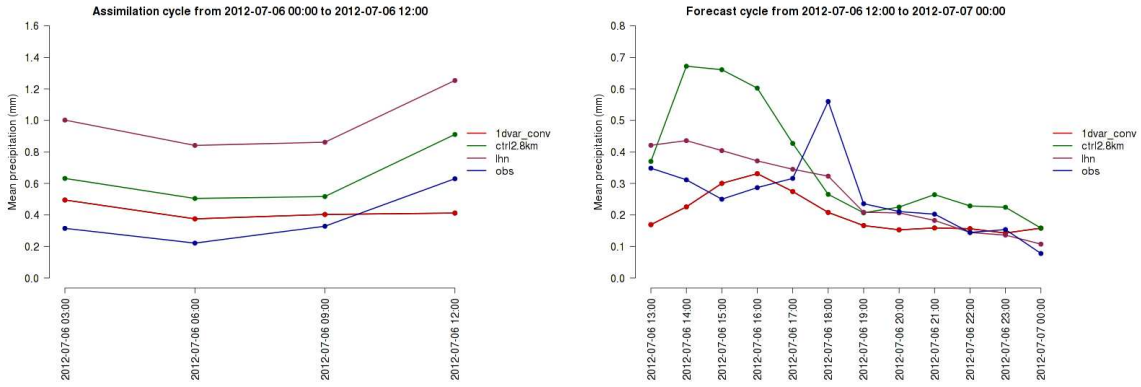

Figure 13: Areal mean precipitation in function of time for the assimilation (left) and forecast (right) cycle for the different runs against observation (blue line) for the 6^{th} of July 2012 case study.

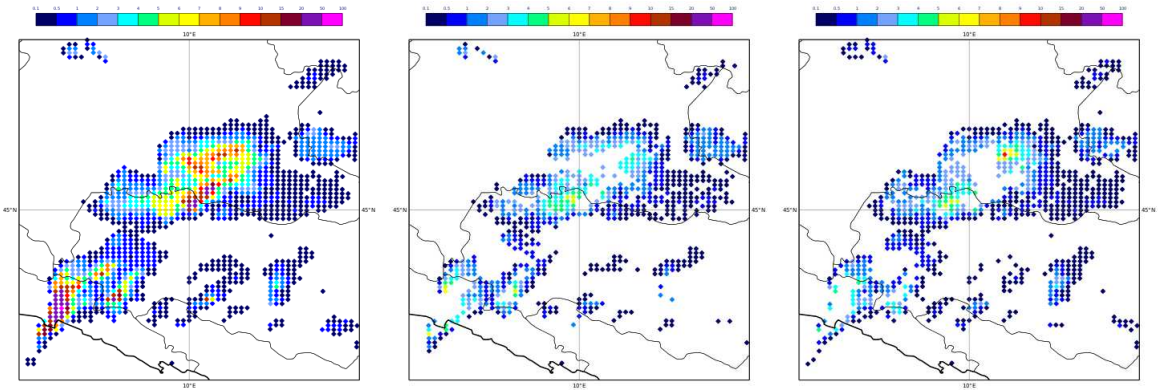

(a) (b) (c)

Figure 14: (a) Observed radar rain rate for the 26^{th} of September 2012; (b) Output from 1D-Var scheme for the standard configuraztion; (c) Output from 1D-Var scheme for the convective configuration.

4 Summary and Outlook

In latest years different attempts were made in order to understand how and how much the assimilation of radar data through the 1D-Var+nudging technique affects the precipitation forecast.

Products were verified subjectively and objectively examining 12 hours accumulated precipitation. Despite changes, results show that LHN scheme outperforms the proposed methodology. These unsatisfactory results are mainly due to two different reasons:

- the moist physics implemented in the 1D-Var differs from the one of the COSMO model;
- the use of a linearized moist physics that has been designed at coarse resolutions is not appropriate to represent intense precipitation events by very high resolution models.

These conclusions imply that this methodology is not suitable for the assimilation with the COSMO model of high density rain rate estimates based on radar data.

References

[1] P. Bauer, P. Lopez, A. Benedetti, D. Salmond and E. Moreau *Implementation of 1D+4D-Var assimilation of precipitation-affected microwave radiances at ECMWF. I: 1D-Var*, Q. J. R. Meteorol. Soc., **132**, 2006,2277–2306.

[2] V. Bondarenko, T. Ochotta, D. Saupe and W. Wergen *The interaction between model resolution, ob-*

servation resolution and observation density in data assimilation: a two-dimensional study, Proceedings 11^{th} Symposium on Integrated Observing and Assimilation Systems for the Atmosphere, Oceans, and Land Surface, San Antonio, Texas, 2007.

[3] Z.-Q. Liu and F. Rabier *The interaction between model resolution, observation resolution and observation density in data assimilation: a one-dimensional study*, Q. J. R. Meteorol. Soc., **28**, 2002, 1367–1386.

[4] P. Lopez and E. Moreau *A convection scheme for data assimilation: description and initial test*, Q. J. R. Meteorol. Soc., **131**, 2005, 409–436.

[5] P. Lopez and P. Bauer *"1D+4D-Var assimilation of NCEP Stage-IV radar and gauge hourly precipitation data at ECMWF*, Mon. Weather Rev., **135**, 2007, 2506–2524.

[6] P. Lopez and P. Bauer *Experimental assimilation of ground-based radar data in ECMWF 4D-Var*, Proc. of 5^{th} European Radar Conference on Radar Meteorology and Hydrology (ERAD), Helsinki, Finland, 30 June–4 July 2008.

[7] P. Lopez 2010 *Direct 4D-Var assimilation of NCEP Stage IV radar and gauge precipitation data at ECMWF*, Tech. Memo., **627**, 2010.

[8] K. Stephan, S. Klink and C. Schraff *Assimilation of radar-derived rain rates into the convective-scale model COSMO-DE at DWD*, Q. J. R. Meteorol. Soc., **134**, 2008, 1315–1326.

[9] M. Tiedtke *A comprehensive mass flux scheme for cumulus parameterization in large-scales models*, Mon. Weather Rev., **117**, 1989, 1779–1800.

[10] A. M. Tompkins and M. Janisková *A convection scheme for data assimilation: description and initial test*, Q. J. R. Meteorol. Soc., **130**, 2004, 2495–2517.

Performance comparison of two COSMO-I2 implementations

M. Giorcelli [1, 2], N. Vela [1, 2], M. Milelli [1], E. Oberto [1], C. Cassardo [2], M. Galli [3]

[1] *ARPA Piemonte*

[2] *Universita' degli Studi di Torino*

[3] *CNMCA, Pratica di Mare, Roma*

1 Introduction

In 2013 ARPA Emilia Romagna has implemented a Rapid Updating Cycle (RUC) based on COSMO-I2 model. RUC is made up of three hours assimilation cycles (00 UTC, 03 UTC, 06 UTC, 09 UTC, 12 UTC, 15 UTC, 21 UTC) followed by 18 hours forecast runs. The aim of RUC is to take advantage of radar data and other "fresh" observations available (e.g. aircraft reports, local surface station networks) for producing a numerical weather forecast having some added value in the nowcasting range.
ARPA Piemonte has implemented a parallel version of the RUC in order to be used as a test suite for some modification which, if successful, could be introduced in the official Italian RUC. In particular this implementation differs in two components: the first one is the assimilation of non-GTS data from the high resolution network of the Italian National Civil Protection Department (DPC) and a the second one is the introduction of the FASDAS (Flux-Adjusting Surface Data Assimilation System) scheme which has been already tested successfully. The aim of the present work is to make a first comparison of the performance of the two different configurations.

2 Model setup: similarities and differences

The ARPA Piemonte and the ARPA Emilia Romagna RUC modelling systems share the same integration area (Northern Italy, surrounding the Alps, figure 1), the grid step of 2.8 Km, the operational COSMO-I2 configuration (default Runge-Kutta dynamics, parametrized shallow convection), the boundary conditions from the operational COSMO-I7. The two modelling systems implement the latent heat nudging using 15 minutes surface precipitation estimated by radar composite provided by DPC. As reported in figure 2, RUC

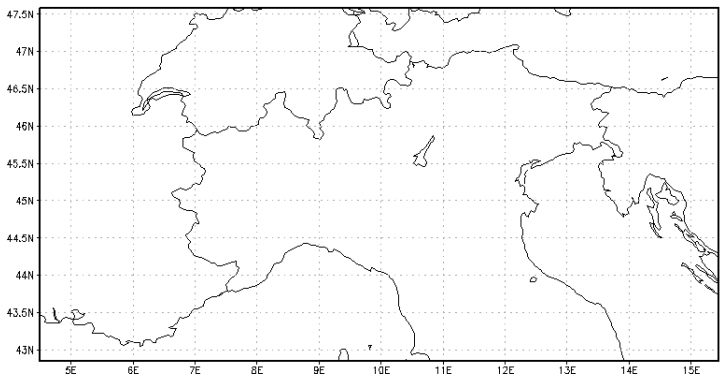

Figure 1: Integration area.

is made up of short cut-off quick assimilation runs covering the last 3 hours followed by 18 hours forecast runs. In order to improve the quality of the model state every 12 hours (00 UTC and 12 UTC) a long cut-off "re-assimilation" run covering the last 12 hours is made; these runs use COSMO-I7 analysis as boundary conditions and more observations than the quick assimilation. The boundary conditions for assimilation run of 03 UTC, 06 UTC, 09 UTC, 12 UTC and the relative forecasts are supplied by COSMO-I7 forecasts initialised at 00 UTC; boundary conditions for assimilation run of 15 UTC, 18 UTC, 21 UTC, 00 UTC and the relative forecasts are supplied by COSMO-I7 forecasts initialised at 12 UTC. This has two consequences: firstly it produces a progressive worsening of forecast quality going from 03 UTC to 12 UTC and from 15

UTC to 00 UTC initialisation time, due to the use of older boundary conditions for assimilation and forecast; secondly between forecasts initialised at 12 and 15 UTC and similarly between 00 UTC and 03 UTC forecasts, there could be a discontinuity due to the use of different forecasts as boundary conditions. The

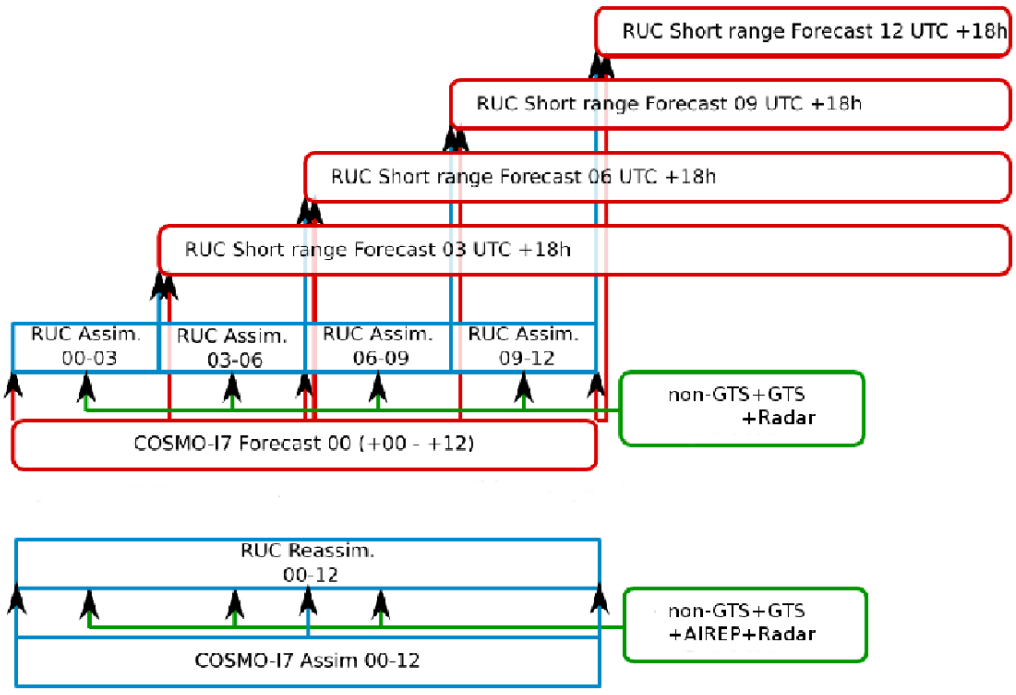

Figure 2: Rapid Updating Cycle scheme.

ARPA Piemonte and the ARPA Emilia Romagna RUC modelling differ in two components. The first one is the assimilation of T2m coming from the high density weather stations network of ARPA Piemonte and DPC. The goal is to take advantage of such a network for enhancing the quality of the COSMO-I2 analysis production. In previous studies, it has been shown how the assimilation of T2m from non-GTS network has a major importance in improving the forecast. The second difference is the use of FASDAS (Flux-Adjusting Surface Data Assimilation System) scheme implemented inside COSMO code. FASDAS is able to improve the scheme involved in the T2m assimilation taking advantage of the great availability of data in the analysis production. FASDAS updates the soil state related variables and the soil to atmosphere fluxes, so it couples temperature and humidity increments in the atmospheric fields with increments in the soil temperature and moisture fields, in order to maintain balanced turbulent heat fluxes between the soil and the atmosphere.

3 Temperature and wind speed verification

The preliminary verification has been made from the 15th of January 2014 to the 15th of February 2014 using the observed data coming from a subset of verification stations not used for assimilation. The stations are all inside the 0-500 m range. Surface variables have been evaluated by comparing the mean error (ME) and the root mean square error (RMSE) of the two simulations for each run (from 00 UTC to 21 UTC) and for each forecast time (from +00 to +18). ME and RMESE have been calculated with respect to all the ground stations included in the integration area for the standard variables (T2m, RH2m, W10m). ME and RMSE are defined as usually by equations:

$$ME = \frac{1}{N}\sum_{i=1}^{N}(P_i - O_i) \tag{1}$$

$$RMSE = \sqrt{\frac{1}{N}\sum_{i=1}^{N}(P_i - O_i)^2} \tag{2}$$

where N is the number of observed-predicted data couples, O_i and P_i represent respectively the ith observed and predicted values.
If we consider T2m mean error (figures 3 and 4) we can see a good improvement of ARPA Piemonte RUC with

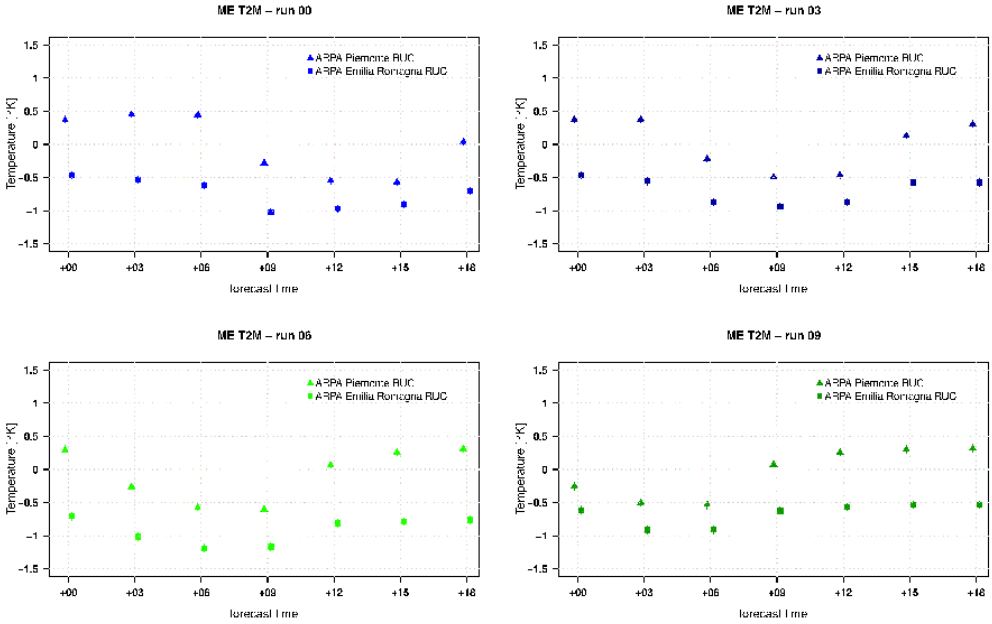

Figure 3: Mean error of two meters temperature for 00 UTC, 03 UTC, 06 UTC, 09 UTC initializations.

respect to ARPA Emilia Romagna RUC for almost all runs. Furthermore, both forecasts show a clear daily cycle: ARPA Emilia Romagna RUC tends to have a greater underestimation during daytime than during night time, ARPA Piemonte RUC tends to overestimate during night time and to underestimate during daytime. This different behaviour probably arises from the introduction of FASDAS scheme because T2m increments is directly correlated to sensible and latent heat fluxes.

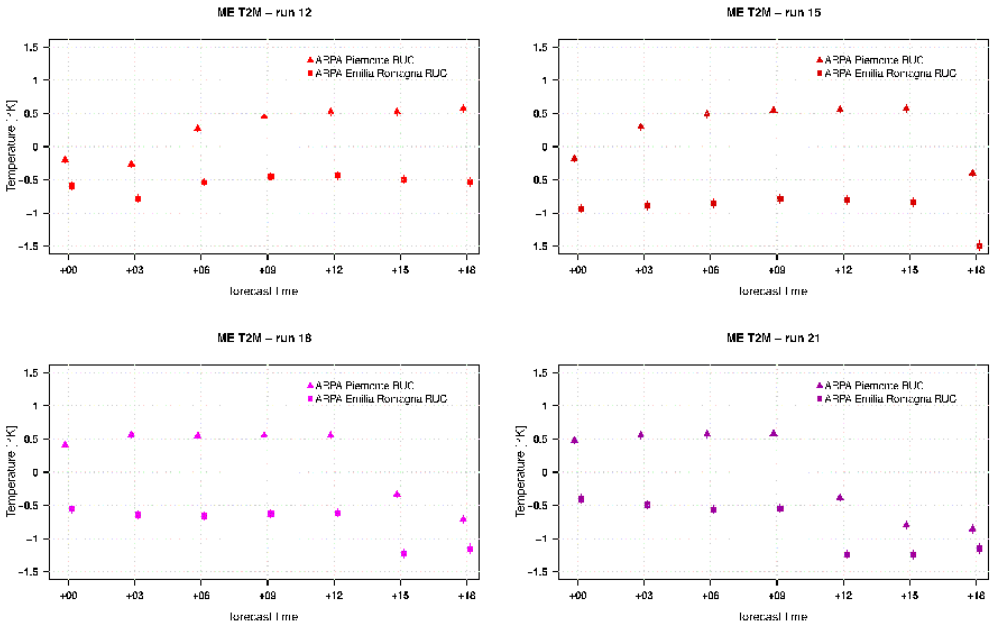

Figure 4: Mean error of T2m for 12 UTC, 15 UTC, 18 UTC, 21 UTC initializations.

As we can see in figure 5 the root mean square error of ARPA Piemonte T2m shows a clear improvement with respect to ARPA Emilia Romagna RUC. If we consider mean error and root mean square error of W10m (figures 6) the two model systems do not show relevant differences, indeed wind speed is not an assimilated variable.

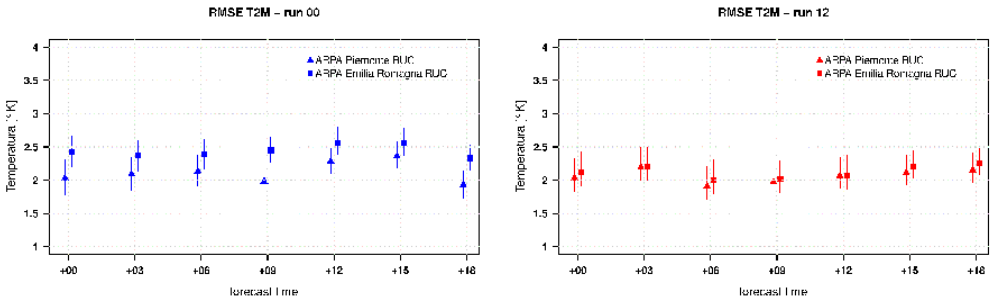

Figure 5: Root mean square error of T2m for 00 UTC and 12 UTC initializations.

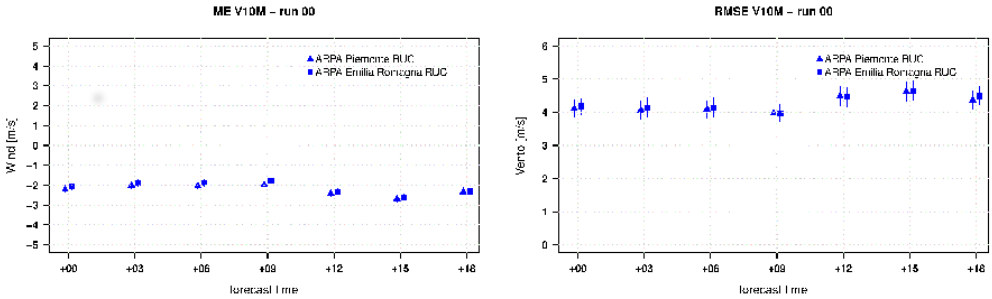

Figure 6: Mean error and root mean square error of W10m for 00 UTC.

3 Precipitation verification

We have carried out also the verification of precipitation using the observed data coming from high density weather stations network of ARPA Piemonte. Thresholds of 1, 2, 4 and 6 mm have been considered and performance diagrams have been made every six hours from +06 to +18 comparing the precipitation predicted and observed. Results are displayed in figures 7, 8 and 9.

In the performance diagram are reported POD (Probability Of Detection) on y-axis, SR (Success Ratio) on x-axis, TS (Threat Score) as solid lines in plot area and BIAS score as dashed lines in plot area defined as follow:

$$POD = \frac{hits}{hits + misses} \tag{3}$$

$$SR = \frac{hits}{hits + falsealarms} \tag{4}$$

$$TS = \frac{hits}{hists + misses + falsealarm} \tag{5}$$

$$BIAS = \frac{hits + falsealarms}{hits + misses} \tag{6}$$

In performance diagram legends RAC stands for ARPA Piemonte system, RUC for ARPA Emilia Romagna system.

There are better performance of ARPA Piemonte RUC for all thresholds due to a general increase in the fraction of the observed precipitation events correctly forecasted (POD). For thresholds of 1 and 2 mm in both models is present a daily effect. In 00 UTC run (figure 7) the first six hours forecast (red in performance diagram) presents a worse SR values and a better POD values than the second six hours forecast (green in

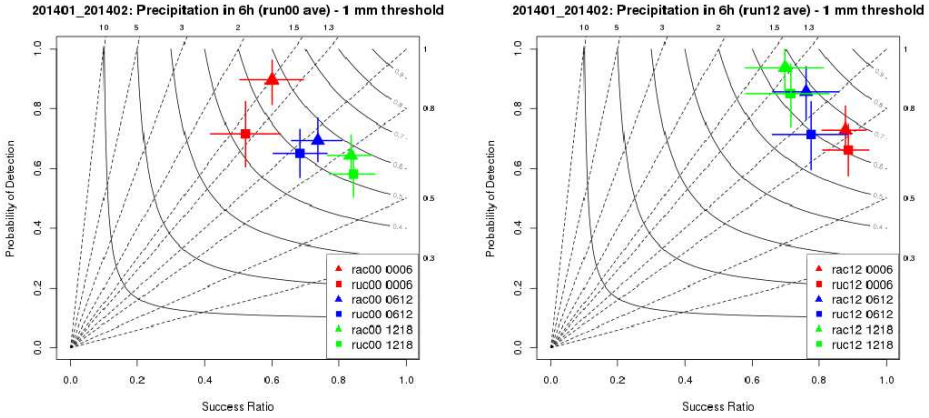

Figure 7: Performance diagram for 1 mm threshold.

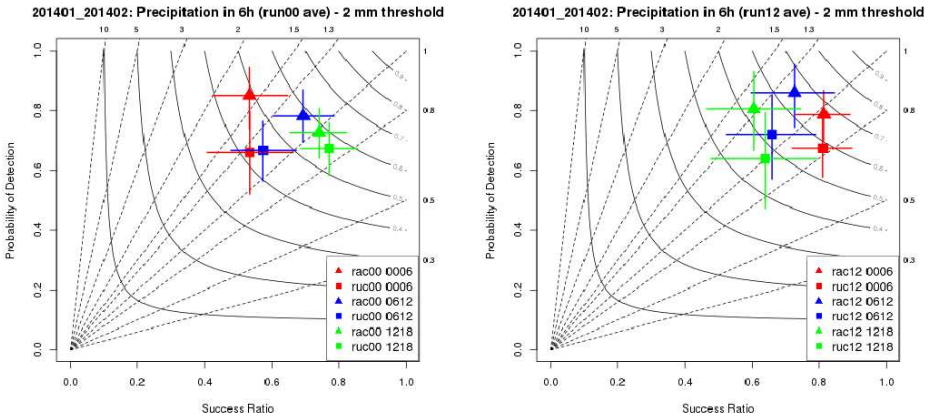

Figure 8: Performance diagram for 2 mm threshold.

performance diagram), but in 12 UTC run (figure 7) the first six hours forecast (red in performance diagram) presents a better SR values and a worse POD values than the second six hours forecast (green in performance diagram); so it means an increment in number of false alarm events during night time.

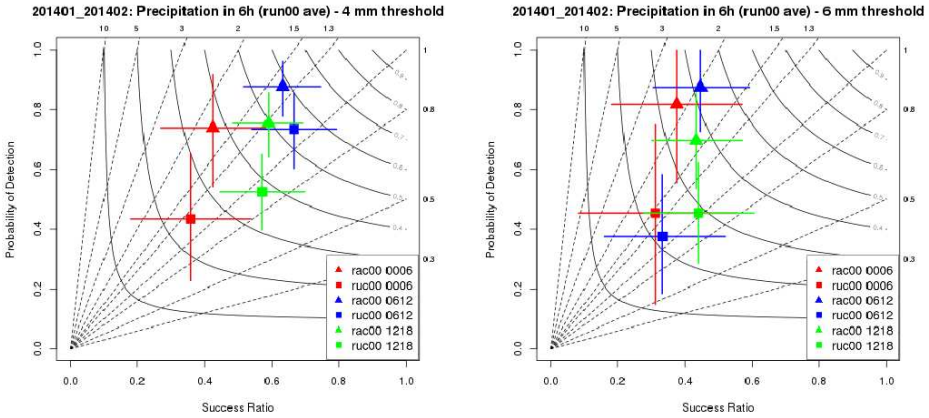

Figure 9: Performance diagram for 4 mm threshold.

4 Summary and future plans

The introduction of FASDAS in the COSMO observation nudging code has a double justification: on the one hand it produces more balanced analysis with respect to the land surface turbulent energy fluxes, and on the other hand it introduces directly in the analysed fields the soil. The soil is characterised by longer response times compared to the planetary boundary layer, so the better initialisation of the soil produces also a better feedback on the model forecasts at on the surface with better values of T2m and precipitation estimates compared to an operational configuration of the COSMO model.
The work goes on because the verification time of one month is quite short, but as soon as the statistics is more solid (and these preliminary results are confirmed), the modifications can be applied operationally.

References

[1] Galli M., Milelli M., Cassardo C., 2011: The effects of T2m assimilation on surface fluxes in COSMO-I2. *COSMO Newsletter, No. 11*, **3-21**.

[2] Alapaty, K., D. Niyogi, F. Chen, P. Pyle, A. Chandrasekar, and N. Seaman, 2008: Development of the Flux Adjusting Surface Data Assimilation System for Mesoscale Models. *Journal of Applied Meteorology and Climatology*, 7, **2331-2350**.

[3] Alapaty, K., N. Seaman, D. Niyogi, A. Hanna, 2001: Assimilating Surface Data to Improve teh Accuracy of Atmospheric Boundary Layer Simulations. *Journal of Applied Meteorology and Climatology*, 7, **2331-2350**.

First COSMO-E Experiments with the Stochastically Perturbed Parametrization Tendencies (SPPT) Scheme

Daliah Maurer, André Walser and Marco Arpagaus

MeteoSwiss, Krähbühlstrasse 58, 8044 Zürich, Switzerland

1 Introduction

COSMO-E is an experimental ensemble prediction system with 21 members for the Alpine area, see Fig. 1. It has a convection-permitting mesh-size of 2.2 km and the forecast range is 120 hours. Lateral boundary conditions (LBC) are taken from IFS-ENS ensemble (30 km mesh size) of the European Center for Medium-Range Weather Forecasts (ECMWF), while the initial conditions (IC) for the ensemble members are taken from the operational COSMO-2 analysis. Uncertainty of the driving model IFS is represented by perturbing LBCs, i.e. using the control and the first 20 members from IFS-ENS interpolated onto the COSMO-E grid. Uncertainty in the assimilation of observations into COSMO-E will be represented later by IC perturbations, provided by an ensemble data assimilation cycle based on a Local Ensemble Transform Kalman Filter (LETKF). This study focuses on sampling the uncertainty of the COSMO-E model, in particular of the physical parametrization schemes, by using the Stochastically Perturbed Parametrization Tendencies (SPPT) scheme. In this work, no IC perturbations are applied and COSMO version 4.26 with single precision is used.

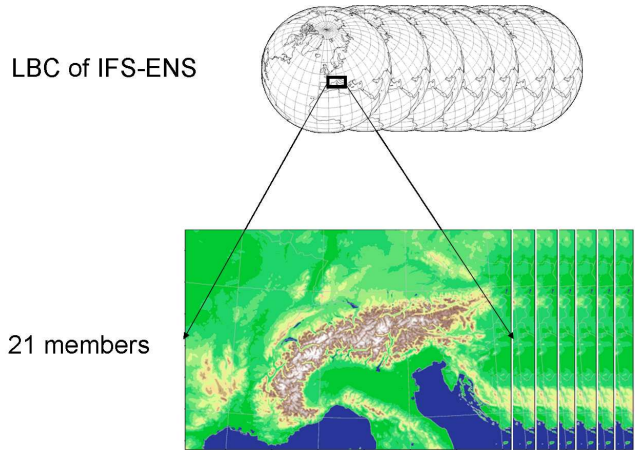

Figure 1: Experimental setup of COSMO-E

2 COSMO Implementation of SPPT

The SPPT scheme has been recently implemented into COSMO by Lucio Torrisi (based on Buizza et al. 1999; Palmer et al. 2009). The code generates a random pattern *ppert*. This random pattern is used to perturb the tendencies of the physical parametrization schemes of the model P_i^X. The total tendency of the prognostic variabe X after one timestep is

$$T^X = \frac{\partial X}{\partial t} = D^X + K^X + (1 + ppert) \sum_{i=1}^{N} P_i^X \ . \tag{1}$$

D^X is the tendency of the dynamics, K^X is the tendency of the horizontal diffusion and P_i^X is the tendency of the i-th physical parametrization scheme. For this work, only the variables zonal (U) and meridional (V) wind components, temperature (T) and specific humidity (QV) are perturbed, and N is the number of physical parametrization schemes producing tendencies for a given variable according to Tab. 1.

During the procedure of generating the random pattern *ppert*, first Gaussian random numbers with standard deviation σ and limited to a given *range* are generated on a coarse grid (Δi,Δj) at lead-time t. These random

T	Radiation,	SSO,	Turbulence,	Shallow convection,	Hydci_pp_gr (microphysics)
QV			Turbulence,	Shallow convection,	Hydci_pp_gr (microphysics)
U		SSO,	Turbulence		
V		SSO,	Turbulence		

Table 1: List of physical parametrization schemes that are active in COSMO-E and produce tendencies for temperature, specific humidity and the horizontal wind components.

numbers are interpolated horizontally in space onto the grid of COSMO-E (fine grid), see Fig. 2. At lead-time $t+\Delta t$ new random numbers are generated in the same manner. The random pattern *ppert* is an interpolation in time of two such sets of random numbers on the fine grid. Vertically *ppert* is constant, except above the tropopause and near surface, where a vertical tapering is introduced by default, see Fig. 3. Moreover, the default SPPT tuning parameters are: no supersaturation check in microphysics, $\sigma = 0.25$, $range = 0.75$, $\Delta i = \Delta j = 5.0^\circ$ and $\Delta t = 6$ hours. In the following, only deviations from the default parameters are mentioned.

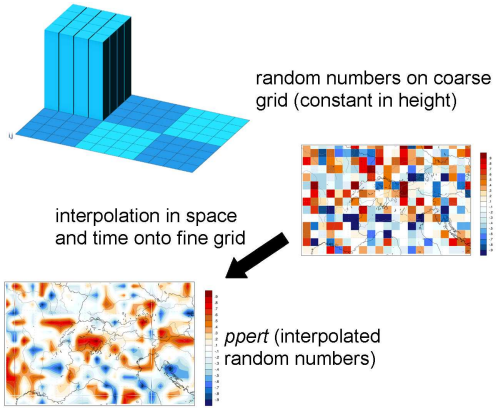

Figure 2: Procedure of generating *ppert*

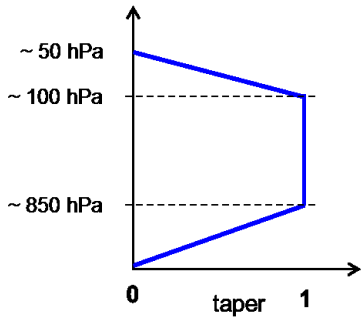

Figure 3: Taper function if the random numbers are tapered above the tropopause and near surface

3 Sensitivity of SPPT Settings

This section investigates the sensitivity of the SPPT tuning parameters on the variation between the ensemble members based on case studies. For the initial time 01.08.2012, 00 UTC, three ensemble forecasts are performed. They differ in the applied amplitude, space and time scales of the random numbers as documented in Tab. 2. The forecast range is 5 days and the same initial and lateral boundary conditions are used for all 21 members, i.e. SPPT is the only perturbation source in these experiments.

small	$\sigma = 0.25$,	$range = 0.625$,	$\Delta i = \Delta j = 0.5^\circ$,	$\Delta t = 0.5$ hours
medium	$\sigma = 0.25$,	$range = 0.625$,	$\Delta i = \Delta j = 5.0^\circ$,	$\Delta t = 6$ hours
large	$\sigma = 0.5$,	$range = 1.0$,	$\Delta i = \Delta j = 5.0^\circ$,	$\Delta t = 6$ hours

Table 2: Three experimental setups in order to check the sensitivity of SPPT

The variation between the ensemble members, also called spread, is measured by the unbiased sample variance of the ensemble members. As it can be seen in Fig. 4, the setup with largest random numbers "large" produces largest spread as expected, while the setup with smaller scales in space and time reveals a significant impact as well, exhibited by a clearly smaller spread in "small" compared to "medium". More specifically, the spread is investigated at three pressure levels 850, 700 and 500 hPa. The setups generally show the largest spread on the lowest level and the smallest on the highest level, even though tapering is switched on below 850 hPa in these experiments, according to Fig. 3. This behaviour is less evident for setup "small". The identical lateral boundary conditions for all ensemble members limit the error growth, i.e the spread of the ensembles. Figure 4 shows a spread saturation at about the same forecast step +40 hours for all setups and at all levels. This rather surprising behavior is confirmed by a second case study for 02.11.2012 (not shown). However, these ensembles show a saturation already at forecast step +15 hours, while the amplitudes of the spread are about

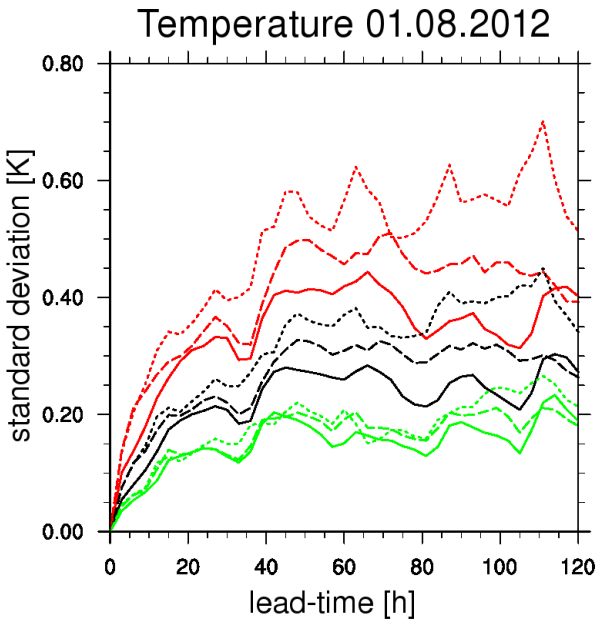

Figure 4: Ensemble spread for temperature averaged over the COSMO-E domain, at 500 hPa (solid line), 700 hPa (dashed line), 850 hPa (dotted line) and for experiment large (red), medium (black), small (green). Forecast initial date is 01.08.2012 00 UTC.

the same as in the present case study.

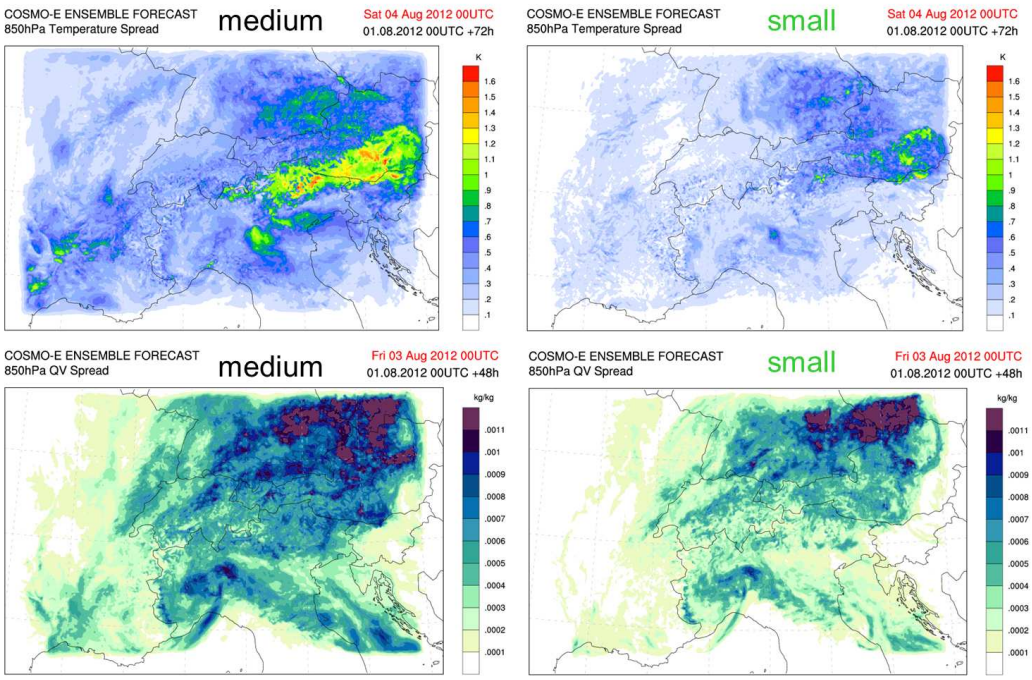

Figure 5: Ensemble spread at 850 hPa for temperature at lead-time 72 hours (top) and for specific humidity at lead-time 48 hours (bottom). Forecast initial date is 01.08.2012 00 UTC.

Figure 5 shows the ensemble spread horizontally at 850 hPa for setup "medium" (left) and setup "small" (right) for temperature (top) and specific humidity (bottom). "Medium" has a coarser structure in the random pattern than "small". This results in a larger amplitude of spread for "medium" but does hardly induce new regions of spread compared with "small".

4 Deterministic Verification

A scheme that samples model uncertainty should not degrade the quality of the individual members of an ensemble forecast. In order to quantify a potential degradation using SPPT, deterministic experiments for different SPPT setups and a reference experiment are performed for a 4 weeks period, both for summer and winter. The relevant validated SPPT setups are listed in Tab. 3.

ex0	no SPPT
ex3	SPPT default settings with $\sigma = 0.5$, $range = 1.0$
ex6	SPPT default settings with $\sigma = 0.5$, $range = 1.0$, $\Delta i = \Delta j = 0.5°$, $\Delta t = 1$ hour, without tapering in the lower troposphere

Table 3: The relevant experimental SPPT setups validated by a deterministic verification.

Observations of approximately 500 stations are used for a standard surface verification by deterministic scores like bias, mean absolute error, standard deviation and frequency bias for common thresholds. Scores of the different setups are compared for surface pressure, 2 m temperature and dew point temperature, 10 m wind speed and direction, 10 m wind gusts, cloud cover and 12 hourly precipitation sums.

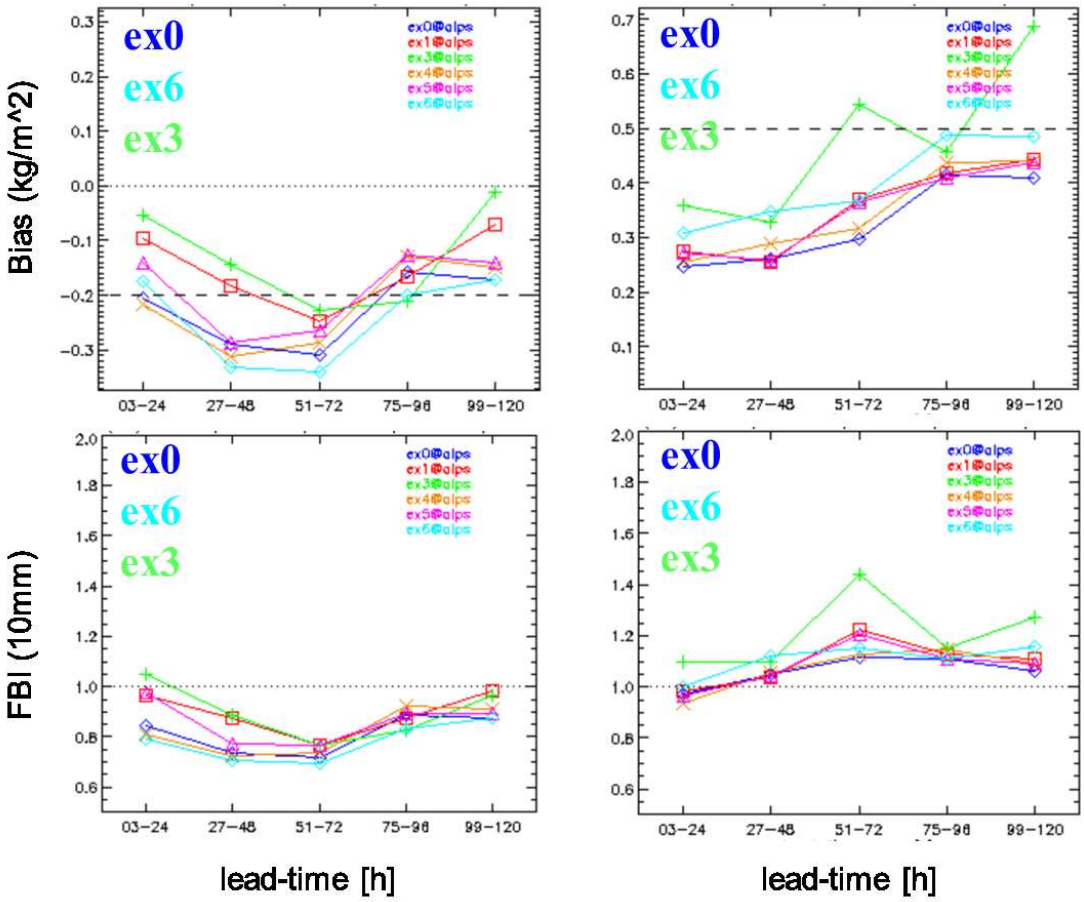

Figure 6: Bias (top) and 10 mm frequency bias (bottom) of 12 hourly precipitation sum for one month in summer (left) and winter (right)

Overall, the scores for the different setups are very similar pointing out that almost no quality degradations are found with SPPT. However, there are a few exceptions: SPPT often induces more precipitation than the reference, see bias in Fig. 6. While this has a positive impact in summer due to a generally negative summer bias of the model, it has a negative impact for the winter period. In particular the scores in winter of setup ex3 lie above the scores of the other setups, see right-hand side of Fig. 6.

In order to measure the quality of the deterministic experiments in the free atmosphere (upper air), these are verified against radio-soundings in terms of bias and the square of standard deviation error (STD) for temperature, specific humidity, geopotential wind speed and direction. Only small differences between the different setups are observed for both the summer and winter period. Figure 7 shows the scores for temperature at 25 pressure levels for all 12 soundings available in the model domain. Both, bias and STD are very similar for all experiments, except ex3 which shows slightly smaller bias but slightly larger STD.

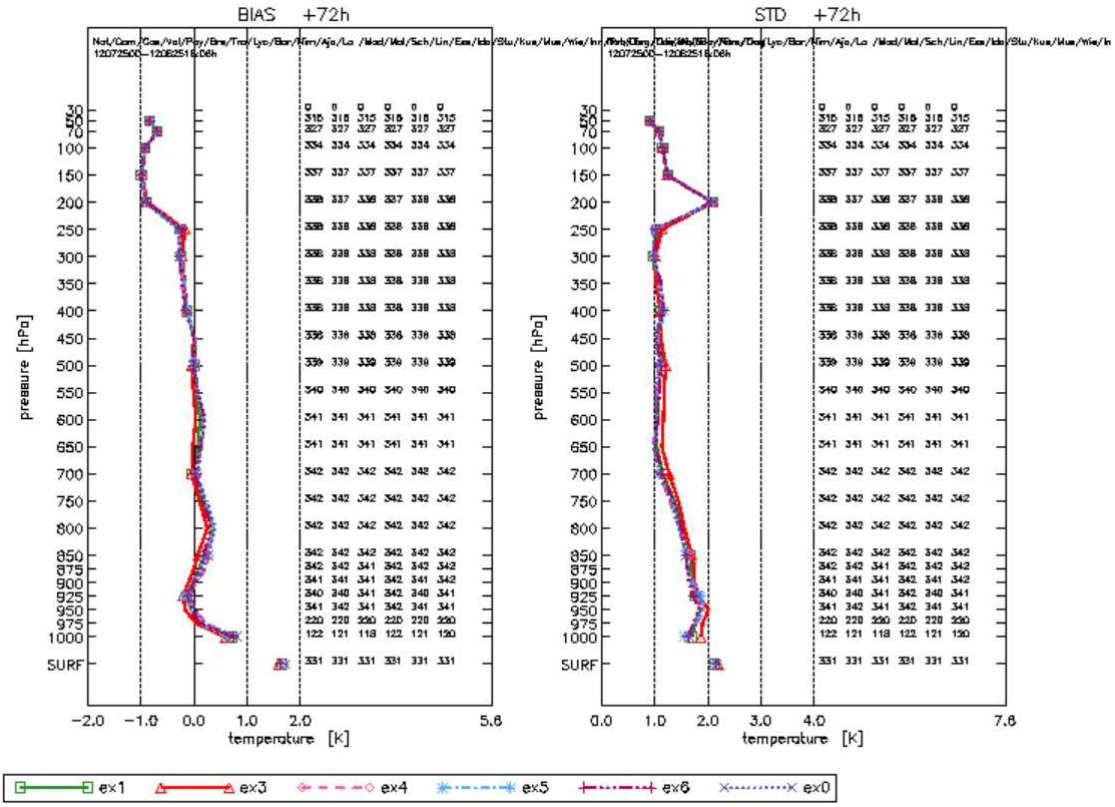

Figure 7: Bias (left) and the square of standard deviation error (right) of the upper air verification of temperature for one month in summer, using all stations in the COSMO-E domain.

In conclusion, surface and upper air verification indicate, unless random numbers as well as space or time scales are increased as much as in ex3, SPPT is hardly detrimental to forecast quality.

5 Ensemble Experiments

This section investigates 00 UTC ensemble forecasts performed for an extended period from 25.07.2012 to 25.08.2012 and 3 experimental setups:

LBC	**L**ateral **B**oundary **C**ondition perturbations alone
LBC+SPPT	SPPT perturbations and LBC perturbations
LBC+PP	**P**arameter **P**erturbations used for COSMO-DE-EPS (Gebhardt et al. 2011) and LBC perturbations

The SPPT setup ex6 is chosen for the LBC+SPPT experiment, because the scale of those perturbations matches the scale of convective events and the scores of the deterministic verification lie in an acceptable range, as pointed out in section 4.

One member of the LBC+SPPT experiments with initial date 24.08.2012 crashed because the CFL-criterion was violated. Therefore, the experiments for this initial date are excluded from the subsequent analyses.

The ensemble forecasts from the three setups have been verified in terms of 12 hourly precipitation sums. Figure 8 shows the Brier skill score against observations from 300 SYNOP stations, with climatology (2001-2010) as reference. SPPT gives a small benefit to LBC at the begin of forecast, i.e. until ∼30 hours lead-time, while almost no differences can be observed between the experiments LBC and LBC+PP. Therefore, in the following we focus on the results of the LBC+SPPT and LBC experiments. Note again, that no IC perturbations are used in these experiments. The benefit of SPPT might be smaller with appropriate IC perturbations.

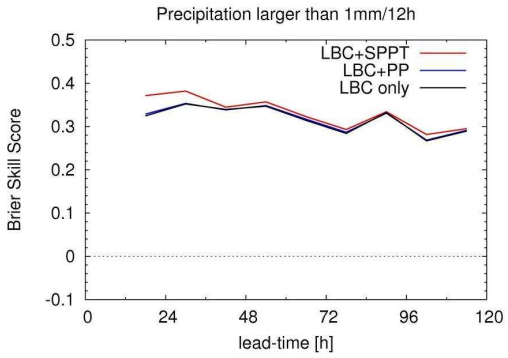

Figure 8: Brier skill score for all three experiments against observations of 300 SYNOP stations for precipitation larger than 1 mm per 12 hours, with climatology (2001-2010) as reference.

According to Jollife et al. (2011), the attribute 'reliability' of a probabilistic forecast characterizes the degree to which the forecast probabilities are consistent with the relative frequencies of the observed outcomes. For a perfectly reliable probabilistic forecasting system, the squared error between ensemble mean and observation and the unbiased sample variance of the ensemble members have the same expectation value. Thus the relation

$$\mathrm{E}_t\left[\left(x_t-\bar{\hat{x}}_t\right)^2\right]=\frac{m+1}{m}\mathrm{E}_t\left[s_t^2\right] \tag{2}$$

should hold. t characterizes the t-th ensemble forecast of m members $\{\hat{x}_{t,1},\hat{x}_{t,2},...,\hat{x}_{t,m}\}$, in our case the lead-time. $\mathrm{E}_t\left[\cdots\right]$ denotes the expectation value and x_t is the observation corresponding to the ensemble forecast. $\bar{\hat{x}}_t \doteq \frac{1}{m}\sum_{j=1}^{m}\hat{x}_{t,j}$ is the ensemble mean and $s_t^2 \doteq \frac{1}{m-1}\sum_{j=1}^{m}\left(\hat{x}_{t,j}-\bar{\hat{x}}_t\right)^2$ is the unbiased sample variance of the ensemble members.
Both sides of Eq. (2) are estimated by calculating the expressions in box brackets at every gridpoint and averaging over the COSMO-E domain and over all initial dates. On the right-hand side of Eq. (2) the estimate is the squared ensemble spread, abbreviated as RMEV_t^2. The left-hand side is estimated by squares of error between analysis and ensemble mean, abbreviated as RMSE_t^2. The model variables often are biased. In that case, the forecasting system is not perfectly reliable, thus the criterion of Eq. (2) will not be fulfilled. Therefore, the left-hand side is estimated by unbiased squares of error between analysis and ensemble mean,

averaged over the COSMO-E domain and over all initial dates, abbreviated as STDE_t^2.

Figure 9 shows the spread (left) and unbiased error (right) of experiment LBC+SPPT for temperature, averaged over the COSMO-E domain and the initial dates. Note that spread and error for lead-time +0 hours are zero by definition due to the use of the verifying analysis as IC for all members. In the lower troposphere (k-levels ∼40-60) the spread is significantly smaller than the unbiased error, at least until a lead-time of ∼60 hours. Above k-level ∼40, spread and unbiased error are quite equal.

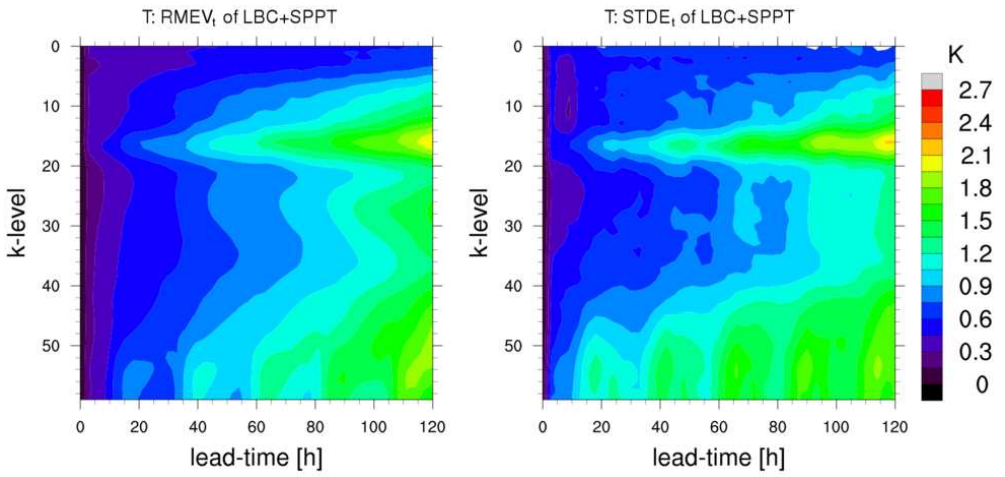

Figure 9: The root of the average over the COSMO-E domain and over the initial dates of ensemble spread (left) and unbiased squares of error between analysis and simulation (right) for temperature. The model levels build the Y-axis and the X-axis is the lead-time.

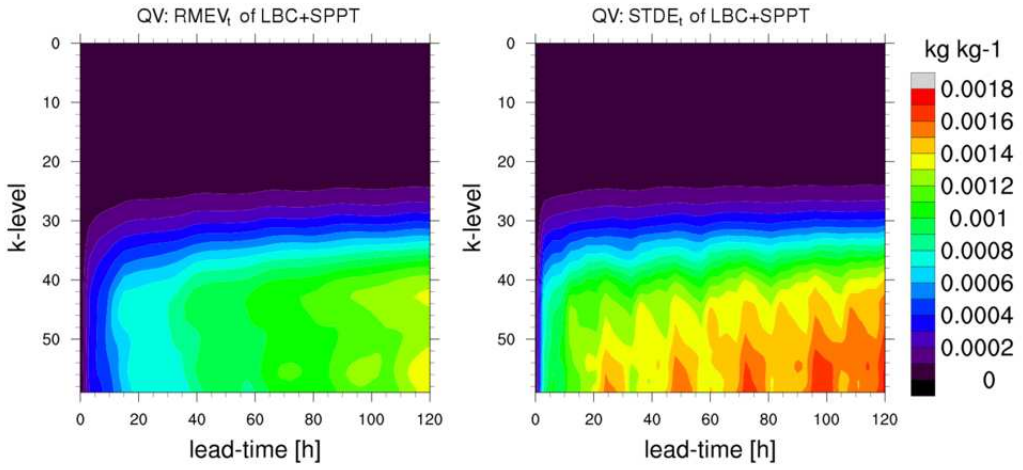

Figure 10: Same as Fig. 9 but for specific humidity

Figure 10 illustrates that for specific humidity the spread is clearly smaller than the unbiased error at k-levels ∼40 to ground, throughout the entire forecast range. For k-levels above ∼40, specific humidity becomes negligibly small and the spread and unbiased error tend to zero as a consequence.

Figure 11 shows the difference in spread amount between the experiments LBC+SPPT and LBC for temperature and specific humidity, averaged over the COSMO-E domain and the initial dates. The spread induced by the SPPT scheme is limited in height to k-levels ∼30-60. After ∼30 hours lead-time, SPPT does no longer give large additional spread to the LBC perturbations.
Investigating the temperature and specific humidity tendencies from the different physical parametrization schemes for a case study in summer (not shown), reveals a very large and horizontally extensive tendency sum in the planetary boundary layer (PBL). Above the PBL, the tendencies are weaker and less extensive. Because

the activity of the SPPT primarily depends on the tendencies of the physical parametrization schemes, this may explain the limitation in height of the SPPT scheme for temperature and why the largest impact of the SPPT scheme occurs in the PBL. The limitation in height of the SPPT scheme for specific humidity is rather caused by the large reduction of specific humidity in height.

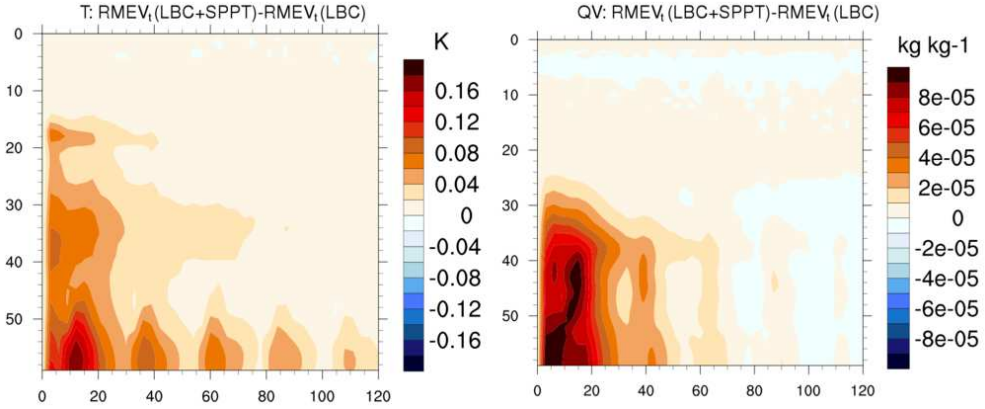

Figure 11: Difference in spread amount between the experiments LBC+SPPT and LBC for temperature (left) and specific humidity (right), averaged over the COSMO-E domain and the initial dates. The model levels build the Y-axis and the X-axis is the lead-time.

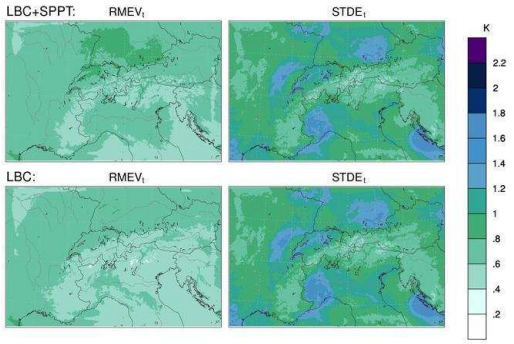

Figure 12: For temperature the root of the average over the COSMO-E domain and over k-levels 40-59 of ensemble spread (left) and unbiased squares of error between analysis and simulation (right) are plotted for the experiments LBC+SPPT (top) and LBC (bottom), at lead-time 24 hours.

The criterion Eq. (2) is examined horizontally as well. For the layer plots in Fig. 12, spread (left) and unbiased error (right) are calculated at lead-time 24 hours averaging over the initial dates and the k-levels 40-59, instead of the COSMO-E domain. For temperature additional spread induced by the SPPT-scheme can be observed in Northern Italy and in the South of Germany. Compared with the unbiased error, the spread of the experimental setup LBC+SPPT is still smaller, but the additional spread mostly occurs in regions where the unbiased error is large. The unbiased error does not change significantly, adding SPPT to LBC perturbations.

6 Caveat

The present idea of SPPT is to model the error of the physical parametrization schemes. However, for the experiments, based on COSMO version 4.26, zonal and meridional wind tendencies of the coriolis subroutine have been erroneously perturbed as well. The large windspeed in in the upper troposphere induces large coriolis force tendencies. Hence, on these levels the SPPT uncertainty terms for the wind components are mainly dominated by the coriolis force tendencies and thus are inappropiate. Therefore, the results for wind are omitted in this report. In COSMO version 5.0 the coriolis force tendencies are no longer perturbed.

7 Summary and Outlook

COSMO-E is an experimental ensemble prediction system with 21 members for the Alpine area. It has a convection-permitting mesh-size of 2.2 km and a forecast range of 120 hours.
The Stochastically Perturbed Parametrization Tendencies (SPPT) Scheme, which perturbs tendencies of the model by multiplying a random pattern, is introduced in order to model the error of the physical parametrization schemes.
Investigating how the variation between ensemble members, also called spread, depends on the parameters of SPPT, it turned out that spread is increased by the increase of random number amplitudes, as one would expect. But surprisingly also the enlargement of space and time scales of the random pattern leads to an increase in spread. A deterministic verification of the SPPT scheme reveals that the forecast quality of individual members is hardly affected, unless random numbers are large ($\sigma \geq 0.5$, cutted at 1.0), and space and time scales are increased up to 5.0° and 6 hours.
Ensemble experiments are performed using a random pattern with space and time scales comparable to the scale of convective events. The forecast time is 5 days starting at initial dates 25.07.2012 to 25.08.2012, 00 UTC. The reference experiment with lateral boundary condition (LBC) perturbations is compared with the experiment which combines LBC perturbations with SPPT. In height, additional spread of SPPT is observed up to ∼7 km, for temperature and specific humidity. The Brier skill score for precipitation larger than 1 mm per 12 hours shows a benefit of the combined experiment until a lead-time of ∼30 hours. Spread and unbiased error between ensemble mean and analysis of temperature and specific humidity show that below a height of ∼5.5 km, the spread is smaller than the unbiased error. Above ∼5.5 km, the spread is in the same range as the unbiased error for temperature. The specific humidity and as a consequence the spread and the unbiased error are negligibly small above ∼5.5 km. Horizontally the additional spread mostly occurs in regions where the unbiased error is large.

In COSMO version 4.26 used for the present study, accidentally the tendencies of zonal and meridional wind of the dynamical subroutine coriolis are perturbed as well. This will be changed for subsequent studies. Moreover, the variation between ensemble members should be increased for specific humidity, and in lower troposphere for temperature, by a further tuning of the parameters of the SPPT scheme. Since the tendencies from the physical parametrization schemes are largest in the planetary boundary layer, there is potential to further increase the ensemble spread with SPPT. Finally, the uncertainty of initial conditions will be modelled by using initial condition perturbations from the ensemble based data assimilation cycle (LETKF).

References

[1] Buizza, R., Miller, M. and Palmer, T.N., 1999: Stochastic representation of model uncertainties in the ECMWF Ensemble Prediction System, *Q. J. R. Meteorol. Soc.*, 125:**2887-2908**.

[2] Gebhardt, C., Theis, S.E., Paulat, M., Ben Bouallègue, Z., 2011: Uncertainties in COSMO-DE precipitation forecasts introduced by model perturbations and variation of lateral boundaries, *Atmospheric Research*, 100 **168-177**.

[3] Jolliffe, I.P., Stephenson, D.B., 2011: Forecast Verification: A Practitioner's Guide in Atmospheric Science. Chapter 8 (Weigel, A.P.): *Verification of Ensemble Forecast*. Wiley.

[4] Palmer, T.N., Buizza, R., Doblas-Reyes, F., Jung, T., Leutbecher, M., Shutts, G.J., Steinheimer, M., Weissheimer, A., 2009: Stochastic Parametrization and Model Uncertainty, *Internal Report from ECMWF*.

Diagnosis of Turbulence Schema in Stable Atmospheric Conditions and Sensitivity Tests

Ines Cerenzia[1], Francesco Tampieri[2], Maria Stefania Tesini[3]

[1] *University of Bologna, Department of Geophysics, Italy*
[2] *CNR Institute of Atmospheric Sciences and Climate, Bologna, Italy*
[3] *Arpa-EMR, Bologna, Italy*

1 Introduction

The sensitivity of NWP models to the representation of the stable boundary layer (SBL) is widely recognised, but unfortunately its simulation is still an open issue. This is partly due to the multiplicity of physical processes at work (turbulent mixing, radiative cooling, interaction with land surface and its heterogeneities, gravity waves, katabatic flow, fog and dew formation) and partly due to the insufficient understanding of them (*Steenveld, 2011*). In the last 15 years, many operational weather forecast models shows a significant benefit in the prediction of synoptic low pressure systems with the introduction of an enhanced mixing in SBL, which compensated in some way the lack from physics (*Holtslag et al., 2013*). The resulted SBL is too deep, with too strong surface drag and eroded low level jet, underestimated wind rotation with height in the lower levels, weak thermal inversion and too warm temperature in the lower part of the PBL (*Cuxart et al., 2006*). COSMO model is not exonerated and hints of the overmixing in the SBL were detected in the too fast dissolving of low level stratus during night (verified at the German Weather Service DWD, 2012), in the overestimation of temperature at 2m (T2m), verified by all COSMO members during nights with particularly stable stratification (clear sky and weak wind) with an extent ranging between 0.5 and 3°C (*COSMO Common Plot 2012-13*) and in the weak structure of thermal inversion and low level jet (observed operationally over Po Valley, Italy).

This study aims to analyse COSMO performance in stable stratified and weak wind (very stable) atmosphere. Due to the particular orography structure, Po Valley provides a large statistics of this conditions. Then a case study has been selected in winter 2012 without any fog and cloud. At first, a diagnosis of the operational simulation is given, underlining the impact of the most active limits and the presence of a time oscillation (section 2). Then, two modified model versions with a decreased mixing are considered. The effect on PBL mixing and temperature is reported, mentioning also the consequences on the observed oscillations. In sections 3 and 4, the focus is on flat area (San Pietro Capofiume (SPC) station is considered as reference) and then it is extended to heterogeneous terrain (sec. 5). Finally the more promising version has been run for three months in a parallel way to the operational COSMO and the results are here summarized (sec. 6). The operational configuration of COSMO-I7 has been used and the output at every timestep is considered.

2 COSMO turbulence scheme in stable conditions

In the operational COSMO setting, the turbulence scheme uses a 1-D closure with a prognostic equation for Turbulent Kinetic Energy (TKE), which corresponds to level 2.5 in Mellor- Yamada notation (*Mellor et al., 1982*). The time trend of TKE , expressed in term of q ($q = \sqrt{2TKE}$) prescribes the balance between different forcings (first three terms r.h.s), the dissipation and its vertical diffusion (4th and 5th terms):

$$\frac{dq}{dt} = -\frac{1}{q}\overline{u'w'}\frac{\partial \overline{u}}{\partial z} + \frac{1}{q}\frac{g}{\theta_v}\overline{w'\theta'_v} + f_C - \frac{\epsilon}{q} - \frac{1}{\overline{\rho}q}\frac{\partial}{\partial z}\left[\frac{1}{2}\overline{\rho q^2 w'}\right] \tag{1}$$

Besides the forcings due to the wind shear and the buoyancy (the first and second terms r.h.s., later called f_m and f_h), some additional contribute to TKE is given by the interaction with the circulations (f_C), i.e. the energy transfer from subgrid scale (SGS) coherent eddies to turbulent scale (Separated Turbulence Interacting with Circulation, STIC approach, *Raschendorfer, 2007-2011*).

Currently in the operational settings, f_C includes only the circulation due to SGS thermal inhomogeneities of the surface [1]. Practically, this term is parameterized as the vertical variation of the product between a length scale (representative of the SGS surface thermal pattern) and the buoyancy forcing: $f_C \propto \frac{\partial}{\partial z}[L_{therm}\,(-f_h)]$.

[1] In COSMO operationally used at DWD also the effect of circulation forced by SGS orography is enabled

The 'thermal' lenght scale is estimated from grid size dynamic variables, external settings (horizontal resolution and one of the namelist parameter) and the SGS clouds coverage. If SGS clouds are not present, L_{therm} does not include any dependency on SGS features [2].

In stable stratification with weak wind shear, the additional energy coming from circulations is relevant with respect to the small amount of TKE forcings and vertical transport. As example see in fig. (1) the TKE budget terms at the lowest main level in increasing atmospheric stability in the case study considered. When buoyancy forcing is negative and wind shear is weak to maintain mixing, the transfer of energy from the circulation scale should support turbulence, avoiding the zero-going of mixing and fluxes.

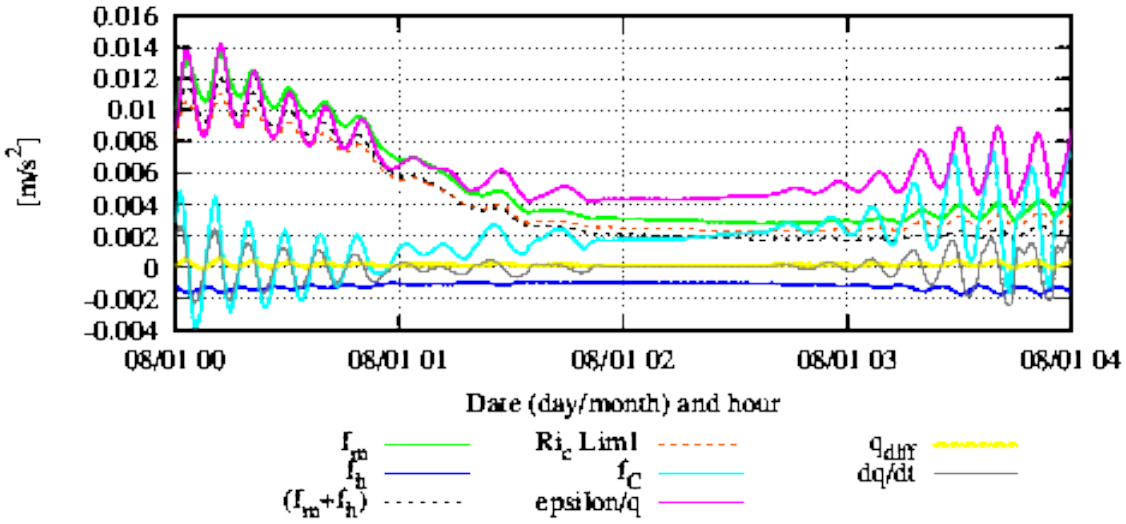

Figure 1: Terms of TKE equation in a stable case in the proximity of $Ri_f = Ri_c$. Ri_c is exceeded at around 01:00 when "Ri_c Lim" line is above the "$f_m + f_h$" line

Nevertheless, some security limitations are active in order to prevent turbulence to decay. The most documented ones are the minimum limits for the vertical diffusion coefficients of momentum and scalars (namelist parameters *tkmmin* and *tkhmin* see *Cosmo User's Guide, 2013*). In principle, they force the system to continue mixing also when the diffusion coefficients would drop below the prescribed minimum values. In the shear driven SBL case study simulated with COSMO Single-Column by Buzzi, the detrimental effect of this measure on the simulation of the SBL structures has been already underlined (*Buzzi et al., 2011*). In the same case study, it appears that the largest minimum limit of the diffusion coefficients not altering the SBL representation is K_{min}=0.01 m^2/s, while in current operational setting it is K_{min}=1 m^2/s (or 0.4 m^2/s as recently suggested by DWD in order to avoid the detrimental effect on boundary layer clouds previously mentioned).

In weak wind SBL, one can expect an even worse effect on the simulation, given that a stronger stratification should be established. In the case study considered here, the limitation to K_{min}=1 m^2/s is frequently occurring (fig. 2). In the next sections, some tests with a reduced K_{min} are described.

Another constraint acts on the sum of buoyancy and wind shear forcings in the TKE equation when the Richardson flux number ($Ri_f = -\frac{f_h}{f_m}$) exceeds the critical value Ri_c (equal to 0.19 in operational setting), i.e. in very stable stratification. Essentially in this case the buoyancy term is excluded from the TKE calculation, so that the forcing sum depends only on mechanical forcing (positive definite), then the sum is prevented to become negative. Therefore, states of the system beyond Ri_c are not described by the TKE equation and are brought back to less stable conditions. In fig. 1 an example of the activation of this limitation is plotted (called "Ri_c Lim"). Neglecting this limitation produces a crash of the model run as soon as the forcing sum ($f_m + f_h$) becomes negative (its square root is required in the TKE calculation). A modulation of this limitation is at the moment tested (Raschendorfer and Cerenzia) and possibly will be included in the next COSMO version 5.1.

According to our experience, these limits strongly affect the simulation of the very SBL.

Furthermore, the operational scheme appears to be not fully stable in stratified atmosphere. In fact, especially when Richardson flux number is close or above the critical value, some high frequency oscillations (about 15 timesteps in the used configuration) are excited (fig. 1, 2). All turbulence related variables (diff. coefficients,

[2] For a detailed description refer to *Raschendorfer, 2007* and *Cerenzia et al., 2013*

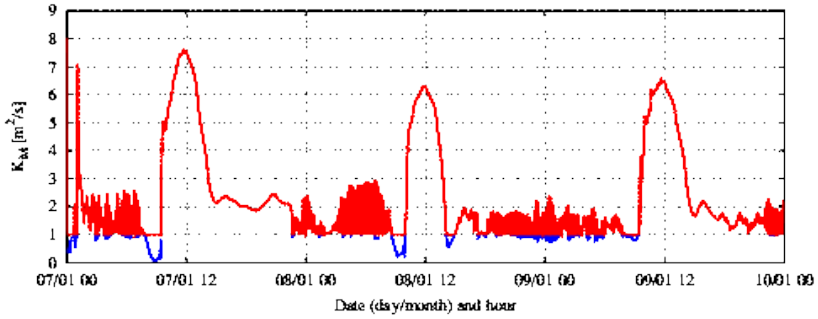

Figure 2: Time series of momentum diffusion coefficient at the lowest model level. Blue segments are the coefficient below the limit $K_M = 1m^2/s$

TKE, wind, temperature, humidity, surface values..) near the surface (three to four levels up to the bottom one) are involved. Some tests performed to check the numerical origin underlined as the oscillations are sensitive to changes of numerical scheme or integration timestep but their behaviour is not directly pointing to a numerical issue (*Cerenzia et al., 2013*).

3 Reduction of minimum limit of vertical diffusion coefficients - Test 1

For this test, the minimum limits of vertical diffusion coefficients are lowered to the value $K_{min} = 10^{-2}m^2/s$. Since values of $K_{M,H}$ below these thresholds are quite uncommon also in very SBL (e.g. *Yague et al., 2006*), then these limits would not reasonably influence the PBL modelling.

At first the flat terrain case is analysed. The closer grid point to SPC station site (2 km away) is considered and the horizontal homogeneity assumption is done in order to compare model results with observations.

In the stable case examined, the diffusion coefficients drop below the default threshold along all the vertical profile (see fig. 3, scalar coefficient not shown but similar to the momentum one). However at 900 hPa a spurious peak is present (described later). Temperature profile indicates a strengthening of stratification in the modified run with lower temperature at the surface and higher at the inversion. Wind speed profile does not show relevant changes, with the exception of the layer at around 900 hPa.

Looking at the time series at the bottom level (fig. 4), the diffusion coefficients slightly reduce in stable cases (on the average also during oscillations despite high mixing is locally produced). This is beneficial for T2m, that shows a lower overprediction of observations each time the diffusion coefficients drop below $K_{min} = 1m^2/s$. Unfortunately a decrease of T2m is present also during day, likely due to an indirect effect since the mixing is not significantly modified. The oscillations visible in stable cases are sensitive to the reduction of the diffusivity limit: their amplitude is strongly enlarged, their period is approximately doubled and they are less wavy and periodic (fig. 4).

4 Elimination of thermal circulation term (f_C) - Test 2

The thermal circulation term resulted as the most active source in increasing the TKE at low levels in stable conditions, especially when the Ri_f exceeds the critical value (fig. 1). Furthermore, it seems to have some special correlation with the oscillations since it anticipates the wave of one-two timesteps with respect to other terms (fig. 1). Therefore, a second case study has been performed switching off the thermal circulation term in TKE budget (setting namelist parameter *patlen*=0) and keeping $K_{min} = 0.01m^2/s$.

The first result is a complete elimination of time oscillations at all levels and in each field. However, preliminary tests (not showed) indicate that the triggering cause of oscillations is not due to an instability in the parameterization of f_C term. Other possible sources of the oscillations (interaction between f_C and the stability functions or with the limitation for Ri_c number, ..) will be further investigated.

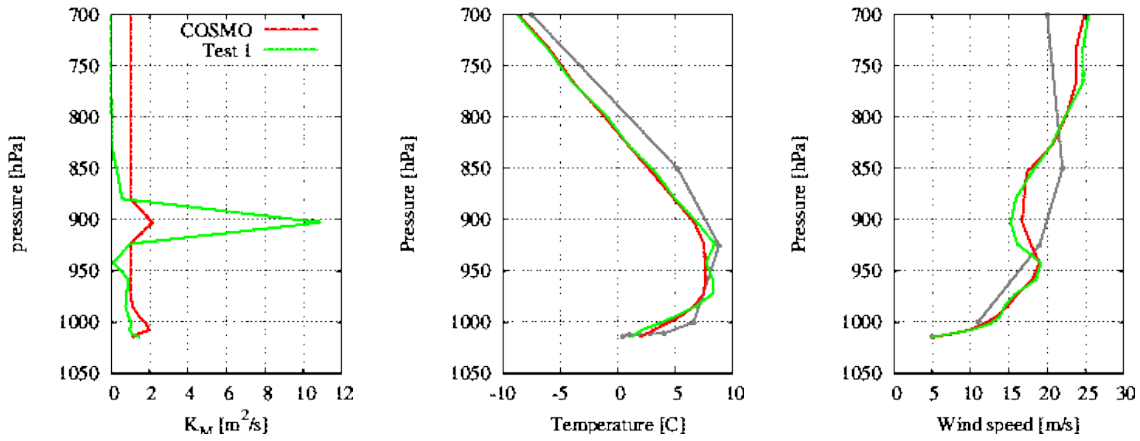

Figure 3: Vertical profiles of Momentum diffusion coefficient(left), Temperature(centre), and Wind speed (right) at SPC site, on the 08/01/2012 at 00:00. Grey line represents the radiosounding observations, if present, red and green lines are COSMO default and Test 1 respectively

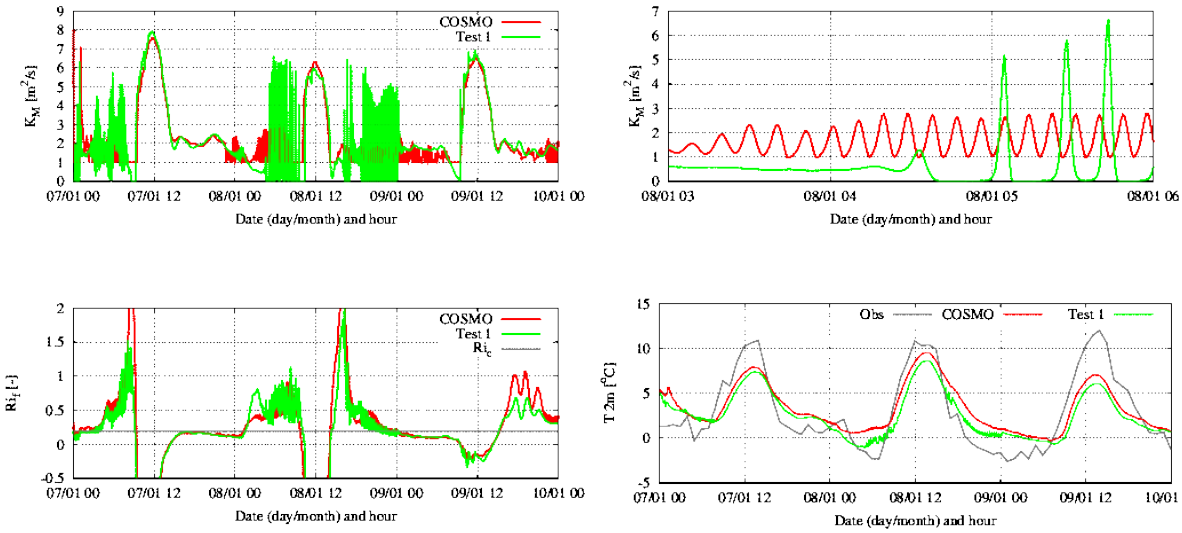

Figure 4: Time trend at the lowest main level of momentum diffusion coefficient (top left) with a zoom during oscillations (top right), Ri_f number (bottom left) and 2 metre temperature (bottom right). Red line represents COSMO default while green line is Test 1. Grey line are observations, if available

In this second case study, the mixing during stable conditions strongly decreases with respect to Test 1, partially because of the disappearance of the oscillations and partially for the lack of the additional TKE production. Consequently, temperature at low levels and at the surface drops (fig. 5, centre), leading to a lower T2m in close agreement with observations (fig. 6). Daily maxima are unchanged compared to Test 1. With respect to the observations, the modified run shows a delay of the surface warming up after sunrise.

The shortcomings rise looking at the vertical profiles of temperature, wind and K_M where some unrealistic "jumps" come now to light (fig 5). The peak of K_M at 900hPa already observed in Test 1 may be attributed to these fluctuations. Another inconsistency is for instance the exceptional positive mixing on the night of 9 January (fig. 6), due to an unstable layer at the bottom level (in fact, Ri_f is negative, not shown).

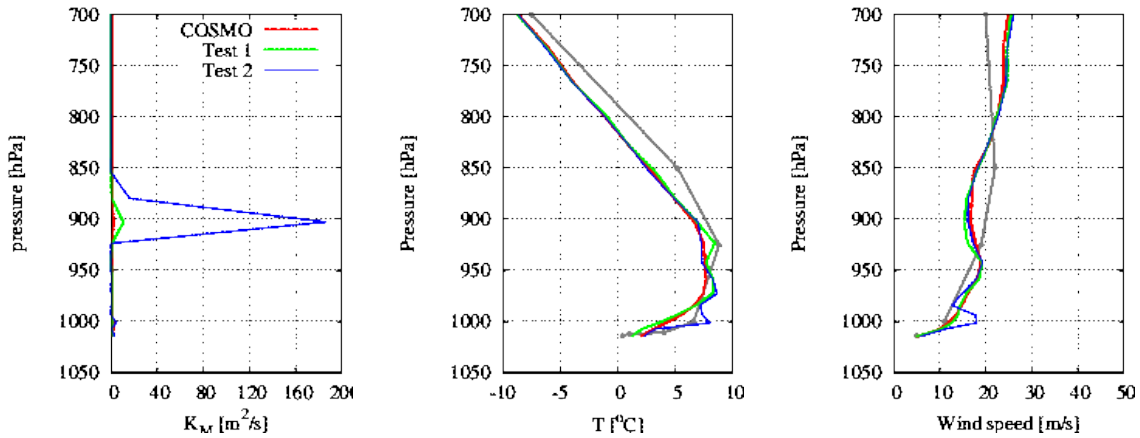

Figure 5: Vertical profiles of momentum diffusion coefficient(left), temperature (centre), and wind speed (right) at SPC site, on the 08/01/2012 at 00:00. Grey line represents the radiosounding observations, if present. Red line is COSMO default, green line is COSMO with $K_{M,H} = 0.01m^2/s$ (Test 1) and blue line is COSMO with $K_{M,H} = 0.01m^2/s$ and $patlen = 0$ (Test 2)

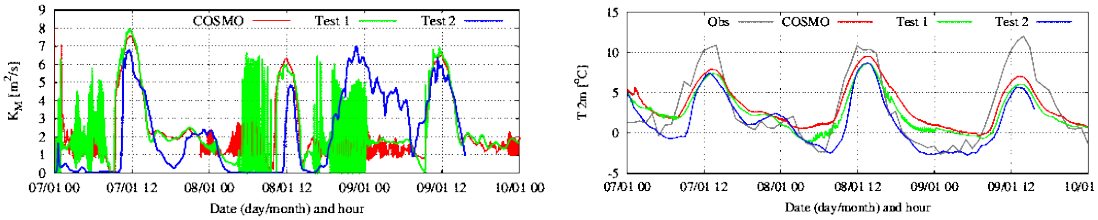

Figure 6: Time trend at the lowest main level of momentum diffusion coefficient and 2 metre temperature. Red line represents COSMO default, green line is Test 1 and blue is Test 2. Grey line are observations, if available

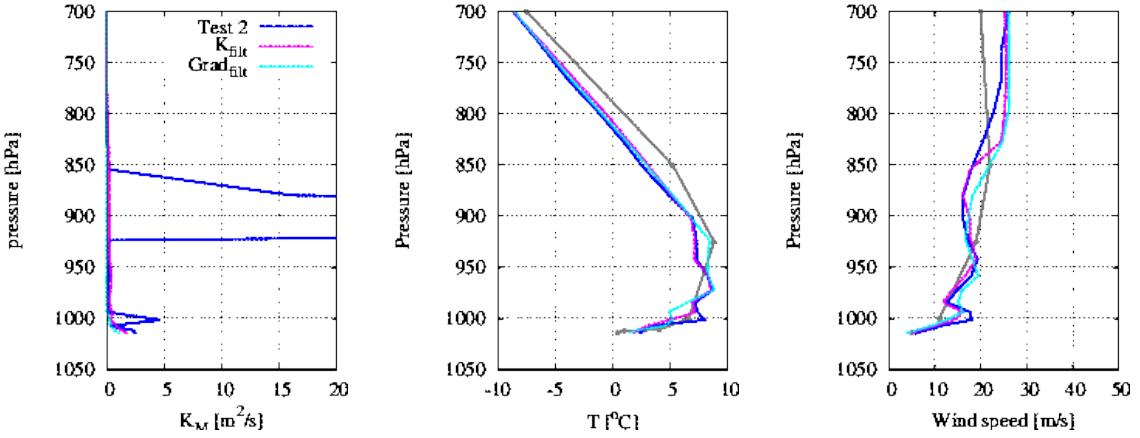

Figure 7: Vertical profiles of momentum diffusion coefficient(left), temperature (centre), and wind speed (right) at SPC site, on the 08/01/2012 at 00:00. Grey line represents the radiosounding observations, if present. Blue line is Test 2, dotted magenta and ceylon lines are the runs with the filter applied respectively on $K_{M,H}$ and on the vertical gradients before evaluating the stability functions

The origin of this vertical fluctuations is still not understood. The thermal circulation term represents in TKE calculation practically the main interaction between different vertical levels in stable conditions, because it includes a second order vertical derivative and it largely exceeds in magnitude the same order term, i.e. vertical TKE diffusion (compare in fig. 1 f_C and q_{diff} terms). Therefore, if it is removed (as in Test 2), the levels are more decorrelated. However, signs of the vertical instability can be seen also in Test 1. Therefore the absence of f_C can not be the only reason of the vertical fluctuations.

Many analogies are present with the instabily detected by Buzzi (2011) in the shear driven idealized case study above mentioned, which is performed with the same configuration (no thermal circulation and reduced $K_{M,H}$ limit). He relates this instability to a physical inconsistency of the stability functions in Mellor-Yamada scheme (*Mellor 2003; Burchards and Deleersnijder 2001*) and he showed that a 5-points vertical filtering of the stability functions and of variables connected to them (diffusion coefficients,wind gradient, dimensionless momentum gradient) is able to completely remove the fluctuation.

In order to test if the origin of the "jumps" seen in the present case study is the same and if the solution is working, the filtering of the diffusion coefficients (named "K_{filt}" in fig. 6) and of both wind and potential temperature gradients before evaluating the stability functions (named "$Grad_{filt}$") are applied to Test 2. In both cases, the spurious peak of K_M at 900hPa is eliminated as a direct effect of the vertical filter. Instead the fluctuations on the profiles of derived variables as temperature and wind are smoothed (with a greater extent in "$Grad_{filt}$") but not removed. This is a hint of the fact that some other source of instability is present in the present case study.

5 Effect of both modifications on Northern Italy area

The results of Test 1 and 2 have been analysed on the Northern Italy scale during the same three days, in order to get a sense of the effects of the two modifications on a non-homogeneous rough terrain. The vertical filtering has not been applied in this study.

If the minimum diffusivity is reduced (Test 1), a decrease of T2m is evident with greater extent on gridpoints sited in flat and hilly area during the more stable periods (fig. 8, left side). There is a minor impact on mountain because in general the stronger wind shear keeps the diffusion coefficients above the value of 1 m^2/s and the atmosphere in a less stable condition. The effect of time oscillations can be retrieved in the onset of some localized peaks at low levels changing location and intensity in time (graph not shown). They are more visible in TKE and diffusion coefficients, coherently with the larger amplitude recognized also at SPC, and they appear only in flat or hilly regions.

Neglecting f_C in the TKE equation together with the diffusivity limit reduced (Test 2) causes a further reduction of mixing in more stable periods accompanying a decrease of T2m (fig. 8). However, the decrease shows different extents on different topography, due to the relative impact of the thermal circulation.

- In flat regions the reduction varies between 1 and 5^oC. In this area, the modified run is overall in agreement with the majority of stations showing anyway a slightly negative mean error (BIAS between $+1^oC$ and -2 ^oC, fig. 9). The overestimation of T2m typical of COSMO operational setting is avoided.
- The lowering is about 5^oC in hilly and low mountain area and the comparison with the observations indicates that it is excessive (fig. 9). In fact, thermal surface inhomogeneities are always present in rough topography (creating a differential cooling and heating) and the additional turbulence production is effectively required.
- Generally, in very high mountain regions there is a small difference between COSMO default and Test 2, again because the atmosphere is less stable due to mechanical forcing and the thermal circulation term has not a leading role in TKE budget.

This suggests some considerations on the correct formulation of f_C, which currently does not include any information on the subgrid scale pattern of temperature or even orography (in absence of SGS clouds, like in this case). Clearly the additional production of TKE due to thermal circulation is not necessary when a SGS heterogeneity is not effectively existing.

As a final consideration on Test 2 performance, the horizontal peak-structures variable in time seen in Test1 disappeared, demonstrating that they are really the manifestation of the time instabilities.

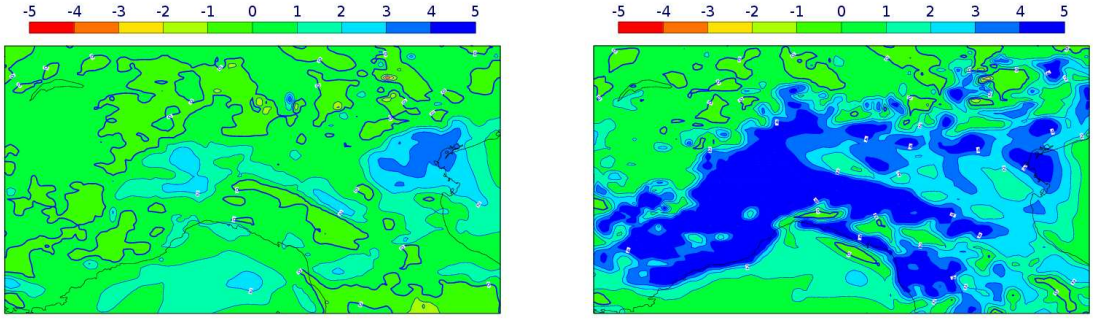

Figure 8: Maps of difference of T2m between COSMO default and Test 1 (left side) and Test 2 (right side). The scale is in [^oC]. The maps refer to the output at 08/01/2012-4:00 am

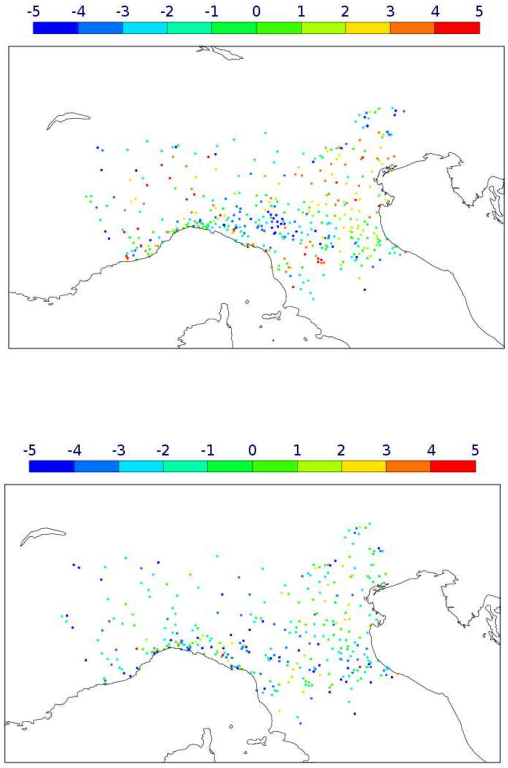

Figure 9: BIAS of T2m in COSMO (top) and in COSMO Test 2 (bottom) against observations. The scale is in [^oC] and red points indicate positive BIAS while blue points negative BIAS. The maps refer to 08/01/2012 at 4:00am

6 Operational verification

A further analysis has been performed running the COSMO version with the reduced limit of diffusivity and without the thermal circulation term (Test 2) on COSMO-I7 domain for three months (no vertical filtering has been applied). The boundary conditions come from GME, while the soil state is obtained from the analysis of the assimilation cycle of Test 2, based on continuous nudging ("independent soil"). The forecasts of T2m are verified and compared to COSMO operational performance (BC taken from IFS, with "independent soil" as well). The deviation on T2m due to the different initializations is negligible compared to the effects of the changes in COSMO version (from a comparison between COSMO-I7 with the BC of IFS and GME, not shown).

The general effects of Test 2 over all meteorological conditions and in all stations in Italy are a modified and smaller daily amplitude of BIAS and an increased RMSE during night with respect to the operational run (fig. 10, left side). The first aspect indicates that the modifications applied in Test 2 strongly impact on T2m forecast. With respect to the observations, T2m appears colder at every hour with a larger extent during night, which means that the nocturnal reduction of mixing is often occurring and is on the average overpowered. The increase of the RMSE during night (when Test 2 modifications are active) is an indication that the changes effect is negative, if applied to all the atmospheric and topographical conditions. This is not surprising, seen that the modifications are led by considerations valid on the very stable atmosphere. Encouraging is the almost unchanged RMSE of T2m during day, suggesting a small influence of the modifications on the error in these hours.

If only conditions favourable to the presence of highly stable stratification (clear sky, low wind intensity and data observed in stations only coming from flat, low altitude regions) are considered, the reduction of the daily cycle of BIAS is even greater (fig. 10, right side). Furthermore, an improvement is visible in both BIAS and RMSE during the first night. Subsequently, the T2m simulated by Test 2 is colder than COSMO-I7 at every hour and it is approximately 1.5°C colder than the observations. This is a hint of the fact that the reduction of mixing which causes the decrease of 2m temperature is slightly excessive also for highly stable stratification in flat area, in agreement with the considerations done on the Northern Italy domain in the case study. Furthermore, after the first night, the RMSE is greater in Test 2 than in COSMO-I7, which implies a larger variability of the error. This is partially due to the the redundant drop of mixing and partially points out the difficulty of the turbulence scheme to represent the very SBL. Moreover, the vertical fluctuations noted in this case can have some effect in increasing outlying results and finally, also the erroneous representation of the stable boundary layer in hilly and low mountain regions can negative affect the large scale flow (due to its sensitivity to SBL simulation), then leading errors also in flat, low level regions.

7 Conclusions

The simulation of PBL in condition of stable stratification (night with clear sky and weak wind) in unsaturated atmosphere has been studied.

In the operational configuration, it appears that the SGS parameterization of sources of TKE and some unphysical limits aim to increase mixing, often in an artificial way. Moreover, an oscillation in time exists in all turbulence related variables at the lower PBL in very stable conditions or close to. Its influence is negligible for operational necessity (e.g. time oscillations on T2m have an amplitude of approx. 0.1-0.2°C), however it is clear that the current turbulence scheme is so far not fully tested in this condition.

A reduction of the limit on the vertical diffusion coefficients to a value not affecting the physics ($K_{min} = 0.01 m^2/s$) generates a stronger stratification and generally improves the simulation of minimum T2m. Unfortunately, this reduction reinforces the previously mentioned time instability. A second test run shows that the time oscillation is related to the term added to the TKE budget considering the turbulent kinetic energy induction by thermal SGS circulations (f_C). In fact, neglecting it, the time oscillation is removed. However, some vertical fluctuations of all fields are now evident. An attempt to solve them through a vertical filter of some variables related to the stability functions (following Buzzi et al., 2011) produces a smoothing of peaks but not the removal of the fluctuations. It is concluded that this second instability has another origin, still to be understood.

A collateral effect of the setting to zero of the thermal SGS circulations term (together with a reduced minimum limit for the diffusion coefficients) is the further reinforcement of the stratification with the drop of T2m, due to the role of strengthening of mixing that f_C assumes in very stable stratification. However, it appears that this drop is excessive on T2m both in flat terrain, where the underestimation is about 1.5^oC (note that the removal of the operational overestimation of T2m during night implies a damping of the daily cycle of BIAS), and mainly in rougher terrain (hilly and low mountain), where the underestimation can reach 5°C. This indicates the necessity to reformulate the parameterization of circulations due to sub-grid scale surface thermal heterogeneities and their effect on turbulence, for example enabling a dependency on some SGS features like SGS orography.

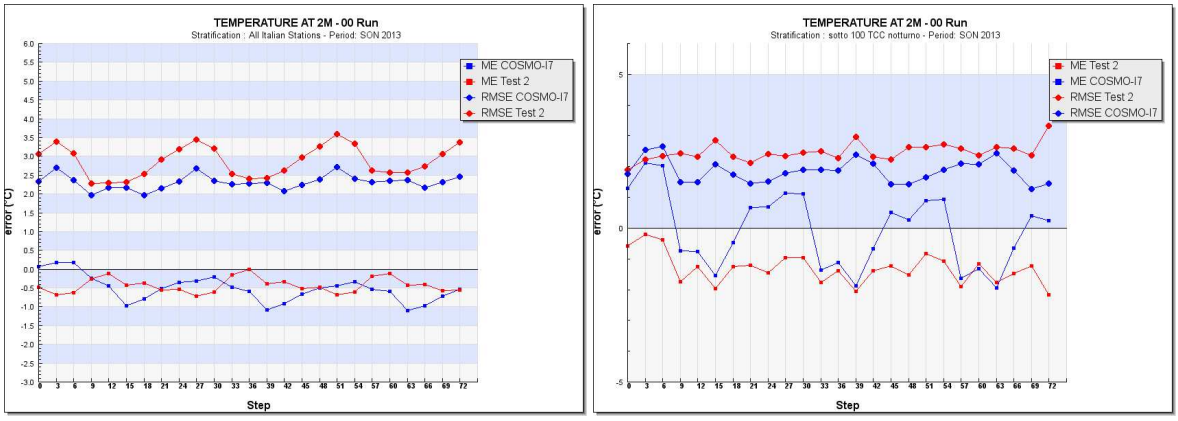

Figure 10: Verification of T2m in COSMO (blue line) and COSMO Test 2 (red line). In the left plot the 3 months data coming from all italian stations are considered while in the right plot only observations in clear sky ($TCC < 25\%$) and low wind ($U_{speed} < 2m/s$) conditions coming from stations sited below 100m of height are verified

References

[1] Burchard, H. and Deleersnijder, 2001:Stability of alegebraic non-equilibrium second order closure models. *Ocean Modelling*, **3**, 33-50

[2] Buzzi, M., M. Rotach, M. Raschendorfer and A. Holtslag 2011: Evaluation of the COSMO-SC turbulence scheme in a shear-driven stable boundary layer. *Meteorologische Zeitschrift*, **20**, 335-350

[3] COSMO WG5, 2013: Common Verification Plots Report DJF 2012-3.

[4] Cerenzia, I. , O. Drofa and F.Tampieri, 2013: Improvement of the PBL parameterization in COSMO model, report 2. Internal document of Arpa-SIMC EMR.

[5] Cuxart, J. and Coauthors, 2006: Single-column model intercomparison for a stably stratified atmospheric boundary layer. *Boundary Layer Meteorology*,**118**, 273-303.

[6] Holtslag, A. A. M., and Coauthors, 2013: Stable Atmospheric Boundary Layers and Diurnal Cycles: Challenges for Weather and Climate Models. *Bull. Amer. Meteor. Soc.*, **94**, 1691-1706.

[7] Mellor, G. L. and Yamada, T., 1982: Development of a Turbulence Closure Model for Geophysical Fluid Problems. *Rev. of Geophys. and Space Phys.*, **20**, 831-875.

[8] Raschendorfer, M. 2007: A new source term in the parameterized TKE equation being of relevance fot the stable boundary layer: the circulation term. *Pres. Workshop on Cloudy boundary layer, Toulouse*

[9] Raschendorfer, M. 2011: Subgrid scale transport by turbulent diffusion. *Pres. CLM Training Course*

[10] Steeneveld, G.J. 2011: Stable boundary layer issues. *Proc. ECMWF Workshop on Diurnal cycles and the stable boundary layer*

[11] Yague, C. and Viana, S. and Maqueda, G. and Redondo, J. M., 2006: Influence of stability on the flux-profile relationships for wind speed, Φ_m, and temperature, Φ_h, for the stable atmospheric boundary layer. *Nonlinear Proc. Geoph.*, **13**, 185-203.

Initial fields of snow cover characteristics preparation for COSMO-Ru

E. Kazakova, M. Chumakov and I. Rozinkina

1 Introduction

Use of present-day mesoscale atmospheric models allows getting more and more realistic forecast information. High grid resolution (several km) of a mesoscale atmospheric model provides higher quality of weather elements forecasting in comparison with traditional use of global atmospheric models with grid sizes of about tens of km. It is well-known that success of mesoscale modeling strongly depends on accuracy of initial fields, as they either remain constant during the whole period or change much slower than atmospheric characteristics.

Initial fields for COSMO-model are prepared with the help of GME-model and standard meteorological observations assimilation. Initial fields have information about snow water equivalent and snow density. Snow depth measurements are determined by snowstake once a day and are included in the list of standard meteorological observations. In Russia snow density and snow water equivalent measurements are also carried out, yet they are held once in 5-10 days on several hydrological stations and can't be used in data assimilation cycles.

Technologies of obtaining of snow depth initial data with its possible following conversion into snow water equivalent in different meteorological centers could be varied, yet in these technologies, as a rule, station measurements of snow depth and satellite information about snow boundary are used ([3], [4], [5]).

Data assimilation systems are also created in Russian Hydrometeocenter ([2], [13]). However they are basically oriented on the use in global atmospheric models.

In weather forecast tasks and while doing applied researches it is necessary to have not only information about snow depth, but also about snow water equivalent. Up to date satellite information has discrepancies with land data ([10], [11]), so obtaining of more reliable values of snow water equivalent according to remote sensing data needs further development of satellite equipment.

In case of cloudy conditions satellite images with high spatial resolution received from synthetic aperture radar are increasingly used for surface characteristics determination ([7]). Yet currently such a data is provided only commercially.

Recently the only use of remote sensing data is insufficient for realistic representation of snow cover, especially for weather and climate forecast tasks and other applied researches. So the common method is to use satellite data as a snow 'mask' in snow models (for example, [6], [9]), which could work independently or be coupled with atmospheric models. Most of such snow models contain rather detailed description of processes in snow cover, as they are designed for solving of specific problems for small territories (for example, for avalanche forming forecasting). As a result - calculation of snow cover characteristics fields requires rather substantial time, that significantly obstruct the use of such models operationally for weather forecast creation.

In winter period different services (utilities, road services, railway services, power station operation, planning of winter competition holding, emergency forecasting and so on) are required adequate information about snow cover characteristics. During snow melting snow equivalent data and information about snow boundary are needed for runoff calculations, prevention of emergencies and agricultural work carrying out.

All the above mentioned determined the need of development of a method for snow cover characteristics initial fields formation for atmospheric models, based on standard meteorological observations at stations in SYNOP-code and satellite data with high resolution. In this article the example of its successful application with the use of mesoscale model COSMO-Ru is given.

2 Materials and Methods

Preparation of initial fields of snow cover characteristics for mesoscale model (the authors made a research taking mesoscale model COSMO-Ru ([12], [14]) with 2.2 km resolution as an example) needs standard observational data done on HMS net and transmitted in SYNOP-code. Scheme of the algorithm for initial fields of snow density and snow water equivalent and surface temperature (covered or not by snow, measured on HMS) construction is shown on figure 1.

Snow density and snow water equivalent values are calculated with the help of the developed snow model SMFE (Snow Model Finite Element) during the whole snow period for stations, where measurements are done, with their further interpolation on regular grid cells using technologies of combination with first guess fields and satellite data.

SMFE algorithm is represented in paper [8]. It should be noted that the model is oriented only on the use of standard observations from HMS. Snow density and snow water equivalent calculation is done with discrecity equal to snow depth measurements carrying out, i.e. once a day for the Russian territory. Snow density is calculated due to equations from [15], which link it with Young's module.

When fresh snow falling its density is calculated in SMFE according to [1] in dependence on air temperature.

The following snow processes are taken into account in SMFE: snow depth acceleration due to dry/wet snow falling and snow depth reduction due to slump, as well as snow melting, percolation and melted water runoff, the process of 'snow blowing' and evaporation/condensation from snow surface.

Remote sensing data are used for snow boundary accurate definition. When stations are densely situated, composite satellite images with 4-km resolution located on NOAA site are employed, which are processed and moved to COSMO-Ru grid cells with the help of special program (authors - U. Alfereov, V. Kopeykin). The field obtained in this way which reflects the space distribution of snow cover is used for correction of snow cover characteristics fields.

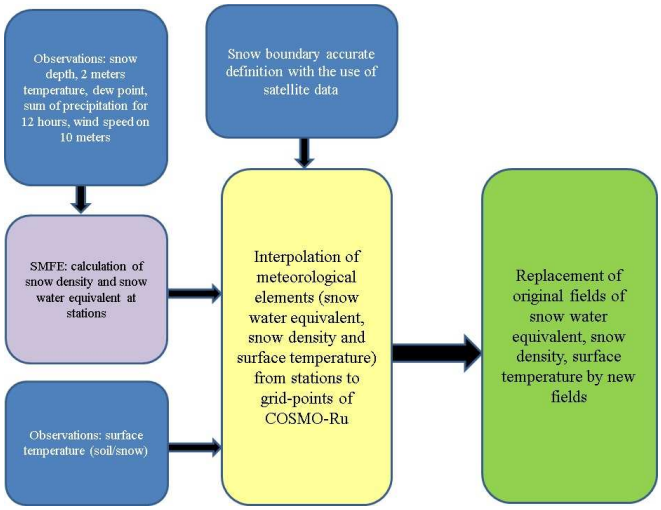

Figure 1: Scheme of the algorithm for initial fields of snow cover characteristics construction (COSMO-Ru as an example model).

In a region with a complicated relief (North-Caucasian region) initial fields replacement requires using composite satellite images with 250-meters special resolution obtained as a result of MODIS data processing, as the use of composite satellite image with 4-km resolution results in gross errors while defining snow cover presence, especially in valleys.

The algorithm based on the use of first guess fields is applied for atmospheric model initial fields construction. Original (operational) fields of snow cover characteristics from GME, which are modified with optimal interpolation method, with the combination of snow cover values from SMFE are used as such fields. Field correction can be done with the use of coefficients, obtained after comparison between operational and modified fields.

Original values of snow cover characteristics (snow density and snow water equivalent) and surface temperature are replaced by modified values in file containing initial fields for mesoscale model. Forecasts with original and modified initial fields of snow cover characteristics were calculated for some days during snow period on the European part of Russia in 2012-2013 with the help of mesoscale model COSMO-Ru. The model was integrated with initial fields prepared for 00 UTC. Experiments were done for two computational areas - Central and North-Caucasian regions.

3 Results and Discussion

Completed numerical experiments show that setting of realistic initial fields of snow cover characteristics lead to forecast quality improvement. It is connected with the fact that snow cover takes part in heat and moisture exchange with the overlying air and influences the heat budget forming. The example of snow water equivalent initial field for mesoscale model COSMO-Ru for Central region territory is shown on fig.2: original (operational) and modified (experiment) versions.

Snow water equivalent values for several stations at 10 April 2013 according to observational data, COSMO-Ru forecasts on 12 hours based on original and modified data are shown in Table 1. As can be seen from this table and fig 2, there is an improvement of initial fields and forecasts of the model COSMO-Ru. Thus, there is an improvement in snow water equivalent forecasting for stations situated on the north of the computational area (Bologoe, Privolzhsk, Buy) when modifying initial data of snow cover characteristics. Snow boundary is in good agreement with observational data. For example, at station Voznesenskoe snow cover was present according to observations, the same result is observed for experiment unlike operational model variant. The similar result is obtained for station Verhov'e, where snow cover has already melted, what was predicted by COSMO-Ru with the use of modified initial data.

For some stations (Spas-Demensk, Karachev) modifications in initial data don't influence forecasting of snow water equivalent, what may be explained as that: in case of presence of snow cover with snow water equivalent value averaged for the region original and modified initial fields may differ from each other too little. Maximum differences between original and modified fields are indicated for maximum values of snow water equivalent (i.e. in the north) as well as on snow boundary.

Feedback from changes in initial fields of snow cover characteristics is observed when calculating forecasts of other meteorological elements. Some changes in low cloudiness were distinguished. Differences between surface albedo forecasts are observed in the region of snow boundary. It's well-known that snow boundary is the zone of maximum contrasts of meteorological elements. As presence/absence of snow cover defines the contribution to surface heat budget, maximum differences between operational version and experiment are observed in 2 meters temperature fields. Let's study stations which were situated in the zone of snow boundary lying.

According to Table 2, there is an improvement of 2 meters temperature forecasts at stations Efremov, Volovo, Verhov'e both for day and nocturnal hours. On stations Unecha and Temnikov changes in initial fields of snow cover characteristics lead to degradation of 2 meters temperature forecasts, yet it is connected with approach to parameterization of 2 meters temperature used in mesoscale COSMO-mode: when snow is present, overlying temperature could be equal to values close to 0^oC. It should be noted that in modified initial fields these stations occurred to be covered with snow, what led to wrong calculations of 2 meters temperature by the model. The derived result indicates that it's necessary to make changes in computational algorithm of 2 meters temperature in COSMO-model.

At station Fatezh there is also some deterioration of forecast of 2 meters temperature. It is connected with the fact that values of snow cover characteristics are used for the previous day for initial data preparation because of snow cover measurements at stations in Russia which are done once a day (at 03 or 06 UTC). At station Fatezh on 9th April snow cover was observed, and on 10th April it has already melted. By virtue of such an observational discrecity some discrepancies in 2 meters calculation for several stations in the zone of snow boundary can be found in case of modified fields of snow cover characteristics using.

Station	Observations	Operational variant	Experiment	Absolute error I	Absolute error II
Bologoe	154	200	139	46	15
Privolzhsk	150	171	167	21	17
Buy	137	196	128	59	9
Kolomna	51	106	68	55	17
Mozhaysk	127	138	110	11	17
Plavsk	86	49	36	37	50
Spas-Demensk	114	106	106	8	8
Suhinichi	102	91	94	11	8
Belgorka	96	118	107	22	11
Karachev	48	37	37	11	11
Poniry	46	15	44	31	2
Voznesenskoe	62	0	32	62	30
Verhov'e	0	16	0	16	0
Mean absolute error				30	15

Table 1: Snow water equivalent (mm) on 10^{th} April 2013 according to observational data, COSMO-Ru forecasts on 12 hours with original and modified initial data. Note. I - difference between observations and operational variant, II - difference between observations and experiment.

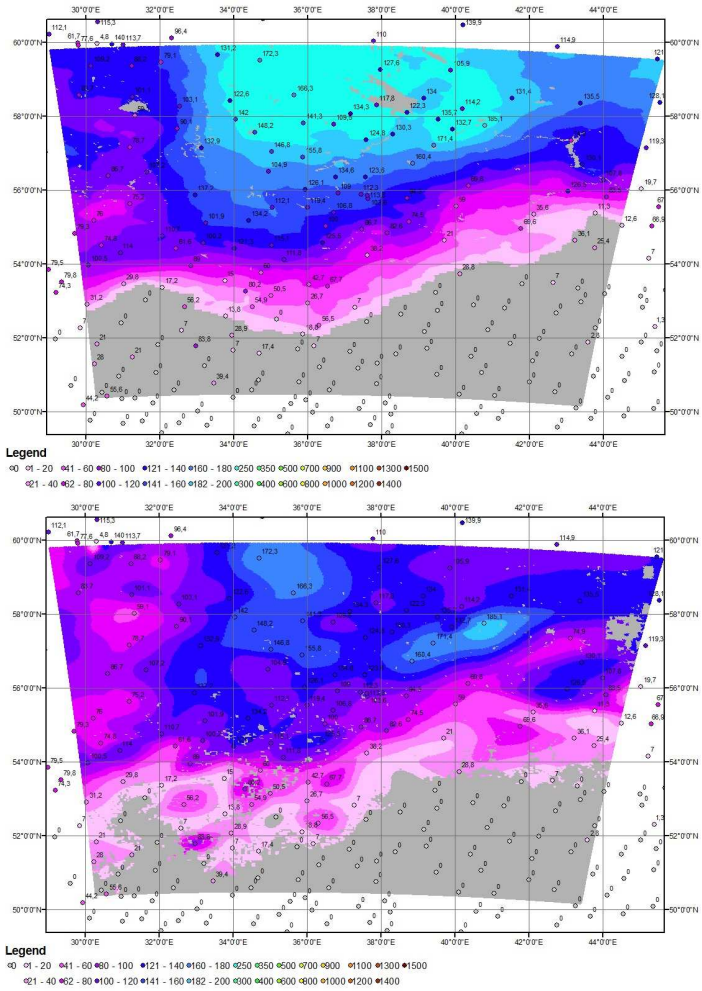

Figure 2: Initial field of snow water equivalent (mm) prepared for mesoscale model COSMO-Ru for Central region: operational variant (top) and experiment (bottom). 00 UTC 10 April 2013.

Station	10 April 2013, 12 UTC			11 April 2013, 00 UTC		
	Observations	Operational variant	Experiment	Observations	Operational variant	Experiment
Efremov	8.0	4.3	6.6	-0.4	-0.5	-0.9
Volovo	6.9	0.6	5.7	-1.1	-3.6	-2.1
Verhov'e	7.0	1.2	6.0	0.8	-1.2	-0.2
Unecha	7.2	6.2	0.6	0.2	0.7	0.0
Fatezh	7.1	6.6	1.3	1.0	0.4	-0.3
Temnikov	8.1	5.6	1.1	-1.5	-3.0	-4.9

Table 2: 2 meters temperature (^oC) at day (12 hours) and nocturnal (00 hours) hours according to observations and forecasts on 12 and 24 hours of mesoscale model COSMO-Ru (operational variant and experiment).

Example of snow water equivalent forecast on 12 hours obtained by mesoscale model COSMO-Ru with original and modified initial data for North-Caucasian region, is shown on fig.3, from which is followed that the proposed method makes it possible to get more realistic ant detailed initial field of snow water equivalent and its forecast, respectfully.

The use of modified initial fields in mesoscale model COSMO-Ru could improve 2-meters temperature in valleys. The example for station Teberda is shown in Table 3. According to this table, forecast values obtained during the experiment are in good accordance with station observations, while operational model version using doesn't provide realistic forecasting of diurnal variation of 2 meters temperature.

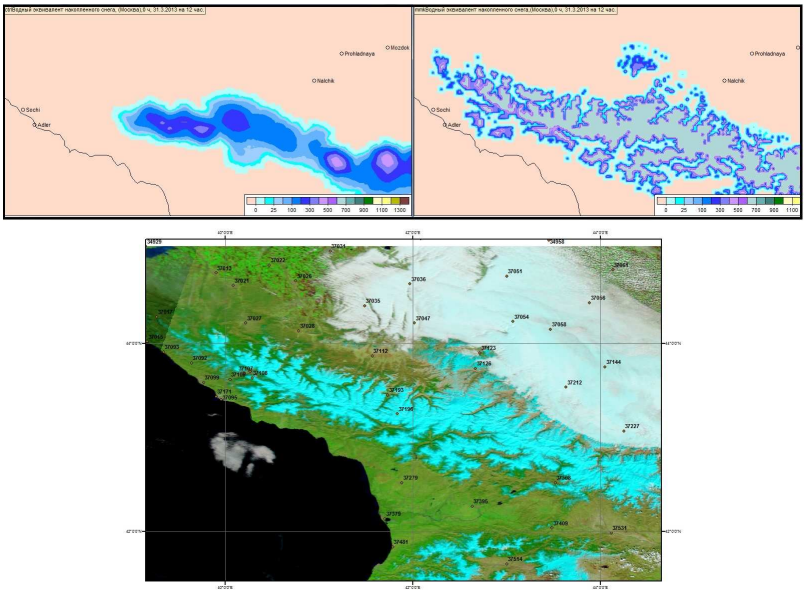

Figure 3: Forecast of snow water equivalent (mm) 12 hours by mesoscale model COSMO-Ru: operational variant (left) and experiment (right). Start - 00 UTC 31 March 2013. Fragment of computational area - the North Caucasus. Bottom - MODIS data with 250-meters resolution for 30 March 2013, snow cover is shown in blue.

Hour	Observations	Operational variant	Experiment
3	3.8	2.3	2.8
6	11.0	3.2	5.9
9	17.0	4.0	10.5
12	16.5	6.3	12.6
15	11.3	5.2	8.8
18	6.9	4.1	5.5
21	6.1	4.5	5.1
0	5.1	5.3	5.7

Table 3: 2 meters temperature (^oC) at station Teberda according to observational data and forecasts of mesoscale model COSMO-Ru (operational variant and experiment). 31 March 2013.

4 Conclusion

So, during the following research it was determined that:

- the proposed method makes it possible to prepare realistic fields of snow cover characteristics;
- changing of initial fields of snow cover characteristics leads to their further more corrective forecast by the mesoscale model;
- the most sensitive to changes in initial fields of surface characteristics is the zone of snow boundary lying;
- changes in initial fields of snow cover characteristics influence on changes in forecast of other meteorological elements (2 meters temperature, low cloudiness, surface albedo).

References

[1] Bartlett, P.A, M.D. MacKay and D.L. Verseghy, 2006: Modified Snow Algorithms in the Canadian Land Surface Scheme: Model Runs and Sensitivity Analysis at Three Boreal Forest Stands. *Canadian Meteorological and Oceanographic Society, ATMOSPHERE-OCEAN* 43 (3), **207-222**.

[2] Bogoslovsky, N.N., A.V. Shlyaeva and M.A. Tolstyh, 2008: Soil and surface variables assimilation in global semi-lagrangian weather forecast model. *Computational technologies* 13, special issue, **111-116** (in Russian).

[3] Cansado, A. and B. Navascues, 2003: Optimum Interpolation Analysis Method for Snow Depth. *HIRLAM Newsletter* 43, **58-64**.

[4] De Ruyter de Wildt, M., G. Seiz and A. Gruen, 2007: Operational snow mapping using multitemporal Meteosat SEVIRI imagery. *Remote Sensing of Environment* 109, **29-41**.

[5] ECMWF, 2010: Technical Advisory Committee. 42nd session. Item12: Snow analysis.

[6] Kuchment, L.S., P.Yu. Romanov, A.N. Gelfan and V.N. Demidov, 2009: Estimation of snow cover characteristics by combined use of models and satellite information. *Earth research from Space* 4, **47-56** (in Russian).

[7] Geldsetzer, T. and J.J. Yackel, 2009: Sea ice type and open water discrimination using dual co-polarized C-band SAR. *Can. J. Remote Sensing* 35 (1), **73-84**.

[8] Kazakova, E., M. Chumakov M. and I. Rozinkina, 2013: Realization of the parametric snow cover model SMFE for snow characteristics calculation according to standard net meteorological observations. *COSMO Newsletter* 13, **39-49**.

[9] Liston, G.E. and C.A. Hiemstra, 2008: A simple data assimilation system for complex snow distributions (SnowAssim). *Journal of Hydrometeorology* 9, **989-1004**.

[10] Nosenko, O.A., N.A. Dolgih and G.A. Nosenko, 2006: Snow cover of the center of the European part of Russia according to AMSR-E and SSM/I data. *Modern problems of Earth remote sensing from Space. IKR RAS press* 3 (1), **296-300** (in Russian).

[11] Pulliainen, J. and M. Hallikainen, 2001: Retrieval of regional snow water equivalent from space-borne passive microwave observations. *Remote Sensing of Environment* 75 (1), **76-85**.

[12] Schättler, U., G. Doms and C. Schraff, 2012: A Description of the Nonhydrostatic Regional Model LM, part 7: User's Guide, **192**.

[13] Tsyrulnikov, M.D., M.A. Tolstyh, A.N. Bagrov and R.B Zaripov, 2003: Global data assimilation system development with variable resolution, *Meteorology and hydrology* 4, **5-24** (in Russian).

[14] Vilfand, R.M., G.S. Rivin and I.A. Rozinkina, 2010: Mesoscale short-term weather forecast in Russian Hydrometeocenter by COSMO-Ru as an example. *Meteorology and hydrology* 1, **5-17** (in Russian).

[15] Yosida, Z. and T. Huzioka, 1954: Some Studies of the Mechanical Properties of Snow. *IAHS Red Book Series*, Publ. no. 39, Gentbrugge, **98-105**.

Experiments in soil physics – case study

Grzegorz Duniec, Andrzej Mazur

Institute of Meteorology and Water Management
National Research Institute.
Department of Numerical Meteorological Forecast COSMO
61 Podlesna str, PL-01-673 Warsaw, Poland

grzegorz.duniec@imgw.pl; andrzej.mazur@imgw.pl

Abstract

A project "New approach to parameterization of Physical Processes in soil in numerical model" started in August 2012 at IMWM-NRI. Basing on overhaul physical phenomena in soil, new parameterizations are being prepared taking into consideration physical processes in soil (microphysics processes in soil, fluid dynamics in porous media, soil dynamics), water cycle in soil and soil-plant-water relation. Parameterizations these are intended to further improve current parameterizations of the TERRA_ML in COSMO model.

At the moment authors are working on new mathematical description of the parameterization of bare soil evaporation, vertical and horizontal soil water transport and the runoff from soil layers. Before incorporating new parameterizations into the TERRA_ML several test cases is being prepared with different soil data sets. In this paper results from testing current TERRA_ML parameterization of the bare soil evaporation for a chosen season are presented. In the first experiment forecasts from COSMO model over the Poland area were compared with the satellite data , received from Satellite Remote Sensing Centre Institute. In the second experiment we tested a "point injection" of the initial soil condition. Later, the results of the 24th hour forecast form the COSMO model were compared with data from meteorological stations.

1 Introduction

Current parameterization of soil processes in meteorological TERRA_ML COSMO model was introduced in the '70s and '80s when the resolution of computational mesh in numerical models was much coarser than today - see Dickenson, 1984 for a comprehensive overview of these parameterizations. Finer resolution demands improved parameterization of the soil and vegetation processes which influence the meteorological forecast. Dickenson was pointed out that his parameterization has a lot deficiencies and although more recently many improvements were incorporated to the original formulation of Dickenson's parameterizations, TERRA_ML still has several weak points (e.g. Duniec and Mazur, 2012, 2013, 2014).

According to Dickenson (1984), parameterization of evaporation is based on:

a) dimensional analysis
b) physical reasoning
c) detail structure was inferred from trial and errors numerical integration

and has several recognized by Dickenson deficiencies , including

a) overestimation of evaporation during morning hours and for wet soil
b) underestimation of evaporation during afternoon hours and for dry soil
c) overestimation of evaporation for wet soil
d) underestimation of evaporation for dry soil
e) it was prepared for low mesh resolution but current version of model has a high mesh resolution (e.g. with grid size of 2,8 km) but the same, "old" soil parameterization schemes

Details of the present parameterizations in TERRA_ML can be found in documentation of COSMO model "*A Description of the Nonhydrostatic Regional Model LM, Part II: Physical Parameterization*".

In the current paper we are presenting results from the numerical experiments which were set in the preparation to improve parameterization of the evaporation processes in the TERRA_ML model. Because knowledge

about forecast of agrophysical and meteorological fields in soil of the COSMO model is very limited, in the first step it was decided to compare numerical forecast with observation data from meteorological stations using the original formulations from the current TERRA_ML model. Soil observation data from meteorological stations belong IMWM - NRI were very poor so it was decided to use an analysis data from two sources. The first set was received from the Satellite Remote Sensing Center Institute of Meteorology and Water Management - National Research Institute, the second - from Institute of Agrophysics Polish Academy of Science.

2 Analysis based on data from Satellite Remote Sensing Center Institute

Satellite Remote Sensing Center receives soil data from satellite MetOp-A . Example of orbit MetOp-A element indicates that it is a pole satellite. Below is an example of element of orbit for epoch 22 of August 2013, 19:37:55 UTC:

- Eccentricity: 0.0000457
- Inclination: 98.7074^o
- perigee height: 819 km
- apogee height: 821 km
- right ascension of ascending node: 293.6326^o
- argument of perigee: 183.6942^o
- revolutions per day: 14.21488536
- mean anomaly at epoch: 176.4232^o

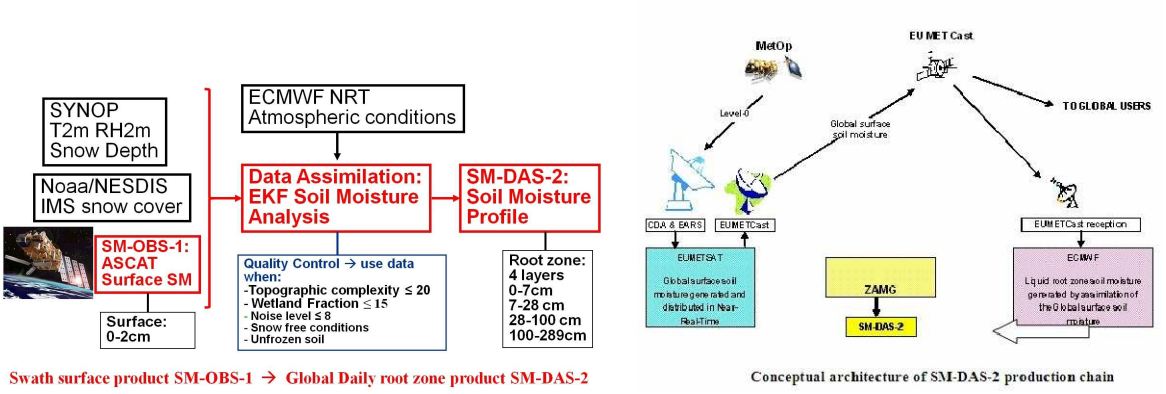

Figure 1: Conceptual schemes architecture of production chain figures from:"Product User Manual for product H14 – SM-DAS-2".

At figure 1 a conceptual schemes architecture of production chain (Information come from Product User Manual – PUM – 14, Product H14 – SM-DAS-2, "EUMETSAT Satellite Application Facility on Support to Operational Hydrology and Water Management", documentation page 6) is shown. Product operational characteristics form the satellite observations are as follow:

- observing cycle: 24 h,
- timeliness: 36 h,
- horizontal resolution: 25 km.

The soil profile is computed for four layers:

a) from surface to 7 cm,

b) 7 cm to 28 cm,

c) 28 cm to 100 cm,

d) 100 cm to 289 cm.

The statistic score of the available for the comparison data is:

a) Mean Bias: 0,043.

b) Standard Deviation: 0,246.

c) Correlation Coefficient: 0,203 or 0,047 m3/m3.

d) Root Mean Square Difference: 0,71.

To the analysis we have selected data from different seasons, keeping in mind a diversity of soil conditions (January, April, August, December in 2012). Next we compared results (forecast) from COSMO model with satellite data, analyzing standard statistic parameters such as Standard Deviation (SD), Correlation Coefficient (CC), Root Mean Square (RMS) and vertical and horizontal profiles. Only selected results for winter season are presented in this paper, namely the case of December 5th, 2012. In the Figure 2 below a synoptic situation in Europe is shown. During this time Poland was under influence of the atmospheric fronts connected with low system pressure with centre on the Baltic Sea, in the result soil was wet and frozen in many regions.

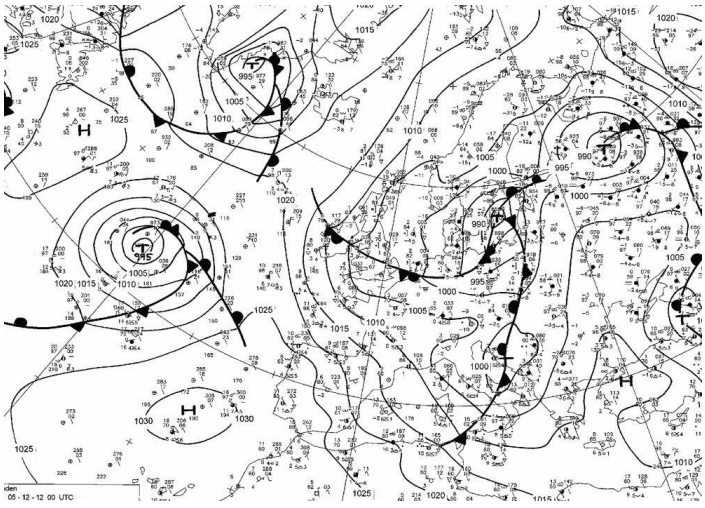

Figure 2: Synoptic situation for December of 5, 2012 for 00 UTC.

At the first step we chose areas with different sort if soil. These area were marked by letter A, B and C (fig. 3) to be further assessed in our numerical experiments.

A - Embryonic soil - Soil in the initial phase of formation, with small level of organic soil. Embryonic soils can be formed usually as a result of erosion of background on hard and loose flowing. Due to low fertility and low resistance to mass movements seldom used in agriculture. Embryonic soils are characterized by a shallow (10 cm) layer of soil with a bedrock located directly below (Uziak et al.). A characteristic feature of initial soil are relatively big rock fragments in the soil, particularly in the lower, less developed layer. In mountain areas an appearance of these soil is temporary due often mass transport down the slope (Skiba et al, 2009). Embryonic soils do not have a distinctive color. It depends on the surrounding rocks that originally form a soil (Uziak et al.).
The most common is the soil profile (A) CC - this abbreviation reads (Trzcinski, 1989):

- A - humus horizon
- C - the level of bedrock

Some authors distinct a separate thin organic layer and then profile description is O-C-AC (Skiba et al.)

B - Fawn (loess) soils - fertile brown soils with A-Eet-Bt-C profile. A characteristic feature of this type is washed-out colloidal clay, transported without decomposition to the lower level of Bt. It can found in the temperate (marine) and transitional zone - in Western and Central Europe, including Poland. It occurs under deciduous and mixed forests.

C - Brown soils - formed in temperate climate, primarily under a vegetation of deciduous and mixed forests. They are formed from various geological origin and various grain, from rocks rich in bases or acids (eg. weathered granite or gneiss) and from dusts (loess and loess-like tracks) . The pH of these soils are strongly acidic.
The brown color of the soils is a result of iron compounds and of brown humus compounds coating grains of soil in a form of thin shells.
In brown soils a cambic subsurface diagnostic level (Bbr) occurs, while in fawn soils - subsurface luvic (Eet) and argillic (Bt) levels (Mocek et al., 2000).

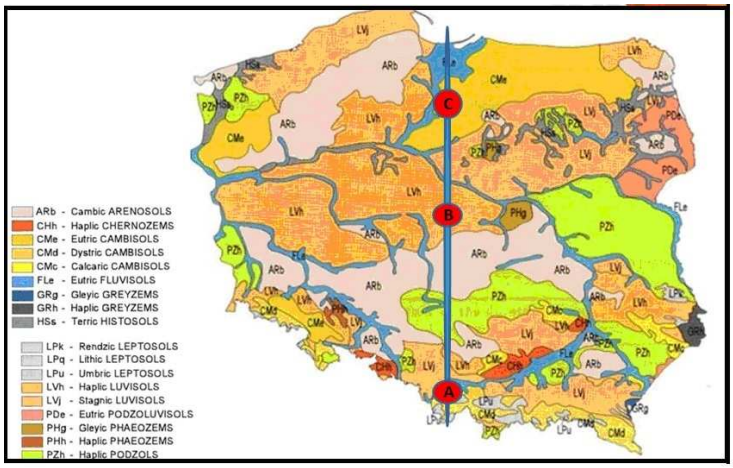

Figure 3: Points selected for analysis.

Next we compared forecast from COSMO model with results from satellite measurements for four soil layers. At figure 4, differences between results from COSMO model and satellite data are shown with green colors indicating areas where values of the Soil Water Content (SWC) from COSMO model was lower in comparison with values from satellite measurements (red colors -higher, respectively).

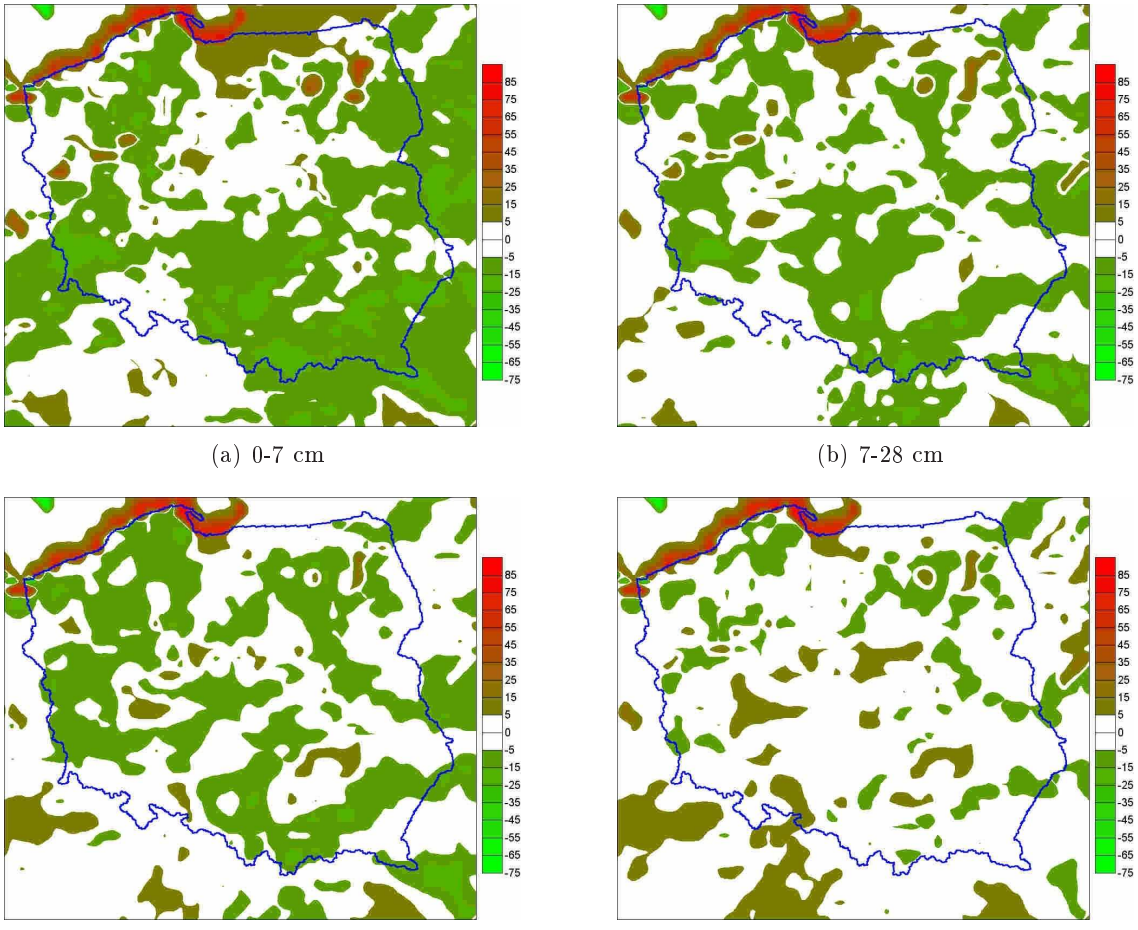

(a) 0-7 cm

(b) 7-28 cm

(c) 28-100 cm

(d) 100-289 cm

Figure 4: Results for December 5th, 2012 – difference of values of SWC in layer

Next we analyzed vertical profiles of SWC for three chosen point (fig. 5). For the first and second layer COSMO model overestimate SWC in comparison with data from satellite. In deeper layer the opposite results were

seen- SWC was underestimated in comparison with satellite data. At the point B only in the upper part of soil humidity was overestimated by COSMO model. In deeper layers situation change to opposite. At the region C, SWC was overestimated by COSMO model only in the fourth layer.

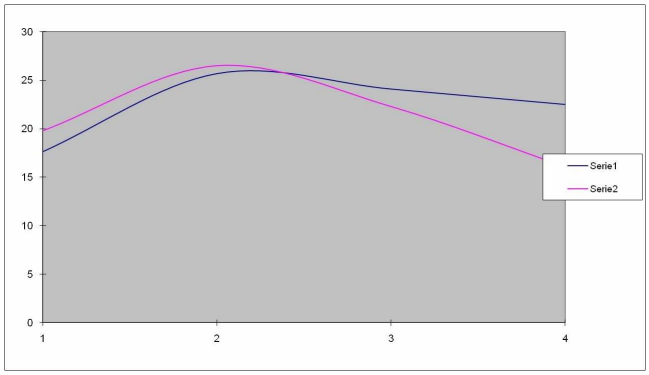

(a) profile of SWC in point A

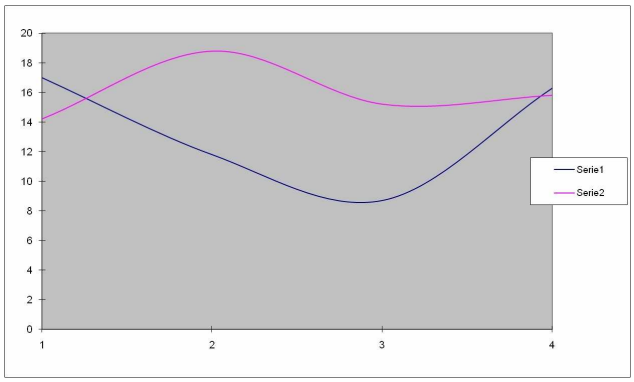

(b) profile of SWC in point B

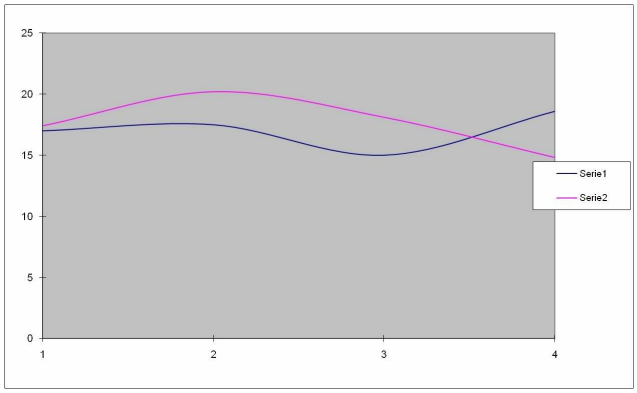

(c) profile of SWC in point C

Figure 5: Results for December 5th, 2012. Blue line represent values SWC from COSMO model and violet line represent data from satellite. Y axis – SWC in percent. X axis – layer number (centre of layer).

In the next step we analyzed cross-section horizontal profile for the four layers (fig. 7) along "blue line", as showed at fig. 6. Along cross-section are following kind of soil: Umbric Leptosols, Haplic Luvisols, Haplic Podzols, Cambic Arenosols, Eutric Cambisols, Eutric Fluvisols.

In the central part of Poland the SWC was underestimated by COSMO model. In the marine area values of SWC were overestimated by COSMO model in comparison with satellite data. In mountain areas values of the SWC are very similar. In the second layer (fig. 7(b)) the SWC was overestimated by COSMO model in comparison with satellite measurements only in coastal region. In the third layer (fig. 7(c)) situation was very similar as for second layer, except that in mountain area values from COSMO model and from satellite measurements were almost identical. In the deepest layer (fig. 7(d)) results from COSMO model were very similar in comparison with results from satellite, except for coastal region where SWC was overestimated.

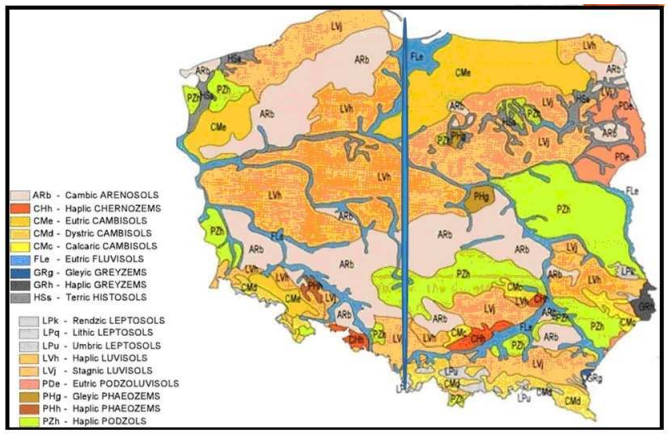

Figure 6: "Blue" vertical line indicate cross-section profile of SWC for the four soil layers.

Basing on numerical experiment for all cases we can summarize this part of the results:

- **Generally for all data:**
  a) Overestimated SWC in coastal area.
  b) Underestimated SWC in mountain area and central part of Poland.
- **In detail for the different soil types:**
  a) Overestimated or underestimated SWC, depending on type of soil and of plant cover, seasons etc.:
  b) for Stagnogleyic Luvisols, Haplic Phaeozems, Haplic Podzols, Cambic Arenosols, – underestimated,
  c) for Eutric Cambisols, Haplic Luvisols – overestimated.

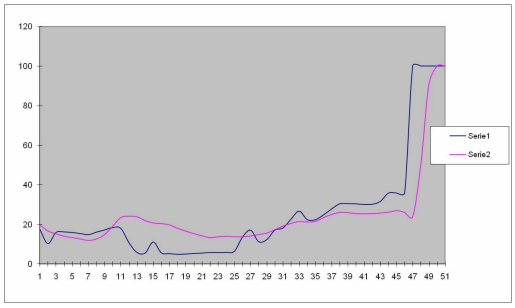

(a) 0-7 cm

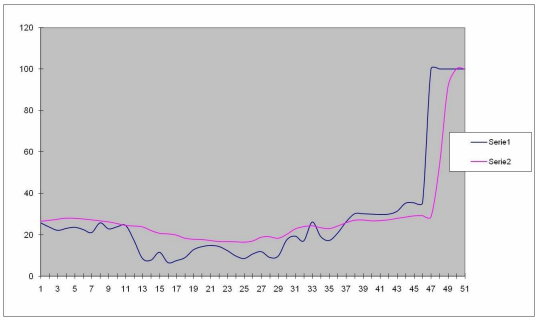

(b) 7-28 cm

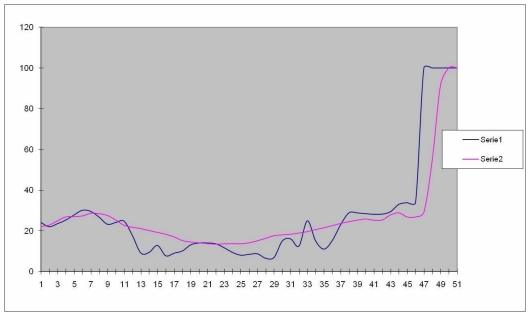

(c) 28-100 cm

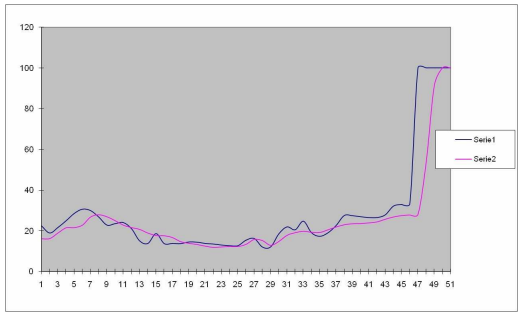

(d) 100-289 cm

Figure 7: Results for December 5th, 2012 – cross section profile of SWC in layer. Blue line represent values SWC from COSMO model and violet line represent data from satellite. Y axis – SWC in percent. X axis – "y" coordinate of COSMO model (small domain).

3 Analysis based on data from Institute of Agrophysics Polish Academy of Science

Second set of data was gained from the Institute of Agrophysics, Polish Academy of Science. That data was received in the frame of formal cooperation established between both Institutes.

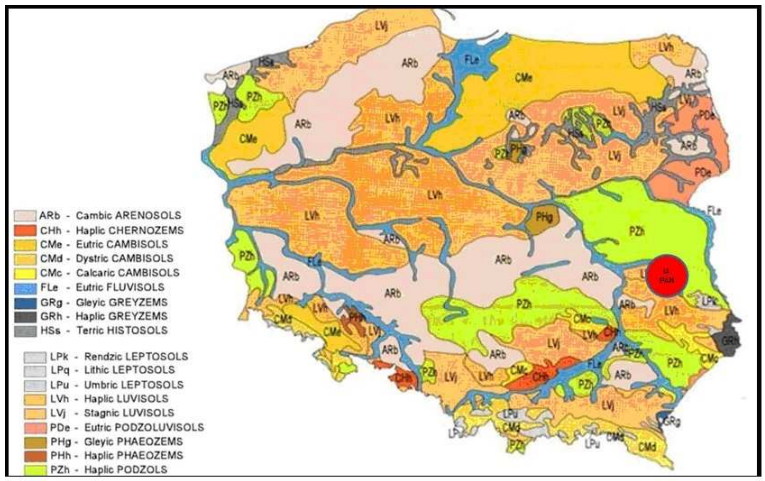

Figure 8: Red circle marks area of measurement.

At the experiment area following parameters were measured:

a) Temperature at 10 cm below ground level

b) Soil water content at 10 cm below ground level

The first set of data was gathered from January 2008 to December 2009.
Data come from the following four different locations in Poland:

a) $\lambda = 23^o06'14.2''$ $\phi = 51^o28'55.2''$ deep soil measurements; soil: sand in pinery,

b) $\lambda = 23^o06'50.5''$ $\phi = 51^o28'23.7''$ surface soil measurements; soil: peat,

c) $\lambda = 23^o07'35.5''$ $\phi = 51^o27'40.1''$ surface soil measurements; soil: peat under grass,

d) $\lambda = 23^o08'6.542''$ $\phi = 51^o27'12.424''$ deep soil measurements; soil: rendzic.

The initial soil conditions for COSMO model were replaced by the field data from Institute of Agrophysics in these four locations. Next, results from "reference" COSMO model with results received after changing initial data (so called COSMO – PAN – version) were compared. We analyzed standard statistic parameters including Mean Bias (MB), Standard Deviation (SD), Correlation Coefficient (CC), Root Square Difference (RMSD) and vertical and horizontal profiles.

Selected data from August 14, 2008 are presented below. Poland was under influence of low system pressure with atmospheric front in the south-eastern part of country (fig. 9). During this day measured soil condition was warm and wet.

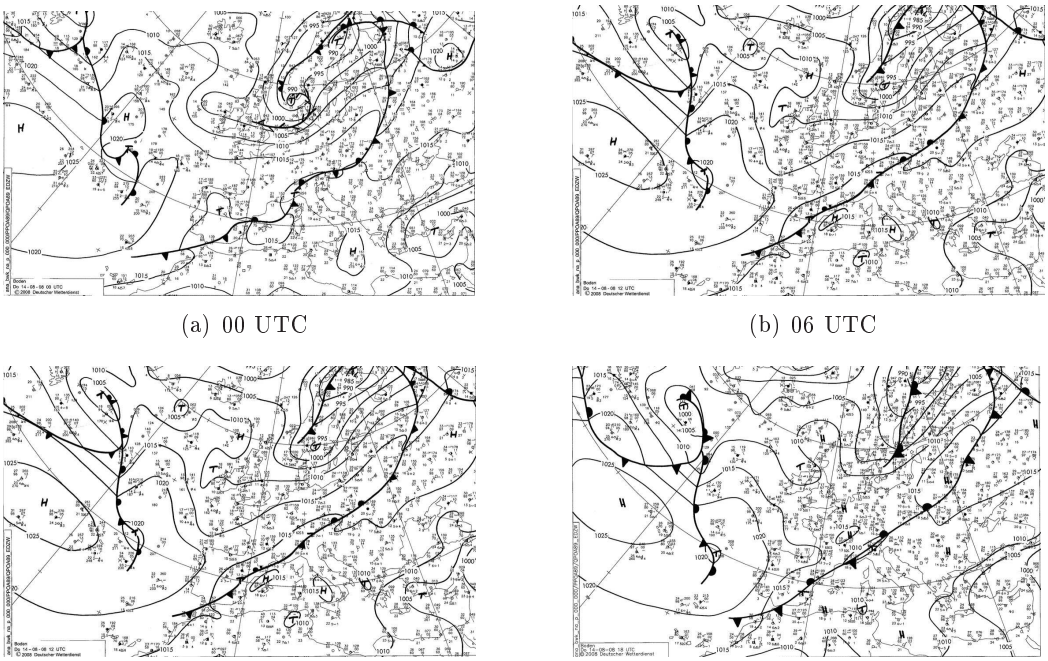

(a) 00 UTC (b) 06 UTC

(c) 12 UTC (d) 18 UTC

Figure 9: Synoptic situation for August 14th, 2008.

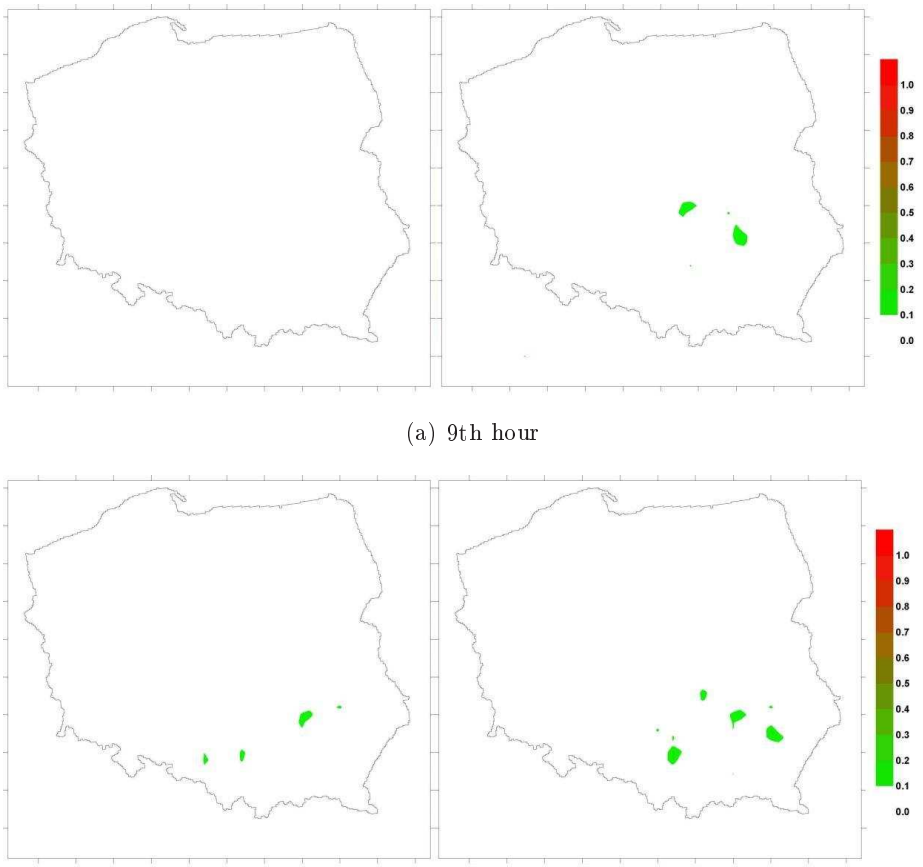

(a) 9th hour

(b) 12th hour

Figure 10: 9th hour and 12th hour forecast for: temperature at 2 m. a.g.l. (left) and temperature of soil surface (right panels). Forecast started at 00 UTC August 14th, 2008.

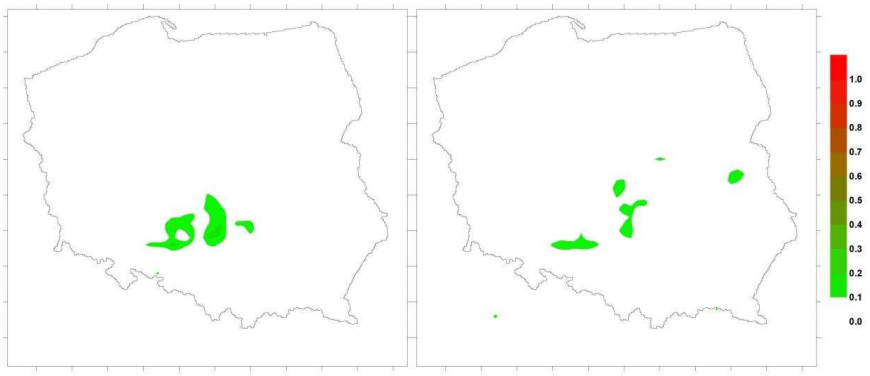

(a) 15th hour

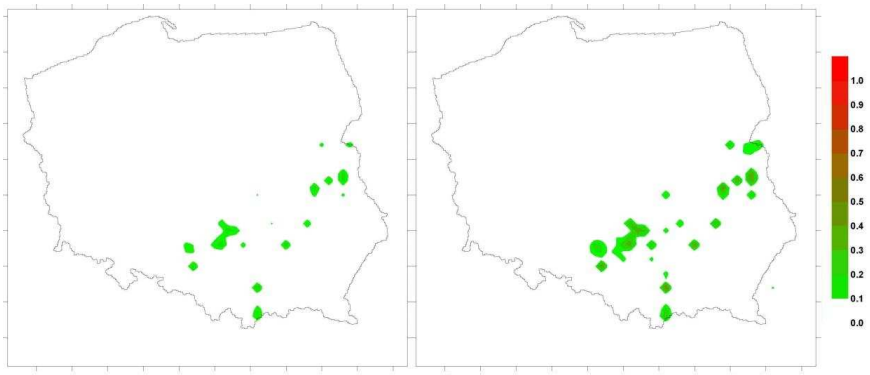

(b) 18th hour

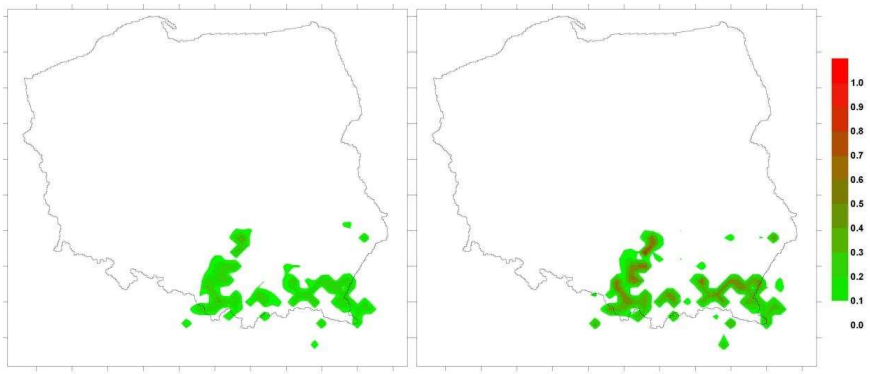

(c) 21st hour

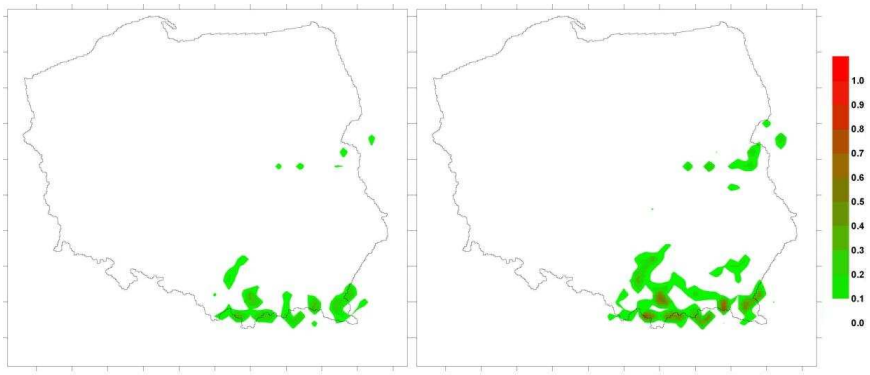

(d) 24th hour

Figure 11: The 15th, 18th, 21st, and 24th hour of forecast for temperature at 2 m. a.g.l. (left) and temperature of soil surface (right). Forecast started at 00 UTC August 14th, 2008.

4 Summary

In this paper preliminary results of the numerical experiments of TERRA_ML model were presented. Current parameterization of soil processes in TERRA_ML COSMO numerical meteorological model give unsatisfactory forecasts of the agrophysical fields like as Soil Water Content (SWC), moisture flux which are very important and influencing on quality of meteorological fields. At first step we studied results from COSMO model and compared them with the data from observations. To make this comparison we used experimental data sets from two sources. The first one was from Satellite Remote Sensing Center, the second – received from the Institute of Agrophysics Polish Academy of Sciences.

Basing on numerical experiment which were made at Institute of Meteorology and Water Management, it was inferred for all cases that Soil Water Content (SWC) were overestimated in coastal area, SWC were underestimated in mountain area and central part of Poland (generally for all data). Consideration results in detail for the different soil types were observed overestimated or underestimated SWC, depending on type of soil and of plant cover, seasons etc.: for Stagnogleyic Luvisols, Haplic Phaeozems, Haplic Podzols, Cambic Arenosols, - underestimated,for Eutric Cambisols, Haplic Luvisols - overestimated. Generally, this effect depends on the type of soil, the plant cover as well as on the season of year.

A very interesting phenomenon can be seen using the second data set. "Point injection" of the initial conditions caused propagation of differences between "modified" and "reference" results, in large distance from the source these changes. The first differences appeared at ninth hour of forecast for temperature of soil at the surface and for twelfth hour of forecast for air temperature at 2 m. a.g.l. This test case will be elaborated in more details in the further studies.

Detailed results will be presented during the next COSMO meeting.

Acknowledgements authors would like to thank prof. C. Slawinski and Dr. K. Lamorski for providing experimental data in the frame of cooperation between IMWM and the Institute of Agrophysics Polish Academy of Sciences.

References

[1] Doms G., 2011; A Description of the Nonhydrostatic Regional Model LM, Part I: Dynamics and Numerics, DWD.

[2] Doms G., Forstner J, Heise E, Herzog H. - J, Mironov D, Raschendorfer M, Reinhardt T, Ritter B, Schrodin R. Schulz, J. - P, Vogel G, 2011; A Description of the Nonhydrostatic Regional Model LM, Part II: Physical Parameterization, DWD.

[3] Dickinson, R. E., 1984; Modeling evapotranspiration for three-dimensional global climate models Climate Processes and Climate Sensitivity. *Geophysical Monograph 29*, Maurice Ewing Volume 5, 5, **58-72**.

[4] *Product User Manual (PUM) for product H14 - SM-DAS-2 Soil Moisture Profile Index in the roots region by scatterometer data assimilation*, EUMETSAT Satellite Application Facility on Support to Operational Hydrology and Water Management, Reference Number: SAF/HSAF/PUM-14, Issue/Revision Index: 1.1, Last Changing 31 May 2012.

[5] Uziak S., Klimowicz Z., Elementy geografii gleb i gleboznawstwa. s. 143 (in Polish).

[6] Skiba S.„ Szymanski W., Medzka M., Predki R. Inicjalne gleby (Lithic Leptosols) pietra polonin w Bieszczadach i Czarnohorze (Karpaty Wschodnie). *Roczniki Bieszczadzkie*. 17, s. **357-358**, 2009 (in Polish).

[7] Trzcinski, W. (red.). Systematyka gleb Polski: Wydanie czwarte. *Roczniki gleboznawcze*. XL (3/4), s. 53-54, 1989. Polskie Towarzystwo Gleboznawcze. PWN, Warszawa. (in Polish).

[8] Mocek,A., Drzymala,S., Maszner,P., 2000; Geneza, analiza i klasyfikacja gleb, Wydawnictwo AR w Poznaniu (in Polish).

[9] Duniec G., Mazur A., 2012; New Approach to Parameterization of Physical Processes In Soil in COSMO Model - Preliminary results, *General Meeting*, Lugano, Switzerland.

[10] Duniec G., Mazur A., 2013; Experiment in Soil physics - results, *General Meeting*, Sibiu, Romania.

[11] Duniec G., Mazur A., 2014; Experiment in Soil Physics - "bare soil" parameterization aspects, *COSMO User Seminar*, Offenbach, Germany, 2014.

[12] Synoptic charts come from website, www.wetter3.de/fax.

First results of simulations with COSMO-1˙ITA and comparison of results with COSMO configurations at different resolutions

M. P. Manzi[1], P. Mercogliano[1,2] and M. Milelli[3]

1 Impact on soil and Coast Division, EuroMediterranean Centre for Climate Change (CMCC),I-81043 Capua (CE), Italy
2 Meteo System & Instrumentation Laboratory, Italian Aerospace Research Center (CIRA), I-81043 Capua (CE), Italy
3 ARPA Piemonte, I-10135 Torino, Italy

1 Introduction

In the framework of the project COSMO-NExT, a configuration of COSMO at 1.1 km of resolution (named COSMO-1) is under development at MeteoSwiss. COSMO-1 has also been used at CIRA, for the realization of some tests, in collaboration with MeteoSwiss and ARPA Piemonte. The first aim of this work concerned the testing of this particular configuration over the Italian domain for a 6 days period. This configuration has been named COSMO-1_ITA. A preliminary activity was constituted by optimization of parameters, mainly concerning the numerics, for the selected domain. Furthermore, to evaluate the performances of the COSMO-1_ITA configuration, different typology of observations have been used for the validation: satellite data and radio soundings, in order to evaluate the configuration performances respectively in the upper layers and through the different layers of atmosphere. Furthermore, a comparison of the results has been realized comparing the output of the 1km simulation with configuration of COSMO at different resolutions: 2.8km and 7km. The last analysis performed over COSMO-1_ITA simulation's results has been the analysis of the kinetic energy spectra to locate the effective resolution of the run.

2 Description of the test cases and features of the simulation

The test case interested a 6 days period, from 25^{th} to 30^{th} of November 2012. The synoptical situation during these six days was quite diversified: in the first day the Mediterranean area was interested by a high pressure ridge (Figure 1) that, in the following days, gradually collapsed pushed towards Eastern Europe by an Atlantic perturbation (Figure 2).

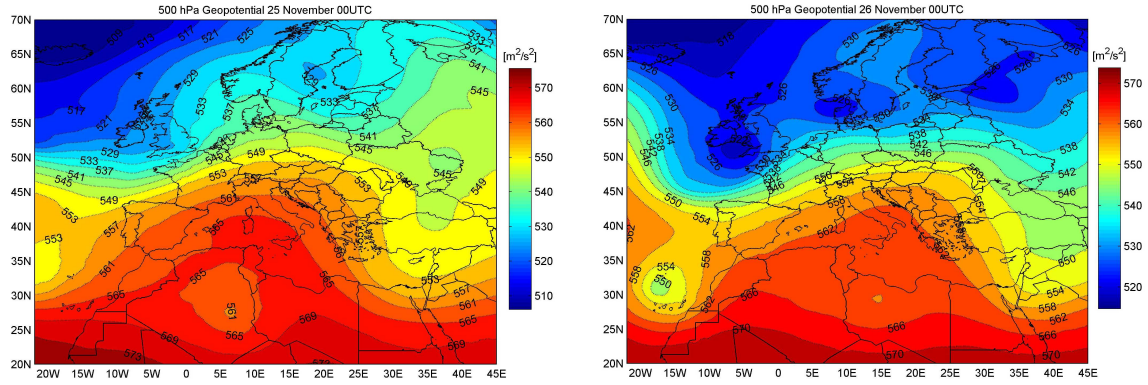

(a) (b)

Figure 1: Geopotential at 500hPa for 25^{th}, 26^{th} at 00UTC. Data taken from the analysis at 00UTC of the ECMWF global model.

From the afternoon of 27^{th} to 30^{th} of November 2012, indeed, Italy was interested by an intense southern moist flow due to a low pressure system centred over the western Mediterranean Sea. This synoptic pattern caused an intense thunderstorm activity with widespread precipitations over the peninsula. The precipitation over the southern Italy, on which the simulation domain is centred, started the 27th of November.

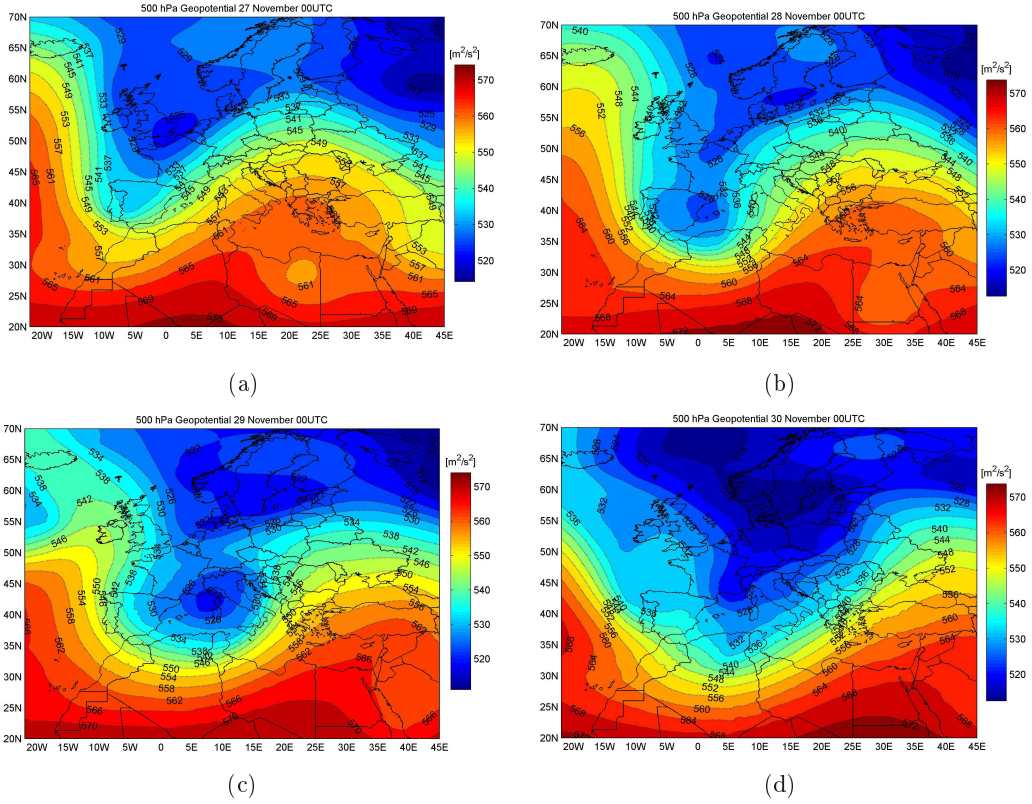

Figure 2: Geopotential at 500hPa for 27^{th}, 28^{th}, 29^{th}, and 30^{th} at 00UTC. Data taken from the analysis at 00UTC of the ECMWF global model.

The choise of this period, then, due to the high variety of weather conditions, made it possible to evaluate the performance of the model under various meteorological conditions.

The nesting strategy used to perform the simulations is shown in Figure 3. The boundary and initial condition for the 7km simulations (COSMO-7_ITA) are taken from the forecast of the T1279 ECMWF model. The output obtained from COSMO-7_ITA is used to initialize the simulations performed with COSMO at 2.8km of resolution (COSMO-2.8_ITA) and with COSMO-1_ITA.

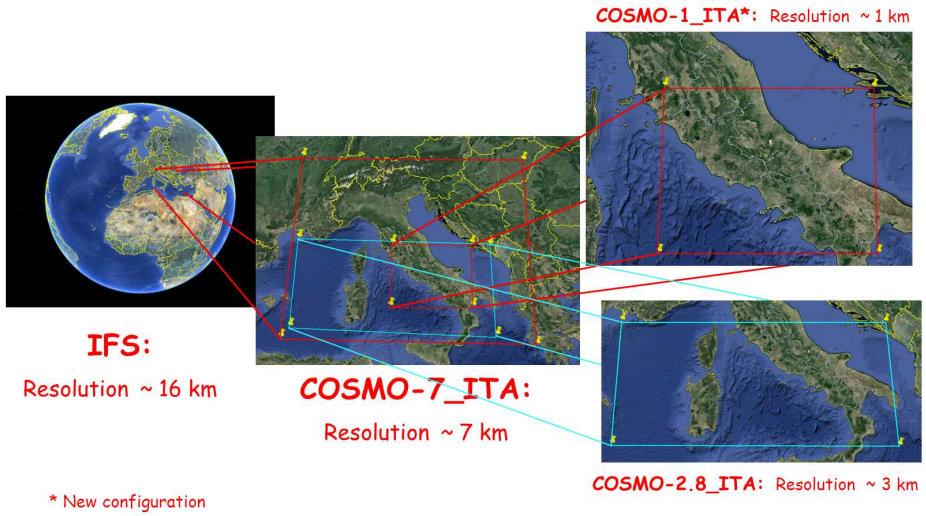

Figure 3: Nesting strategy used for COSMO-7_ITA, COSMO-2.8_ITA, COSMO-1_ITA configurations.

In Figure 3, in the upper right image, is shown the computational domain used for the optimized version of 1km simulations. A first optimization, indeed, interested the selection of the domain's dimension: the new simulations of COSMO-1_ITA were performed on a bigger domain. In Figure 4 is shown the difference between old (a) and new (b) domain.

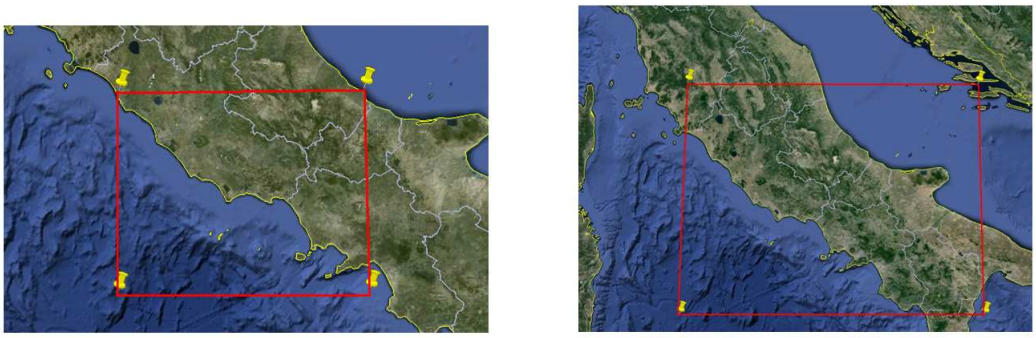

(a) (b)

Figure 4: Comparison between old (a) and new (b) domain.

Moreover, some parameters in model dynamics have been changed (Baldauf, 2010). Some of the most relevant settings for the two configurations are shown below in Table 1.

Parameter name	**New configuration**	**Old configuration**
Grid characteristic	ie_tot=400, je_tot=300, ke_tot=60	ie_tot=225, je_tot=120, ke_tot=60
Time step (s)	dt = 5.0	dt = 5.0
Coefficient for divergence damping	xkd=0.1	xkd=0.01
Fast wave solver	itype_fast_waves=2	itype_fast_waves=2
Bottom boundary condition	itype_bbc_w=114	itype_bbc_w=4
Runge Kutta advection scheme	iadv_order=5	iadv_order=5

Table 1: Namelist comparison between old and new (optimized) versions of COSMO-1_ITA.

To summarize, the most important settings choosen for each one of the three configuration are reported below in Table 2.

Parameter name	**7km**	**2.8km**	**1.1km**
Grid characteristic	ie_tot=240, je_tot=160, ke_tot=40	ie_tot=400, je_tot=175, ke_tot=60	ie_tot=400, je_tot=300, ke_tot=60
Time step (s)	dt = 40.0	dt = 20.0	dt = 5.0
Interval between two consecutive boundary data	hincbound=3.0	hincbound=1.0	hincbound=1.0
Subgrid-scale convection	lconv=.true., itype_conv=0,	lconv=.true., itype_conv=3,	lconv=.true., itype_conv=3,
Switch for nudging	lnudge =.TRUE.,	lnudge =.FALSE.,	lnudge =.FALSE.,

Table 2: Comparison between parameters settings for the three configurations.

The number of vertical levels has been increased from 40^{th} for the 7km run to 60^{th} for 2.8km/1.1km runs. In Figure 5 is reported the distribution of the vertical levels described above. Anyhow no further investigation has been carried out in this work about the number of the vertical levels to be used in COSMO-1_ITA, since previous studies show that the model behavior substantially does not change, changing the number of vertical levels (Milelli, 2012).

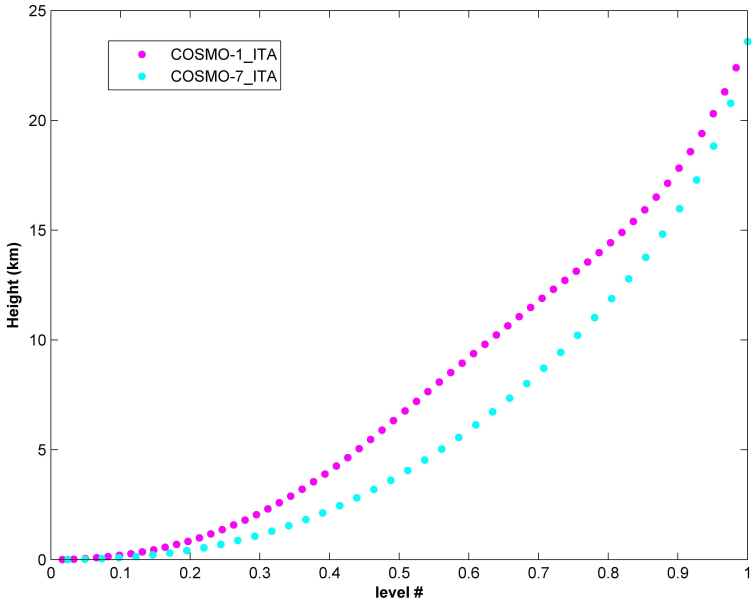

Figure 5: Distribution of the vertical levels for COSMO-7_ITA and COSMO-1_ITA configurations. Note that the same distribution of COSMO-1_ITA has been used even for COSMO-2.8_ITA.

The assimilation is performed through the use of the nudging technique only for the 7km simulations. As reported in Figure 6, at 12UTC a simulation of COSMO-7_ITA has been realized with a forecast range of 12 hours and with assimilation enabled. The output of this run has been included in the initial conditions of COSMO-7_ITA at 00UTC. In their turn the outputs of the 7km run at 00UTC have been used for the nesting of 1km and 2.8km runs, performed only at 00UTC.

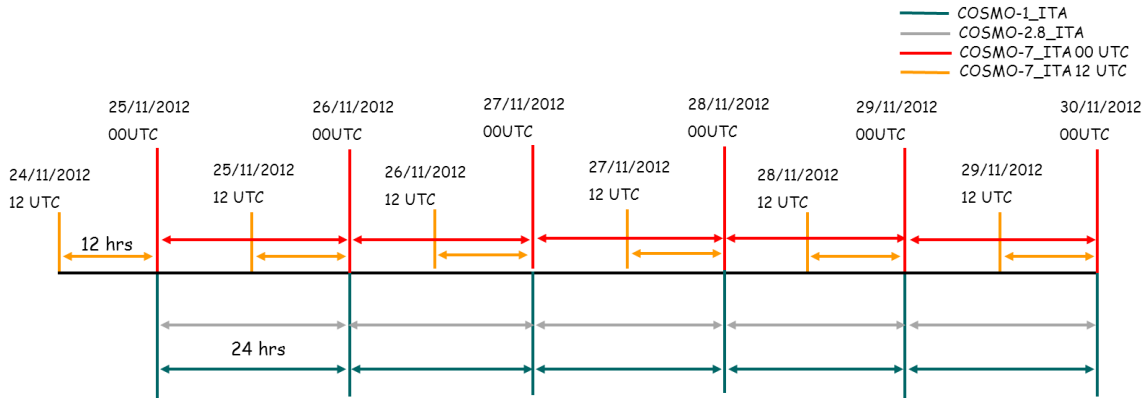

Figure 6: Scheme of performed simulations.

The increasing in spatial resolution means also a more accurate description of the analyzed domain characterized by a complex orography in which are present, at very low distance, Mediterranean Sea and Appennines (Figure 7).

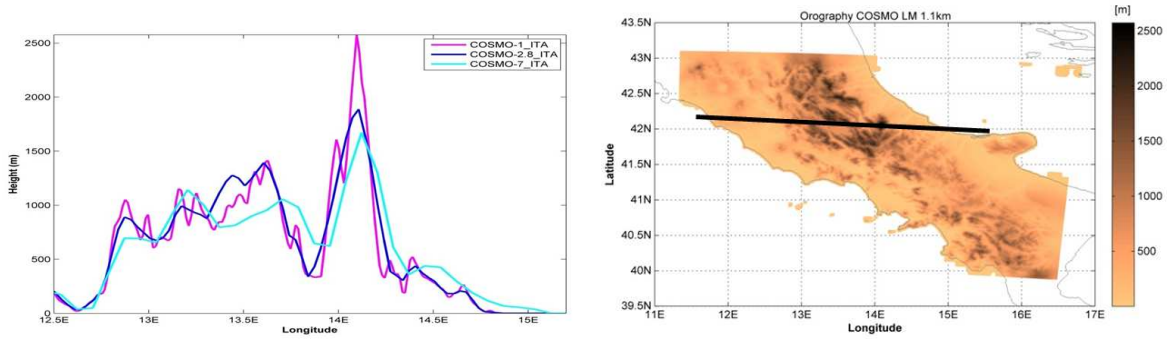

Figure 7: Comparison between the three orographies of the three simulations at the fixed latitude of 42^o.

There is therefore the necessity of a proper treatment of orography and filtering in the passage from 7km to 2.8km and 1km. In the Table 3 are reported the main characteristics for orography filtering.

Parameter name	**int2lm 7km - 1km and int2lm 7km - 2.8km**
Type of low pass filter and number of sequential applications of filter	lfilter_oro=.true., ilow_pass_oro=4, numfilt_oro=1,
Parameter for filtering and order of the orography filtering	eps_filter=0.1, norder_filter=5,
Extra smoothing of steep orography	ilow_pass_xso=6, lxso_first=.FALSE., numfilt_xso=6, rxso_mask=300.0,

Table 3: Treatment of orography and filtering in int2lm.

3 Performances evaluation

The performances evaluation has been realized through the use of satellite images and sounding data. The observed satellite data have been provided by courtesy of University of Sannio, while sounding data were freely available on internet. The decision to use these two different types of data is derived from the specific characteristics that belong to each of them and that in some ways make them complementary.

Indeed, although satellite data have the great advantage of high resolution in space and time and give information of the weather in areas where no other observations are available, the use of satellite data offers only the possibility to make an analysis of the situation of the upper part of the atmosphere. For this reason a second kind of validation has been performed.

In order to better understand the behavior of the atmosphere also through the different layers, the second part of the validation work has been carried out through the comparison of observed soundings and simulated soundings obtained from the three simulations.

As regards the comparison via satellite images, two channels have been used: 10.8 μm (infrared channel) and 6.2 μm (water vapor channel), which are typically used for the detection of clouds. The results have been analyzed for two particular cases: one cloudless and the other one cloudy which show, respectively, the best and the worst results. In Figure 8 are shown the differences between observed and synthetic satellite images (Saunders, 2008 and 1999), for the three simulations (column-wise) and for the two considered channels (row-wise) for the 4th hour of forecast of 26^{th} November. In this case the error is quite low for all the simulations, for both channels.

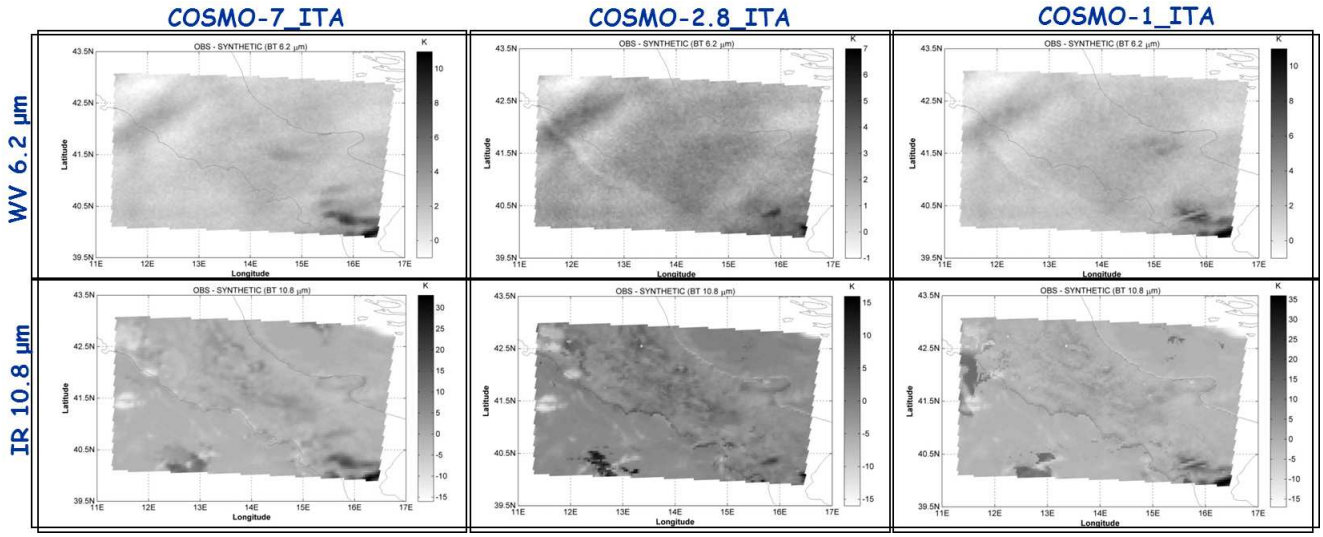

Figure 8: Comparison of observed and synthetic satellite images for the three simulations, in the two selected channels, for 26^{th} November 2012 at 04UTC.

In Figure 9 are shown the differences for the 13^{th} hour of forecast of 30^{th} November. In this case, especially for the 10.8 μm channel, the error is higher for all the simulations: white areas in the images (highlighted by red circles) denote values of model higher than observed, in other words the model is hotter than reality; dark areas (highlighted by blue circles), instead, denote model values lower than observed, in this case the model is colder.

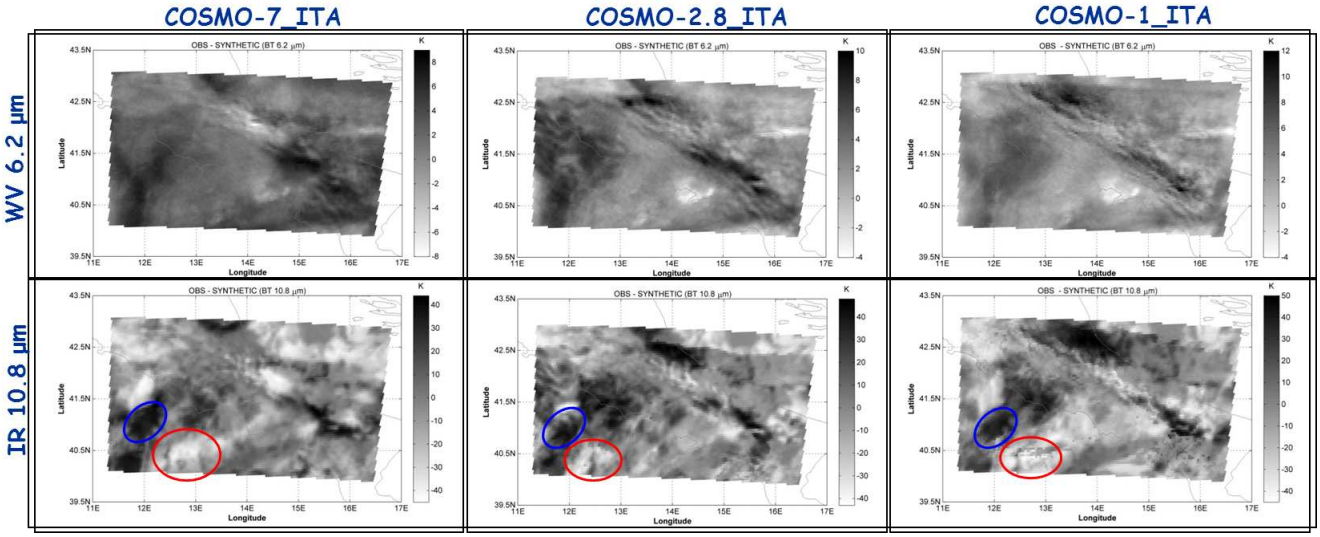

Figure 9: Comparison of observed and synthetic satellite images for the three simulations, in the two selected channels, for 30^{th} November 2012 at 13UTC.

To summarize the results obtained for all the days of simulation two statistical indices have been calculated, as described in Reichert et al., 2005. The first is the correlation coefficient, calculated as reported in (1):

$$r = \frac{\sum (x_i - \bar{x})(y_i - \bar{y})}{\sqrt{\sum_{i=1}^{n} (x_i - \bar{x})^2 \sum_{i=1}^{n} (y_i - \bar{y})^2}} \tag{1}$$

where x are pixel values of the synthetic image, y are the pixel values of the observed image and n is the number of pixels in image. The second index used is the Root Mean Square Error, calculated as in (2):

$$RMSE = \sqrt{\frac{\sum_{i=1}^{n} (x_i - \hat{x})^2}{n}} \tag{2}$$

where x are the pixel values of the observed image, $\hat{x}$ are the pixel values of the synthetic image and n is the number of pixels in image.

In Figure 10 is reported the comparison between the correlation coefficients of the three simulations for the 10.8 mum channel (upper image) and the 6.2 mum channel (lower image).

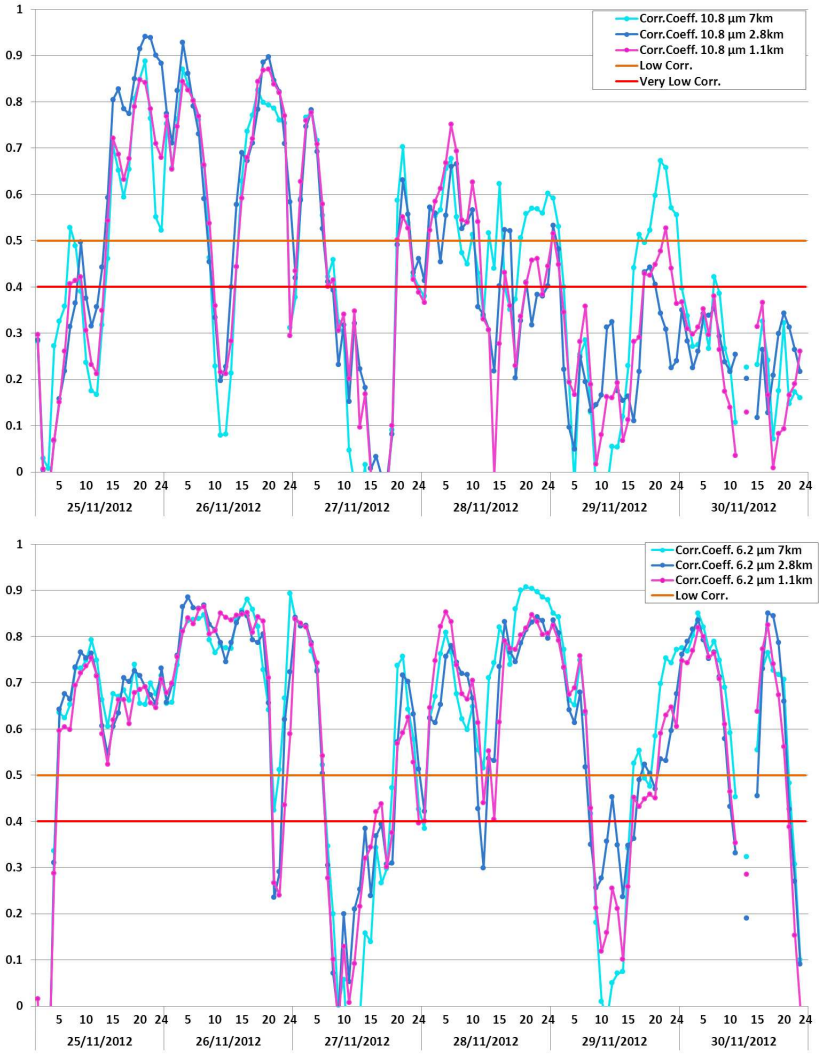

Mean Corr.Coeff. 10.8 µm

	25	26	27	28	29	30
7km	0,46	0,62	0,32	0,51	0,32	0,25
2.8km	0,52	0,67	0,36	0,44	0,25	0,26
1.1km	0,46	0,64	0,36	0,45	0,29	0,22

Mean Corr.Coeff. 6.2 µm

	25	26	27	28	29	30
7km	0,56	0,76	0,40	0,74	0,49	0,64
2.8km	0,56	0,74	0,45	0,69	0,51	0,61
1.1km	0,54	0,74	0,43	0,71	0,48	0,60

Figure 10: Comparison between the correlation coefficients of the three simulations for the two channels. In the tables are reported the mean values of correlation coefficient for each day.

The simulations at different resolution show almost the same pattern except for results obtained for $28^{th}/29^{th}$. For these two days the best results are obtained from COSMO-7_ITA configuration. Moreover, is visible a general good agreement with observations for periods without clouds for both channels. Instead a lower agreement between observations and synthetic satellite images characterizes cloudy periods, especially for IR 10.8 mum channel.

A consistent result is also obtained in terms of RMSE (Figure 11).

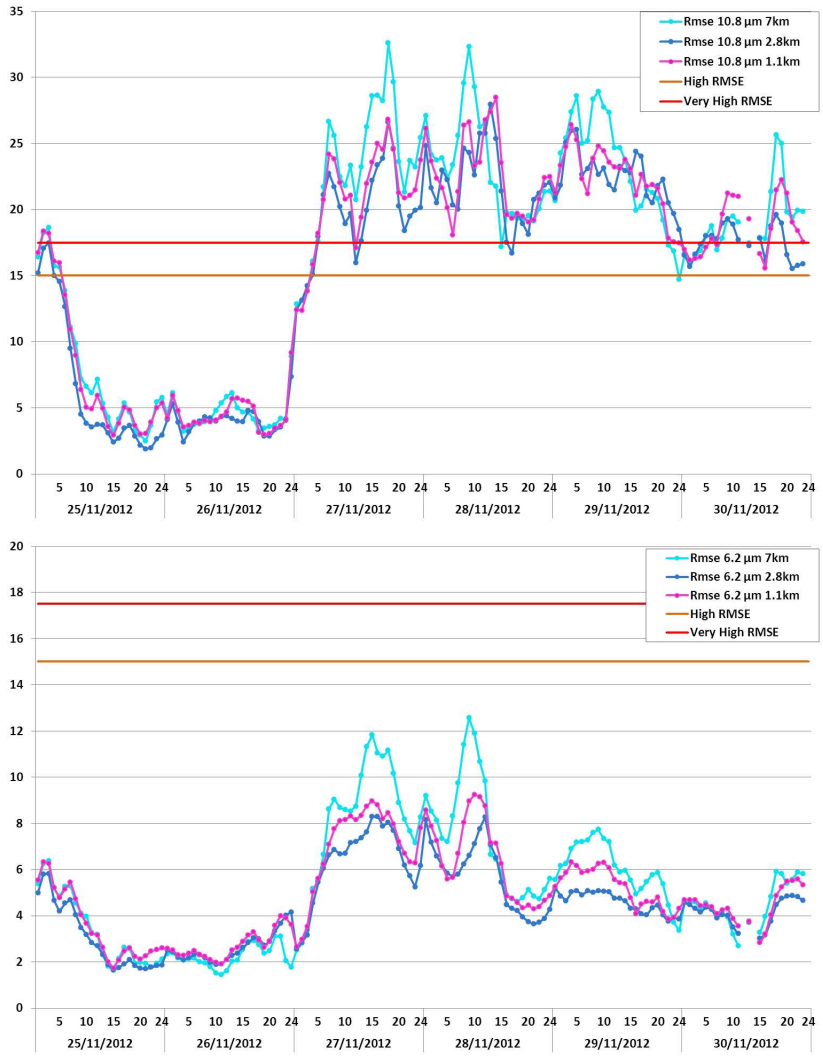

Mean Rmse 10.8 µm

	25	26	27	28	29	30
7km	8,21	4,56	22,93	23,11	23,16	19,02
2.8km	6,56	4,07	19,56	21,96	22,51	17,48
1.1km	7,92	4,50	20,69	22,56	22,36	18,62

Mean Rmse 6.2 µm

	25	26	27	28	29	30
7km	3,43	2,24	8,12	7,43	6,01	4,57
2.8km	3,05	2,63	6,30	5,69	4,59	4,14
1.1km	3,55	2,71	6,97	6,40	5,24	4,44

Figure 11: Comparison between the RMSE of the three simulations for the two channels. In the tables are reported the mean values of RMSE for each day.

Indeed, even in terms of RMSE the three simulations show almost the same pattern. The error is lower for periods without clouds for both channels and is higher for cloudy periods, especially for IR 10.8 mum channel. Concerning the WV 6.2 mum channel, instead, there is almost no error for the entire period.

An analysis in terms of statistical indices has been realized also between the two different configurations of COSMO-1_ITA, the old and the optimized one. The results are shown in Figure 12.

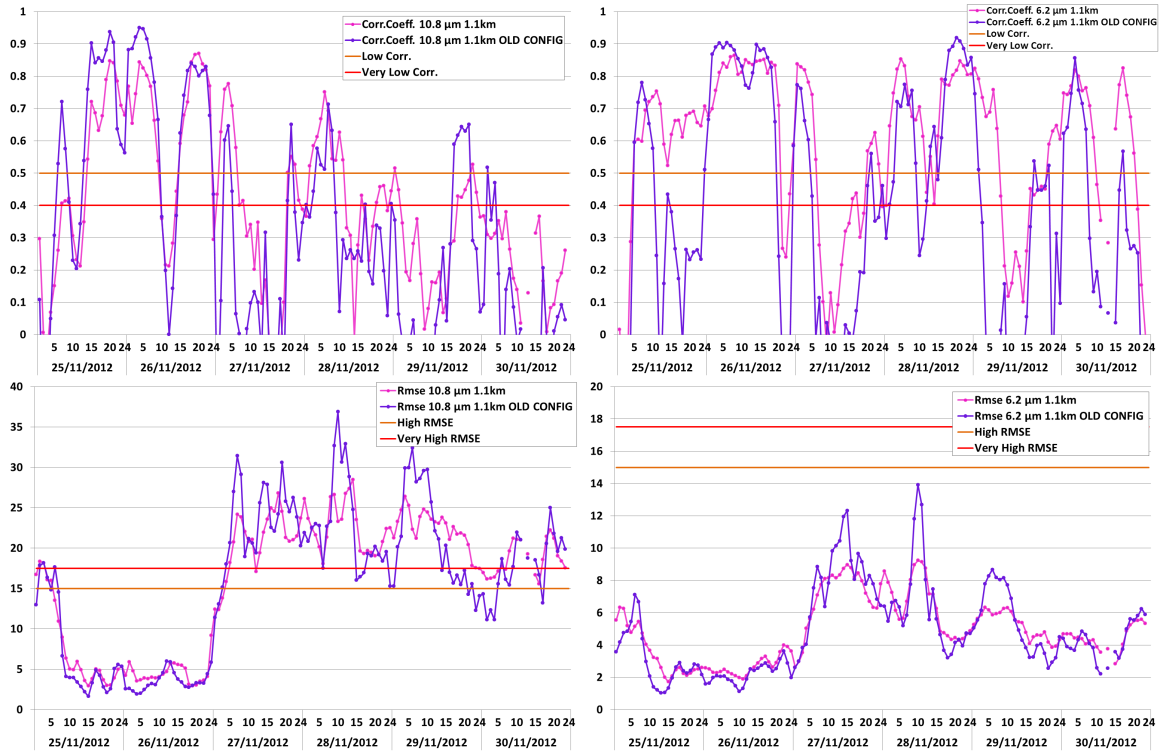

Mean Corr.Coeff. 10.8 μm

	25	26	27	28	29	30
new	0,46	0,64	0,36	0,45	0,29	0,22
old	0,50	0,68	0,15	0,34	0,17	0,08

Mean Corr.Coeff. 6.2 μm

	25	26	27	28	29	30
new	0,54	0,74	0,43	0,71	0,48	0,60
old	0,27	0,68	0,22	0,65	0,15	0,35

Mean Rmse 10.8 μm

	25	26	27	28	29	30
new	7,92	4,50	20,69	22,56	22,36	18,62
old	7,38	3,50	22,82	22,57	21,25	17,65

Mean Rmse 6.2 μm

	25	26	27	28	29	30
new	3,55	2,71	6,97	6,40	5,24	4,44
old	3,10	2,22	7,74	6,34	5,43	4,26

Figure 12: Comparison between the correlation coefficients of the three simulations for the two channels. In the tables are reported the mean values of correlation coefficient for each day.

From Figure 12 is visible a general improvement of the results with the use of the new configuration of COSMO-1_ITA. Indeed the correlation between observed and synthetic satellite images is higher and the maximum RMSE is lower than the one obtained with old configuration, for both channels.

Furthermore, soundings data have been used to analyze two particular cases: one of good agreement with observation (26^{th} of November at 04UTC) and one of lower agreement (30^{th} of November at 13UTC) which correspond to, respectively, high correlation (low RMSE) and low correlation (high RMSE). The evaluation of the performances for these two cases has been carried out through the use of soundings. The observed soundings are taken from the station of Pratica di Mare, that is located inside the simulation domain (Figure 13), at 00UTC and 12UTC.

Figure 13: Location of observation station of Pratica di Mare.

Simulated soundings are realized using the nearest grid point of the model to the observation station, for the different resolutions, at 00UTC and at 12UTC. The simulated soundings at 00UTC are obtained through the use of the analysis data (which in this case is the model output at 00UTC).

In Figure 14 are reported the results for the best case (26^{th} of November) at 00UTC and at 12UTC. In this case COSMO-7_ITA, COSMO-2.8_ITA and COSMO-1_ITA show almost the same pattern and there's a general good agreement with the pattern of the observation soundings. For the worst case (30^{th} of November, Figure 15), in the results of 00UTC the three simulated soundings show the same pattern, different from the observed one. In particular, the analysis differs for lower levels (900-700 hPa) and for middle levels (600-350 hPa). Also in the image of 12UTC the simulations show a pattern quite different from the observations, even if here the 7km simulation exhibits a different behavior compared with the others two configurations. In general, as regards the worst case, the model shows a greater error in the reproduction of the thermodynamic state of the atmosphere.

These results are in agreement with what has been already seen in Figure 10 and in Figure 11, since the best case shows good results even in terms of correlation and error, as well as the worst case shows worse results in terms of correlation and error. Therefore it is possible to say that a bad description of the state of the atmosphere through the different layers, in turn, leads to a worse quality of the forecast. Moreover, while in WV channel results are always quite good, in the IR channel error is higher, especially in cloudy periods. This could mean that the cloud is rightly localized, since the error in terms of water vapour is low, but the cloud temperature is not well identified.

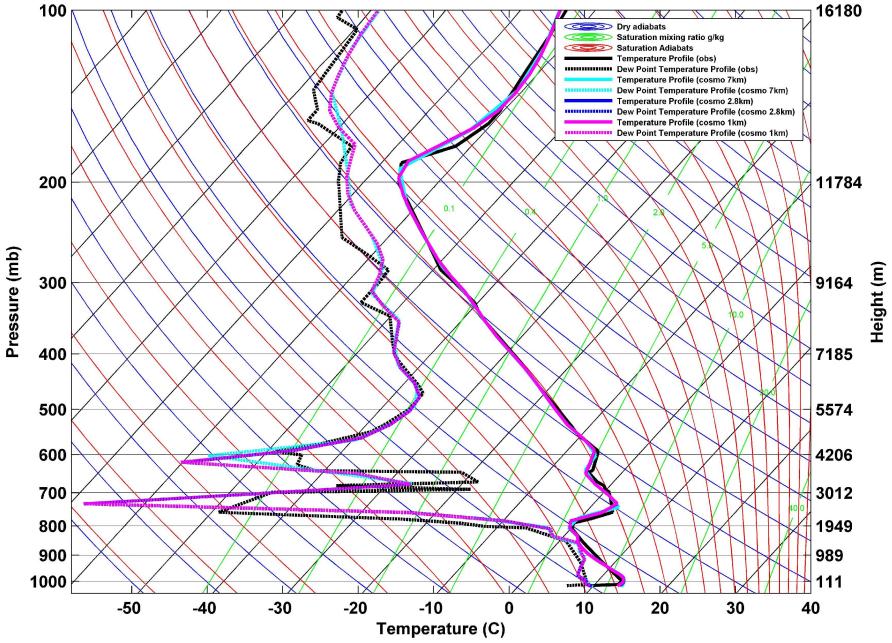

(a)

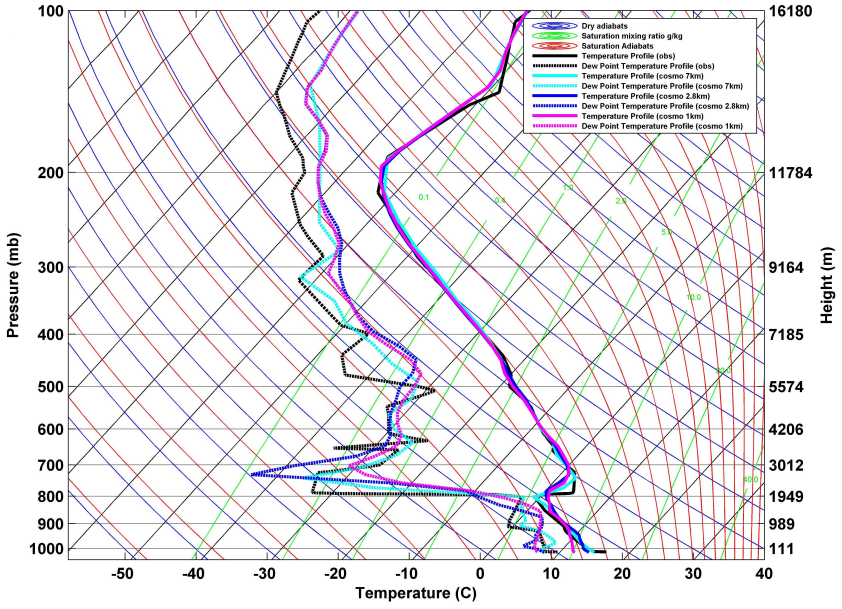

(b)

Figure 14: Comparison between observed and simulated soundings for the different simulations for 26*th* of November at 00UTC (a) and 12UTC (b).

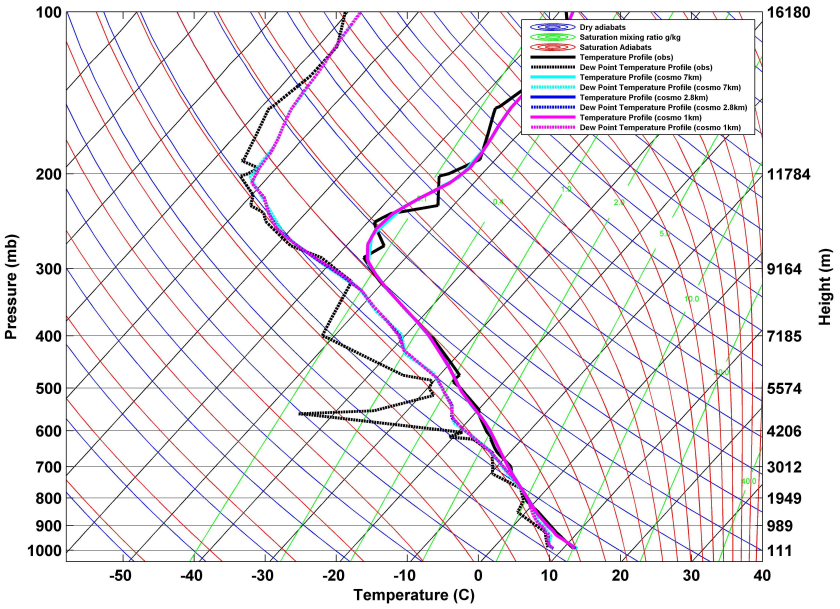

(a)

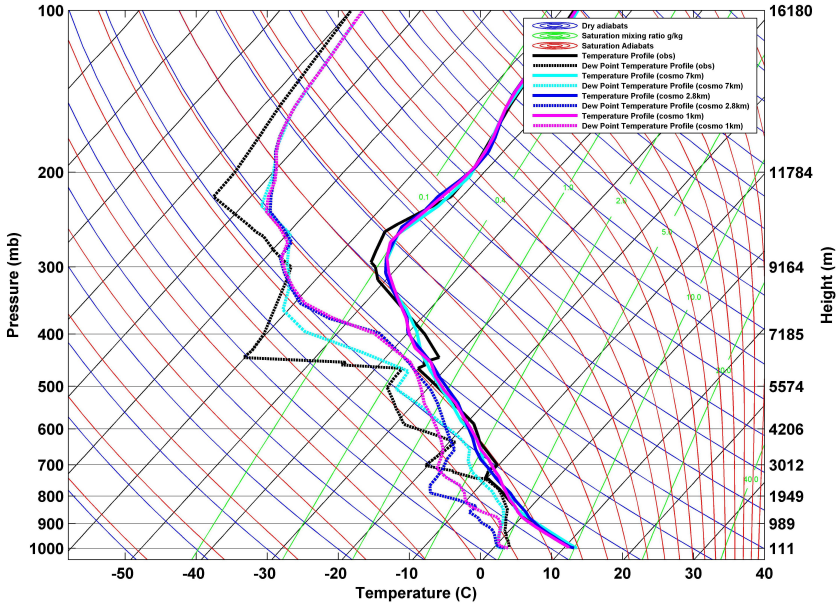

(b)

Figure 15: Comparison between observed and simulated soundings for the different simulations for $30th$ of November at 00UTC (a) and 12UTC (b).

The last analysis performed in the present work regards the study of kinetic energy spectra, used to evaluate the effective resolution of the COSMO-1_ITA simulations. A spectral decomposition was made with 2D-DCT (Denis et al., 2002) of the horizontal components of wind at different heights (200 hPa, 250 hPa, 300 hPa, 400 hPa, 500 hPa, 600 hPa, 700 hPa). The results obtained with this procedure have been avaraged daily. In Figure 16 are shown results only for $26th$ and $30th$ November, but these results are confirmed also for the other days.

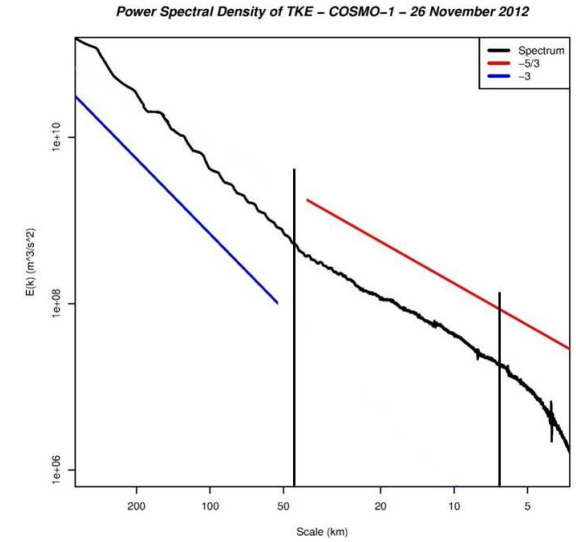

(a)

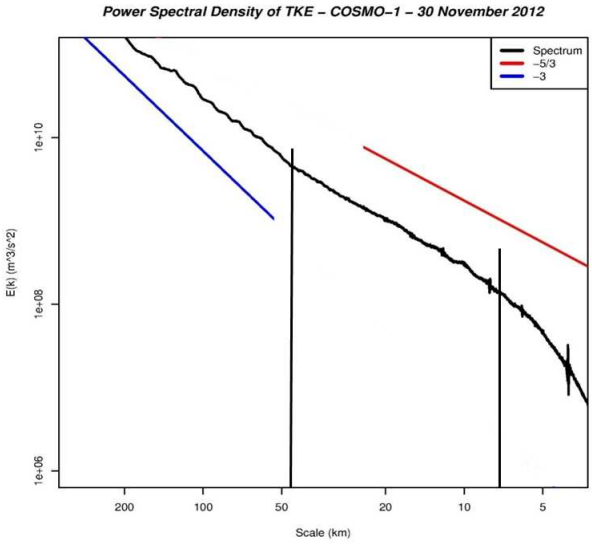

(b)

Figure 16: Power spectral density of TKE for 26 (a) and 30 (b) November.

The results are in agreement with experimental spectra by Skamarock, 2004 since for the largest spatial scale the spectral solpe is approximately -3. The transition from -3 to -5/3 is around 50 km. The loss of information is between 10 and 5 km, that is in the range of 5-10 times the nominal resolution of the model. Further experiments show that for the same test case the cofiguration at 7 km of resolution has a lower effective resolution, as expected. In Figure 17 are shown results for COSMO-7_ITA for $26th$ and $30th$ November. In this case the resolution of the model is too coarse to reproduce the -5/3 spectral slope, so it can only reproduce the -3 slope.

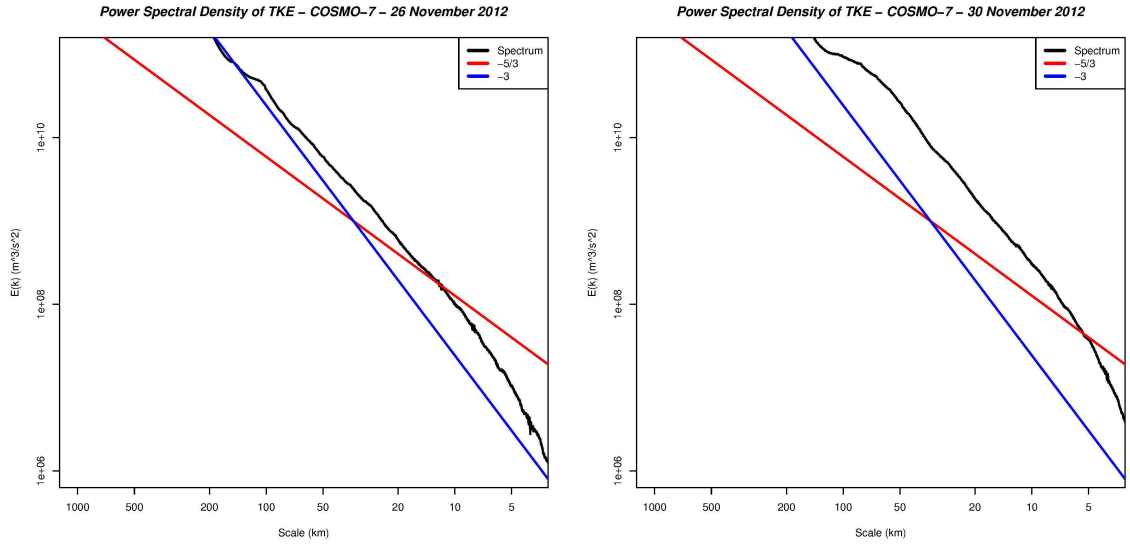

(a) (b)

Figure 17: Power spectral density of TKE for 26 (a) and 30 (b) November for COSMO-7_ITA simulation.

4 Conclusion

The aim of the work was the evaluation of the performances of COSMO-1 model over the Italian domain with different kinds of observations, suitable for the high resolution of the model, and with different configurations of COSMO (different resolutions: 7 km and 2.8 km).
The behavior of COSMO-7_ITA, COSMO-2.8_ITA and COSMO-1_ITA is quite the same for almost every variable analyzed in the validation, even if, for the cloudy days analyzed, the three simulations have worst performances. In this regard it is necessary to perform further analysis, even on the longest test case, since six days are a relatively short period to make precise estimates of error. In addition, further testing should be performed also on other variables.
The analysis of kinetic energy spectra shows a good agreement with experimental spectra by Skamarock. The loss of information is between 10-5 km, which is the effective resolution of the model. Is possible to conclude that, using a higher resolution, is possible to analyze meteorological structures characterized by a higher resolution with respect to that of 7 km and 2.8 km. This confirms that the nesting strategy used is correct and an increase of resolution can increase the capacity of the model to forecast structures more localized in space and time. Anyhow this should be verified with observations suitable for the validation of such high resolutions, such as radar or non-GTS stations.

References

[1] Reichert, B. K., Träger-Chatterjee, C. and Asmus, J., 2005: Using synthetic satellite images for automatic monitoring of NWP fields: operational applications, *Meteorol. Sat. Conf.*, EUMETSAT, Darmstadt, Germany., pp. **67-74**.

[2] Baldauf, M., 2010: Linear Stability Analysis of Runge-Kutta-Based Partial Time-Splitting Schemes for the Euler Equations, *American Meteorological Society*.

[3] M. Milelli, Sensitivity of COSMO-1 to vertical levels distribution, COSMO GM 2012, http://www.cosmo-model.org/content/consortium/generalMeetings/general2012/wg4-corso

[4] U. Schaettler, G. Doms, and C. Schraff, 2012: A Description of the Nonhydrostatic Regional, COSMO-Model Part VII: *User's Guide*.

[5] R. Saunders et al., 1999: An improved fast radiative transfer model for assimilation of satellite radiance observations, *Q. J. R. Meteorol. Soc.*

[6] R. Saunders et al., 2008: RTTOV9.1 Users Guide, EUMETSAT

[7] Skamarock, W. C., 2004: Evaluating Mesoscale NWP Models Using Kinetic Energy Spectra, *American Meteorological Society*.

[8] Errico, R. M., 1985: Spectra computed from a limited area grid, *American Meteorological Society*.

[9] Denis, B. et al., 2002: Spectral Decomposition of Two-Dimensional Atmospheric Fields on Limited-Area Domains Using the Discrete Cosine Transform (DCT), *American Meteorological Society*.

Between forecasting and nowcasting strong convective events

Jan Parfiniewicz

Institute of Meteorology and Water Management 61 *Podlesna str., PL*-01673 *Warsaw, Poland*

1 Introduction

Let me refer to formulas presented in Newsletter 13. The 1st Formula, the best filter for strong Tornado or Downburst events expresses Fujita scale as a square root function merely of the IntraCloud discharges densities, while, the second for less severe events takes into account both: IntraCloud and Cloud-to-ground lightning discharges densities. It has occurred, that both formulas might have clear physical interpretation. Indeed, Formulas (1) and (2) distinctly differentiate between specific lightning activity that is characteristic for two various developing thunderstorm stages, i.e., for the mature and very active one , with dominant IC lightning activity and the second for the dissipation thundercloud formation, when CG flashes initiation is increasing and is more pronounced. Expression (1) by explicit inclusion of the ICi component is confirming well known fact that so-called spider lightning with great number of branches, with the great ICi points are appearing frequently during mature stages of supercells.

2 Action & Result

Operational monitoring of tornados that were observed over Poland showed that extreme Tornado or Downburst events are strictly correlated to IntraCloud number of flashes aggregated in cells over a 15 km radius area. Here, densities are calculated on the 7 by 7 km square grid. But to remain the accordance with typical supercells diameter I should enhance the commonly used values by a factor that varies from 5 to 12, according to weighting function which is growing with the distance from a square centre. (Parfiniewicz, EXPO2013).

Let's turn to Nowcasting and Forecasting SCE. The 3 categories are highlighted to distinguish between Nowcast and Forecast: ,i.e., lead time, the method used, and finally the targeted product. For lead time: we have tens of hours against 1 hour, for methodology: probabilistic interpretation of the model against tendency plus probabilistic interpretation plus possibly HD accurate simulations - if occurred, and finally: danger zones against accurate location. The successful nowcasting in fact is measured in minutes (after James Anderson, EXPO2013). What we have now in Poland on (http://awiacja.imgw.pl/index.php?product=burze) is the Observed Storms category which serves merely as an introduction to Nowcasting SCE showing their possible growth or decay and helps to understand how will they propagate.

References

[1] Anderson J., 2013: Generating intelligent weather forecasts and advanced alerting with real-time observations. *Meteorological Technology World Expo 2013*, Brussels, Belgium, 15 -17 oct.

[2] Parfiniewicz J., 2013: On thunderstorm quantification. *COSMO Newsletter No. 13*, April 2013 (http://www.cosmo-model.org/content/model/documentation/newsLetters).

[3] Parfiniewicz J., 2013: Nowcasting strong convective events (SCE) – the Thunderstorm Thermometer. *Meteorological Technology World Expo 2013*, Brussels, Belgium, 15 -17 oct.

[4] www.ukintpress-conferences.com/uploads/SPMTWX13/Breakout_Session_d2_s2_p5 _Jan_Parfiniewicz.pdf

COSMO in Single Precision

Stefan Rüdisühli, André Walser, and Oliver Fuhrer

MeteoSwiss, Zürich

Abstract

Reducing arithmetic precision in a numerical weather prediction model, and thus reducing the number of bytes required to store a floating point number, can be advantageous for an application such as COSMO both in terms of runtime and memory consumption. But, since the COSMO model has been written and applied only using double precision floating point numbers, reducing arithmetic precision requires careful consideration. In this article, we present the modifications necessary to the COSMO model to reduce the arithmetic precision of floating point numbers to single precision. Using concrete examples from the current code that did not work in single precision, we illustrate critical algorithmic patterns that should receive special attention from developers in order not to rely on double precision in the future. We present results from detailed tests as well as a standard verification of the newly developed model version. Results indicate that the new version exhibits the same forecast skill as the reference version, both in single and double precision mode. In single precision, the runtime drops to $\approx 60\%$ and memory consumption is reduced considerably, as compared to the double precision mode.

1. Introduction

Numerical Weather Prediction (NWP) models consume immense amounts of computer resources and, as a consequence, electrical energy. Model development and application is thus constrained by both monetary and technical limits. Considering the ever-increasing demand for computer resources, fueled by current trends such as cloud-resolving modeling or ensemble predictions, techniques to make models faster and more energy efficient are highly welcome.

One approach which promises a significant speedup is running models with reduced arithmetic precision. Current computer hardware typically supports floating point computations in single precision (SP) and double precision (DP). While it is still customary to use DP for NWP, reducing arithmetic precision to SP has several advantages. First and foremost, less information has to be moved to the floating point unit of the microprocessor in order to perform a computation. Second, microprocessors are typically capable of performing more floating point operations per second (FLOPS) in reduced precision. Third, the memory consumption of an application can be significantly reduced. Often, reducing the arithmetic precision of an application can be achieved with relatively little changes to the code, as compared to other approaches such as code optimization or porting to more efficient hardware such as GPUs. The latter often requires substantial code modifications or even partial rewrites. Several other weather and climate models are already capable of running in SP [5, 3] or are in the process of being adapted to SP [2].

In this article, we present the steps which are required to adapt the COSMO model to run in SP. In the new code version, the working precision (WP) of the model can be chosen using a single switch. By means of extensive validation, we show that our adapted code in DP can replace the previous code, and that it's skill in SP should be sufficient for many applications. We confirm and build upon findings of preliminary work, which showed that not only the dynamical core [4], but the whole model can be run in SP (Despraz and Fuhrer, *pers. comm.*) without significant loss in forecast quality, and with only few changes to the code.

2. Background

2.1. Floating Point Numbers and Precision

Floating point numbers (FPNs) on computers are stored in binary form. They consist of three parts: the sign (plus/minus), the exponent (order of magnitude), and the mantissa (significant digits). On most common hardware architectures, the representation of FPNs follows a standard [1] on most current microprocessors. This standard defines how FPNs are stored in binary form and how operations between two FPNs have to

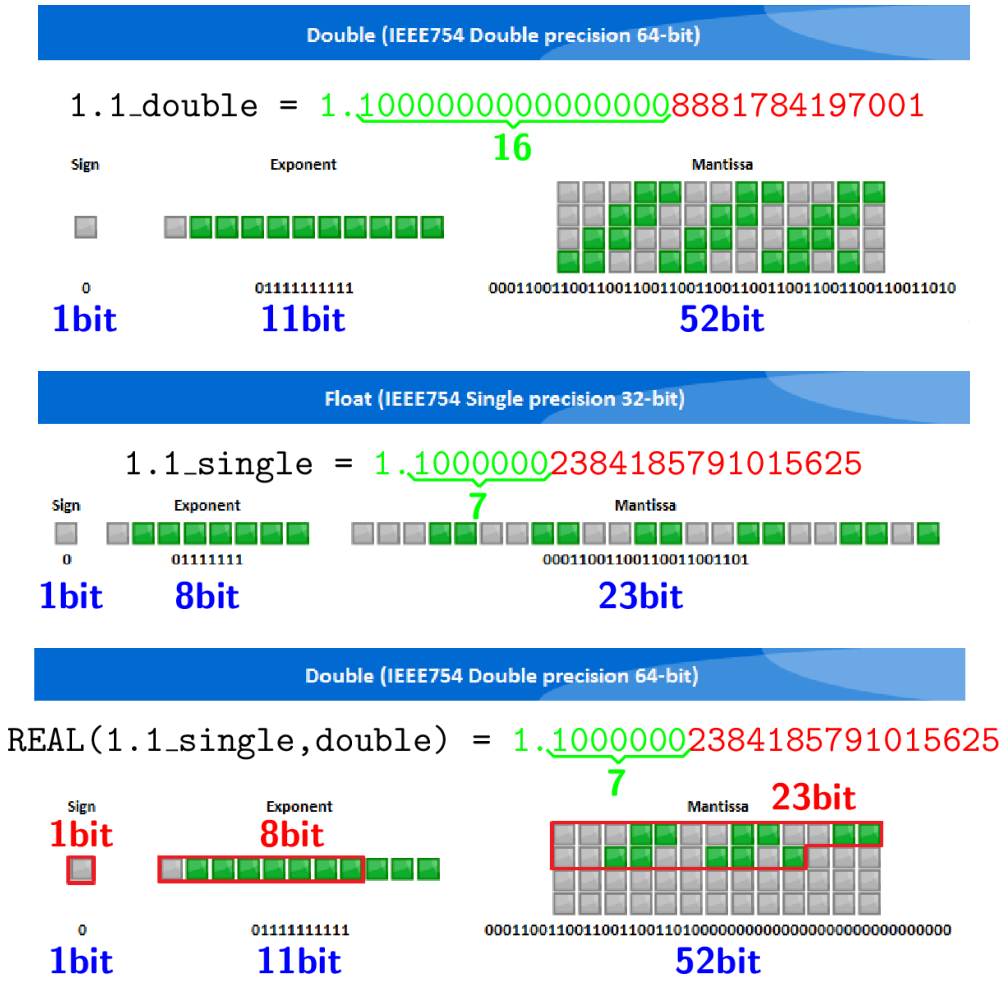

FIGURE 1: Binary representation of DP and SP floats on computers using the example of 1.1. Each square corresponds to one bit, grey standing for 0 and green for 1. The number of bits of all three components of FPNs is indicated. They add up to 64 and 32 bits for DP and SP, respectively. In DP (top), 1.1 is accurate to 16 decimal digits behind the decimal point, but only to 7 decimal digits in SP (center). If 1.1 in SP is assigned to a DP variable (bottom), only the first 23 bits of the mantissa carry information (red border). All bits outside this area are 0, which reduces the accuracy to 7 decimal digits behind the decimal point. *Source:* `http://www.binaryconvert.com`

be implemented. The magnitude and precision ranges of FPNs in DP and SP are listed in Table 1. How FPNs are stored in binary form is illustrated in Figure 1, using the number 1.1 as an example. The top and center panels show how the example FPN is stored in binary form in DP and SP, respectively. If converted from binary to decimal form, the number of significant decimal digits after the floating point is 16 and 7, respectively, determined by the size in bits of the mantissa. The digits beyond (marked red) may seem to be random, but they are not. They are the deterministic product of the conversion from binary to decimal. This is illustrated in the bottom panel, where 1.1 in SP resolution is shown in DP. The difference between the FPNs resulting from the conversion (i.e. `1.1_double-REAL(1.1_single,double)`) stems from the bits which are 1 (green) in the top, but 0 (grey) in the bottom panel.

precision	total size	max	min	digits	precision
single	32 bit	10^{38}	10^{-38}	7.2	10^{-7}
double	64 bit	10^{308}	10^{-308}	16.0	10^{-16}

TABLE 1: Magnitude and precision ranges of SP and DP FPNs according to the IEEE 754 standard. The maximum and minimum magnitudes are determined by the size of the exponent, the number of digits by the mantissa. The precision of FPNs on the order of 1.0 is determined by the number of digits.

2.2. Precision in Fortran

In Fortran, FPNs are represented by the basic type real. Typically reals are SP by default, although this may depend on the specific compiler used. To ensure a program runs in a certain precision, the kind of every real variable as well as of every FPN in the program has to be declared explicitly, which determines the number of bytes used to store a real. It is set with an integer parameter. Often, it directly corresponds to the size a FPN in bytes, i.e. 4 and 8 for SP and DP, respectively. As this is platform-dependent, however, intrinsic routines are provided to obtain the correct values. The kind parameter used in COSMO is called `ireals`[3]. How it is used to set the precision of variables, of FPNs, as well as in type conversions is illustrated with the following line of code. A real variable is defined and initialized to the sum of a FPN and an integer variable.

```
REAL(KIND=ireals) :: var = 3.5_ireals + REAL(intvar,ireals)
```

If the '`_ireals`' following a FPN (3.5 in this case) is omitted, it is typically defined in SP by default. This introduces arbitrary inaccuracies of relative order of magnitude $O\left(10^{-7}\right)$ as illustrated in Figure 1.

2.3. Epsilons

Epsilons are small numbers used for various numerical purposes in a code. They are used to account for inaccuracies resulting from the limited ability of computers to represent FPNs. Furthermore, they are used as tolerances in both numerical and physical contexts. Three examples of popular applications of epsilons are the following.

1. In divisions to avoid division by zero (DBZ), e.g. `x = y / MAX(z,eps)`[4].
2. In comparisons of FPNs, e.g. `IF (ABS(a-b) < eps) equal = .TRUE.`).
3. In iterations as abort criteria, e.g.
   `IF (MAXVAL(ABS(p_new(:,:,:)-p_old(:,:,:))) < eps_abort) EXIT.`

Two basic kinds of epsilons can be distinguished. On the one hand, there are those epsilons the magnitude of which is only determined by the precision. On the other hand, many epsilons additionally have some meaning in an algorithm or physical context, which puts additional constraints on the magnitude. These two basic kinds will henceforth be referred to as *precision-limited* and *algorithmic* epsilons. Note that algorithmic epsilons are precision-limited, too, as, after all, all FPNs are. This means that the subsequently described limitations apply to them as well, but *precision-limited* will refer exclusively to those epsilons upon which no further limitations of algorithmic or physical nature are imposed.

Precision-limited epsilons can be further classified according to the factor which determines their minimal magnitude. To which group a specific epsilon belongs depends on it's context of use. Either the limiting factor is the minimal order of magnitude (*range-limited*) or the maximal number of decimal digits (*digit-limited*) that can be resolved, i.e. the exponent or mantissa, respectively. Range-limited epsilons are used to avoid floating point exceptions (FPEs) in operations where zero is not allowed as an operand, such as divisions or logarithms. Digit-limited epsilons, on the other hand, are used to account for inaccuracies in comparisons of FPNs.

The epsilon in the first of the three examples above is range-limited, and that in the second is digit-limited. Both are precision-limited epsilons. That in the third example is also digit-limited, but probably has some additional algorithmic constraints. However the distinction between precision-limited and algorithmic epsilons is not always straight-forward, and the context has to be taken into account in all but the most obvious cases. The epsilon in example two, for instance, might need to be bigger in certain algorithms with unusually large error growth, which would make it algorithmic. Also, using the minimal representable positive number larger than zero in the first example, may lead to erroneous results later on in the computation if the algorithm has not been designed carefully (for example by limiting the maximum result of the division to a physically reasonable value). However, it is most important to make this distinction in obvious cases where it is easy to draw the line, such as if the epsilon carries a physical unit.

Range-limited epsilons can theoretically be as small as 10^{-37} and 10^{-307} in SP and DP, respectively. However the magnitude of the dividend must be taken into account to avoid arithmetic overflow, e.g. if it is on the

[3] It is currently planned to unify the constant used to denote the WP across the COSMO, ICON, and 3DVAR codes. It is likely that in the future `ireals` will be renamed to `wp` which has the advantage of brevity.

[4] Note that this is only valid if `z` is strictly positive.

order of 10^7 the epsilon must be at least of magnitude 10^{-30} and 10^{-300}. As these values are still minuscule in a NWP model such as COSMO, it is sufficient to simply chose a value a couple of orders of magnitudes (e.g. 10^8) above the absolute minimum without further considerations, even in SP.

Digit-limited epsilons, on the other hand, must have a minimal magnitude – relative to 1.0 – of 10^{-7} and 10^{-16} in SP and DP, respectively. Taking into account the order of magnitude of the involved numbers is much more important than in the range-limited case, especially in SP, since 10^{-7} is not far from physical significance in many cases, for example for trace gas concentrations. Simply increasing the epsilon by some orders of magnitude to account for the magnitude of the other involved numbers is thus not a good solution. Rather the relative character of digit-limited epsilons should be accounted for in the way they are used in the formula, i.e. by not inserting them by addition (`a < b + eps`), but by multiplication (`a < (1.0 + eps)*b`). This much more robust implementation ensures that the epsilon does not vanish when large numbers are involved. Note that such a relative-epsilon implementation is more difficult when trying to determine the equality of two FPNs, e.g. `ABS(a-b) < eps`. Making the epsilon relative in this case would result for instance in `ABS(a-b) < ABS(a)*eps`, which is already quite complicated.

2.4. Numerical Errors

Numerical error growth can be minimized if certain formulas are written in a numerically robust form. What should be avoided wherever possible are subtractions of very similar numbers, as well as raising numbers to high powers. This is usually not a major concern in DP. In SP, however, error growth from such subtractions can be substantial, and high powers may even provoke arithmetic under- or overflow, leading to model crashes.

A good example to illustrate precision loss in subtractions of similar numbers is the computation of a small difference between two temperatures, e.g. `274.00000 - 273.15000 = 0.85000???`. In this case, three significant digits are immediately lost, as indicated by the three trailing digits in the result, which are subject to rounding error. An epsilon inserted by addition (which, unfortunately, is the usual practice) in such a formula in SP must be at least of absolute magnitude 10^{-5} in order not to completely vanish. This has to be considered when using epsilons in such cases by either increasing their magnitude or inserting them by multiplication. This is a common problem with temperature and pressure, which can easily be avoided if deviations from some reference are used instead of absolute values.

3. Changes to the Code

The COSMO model has been developed for and tested in DP. Therefore, there are many places in the code where something goes wrong in SP that works perfectly fine in DP. This has required us to conduct a variety of changes to the code to run COSMO in SP. These modifications can be broadly grouped into three categories.

- Obtain a pure DP code by adding all missing `ireals` declarations.
- Conduct various local changes.
  - Add epsilons to divisions to prevent FPEs by DBZ.
  - Adapt epsilons which might vanish in SP to be precision-dependent.
  - Optimize formulas that might cause numeric overflow or other problems.
- Implement mixed precision (MP) form of radiation.

3.1. Ireals declarations

The real kind parameter `ireals` in COSMO, which determines the WP, is set to DP by default. However, a large number of `ireals` declarations are missing in the current code, which introduces many SP reals into the model, thereby lowering the precision. The first step is therefore to add all these missing declarations in order to obtain a code running in pure DP. Because of the large number of missing declarations (see Table 2), we have written a script which automatically finds and declares all undeclared real variables and FPNs.

The consequence of the additional `ireals` declaration is that the model results of the new code differ from those of the old code (numerically, not meteorologically). This difference is due to the removal of the inaccuracies introduced by the undeclared reals, which corresponds to a perturbation of relative order of magnitude $\mathcal{O}\left(10^{-7}\right)$. Validation of this pure DP code by means of comparing results against simulations with random perturbations of similar magnitude is provided in Section 4.1.1. It is worth noting that these changes are the

only ones we have introduced which cause different model results in DP. All other code changes are neutral in DP and only have a significant effect in SP.

	nf	nf*	nold	del	del%	del%*
src_*	60	43	6276	4299	68.5	81.9
data_*	27	4	791	1141	144.3	967.0
rest	44	25	3026	682	22.5	26.6
total	133	72	10093	6122	60.7	76.2

nf	total number of files	del	number of _ireals added (delta)
nf*	number of changed files	del%	relative delta (all files)
nold	initial number of _ireals	del%*	relative delta (only changed files)

TABLE 2: Statistics of occurrences of `ireals` declarations before and after our modifications. The source files are sorted into three groups. Overall,we have added roughly 60% additional declarations.

3.2. Local Modifications

A number of local modifications are necessary to run COSMO in SP. They are listed in detail in Table 3. Those which are critical for the model not to crash in SP are emphasized.

3.2.1. Critical Epsilons

Epsilons are either range- or digit-limited, as established in Section 2.3. To account for this, we have introduced the two precision-dependent parameters *repsilon* and *rprecision*. They are defined in *data_parameters.f90* as shown below. Their magnitudes in SP/DP are $10^{-30}/10^{-300}$ and $10^{-7}/10^{-16}$, respectively.

The values chosen for epsilons in COSMO are typically between `repsilon` and `rprecision` in SP, for instance 10^{-15} or 10^{-8}. Thus they are big enough for range-limited cases, but might vanish in digit-limited contexts. Therefore, in range-limited cases, i.e. mostly in divisions, problems occurred in places where there had not been an epsilon previously, and we have had to add epsilons, predominantly in divisions where the divisor vanishes in SP. In digit-limited cases, on the other hand, an epsilon was usually already present in places where problems in SP occured, but with a too small magnitude. Thus, we have usually had to identify the respective epsilon parameter and limit is's magnitude to `rprecision` in SP using the `MAX()` function. Additionally, in some places, instead of a parameter a hard-coded epsilon has been used, e.g. 10^{-30}, usually in divisions. We have replaced those by epsilon parameters. The chosen magnitude of these hard-coded epsilons has usually not been critical in SP, except for one case where 10^{-50} was used.

In most cases, epsilon-related problems in SP manifested themselves in model crashes or deadlocks, i.e. were rather easy to recognize and track down. In one case where an epsilon vanished in SP, however, the implications were much more subtle, namely only impacted the model physics, and the problem was accordingly much more difficult to identify and resolve. This case is described in detail in Section 4.2.1.

data_parameters.f90

```
161   REAL (KIND=ireals), PARAMETER  ::                                  &
162        repsilon = 1.0E8_ireals*TINY(1.0_ireals),                     &
163                !
164                ! Very small number near zero.
165                ! To be used mainly to avoid division by zero, e.g.
166                ! eps_div = repsilon ; x = y / MAX(z,eps_div) ! for z >= 0.
167                ! Note that the factor 1.0E-8 has been chosen rather
168                ! arbitrarily to get some distance to zero to account
169                ! for the magnitude of the dividend, which might be 1.0E5
170                ! in case of pressure, for instance.
171                !
172
```

File	Modifications
data_obs_lib_cosmo	**limit `epsy` to `rprecision` in SP**
data_soil	new epsilons: ∘ `eps_div` - avoid DBZ ∘ `eps_soil` - threshold for computations ∘ `eps_temp` **- check if temperature below zero**
data_turbulence	replace `epsi` by `eps=repsilon`
near_surface	remove `zepsi`, use `repsilon` instead
numeric_utilities	∘ remove local epsilons (`zeps`) ∘ introduce module-wide variable `eps_div` instead
numeric_utilities_rk	∘ remove `zeps` ∘ new epsilons `eps_div` and `eps_adv`
organize_data	add definition of `epsy`
pp_utilities	∘ rename `eps` to `eps_conv` ∘ **reformulation** `m2s**4/m3s**3` →`m2s*(m2s/m3s)**3`
src_gscp	∘ replace `zeps` by `repsilon` where used as small number ∘ **reformulation** `m2s**4/m3s**3` →`m2s*(m2s/m3s)**3`
src_lheat_nudge	replace `epsilon`/`epsy` by `epsy` from *data_obs_lib_cosmo.f90*
src_obs_cdfin_print	use `epsy` from *data_obs_lib_cosmo.f90*
src_obs_cdfin_util	use `epsy` from *data_obs_lib_cosmo.f90*
src_obs_rad	add `ireals` to `REAL()`
src_output	replace `EPS` by `repsilon`
src_setup	add output `RUNNING IN DOUBLE/SINGLE PRECISION`
src_soil	replace `zepsi` by `eps_soil` from *data_soil.f90* or by `repsilon`
src_soil_multlay	replace `zepsi` by `eps_*` from data_soil
turbulence_tran	replace `epsi` by `eps` (both from *data_turbulence.f90*)
utilities	∘ **replace hard-coded `1E-50` by `repsilon`** ∘ **overload `check_field_NaNs()` for SP/DP**

TABLE 3: Detailed overview over conducted all changes, except those related to `ireals` declarations and the mixed precision (MP) radiation. Critical modifications are emphasized. These are necessary for the code to compile and run in SP, whereas the others can be considered code cleanup. Note that a number of epsilons added to divisions to avoid DBZ are not listed explicitly in this table.

data_parameters.f90

```
172        rprecision = 10.0_ireals**(-PRECISION(1.0_ireals))
173                !
174                ! Precision of 1.0 in additions/subtractions.
175                ! To be used for instance to check equality of reals, e.g.
176                ! eps_fpn = rprecision ; IF (ABS(a-b) < eps_fpn) equal=.true.,
177                ! or to increase the magnitude of an epsilon only in SP, e.g.
178                ! epsilon = MAX(1.0E-8_ireals,rprecision) when 1E-8 is too small
179                ! but the value should stay the same in DP.
180                !
181                ! Approximate magnitudes:
182                ! -----------------------
183                !
184                !       | repsilon | rprecision
185                !   ----+----------+------------
186                !    SP |  1.0E-30 |   1.0E-7
187                !   ----+----------+------------
188                !    DP | 1.0E-300 |  1.0E-16
189                !
```

3.2.2. Non-Critical Epsilons

Many of the epsilon-related changes listed in Table 3 are not strictly necessary to run COSMO in SP, but we have taken the opportunity to do some code cleanup, as the use of epsilons in the model is far from consistent, which is no surprise considering the large number of different people that have contributed it. Whereas in some parts of the code, such as the assimilation, centrally defined epsilons used by multiple source modules already exist, in other parts epsilons are defined very locally, i.e. on the subroutine level. In some cases the same epsilon parameter has been defined many times per file. This might be appropriate in special cases, such as utility routines, which should be as self-contained as possible. In most cases, however, one single definition of an epsilon per file is a much better and cleaner solution.

Soil Model

In the soil model (*src_soil.f90, src_soil_multlay.f90*) the same epsilon *zepsi* has been used for various purposes. We have replaced *zepsi* by the three new variables `eps_soil`, `eps_div`, and `eps_temp` Their definitions and descriptions are shown in the following code excerpt.

data_soil.f90

```
249   REAL  (KIND=ireals), PARAMETER :: &
250
251     ! Avoid division by zero, e.g. x = y / MAX(z,eps_div).
252     eps_div  = repsilon       , &
253
254     ! Threshold for various computations in soil model (former zepsi).
255     eps_soil = 1.0E-6_ireals  , &
256
257     ! Small value to check if temperatures have exceeded a fixed threshold
258     ! such as the freezing point.  In double precision (16 decimal digits)
259     ! a value as small value such as 1.0E-6 can be used. In single
260     ! precision (6-7 decimal digits), however, the value has to be larger
261     ! in order not to vanish. The current formulation is save for
262     ! temperatures up to 500K.
263     eps_temp = MAX(1.0E-6_ireals,500.0_ireals*EPSILON(1.0_ireals))
```

Assimilation

In the assimilation, there is one general-purpose epsilon variable called `epsy`, which is centrally defined in *data_obs_lib_cosmo.f90* and used in the files listed below.

data_obs_lib_cosmo.f90

```
 87   REAL    (KIND=ireals)        , PARAMETER  :: &
 88     epsy   = 1.0E-8_ireals    ,&! commonly used very small value > 0
```

- organize_assimilation
- src_correl_cutoff
- src_gather_info
- src_lheat_nudge
- src_mult_local
- src_mult_spread
- src_nudging
- src_obs_cdfin_blk
- src_obs_cdfin_comhead
- src_obs_cdfin_gps
- src_obs_cdfin_mult
- src_obs_cdfin_org
- src_obs_cdfin_print
- src_obs_cdfin_sing
- src_obs_cdfin_util
- src_obs_cdfout_feedobs
- src_obs_print_vof
- src_obs_proc_air
- src_obs_proc_aof
- src_obs_proc_cdf
- src_obs_processing
- src_obs_proc_util
- src_obs_use_org
- src_sfcana
- src_sing_local
- src_sing_spread

As the vast number of files suggests, `epsy` is used in a large variety of contexts, both precision-limited and algorithmic, and even physical. It's magnitude of 10^{-8} is a well thought-out compromise between all those use cases. While this works well in DP, we have run into problems in SP. For example, in one place, `epsy` is used in an abort criterion of an iteration. As it is digit-limited in this context, the minimal relative magnitude required is 10^{-7}. Because `epsy` is smaller (10^{-8}), it vanishes and the loop never terminates. We have fixed this by limiting `epsy` to `rprecision` in SP in-place.

src_gather_info.f90

```
4168       ELSEIF (    MAX( zwts1t1,zwts1t2 ) &
4169                 >= MAX( zwts0t1,zwts0t2 )+MAX(epsy,rprecision)) THEN
 ...
4172       ELSEIF ((    MAX( zwts1t1,zwts1t2 ) &
4173                  >= MAX( zwts0t1,zwts0t2 )-MAX(epsy,rprecision)) &
4174         .AND. (zwts1t2 > zwts0t2+epsy)) THEN
```

There are, however, many similar places in the code where `epsy` is not used in a robust way and might thus potentially cause problems. Globally limiting `epsy` to `rprecision` in SP is not a solution, because `epsy` is also used in physical contexts. Therefore, increasing it's magnitude in SP would have undesired impacts on the model physics. The many different contexts in which `epsy` is used, along with it's vast number of occurrences, suggest it might be advisable to replace it by several purpose-specific epsilons, analogous to our epsilon implementation in the soil model. However, such a clean implementation which would be robust in SP has not been done yet. We have only limited `epsy` to `rprecision` in-place in some critical cases, such as the one shown above, as a preliminary solution.

3.2.3. Optimized Formulas

We have conducted some reformulations of critical formulas to increase their accuracy and stability in SP, i.e. to avoid large error growth and model crashes. In addition, we have tested two reformulations for the numerical error they introduce in SP.

Critical Reformulations

There is one formula in the code which consitently caused the model to crash in SP in it's previous formulation (commented out in the code below). It occurs once in *pp_utilities.f90* and twice in *src_gscp.f90*.

pp_utilities.f90

```
3094 !    zn0s = 13.50_ireals * m2s**4 / m3s**3
3095      zn0s = 13.50_ireals * m2s*(m2s/m3s)**3
```

The values of `m2s` and `m3s` are on the order of 10^{-6} and 10^{-10}, respectively, plus/minus 2 orders of magnitude, i.e. both are already very small numbers before they are raised to higher powers. However as they are, they become minuscule, and `m3s**3` might even vanish in SP when it becomes $< 10^{-38}$, which causes FPEs due to DBZ. A simple reordering of the terms of the formula resolves the problem. In the new formulation the dividend and the divisor are both moderately small instead of minuscule numbers, as is the result of the division, and the third power does not cause any more issues.

Potential Precision Loss

Two potentially critical formulations in *src_radiation.f90* have been identified in previous work (Despraz and Fuhrer, *pers. comm.*). Both can be formulated in a different way, which might improve numerical accuracy. The first formula involves a sine and cosine of a variable. In the original code, the cosine is not computed directly from the operand, but from the sine, which saves an extra cosine array. However, computing it directly from the operand, without the intermediate sine, might be numerically more precise.

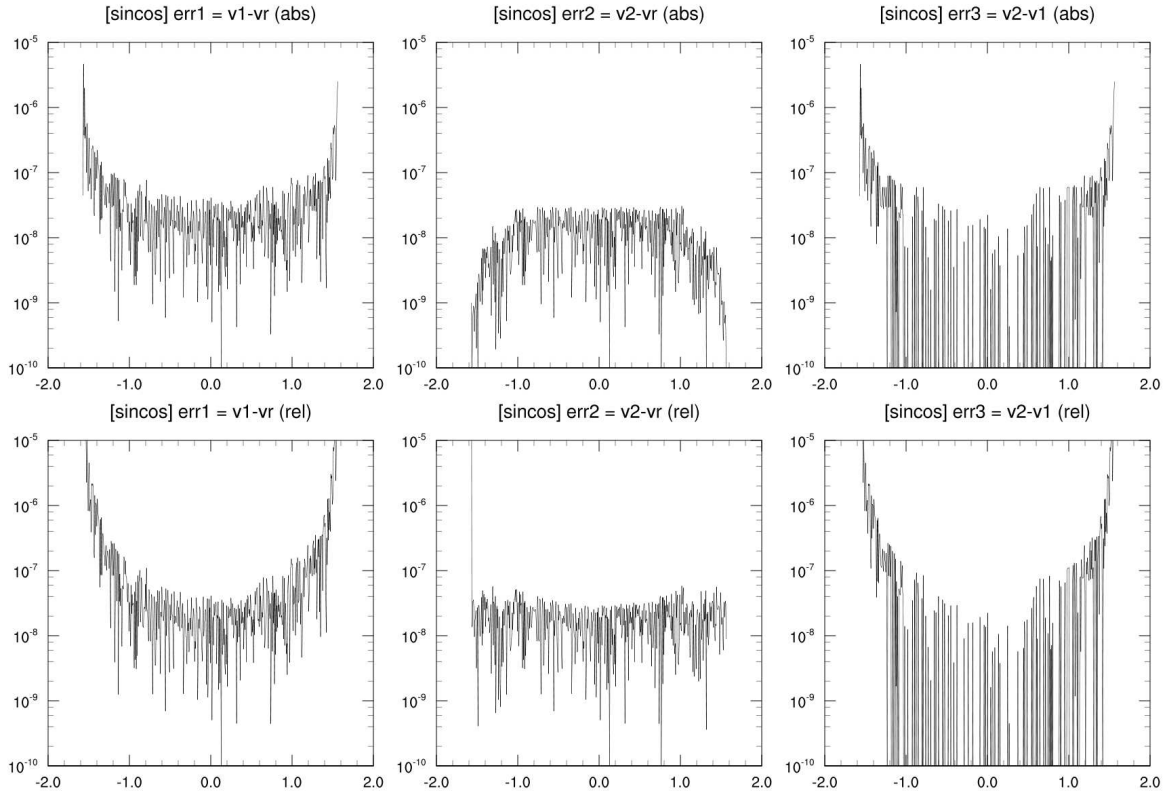

FIGURE 2: Numerical error in SP compared to $cos_x = cos(x)$ in DP of $cos_x = \sqrt{1 - sin(x)^2}$ (left) and $cos_x = cos(x)$ (center), as well as the difference between them (right). The difference corresponds to the gain in precision when substituting $cos_x = \sqrt{1 - sin(x)^2}$ by $cos_x = cos(x)$. The top panels show the absolute error, the bottom panels the relative error.

src_radiation.f90

```
1006        zsinphi  = SIN (degrad*(90.0_ireals-ABS(pollat)))
1007        zcosphi  = COS (degrad*(90.0_ireals-ABS(pollat)))
1008      ELSE
1009        zsinphi  = SIN(rlat(i,j) )
1010        zcosphi  = COS(rlat(i,j) )
1011      ENDIF
1012 !!     zcosphi  = SQRT(1._ireals-zsinphi**2)
 ...
2140             DO  i = 1, ie_tot
2141               zsinphi(i)      = SIN (rlattot(i,js))
2142               zcosphi(i)      = COS (rlattot(i,js))
2143             ENDDO
```

The second formula involves two formulations of the form $\left(1 - a^2\right)$, which can be reformulated to $(1 - a)(1 + a)$. Eliminating the square might be favorable in terms of numerical precision.

src_radiation.f90

```
5959 !!      pa1f(j1,j2) = ztau*(1.0_ireals-(zrho**2)) &
5960 !!                         *(1.0_ireals/(1.0_ireals-(zrho**2)*(ztau**2)))
5961       pa1f(j1,j2) = ztau*(zrho-1.0_ireals)*(zrho+1.0_ireals) &
5962                           /((zrho*ztau-1.0_ireals)*(zrho*ztau+1.0_ireals))
```

To assess the gain in precision in SP of the supposedly better formulations, we have computed the error of both formulations in SP relative to the better supposedly formulation in DP for all possible values. The errors

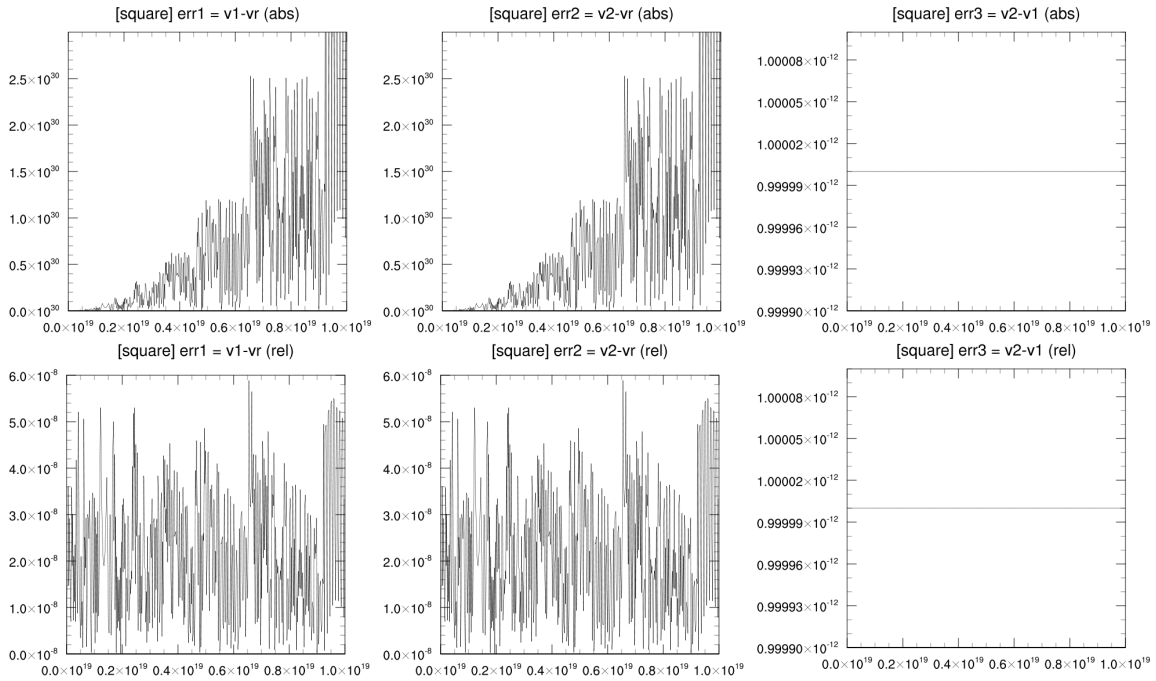

FIGURE 3: As in Figure 2, but for $1 - a^2$ (left) and $(1 + a)(1 - a)$(center) in SP relative to $(1 + a)(1 - a)$in DP. In this case, both formulations are totally equivalent with respect to precision.

in SP relative to DP, as well as their difference, are shown in Figures 2 and 3. The left and center panels show the error in SP of the old and new formulations, respectively. The difference between them in the right panels corresponds to the gain of using the supposedly better formulation. In case of the first formula, this gain is significant, which is why we have replaced the old formulation in the code. In case of the second formula, on the other hand, there is no gain, i.e. both formulations perform equally well in SP.

3.3. Mixed Precision Radiation

The only part of the code where substantial modifications are necessary to run it in SP is the radiation, which in it's current form has to run partly in DP regardless of the model's WP. It should be noted that we have not proven the algorithms in the radiation code to strictly require DP but rather have simply not succeeded in finding the critical modifications required to enable SP also for the radiation code.

The subroutine structure of *src_radiation.f90* is shown in Figure 4. The subroutines always running in DP are highlighted in yellow, those that are critical in orange. Figure 5 shows the dataflux between the main radiation subroutines, as well as that between them and the radiation data module, again with the critical and the DP subroutines highlighted. The dataflux by argument arrays at the interface of the WP and the DP part of the code (i.e. the calls to `fesft()` and `opt_th/so()`) is organized in such a way that the precision conversion of the `IN`-arrays is handled by the calling, and that of the `OUT`- and `INOUT`-arrays by the called subroutines[5].

The critical subroutines that only work in DP are the inversion routines `inv_th/so()`, along with their sub-subroutines `coe_th/so()`. Although `fesft()` works fine in SP, we have included it in the DP-part of the radiation because `inv_th/so()` are called so often by `fesft()`. If the conversion to DP and back were done on each of these calls, the model would be slowed down considerably. The second pair of subroutines called by `fesft()` are `opt_th/so()`. We have chosen to run them in WP despite their calling subroutine being run in DP, although this requires conversion of all argument arrays to WP and back on all calls. These conversions, however, do not effect the runtime as those on calls to `inv_th/so()` would, and the gain in terms of code simplicity is substantial. All arrays from *data_radiation.f90*, except for `cobi`, `coali`, `cobti`, `coai`, `planck`, `solant`, `zketypa`, and `zteref`, are only used in `opt_th/so()`[6]. Running `opt_th/so()` makes any DP

[5]Note that conversion is only done if necessary, i.e. if the model is run in SP. If the WP is DP, direct assignment is sufficient and the conversion is omitted.

[6]They are also used in `init_radiation()`, but this subroutine is always run in WP anyway.

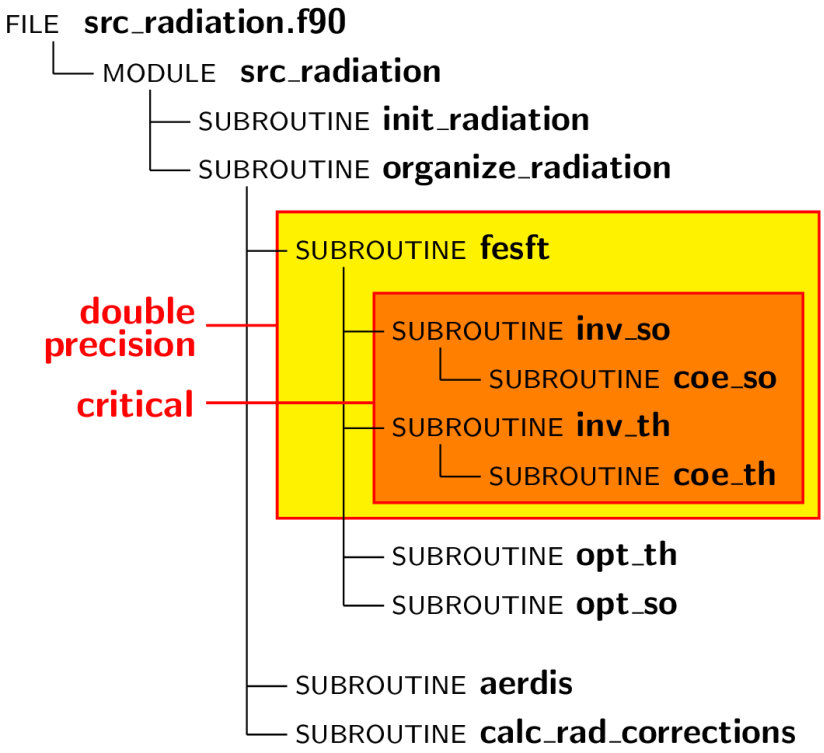

FIGURE 4: Structure of the source file *src_ radiation.f90*. The subroutines are nested according to how they call each other, the called subroutines indented with respect to the caller. The orange box encloses the subroutines that are critical with respect to precision, i.e. need to be run in DP regardless of the WP. The DP part has been expanded to what is enclosed by the yellow box due to performance considerations.

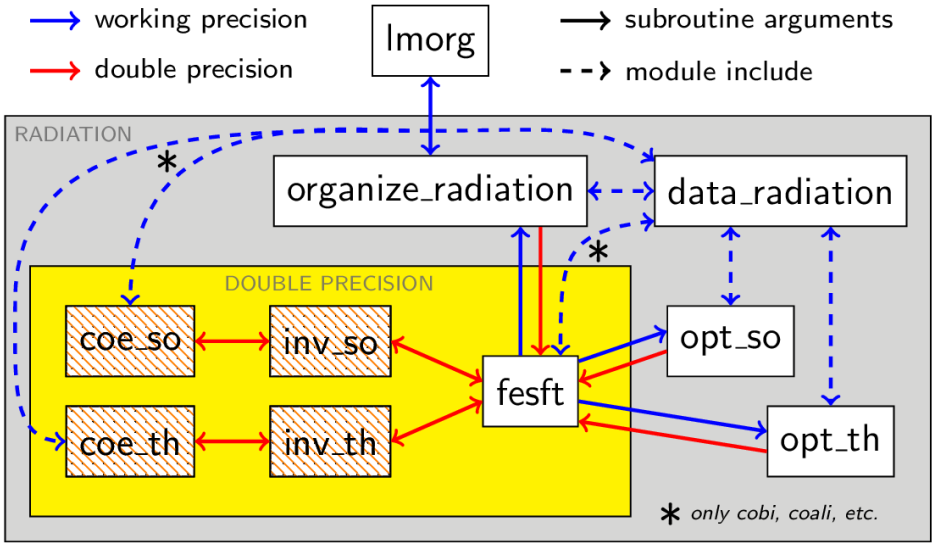

FIGURE 5: Data flux between the subroutines of the MP radiation. The DP part is enclosed by the yellow box, and the critical subroutines that only work in DP are emphasized by orange stripes. Solid arrows show data flux as array arguments, and dashed arrows show data exchange through the shared data module. Data flux happens in WP along blue arrows and in DP along red arrows. The precision transformation of `INOUT`- and `OUT`-arrays is handled by the called routine, wherease the handling of `IN`-arrays is left to the caller. Module data is only used by WP-subroutines, with the exception of the arrays `cobi`, `coali`, `cobti`, `coai`, `planck`, `solant`, `zketypa`, and `zteref`. The precision transformation of these arrays is handled by the DP subroutines that use them.

declarations of arrays in *data_ radiation.f90* unnecessary and thus restricts the changes to *src_ radiation.f90*. The three exceptions are handled by the DP subroutines using them.

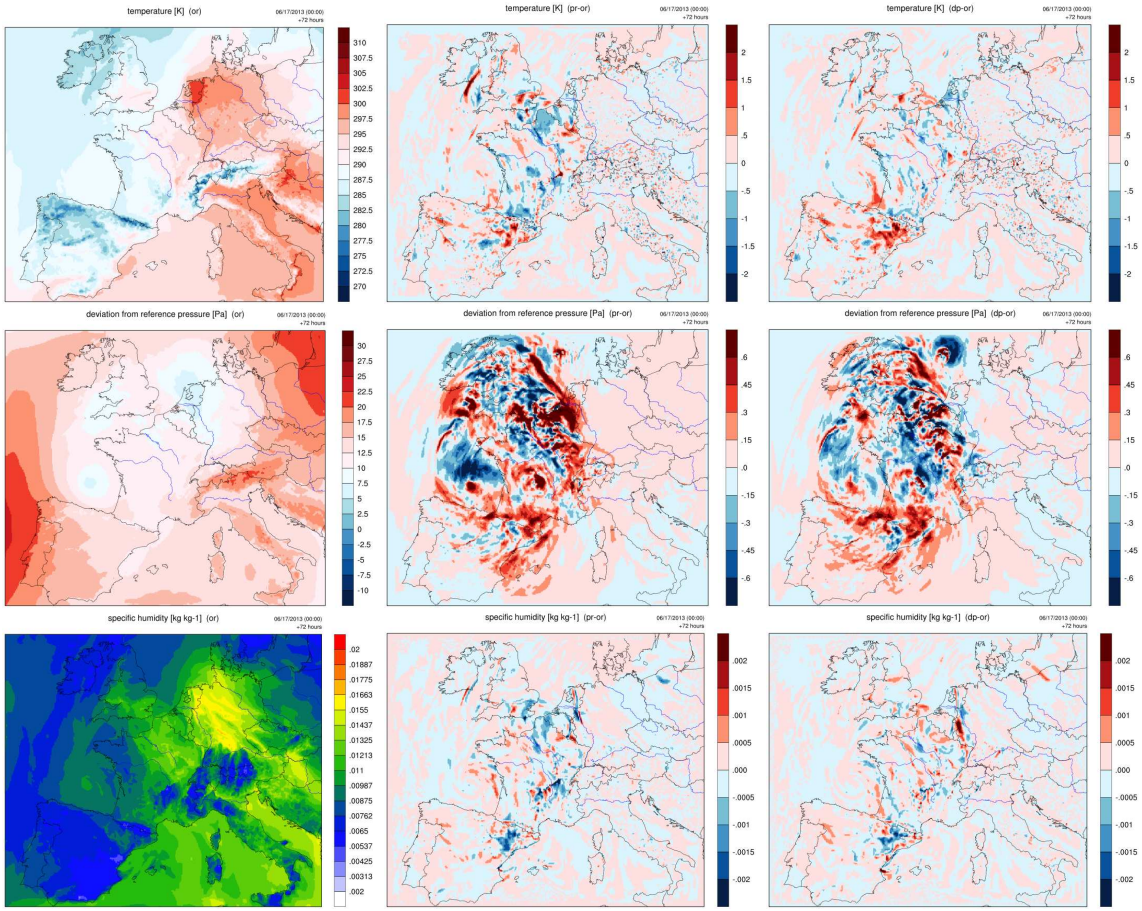

FIGURE 6: Results of the perturbation sensitivity experiments for temperature (top), pressure deviation (center), and specific humidity (bottom). The left panels show the absolute fields of **OR**, those in the center the deviations **PR-OR**, and those on the right **DP-OR**on the lowermost model level after 72h. The deviations **PR-OR** are comparable in magnitude to those of **DP-OR**.

4. Experiments and Results

To asses the performance of the new code, we have chosen a two-step approach. First, we conduct sensitivity experiments to test it from a numerical point of view. Second, we test it's performance against observations.

4.1. Sensitivity Experiments (COSMO-7)

To validate the new code from a numerical standpoint, we have conducted two major sets of sensitivity experiments. In a first step, we validate it in DP by simulating the effect of the additional `ireals` declarations. In a second step, we assess its performance in SP. The aim of these sensitivity experiments is to get a general feeling for the magnitude of the deviations between various code versions in a realistic setup, without aiming for meteorological representativeness. We use data from a period from last summer (June 17-19 2013). The model setup corresponds to MeteoSwiss operational COSMO-7 setup with a lead time of 72h.

4.1.1. Perturbation Experiments

The new code in DP, subsequently referred to as **DP**, will replace the original code (**OR**). Therefore, it is of high importance to make sure it yields results of equal quality. There are apparent differences between the results of the new and the original code. Considering the code changes we have carried out, those differences should be dominated by the effect of the correct type declaration of previously erroneously typed FPNs documented in Section 3.1. These may be seen as a random perturbation of relative magnitude $\mathcal{O}\left(10^{-7}\right)$. To assess the impact of such perturbations on the model physics, we have developed a new code (**PR**) based on

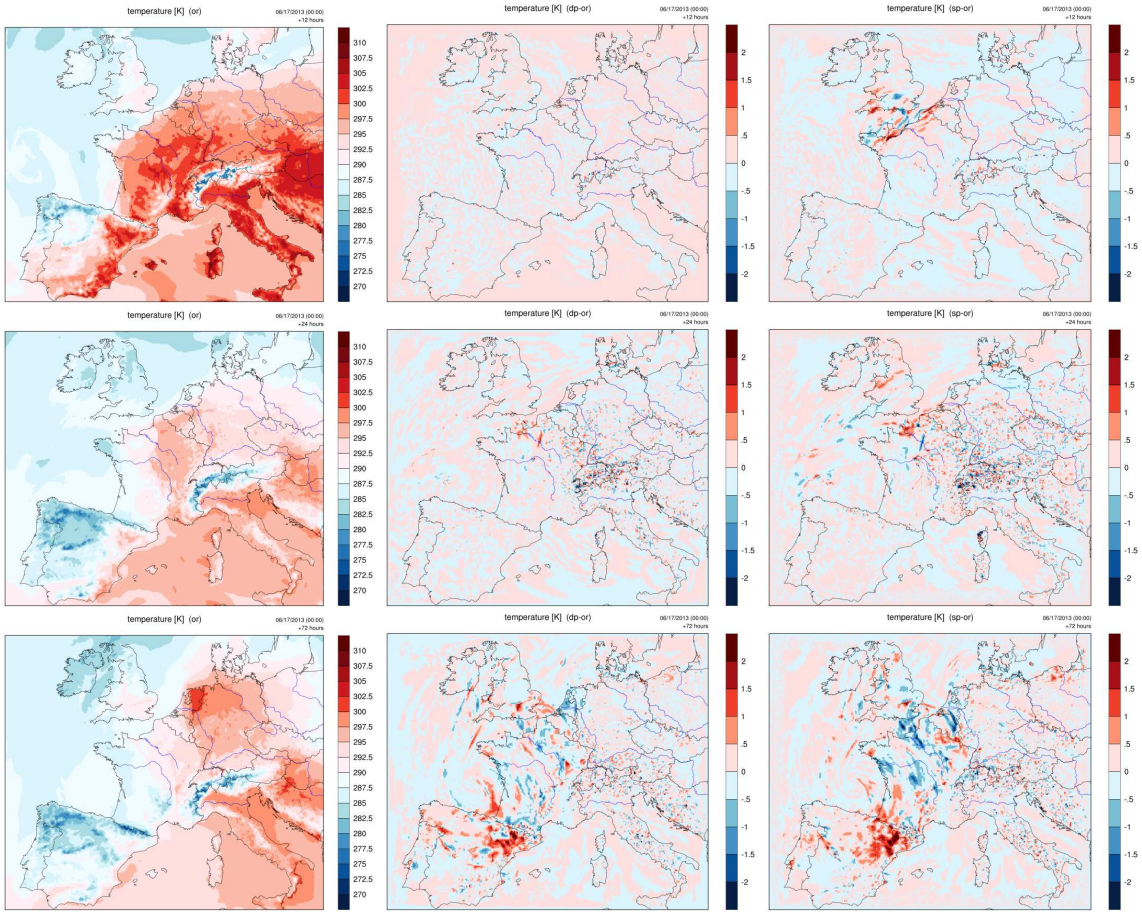

FIGURE 7: Results of the SP sensitivity experiments. Shown is temperature on the lowermost model level. Shown are the absolute field of **OR** (left), the deviations **DP-OR** (center), **SP-OR** (right). The lead times are 12h (top), 24h (middle), and 72h (bottom). The error growth is faster in **SP** than in **DP** with respect to **OR**, but the difference between **DP-OR** and **SP-OR** is already much smaller after 24h, and is gone after 72h, when they are of comparable magnitude.

the reference code, where all prognostic fields are randomly perturbed at every time step by a factor on the order of 10^{-7}. We run our test case with the three code versions **OR**, **DP**, and **PR** and compare the differences after 72h. Figure 6 shows the results of these experiments for temperature (top), pressure deviation (center), and specific humidity (bottom). Shown are the absolute fields of **OR** (left) as well as the differences **PR-OR** (center) and **DP-OR** (right) on the lowermost model level after 72h. The difference plots show perturbations of comparable magnitude for all three variables. These results confirms that the observed differences between **DP** and **OR** are mainly the result of the additional type declarations.

4.1.2. Single Precision Experiments

To assess the quality of the simulations with the new code in SP (**SP**), we run our test case with **OR**, **DP**, and **SP** and compare the fields after 12h, 24h, and 72h. The results are shown in Figures 7 and 8 for temperature and pressure deviation, respectively, after 12h (top), 24h (center), and 72h (bottom). After 12h, the deviations of **SP** from both **DP** (not shown) and **OR** are clearly larger than **DP-OR**. After 72h, however, the deviations between all model versions are of similar magnitude. No systematic biases are observed. We can conclude that perturbations due to numerical truncation errors seem to be slightly larger in **SP**, but physical error growth rapidly dominates. We have not found any indications that **SP** does not perform as well as **DP** in any of the experiments or variables analyzed.

4.2. Verification (COSMO-2)

The test which a NWP model eventually has to pass is verification against observations. From a numerical

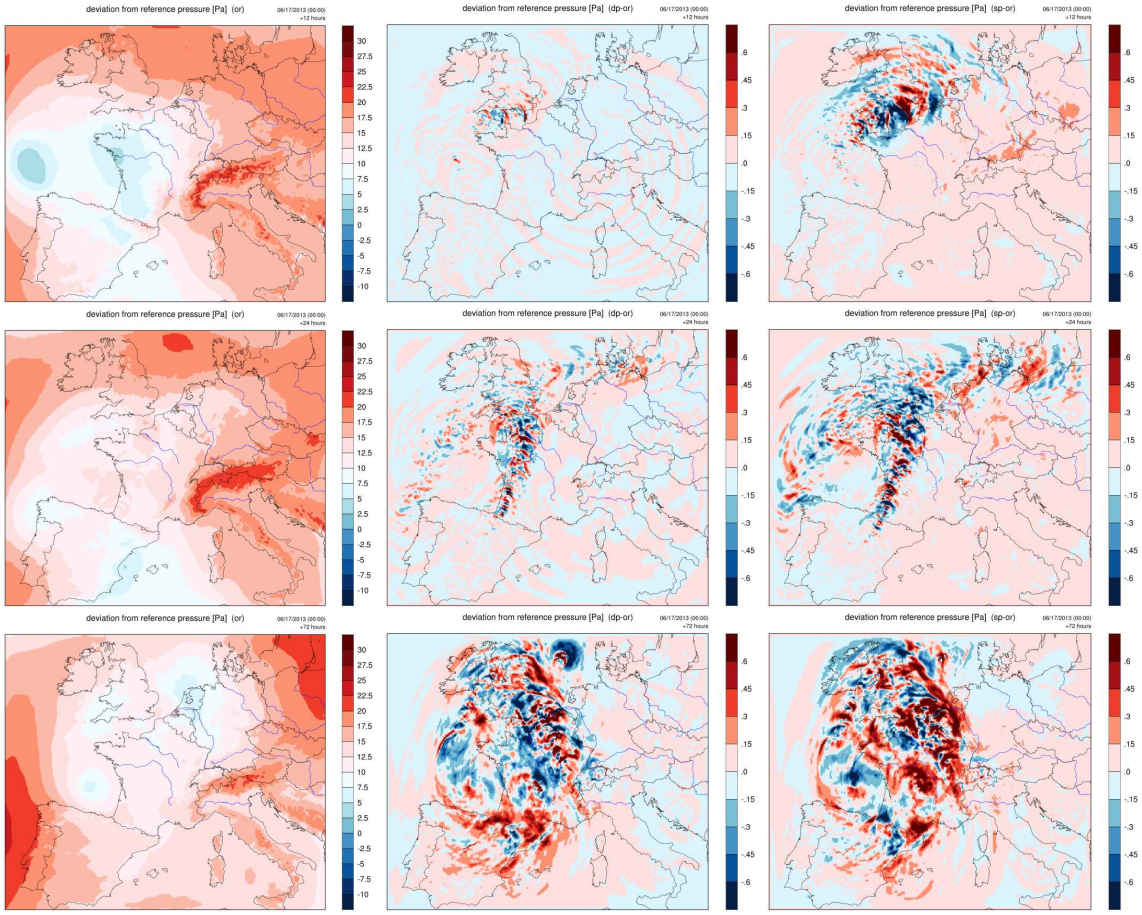

FIGURE 8: As Figure 7, but for pressure deviation.

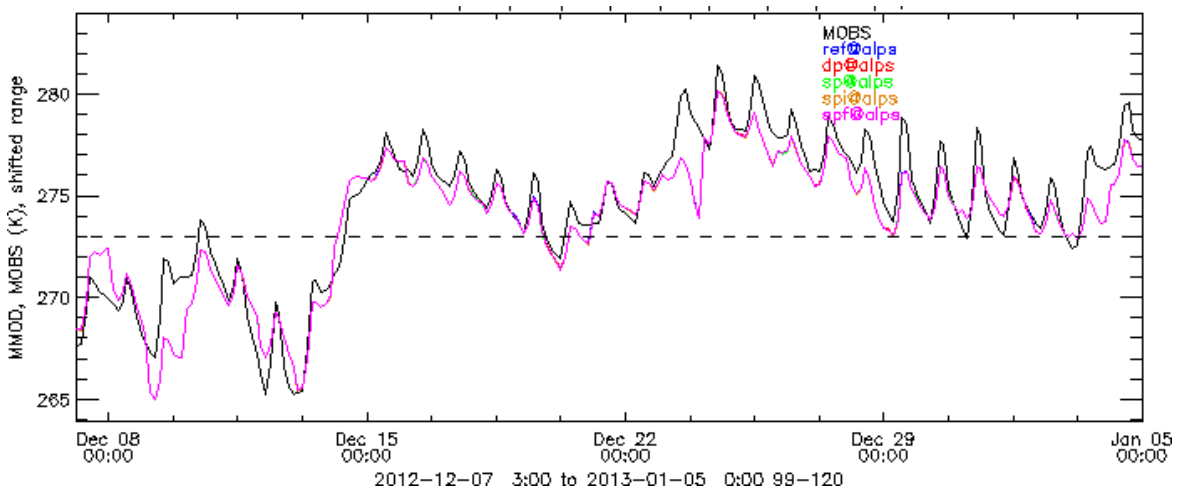

FIGURE 9: Verification against observations (black line) of OR (blue), DP (red), and SP (green, orange, purple) line). Shown is the mean 2m temperature for forecast day 5. The model forecoasts differ from the observations, but not at all from each other.

point of view, this test is far less restrictive than the sensitivity experiments presented in the previous section, as it allows for much larger deviations from the reference simulation. The verification runs are much more meteorologically representative, though, as a larger number of different situations occur during two months than during 72h, especially as both summer and winter are tested. Therefore it is much more likely for bugs in SP to show up in these runs than in those with the previous setup. The verification is done in the COSMO-2 setup. Simulations with lead time +120h are started every 24h during one month in both summer

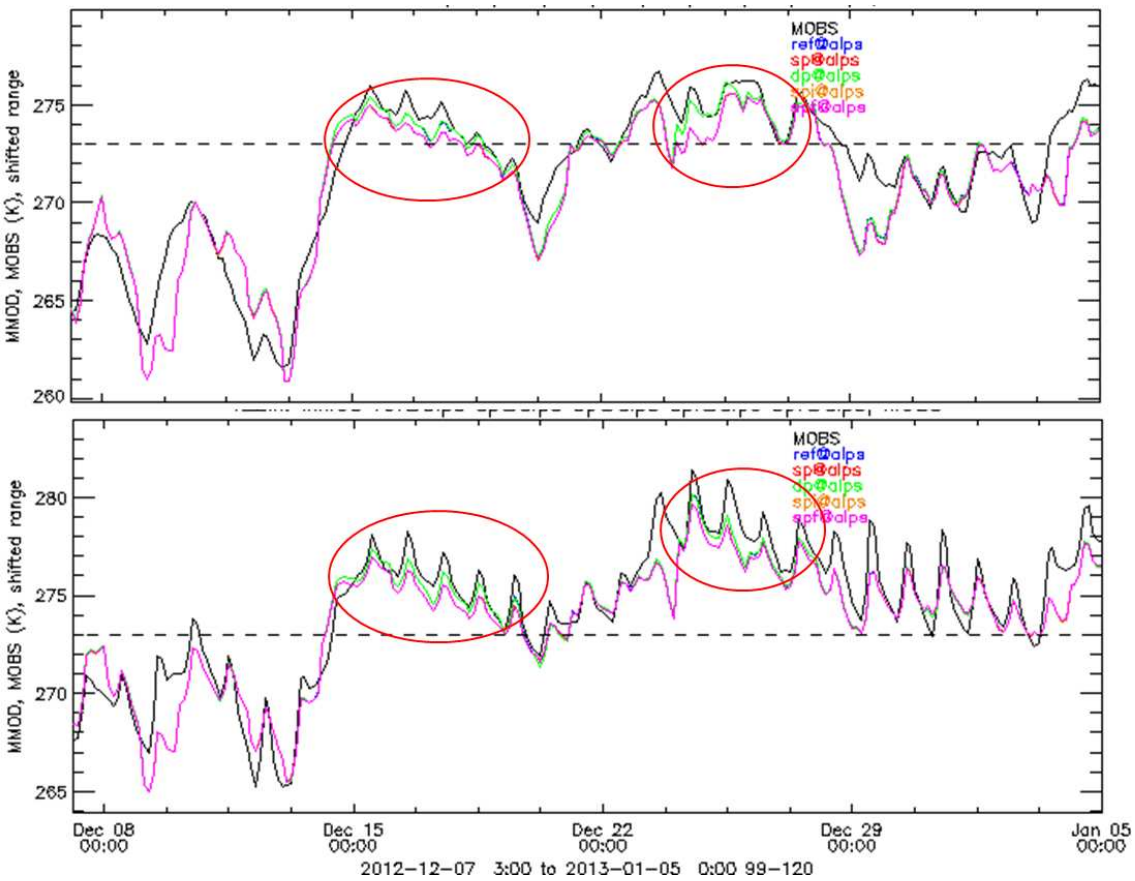

FIGURE 10: Verification against observations (black) of the code with the winter bug in DP (green) and SP (red, orange, purple). Shown are mean dew point temperature (top) and absolute temperature (bottom) for forecast day 5. The two periods where **SP** differs significantly from **DP** are emphasized by red circles. These differences have been caused by a bug in the soil model related to the melting of snow.

(August 2012) and winter (December 2012) and the results statistically compared to ground observations (up to +120h) and soundings (up to +72h).

The results of the **SP** and **DP** simulations are indistinguishable in most of the graphical products generated by the standard verification package. As an example, Figure 9 shows a time series of temperature on forecast day five. The forecasts (colored) are clearly distinguishable from the observations (black), however not from each other. We can conclude from the results that all code version (**OR**, **DP**, **SP**) perform equally well and are meteorologically not distinguishable.

4.2.1. The Winter Bug

In contrast to the final version, the first working **SP** code yielded ambivalent verification results. In summer, the performance of **SP** was comparable to that of the other codes. In winter, however, it was clearly inferior. Time series of absolute and dew point temperature showed significant deviations of **SP** from **DP** and **OR**, as shown in Figure 10 with the respective periods emphasized. Plots of the fields during these periods revealed strong temperature anomalies which quickly grew to large size by advection, with the source regions fixed in space, as shown in Figure 11 (top) for temperature at +96h (left) and +120h (right). On first sight the anomalies seemed to be spatially related to topography in some way. Investigation of various fields, however, eventually hinted towards differences in snow cover, as the source regions of the anomalies corresponded to the margins of snow covered regions. This led us to inspect the soil model code. We eventually identified the bug in *src_soil_multlay.f90*. It had been caused by an epsilon used to check whether a temperature has a certain minimal distance to the freezing point. We have replaced the epsilon variable `zepsi` by `eps_temp` in the critical places, as illustrated by the following code excerpt. The magnitude we have chosen for `eps_temp` is save up to temperatures of $500K$.

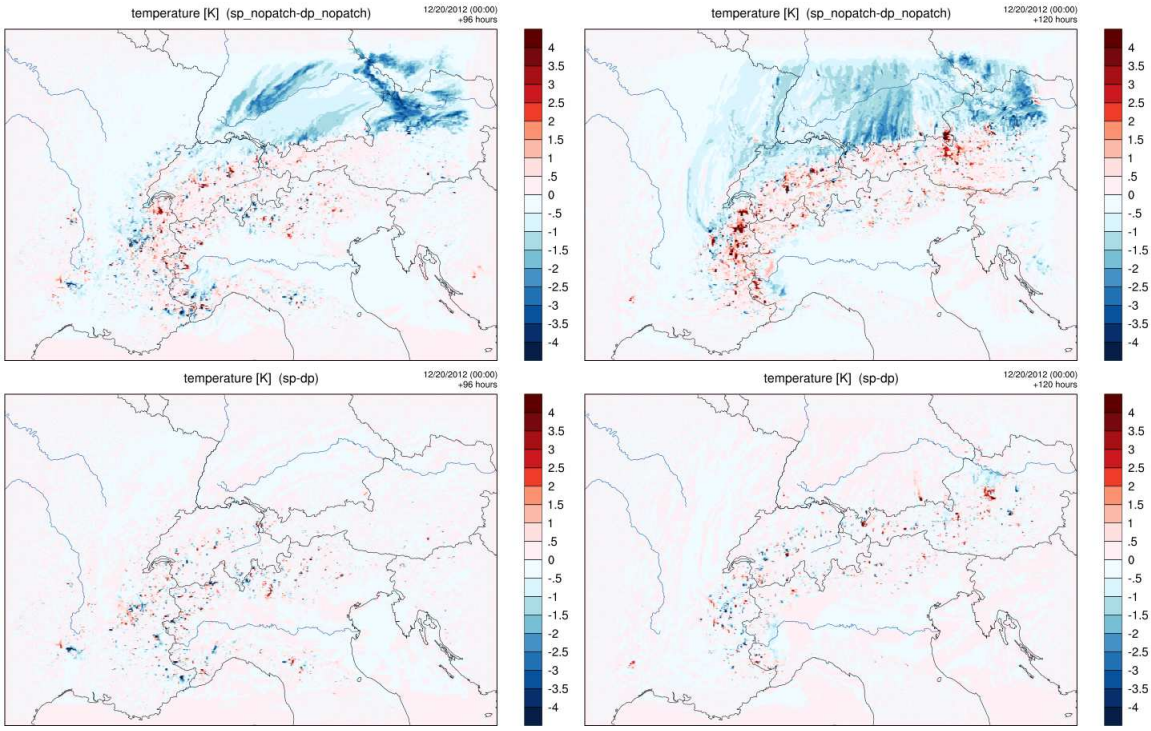

FIGURE 11: Difference in temperature between SP and DP with (top) and without (bottom) the winter bug after 96h (left) and 120h (right). (Top) The anomalies start to grow in specific places such as NW of Switzerland roughly parallel to the Jura mountains and along the Danube river valley, and from there grow by NE-ward advections. (Bottom) With the winter bug patch, the large deviations have disappeared, and only small, noisy signals over the alpine region remain.

src_soil_multlay.f90

```
 427   REAL     (KIND=ireals   ), PARAMETER ::  &
 428 !    zepsi  = 1.0E-6_ireals , & ! security constant
 429      eps_temp = MAX(1.0E-6_ireals,500.0_ireals*EPSILON(1.0_ireals))
 ...
3560 !          IF(t_so(i,j,kso,nnew).LT.(t0_melt-zepsi)) THEN
3561           IF(t_so(i,j,kso,nnew).LT.(t0_melt-eps_temp)) THEN
3562             zaa     = g*zpsis(i,j)/lh_f
```

This is a digit-limited case, i.e., the minimal relative epsilon in SP is 10^{-7}. The epsilon of magnitude 10^{-6} thus seems to be big enough at first sight. However, three significant digits are lost because of the order of magnitude of the temperatures (cf. Section 2.4), which increases the minimal magnitude of the epsilon by 10^3. `zepsi` therefore vanished in SP, introducing a hard-to-find bug. Replacing it by a new epsilon with a sufficiently large magnitude in SP solved the problem. The temperature fields from a model run with this patch are shown in Figure 11 (bottom). A comparison to the top panel shows that the large deviations have vanished, and that only a noisy signal of very localized deviations spread over the Alps remains, reminiscent of the deviations observed in the sensitivity experiments.

4.2.2. Timings

The major benefit of running the COSMO model in SP is a significant reduction in runtime. The mean runtime statistics with various model versions running on a Cray XE6 with AMD Magny-Cours processors are summarized in Table 4. Switching from DP to SP reduces runtime by almost 40%. This is substantial, as for example for an ensemble forecast the number of members could be increased by almost 70% on a given hardware.

OR	DP	SP	SP_i	SP_f
100.0%	102.0%	60.2%	56.2%	55.9%

TABLE 4: Mean runtimes of all sensitivity experiments relative to OR. SP_i and SP_f are SP with aggressive optimization at compilation (both without strict IEEE conformance, and SP_f additionally with less accurate library functions). The runtime of the most aggressively optimized code drops below 56%, i.e. it is almost twice as fast than the reference.

5. Discussion

5.1. Caveats

We have only tested the model configurations most important for MeteoSwiss. While this should cover the main parts of the model, we must emphasize that testing is required before using it in SP. It is in the user's responsibility to make sure his configuration of choice works in SP, especially if less common parts of the code are to be run. Critical in this respect is the assimilation due to the unresolved epsilon issue presented in Section 3.2.2.

The synthetic satellite image package RTTOV7 does not work in SP. This is why we have written wrapper subroutines for all RTTOV7 subroutines used in COSMO. They convert the input arguments from WP to DP, call RTTOV7 in DP, and convert back the output arguments.

5.2. Epsilon Recommendations

In this article, we have presented several epsilon-related pitfalls and some often-made mistakes in COSMO. To help avoid such problems in the future, some of which are critical to run the model in SP, we have compiled a few recommendation.

Use purpose-specific epsilon-parameters. Try to avoid multi-purpose epsilon parameters the magnitude of which is a compromise between various use cases. We recommend to consider the use of at least three distinct epsilon parameters.

- `eps_div`: Range-limited epsilon to avoid division by zero (DBZ).
- `eps_fpn`: Digit-limited epsilon for FPN comparisons.
- `eps_???`: Algorithmic epsilon(s) for all other purposes.

Insert digit-limited epsilons by multiplication, not by addition. Digit-limited epsilons are those the magnitude of which, relative to other involved numbers, is the important factor. This is predominantly the case in comparisons of FPNs. Inserting such epsilons by multiplication (`a < (1.0 + eps)*b`) considers this relative nature and is much more robust than the usual insertion by addition (`a < b + eps`).

Define epsilon parameters neither too locally, nor to globally. Neither should they be redefined in every subroutine in a file, nor should only a single epsilon be used throughout the whole model. A good compromise is usually one definition per file/module, or, if there is one, in a data module, which might be shared by multiple source modules. Do not hardcode the values of epsilons, but use the newly introduced precision-dependent parameters `repsilon` and `rprecision` to define range- and digit-limited epsilons, respectively.

Name epsilon parameters in a way that reflects their purpose. Especially algorithmic epsilons should be marked as such in order for them not to be confused with precision-limited epsilons, e.g. `eps_soil` instead

of a plain `epsilon`. Also clearly state the purpose of an epsilon parameter in a detailed comment next to it's definition.

Be aware of rounding error. Think about rounding error when writing new code and be aware of users running the COSMO model in reduced precision. Test your code in reduced arithmetic precision (single precision), if possible. If it runs and validates, it is highly likely to work correctly in higher precision arithmetic (double precision).

5.3. Summary and Conclusions

In this article, we have presented the modifications necessary to run the COSMO model in single precision (SP) instead of double precision (DP), and how this modified version of COSMO performs in both DP and SP. Three types of modifications are necessary. In a first step, all real type declarations (`ireals`) currently missing in the code are added to obtain a model running purely in DP. These are the changes which alter the results of DP-runs of the model (in a numerical sense). In a second step, various local modifications are introduced. These are mainly related to epsilons, i.e. additional epsilons to prevent model crashes in SP, or working precision-dependent modifications of the magnitude of some epsilons. For the latter purpose, we have introduced two precision-dependent parameters. Furthermore, a few formulas need to be reformulated to a numerically more precise form. The third step towards SP is a mixed precision implementation of the radiation, which in it's current form does not work in SP. A substantial part of the radiation is therefore always run in DP.

We have validated the code in two steps. First, sensitivity experiments have shown that the differences between the new code in DP and the reference code can be explained by the addition of the missing real kind declarations, and that, despite slightly faster error growth, the differences between the new code in both SP and DP from the reference do not show any systematic biases and are of the same order of magnitude for longer lead times. Second, validation against observations has shown that the forecast quality is unaffected by the switch from DP to SP. The gain of the switch to SP is a reduction of the model runtime to roughly 60% accompanied by a significant reduction of required memory.

Running COSMO with reduced precision should be a good choice for many applications. However, we must emphasize that our tests of the model in SP have been far from exhaustive. There might still be places in the code where problems occur in SP that have yet to be discovered. The elaborate documentation of the changes and problems we have presented in this article may serve as a guideline to cope with future problems with either previously untested or new code in SP.

References

[1] ANSI/IEEE 754 (2008). IEEE standard for binary floating-point arithmetic.

[2] Düben, P. D., McNamara, H., and Palmer, T. N. (2013). The use of imprecise processing to improve accuracy in weather and climate prediction. *J. Comp. Phys.*, in press.

[3] Govett, M., Middlecoff, J., and Henderson, T. (2010). Running the NIM next-generation weather model on GPUs. In *10th IEEE/ACM International Conference on Cluster, Cloud and Grid Computing (CCGrid)*, pages 792–796.

[4] Riedinger, K. (2011). Mixed precision im dynamischen kern eines numerischen wettervorhersagemodells. Bachelor's thesis, University Innsbruck.

[5] Skamarock, W. C., Klemp, J. B., Dudhia, J., Gill, D. O., Barker, D. M., Duda, M. G., Huang, X.-Y., Wang, W., and Powers, J. G. (2008). A description of the advanced research WRF version 3. NCAR technical note, National Center for Atmospheric Research, Boulder, CO, USA.

Ensemble forecasting for Sochi-2014 Olympics: the COSMO–based ensemble prediction systems

Andrea Montani[1], D. Alferov[2], E. Astakhova[2], C. Marsigli[1], T. Paccagnella[1]

[1] *ARPA–SIMC, Bologna, Italy*
[2] *Roshydromet, Moscow, Russia*

1. Introduction

In the framework of the forthcoming Winter Olympics and Paralympic Games, taking place in Sochi, Russia, from 7 to 23 February 2014 and from 7 to 16 March 2014, WMO WWRP initiated a dedicated blended Forecast Demonstration/Research and Development Project (FDP/RDP). **FROST-2014** (**F**orecast and **R**esearch in the **O**lympic **S**ochi **T**estbed; http://frost2014.meteoinfo.ru/) aimed at advancing the understanding of nowcasting and short-range prediction processes over complex terrain, since the region of Sochi is characterized by a complex topography, with the Caucasus mountains in the vicinity of the Black Sea (Kiktev, 2011), as shown in Fig. 12, where the main features of the Olympic venues are presented.

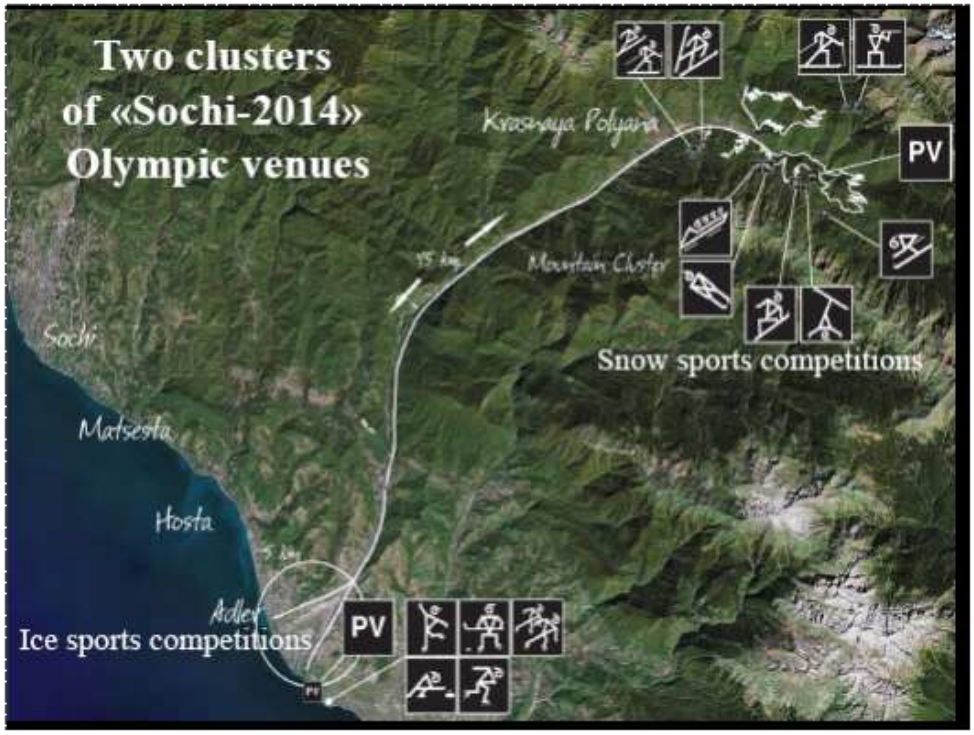

Figure 12: Main features of the Olympic venues for Sochi–2014.

Since Russia belongs to the COSMO consortium (http://www.cosmo-model.org), several activities have also been undertaken within the consortium to support NWP aspects of the FROST-2014 project. The COSMO tasks within FROST-2014 are organized in the framework of the Priority Project CORSO (Consolidation of Operation and Research results for the Sochi Olympic games), which deals with the following topics:

1. deterministic forecasting,
2. probabilistic forecasting:
   (a) FDP part: relocation of COSMO-LEPS (Montani et al., 2011) over the Sochi area, generating a new system named COSMO-S14-EPS ("S" stands for Sochi);
   (b) RDP part: development of a convective-scale ensemble system for the Sochi area, referred to as COSMO-RU2-EPS ("RU2" stands for Russian 2.2 km);
3. post-processing and product generation;
4. verification (development of VERSUS software for probabilistic verification).

As for 2(a), the main activities include the set-up, generation, implementation and maintenance of COSMO-S14-EPS, the convection-parameterized ensemble prediction system based on COSMO model and targeted for the Sochi-area. In addition to providing probabilistic guidance for the prediction of high-impact weather over the Olympic mountainous areas in the short range (up to day 3), COSMO-S14-EPS is also meant to provide both initial and boundary conditions for activity 2(b), linked to the generation of the convective-permitting ensemble, COSMO-RU2-EPS, running on a quasi–operational basis during winter 2013.

2. Methodology and implementation

As previously mentioned, COSMO-S14-EPS is a relocation of COSMO-LEPS over the area interested by the Olympic competitions. As such, it shares some features of the COSMO-LEPS methodology for its generation. On the other hand, computer-time constraints and the interest towards the short-range made it necessary to make some changes. The main characteristics of COSMO-S14-EPS are summarized in Table 5, which also reports some details relative to the global ensemble ECMWF-EPS.
It is worth pointing out that those ECMWF EPS members providing both initial and boundary conditions to COSMO-S14-EPS, are selected via a clustering technique performed between t+48h and t+72h on the basis of four variables (Z, U, V, Q) at three pressure levels (500, 700, 850 hPa). In addition to that, the lower boundary condition for all COSMO-S14-EPS members is taken from COSMO model run in hindcast mode (short-range forecast nested on ECMWF analyses).

TABLE 5: Main features of the present implementations of ECMWF-EPS, COSMO-S14-EPS and COSMO-RU2-EPS.

	ECMWF-EPS	COSMO-S14-EPS	COSMO-RU2-EPS
Hor. res.	$\sim$ 31 km	7 km	2.2 km
Vert. res.	62 ML	40 ML	50 ML
Forecast length	240h	72h	48h
Ensemble size	50+1	10	10
Initial time	00/12 UTC	00/12 UTC	00/12 UTC
Convection	Parameterized	Parameterized	Resolved
Running at	ECMWF	ECMWF	Roshydromet
ICs and BCs	SV ini pert + EDA	from selected ECMWF-EPS members	from COSMO-S14-EPS members
Model perturbations	Stochastic physical tendencies + backscatter	Physical parameterizations	

COSMO-S14-EPS was implemented on ECMWF super–computers in November 2011 and has been running on a regular basis since 19 December 2011 thanks to the billing units provided by the ECMWF Special Project SPCOFROST. COSMO-S14-EPS generates a set of standard probabilistic products, including probability of surpassing a threshold, ensemble mean and ensemble standard–deviation for several surface and upper-air variables. These products are delivered in real time to the Hydrometcenter of Russia (Roshydromet), further disseminated to Sochi forecasters and presented at the FROST-2014 Web-site (`http://frost2014.meteoinfo.ru/forecast/goomap` and `http://frost2014.meteoinfo.ru/forecast/arpa-new/cosmo-s14-eps-maps`). In addition to this, all forecast members for a specially defined area are transferred to Roshydromet where the epsgrams for predetermined points are prepared (see `http://frost2014.meteoinfo.ru/forecast/arpa-new` (authorization required)). The generation of the different types of non-graphical products makes use of

"Fieldextra", the official COSMO post-processing software (for information about Fieldextra, please refer to `http://www.cosmo-model.org`). The graphical products are prepared using the GRADS package.

In addition to the ensemble products, initial and hourly-boundary conditions (up to t+48h) are provided to Roshydromet for the experimentation with the convection-resolving ensemble COSMO-RU2-EPS, whose main features are also summarized in Table 5.

Figure 13 reports the orography for the three systems of Table 5 and is meant to indicate the potential impact of increased horizontal resolution in the description of orographic and mesoscale-related processes.

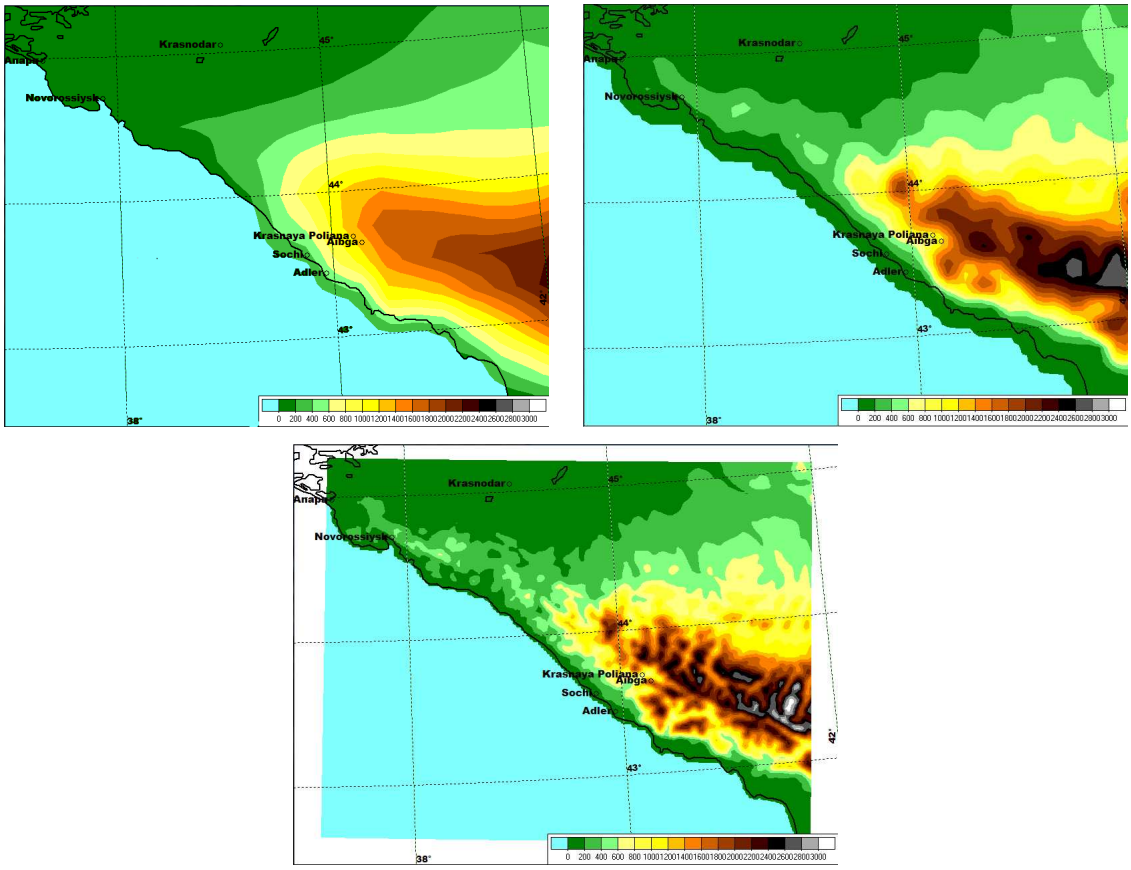

FIGURE 13: Model orography (in m) for ECMWF-EPS (Δx = 31 km, top-left panel), COSMO-S14-EPS (Δx = 7 km, top-right panel) and COSMO-RU2-EPS (Δx = 2.2 km, bottom panel) in the Olympic region.

ECMWF-EPS orography (top-left panel) shows almost no evidence of the valley running for about 40 kilometres from Sochi-Adler, the "Coastal cluster" where ice-sport competitions will take place, towards Krasnaya Polyana, located in the area of the "Mountain cluster" for snow-sport competitions (see also Fig. 12). COSMO-S14-EPS (top-right panel of Fig. 13) already offers a better description of the complex topography of the area, although it has to be pointed out that only with the 2.2 km grid-size of COSMO-RU2-EPS (bottom panel) some important details of the geography (e.g. the eastward turn of the valley after Krasnaya Polyana) can emerge. It is clear that the simple increase of horizontal resolution does not automatically guarantee a better simulation of the flow over orography and an overall higher prediction skill of precipitation. On the other hand, it has already been shown (Montani et al., 2013), that COSMO-S14-EPS outperforms ECMWF-EPS in terms of probabilistic prediction of precipitation events in the short range. These results, although based on only three months, have shown the potential of limited-area ensemble forecasting for the prediction of precipitation with high spatial detail.
In the next section, we analyse the performance of COSMO-S14-EPS and COSMO-RU2-EPS for a number of high-impact weather events occurred during the last winter and we try to assess the impact of higher -resolution in the probabilistic prediction of heavy precipitation and surface temperature.

3. Case-study results

Here, the attention is focused on the performance of the limited-area ensemble prediction systems for two high–impact weather events:

• heavy precipitation event on 13 January 2013 with 21 mm of rain during the day on the coast (Sochi/Adler) and 33 mm of snow-water equivalent in the mountain (Krasnaya Polyana);
• Foehn event on 14-15 February 2013 with a sudden 10–degree warming.

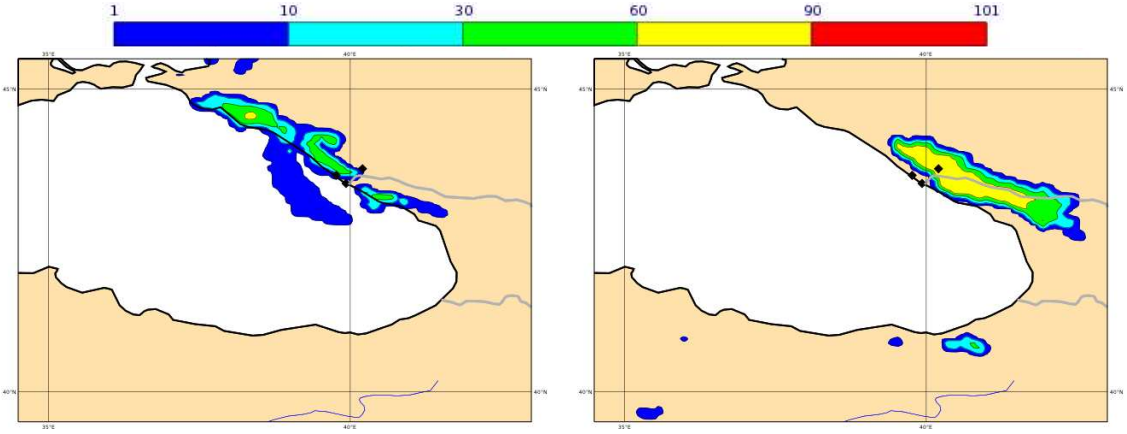

FIGURE 14: COSMO-S14-EPS run starting at 00UTC of 11 January 2013 (48-60 hour forecast range): probability of 12–hour rainfall exceeding 20 mm (left panel) and of 12-hour snowfall exceeding 15 mm of water equivalent. The black squares on the coast denote Sochi and Adler; the black square inland denotes Krasnaya Polyana.

3.1 Heavy precipitation event

Figure 14 reports the performance of COSMO-S14-EPS in terms of probabilistic prediction for two variables: probability of 12–hourly accumulated rainfall exceeding 20 mm (left panel) and probability of 12–hourly simulated snowfall exceeding 15 mm of equivalent water. The ensemble runs start at 00UTC of 11 January and the attention is focused on the 48-60 hour forecast range: it can be noticed that COSMO-S14-EPS provides a quite accurate forecasts giving large probability of heavy precipitation. Despite the steepness of the orography and the length of the forecast range, the system is able to distinguish between the area more likely affected by rainfall (along the coast, left panel) and the region mainly interested by snowfall (in the mountains, right panel). This is an interesting result, as the knowledge of the possibility of this weather event, with an advance of about 2 days, gives organizers the chance of taking counter–measures and relieving the weather-related problems. Let us compare the COSMO-S14-EPS forecasts to COSMO-RU2-EPS. The attention is fixed on the ability of both systems to predict the possible occurrence of heavy snowfall inland. More precisely, we consider the predictability of the following event: "probability of 12h snowfall exceeding 15 mm of equivalent water". In Fig. 15, the left–column (right–column) panels report the performance of COSMO-S14-EPS (COSMO-RU2-EPS) for the forecast ranges 36-48 hour and 24-36 hour (top-row and bottom-row panels, respectively). It can be noticed that the signal by COSMO-S14-EPS forecasts (left–column) is consistent for the different prediction ranges, with a probability of snowfall above 90% in the area actually affected by the weather event. It is also worth pointing out that no snowfall is predicted along the coast at any forecast range (probabilities below 1%), consistently with observations. A straight comparison of COSMO-S14-EPS against COSMO-RU2-EPS forecasts indicates that the higher–resolution ensemble (right–column panels of Fig. 15) provides more detailed information in terms of location of the regions affected or not by heavy snowfall. In the convective–resolving ensemble, the extent of the coastal region not interested by snowfall turns out to be more evident. At the same time, the higher-resolution ensemble is more confident in giving larger probabilities of snow in the mountainous region. Since more and more spatial and time details are usually required to the forecasts for shorter time ranges, COSMO-RU2-EPS seems to have, on the basis of this case study, the potential to provide a larger amount of information to local forecasters and event organizers.

3.2 Foehn event

Sudden temperature changes in the Olympic areas are considered high–impact weather events possibly affecting outdoor competitions. Therefore, the prediction of this type of event is an important benchmark for the usefulness of ensemble prediction systems. Note that the event considered below was regarded as hardly predictable by local forecasters.
Figure 16 shows the evolution of surface temperature in Krasnaya Polyana from 13 to 16 February 2013. Linked to the onset of Foehn winds, a marked increase took place between 13 and 15 February, affecting both day–time and night–time temperatures. On 14 and 15 February, the observed peaks amounted to 6 and 10 ^{o}C, respectively.

As for the ability of COSMO-S14-EPS (the only system analysed in this case study) to predict this temperature

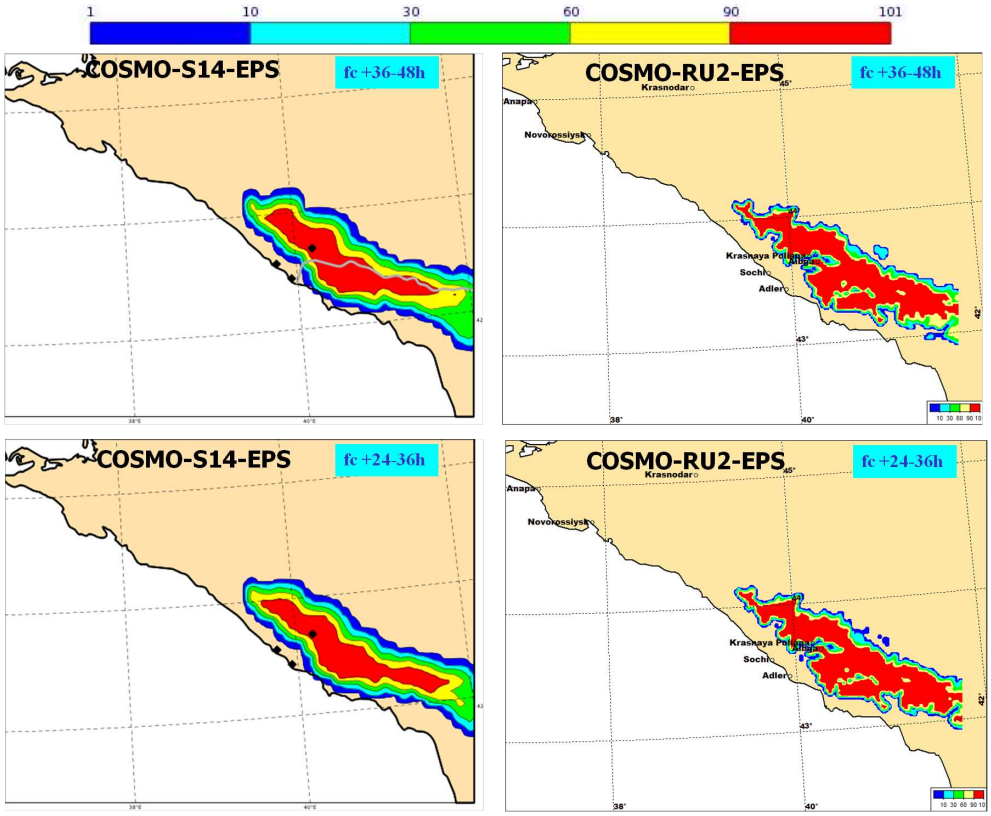

FIGURE 15: Probability of 12–hour snowfall exceeding 15 mm of equivalent water: COSMO-S14-EPS runs starting at 12UTC of 11 January (top-left panel, t+36-48h) and at 00UTC of 12 January (bottom-left panel, t+24-36h) and COSMO-RU2-EPS runs starting at 12UTC of 11 January (top-right panel, t+36-48h) and at 00UTC of 12 January (bottom-right panel, t+24-36h). All forecasts verify at 12UTC of 13 January 2013. As in Fig. 14, the black squares in the left panels denote Sochi, Adler and Krasnaya Polyana.

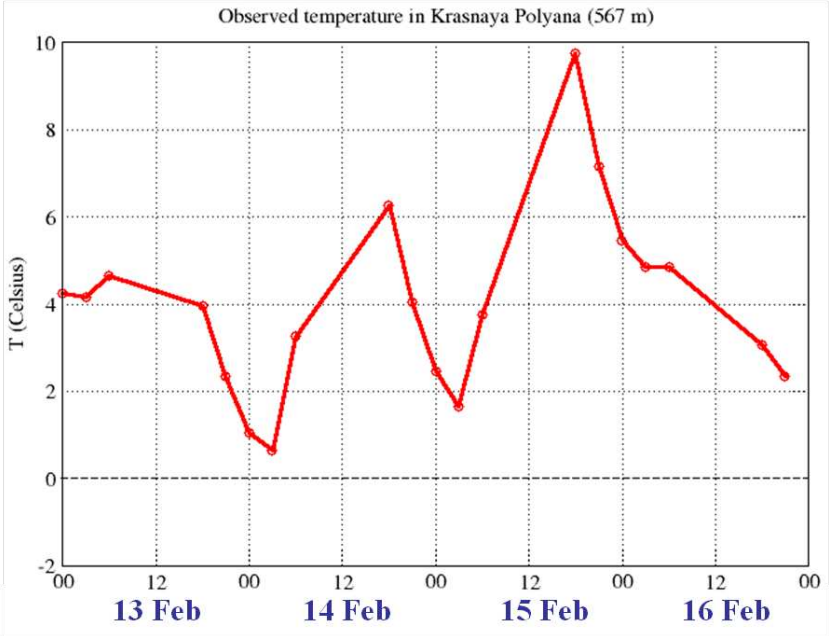

FIGURE 16: Observations of 2-metre temperature in Krasnaya Polyana (data from FROST database).

increase, Fig. 17 reports the meteograms computed over the station point of Krasnaya Polyana, in terms of 2-metre temperature, for different starting times. The top panel of the figure indicates that, already at the 72–hour range (forecasts starting at 12UTC of 12 February), the COSMO-S14-EPS members predict the temperature increase of 14 and 15 February, with peaks close to, or above, 10 °C. In this panel, as well as in

the others, some discrepancies between observed and predicted temperature are evident, but the differences are partly related to the model orography, which locate Krasnaya Polyana at about 941 m, instead of 567 m. The accuracy of 2–metre temperature forecasts seems related, among other factors, to the good prediction of the onset of the Foehn winds, in terms of both location and intensity (not shown).

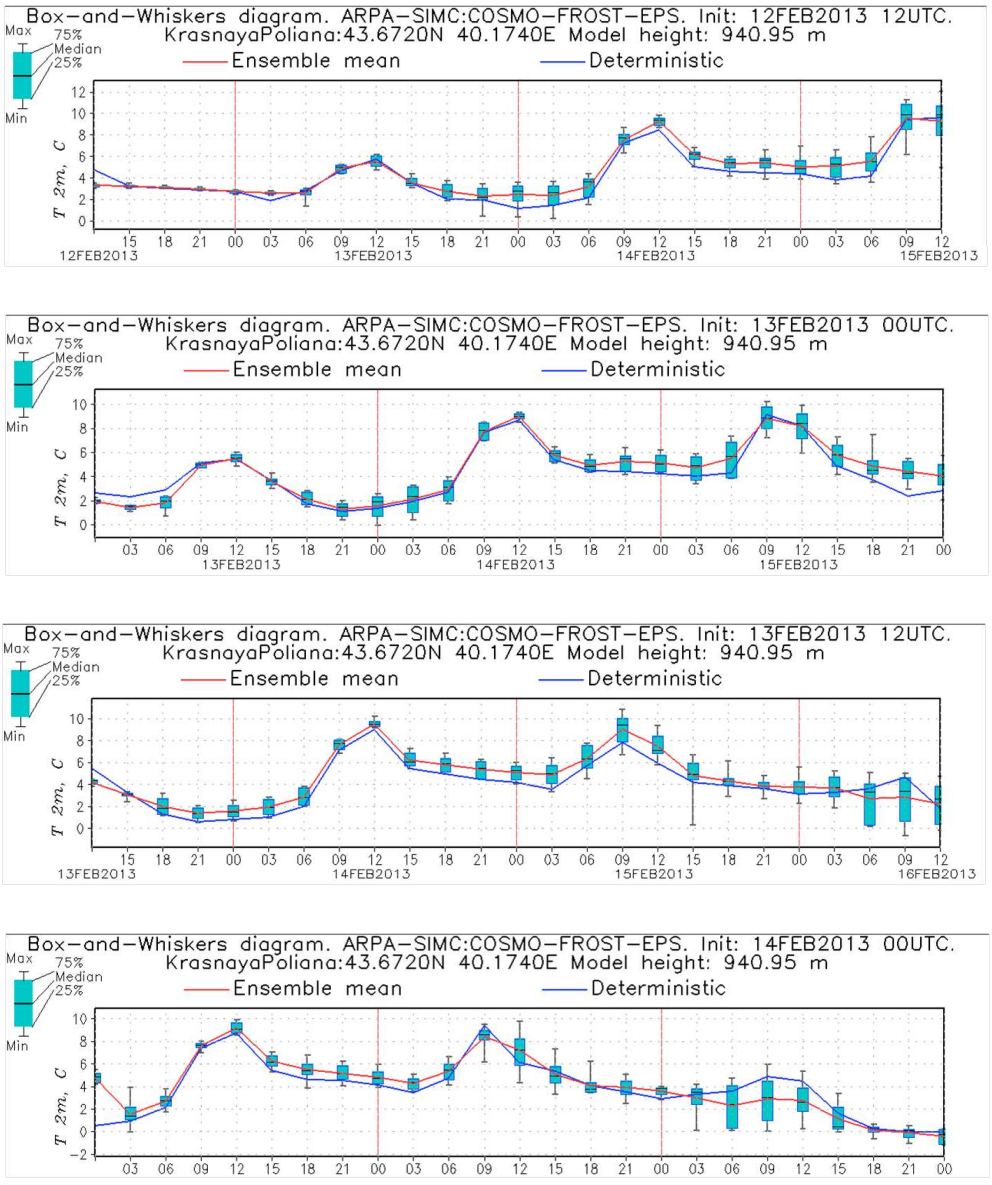

FIGURE 17: Point meteograms in terms of 2–metre temperature over Krasnaya Polyana based on COSMO-S14-EPS and starting at: (a) 12UTC of 12 February, (b) 00UTC of 13 February, (c) 12UTC of 13 February and (d) 00UTC of 14 February.

4. Summary and Outlook

The main results of the ensemble prediction system experimentation within FROST-2014 can be summarized as follows:

- The new COSMO-based ensemble systems over the Sochi-area (COSMO-S14-EPS and *COSMO-RU2-EPS*) were implemented and run on an operational/*quasi–operational* basis;
- COSMO-S14-EPS was shown to be able to capture the possible occurrence of intense and localized weather events in the Olympic venues with a few days in advance;
- COSMO-S14-EPS products are getting more and more used in operational forecasting and the use of probabilistic products among Olympic forecasters is increasing.

As for the future, it is planned to consolidate the generation/transmission/use of probabilistic products from ECMWF to the Sochi forecasters and to quantify the added value of the higher resolution in COSMO-RU2-EPS forecasts.

References

[1] Kiktev D., 2011: Forecast and Research: the Olympic Sochi Testbed (FROST-2014). Concept paper. Available at http://frost2014.meteoinfo.ru.

[2] Montani A., Cesari D., Marsigli C., Paccagnella T., 2011. Seven years of activity in the field of mesoscale ensemble forecasting by the COSMO-LEPS system: main achievements and open challenges. *Tellus*, **63A**, 605-–624. DOI: 10.1111/j.1600-0870.2010.00499.x

[3] Montani A., Marsigli C., Paccagnella T., 2013. Development of a COSMO-based limited-area ensemble system for the 2014 Winter Olympic Games. *Cosmo Newsletter No. 13*, 93-99. Available at http://www.cosmo-model.org

A sensitivity test to assess the impact of different soil moisture initializations on short range ensemble variability in COSMO model

Riccardo Bonanno and Nicola Loglisci

Arpa Piemonte

1 Introduction

A well-known problem with mesoscale ensemble forecasts is their lack of variability between members near the surface.

Surface condition uncertainties are generally not taken into account in ensemble systems, and ensemble forecasts often use the same surface conditions for all members.

However, the sensitivity of moist atmospheric processes to soil conditions has been demonstrated in numerous studies.

Sutton et al. (2006) used two soil moisture analyses originating from two different land surface models (LSM) forced with exactly the same meteorological data. The results showed significant differences in near-surface temperature and precipitation and suggested that the variability induced by soil moisture differences can, in fact, increase the spread of ensemble members and improve on the short-range weather forecasting.

Aligo et al. (2007) used a similar approach showing that perturbations applied only to soil moisture might not be enough to produce sufficient variability to precipitation forecast and a better ensemble set can be constructed from perturbing also other aspects such as atmospheric initial conditions.

Quintanar et al. (2008) used a similar approach to that used by Sutton et al. (2006) and Aligo et al. (2007) providing additional insight for soil moisture impacts on ensemble spread. They evaluated, in addition to precipitation and temperature, also ensemble spread in terms of relative humidity, horizontal and vertical wind and showed that soil moisture perturbations can produce sufficient spread for vertical velocity (thus, precipitation) but not for RH, T and horizontal winds. They also suggested that additional experiments need to be undertaken where soil moisture and atmospheric initial conditions perturbations and model physics would be considered simultaneously.

Klüpfel et al. (2011) investigated the impact of soil moisture on precipitation amount and distribution in model simulations for West Africa with the COSMO model at 0.025^o resolution. They used three analysis fields, satellite measurements, and model output from a Land Surface Model to initialize five convection-permitting model runs of COSMO, forced by reanalyses from the European Centre for Medium-Range Weather Forecasts. The spread between the five precipitation forecasts suggests that a high-resolution limited area ensemble built by applying atmospheric variations as well as variations of the initial land surface conditions lead to an improvement of the prediction of mesoscale convective systems and convective precipitation for West Africa.

Considering all these studies, it is clear that it would be very important to integrate surface perturbations into an ensemble system to account for uncertainties in surface conditions and to effectively increase the ensemble spread near the surface.

In this regard, some techniques have been proposed in the recent years. Sutton and Hamill (2004) implemented an empirical orthogonal function (EOF) method that was used to generate random perturbations with the same spatial structure as the daily deviations of soil moisture from a running-mean climatology.

A non-cycling surface breeding method was proposed by Wang et al. (2010), where short-range surface forecasts driven by perturbed atmospheric forcing are used for generating the perturbation to surface ICs. A simple method proposed by Hacker (2010), consists in the construction of perturbations of the soil moisture field that represent random, spatial correlated errors, to quantify the response to soil moisture perturbations. He recognized that this method is not suited for reproducing the characteristics of the actual soil moisture uncertainty, which varies locally with the properties of the soil, vegetation and background moisture itself (Hacker, 2010).

Lavassey et al. (2013) used a similar approach to assess the impact of uncertainties in surface parameter and initial conditions on numerical prediction with the Canadian Regional Ensemble Prediction System (REPS). In this work, perturbations at the initial time of one or several surface parameters or prognostic variables (soil

moisture and temperature) are generated using a two-dimensional random function on the sphere correlated in space, with a probability density function symmetric around the mean. This preliminary study of the impact on the ensemble forecast showed that the inclusion of the surface perturbations tends to increase the ensemble spread for all screen-level variables especially for 2-m temperature and 10-m wind speed and significantly increase the 2-m temperature and 10-m wind speed skill.

Cloke et al (2012) proposed a simple method, perturbation of 2 soil scheme parameters, in the ECMWF seasonal forecasting system.

In the COSMO Priority Project CONSENS a methodology for soil moisture perturbation based on Sutton and Hamill (2004) was developed by the Hellenic National Meteorological Service (COSMO Technical Report No. 22). The method was never tested in ensemble mode but it could be revived and tested on the new ensembles under development.

At DWD a simple method was developed to derive initial condition soil moisture perturbations from differences between COSMO-EU und COSMO-DE soil moisture. This approach is now implemented in COSMO-DE-EPS.

The goal of this study is to perform a sensitivity test to assess the response of the COSMO model to different lower boundary initial conditions in the framework of the COTEKINO (COsmo Towards Ensembles at the Km-scale IN Our countries) Priority Project, aimed at developing convection-permitting ensembles in the COSMO countries. In fact, even if the sensitivity of the atmospheric moist processes to different soil condition initializations has been demonstrated in several studies previously mentioned, it cannot be generalized to a completely different modeling system. Hence, it would be wise to verify a sensitivity in COSMO model before implementing soil moisture perturbations, and to have a quantification of the model reaction. The study of Klüpfel et al. (2011) for the West Africa lead us to imagine positive results also for our test.

2 Dataset and methodology

Different models with different spatial resolution have been chosen to ensure a good variability among the soil moisture fields used to initialize COSMO model for the sensitivity test.

Model	COSMO EU analysis	ECMWF analysis	GFS analysis	GLDAS-NOAH LSM reanalysis	UTOPIA LSM reanalysis
Resolution (^{o})	0.063	0.125	0.500	0.250	0.250
Soil levels depth (cm)	1, 2, 6, 18, 54, 162, 486, 1458	7, 28, 100, 289	10, 40, 100, 200	10, 40, 100, 200	1, 2, 6, 18, 54, 162, 486, 1458

TABLE 1: List of the analyses and reanalyses used to initialize COSMO model with the correspondent spatial resolution and soil level depths in cm.

As regards the reanalysis of land surface state coming from NOAH LSM, this is driven by a Global Land Assimilation System (GLDAS). GLDAS is a system that integrates satellite and ground-based data within multiple offline LSMs to produce fields of land surface states and fluxes at several spatial resolution (See Rodell et al., (2004) for further details).

The UTOPIA (University of TOrino land Process Interaction in Atmosphere, Cassardo et al. (2006)) model is a diagnostic one-dimensional land surface model (similar to TERRA LSM) developed at the University of Torino since 1989, and can be categorized in the class of the SVAT schemes. UTOPIA can be used both as a stand-alone model or coupled with an (global or mesoscale) atmospheric circulation model, behaving as its lower boundary condition.

A first step towards the creation of a soil moisture field ready to initialize COSMO model, is to take into account the soil texture distribution of the original soil model. To this end, we computed the degree of saturation S:

$$S = \frac{\eta_w}{\eta_S} \tag{1}$$

where η_w is the volumetric soil water content and η_S is the soil porosity of the original model depending on the spatial distribution of the soil texture used in the original model. For this computation, the soil texture map for each model considered was necessary, together with the raw initial soil moisture fields.

Afterward, the vertical interpolation of S over TERRA-LM soil levels was performed and then also the rotation and the spatial interpolation over the finer COSMO 0.025^o grid. As regards the vertical interpolation over TERRA LM soil levels, we noticed that for most of the models the depth of the bottom soil level is lower than the one in TERRA LM (289 cm for ECMWF, 200 cm for NOAH and GFS vs. 1458 cm for TERRA LM). Hence for these models, being the vertical interpolation not possible for the two deepest levels of TERRA LM (486 and 1458 cm), we extrapolated the values at these two depths using the soil moisture values of the bottom soil level of the original model (289 cm for ECMWF, 200 cm for NOAH and GFS). Finally, the final value of the volumetric soil water content $\eta_{w\,final}$ ready to initialize the model is computed by multiplying the degree of saturation S by the soil porosity of COSMO model at 0.025^o resolution $\eta_{S\,COSMO}$:

$$\eta_{w\,final} = S\,\eta_{S\,COSMO} \tag{2}$$

The only exception to this preprocessing procedure was for the COSMO EU fields for which only rotation and spatial interpolation over the COSMO 0.025^o resolution grid was performed.

The procedure adopted here is different from the one used operational version of INT2LM. Setting in the namelist l_smi=TRUE, the soil moisture index SMI is used instead of the degree of saturation S:

$$SMI = \frac{\eta_w - \eta_{wp}}{\eta_{fc} - \eta_{wp}} \tag{3}$$

where η_{wp} and η_{fc} are the wilting point and field capacity of the original model.

Further considerations have to be done for the reanalysis coming from UTOPIA LSM. The model needs the following boundary atmospheric condition to run: 2m air temperature, relative humidity RH, X and Y components of the wind speed, total cloudiness, low cloudiness, and precipitation. The first 6 variables are taken from ECMWF analyses, whereas for the last one (precipitation) the TRMM gridded precipitation dataset has been used. TRMM (Tropical Rainfall Measuring Mission) is a gridded precipitation product at 0.25^o resolution coming Multisatellite Precipitation Analysis (see Huffman et al., 2007 for further details). Despite the higher resolution of ECMWF analyses (0.125^o), all the initial boundary conditions for UTOPIA LSM coming from the IFS are upscaled at 0.25^o resolution to ensure the homogeneity of resolution with the gridded precipitation product. Another possibility was to use ERA-Interim reanalysis to obtain the gridded precipitation data that we needed, but for this product the horizontal resolution was too small for our purposes ($\approx$ 80 km of ERA-Interim 0.5 vs. $\approx$ 25 km of TRMM 0.25 precipitation data).

Since the soil moisture and temperature in UTOPIA LSM were initialized arbitrarily at the beginning of the simulation, a spin up period was necessary to let the two fields approach real values. To this end, two months simulation before the desired date were performed for each case study considered here.

Snow depth initialization was also taken into account at the beginning of each simulation using the ECMWF analyses, because of the important role of the snowpack on the soil water budget, especially over the alpine region and in the winter case studies.

3 Case studies

For this sensitivity test several few case studies taking into account summer and winter conditions were selected to evaluate the (potential) differences in sensitivity of the COSMO model in the different seasons.

As regards the summer case studies, we have chosen a case with strong synoptic forcing (a cold front approaching Northern Italy, 29-06-2011), and a second case with a weaker forcing (an upper level trough moving westward from eastern Europe, 25-05-2012). The aim was to assess if differences in the synoptic condition could lead to changes in the sensitivity of the model.

As regards the other case studies, we considered two typical autumn/winter conditions. The first one is characterized by a strong katabatic wind (foehn) over the Po valley (10-11-2013) with the subsequent formation of a low pressure system over the Tyrrhenian sea; the second one (26-01-2013) consists in a stable atmosphere with an inversion over the Po valley causing dense fog over most part of the plain. In this last case, we opted to start the run the 25-01-2013 at 12 UTC. In fact, because the fog in winter season appears in the late afternoon after the sunset, we thought it would be more appropriate to start the run before the beginning of the event (at 12 UTC) instead of in the middle (at 00 UTC of 26-01-2013). In figure 1, the synoptic description of the case studies considered in our experiment is reported, whereas in figure 2 an example of soil moisture fields used to initialize the COSMO run for the 29-06-2011 case study is shown.

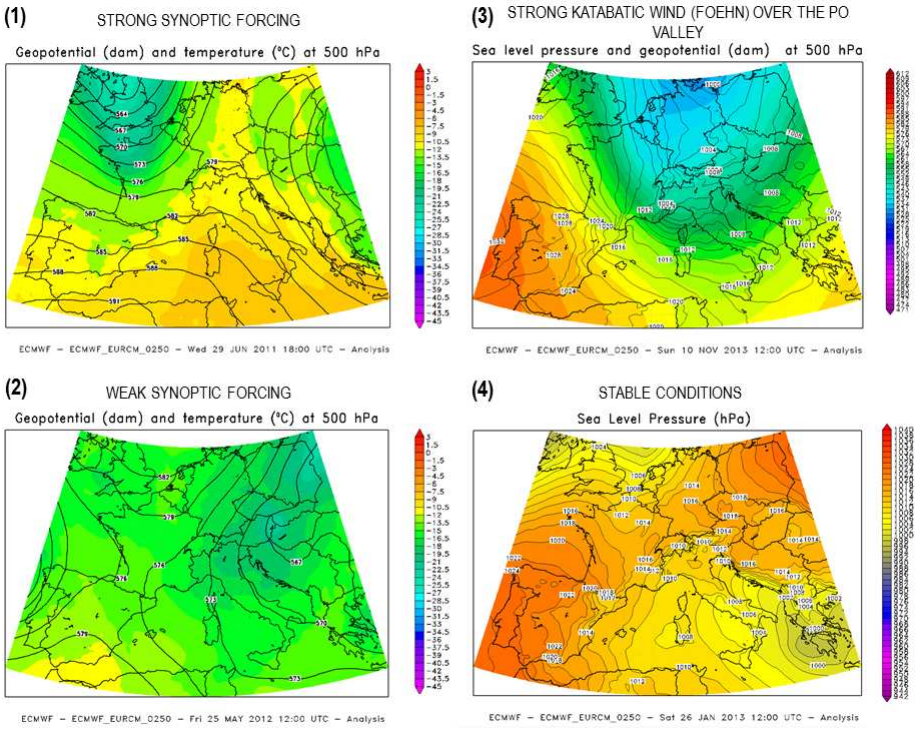

FIGURE 1: Synoptic maps of the case studies considered in the sensitivity test. The top left figure (1) represents the case of strong forcing with a cold frond approaching the Alps (29-06-2011), the bottom left figure (2) represents the weaker synoptic forcing with the upper level trough moving from the east Europe toward the north Italy (25-05-2012), the top right figure (3) represents the foehn condition generated by the strong pressure gradient across the Alps (10-11-2013), the bottom right figure (4) represents the fog condition with the north Italy crossed by a corridor of high pressure connecting the Azores anticyclone with the Siberian one.

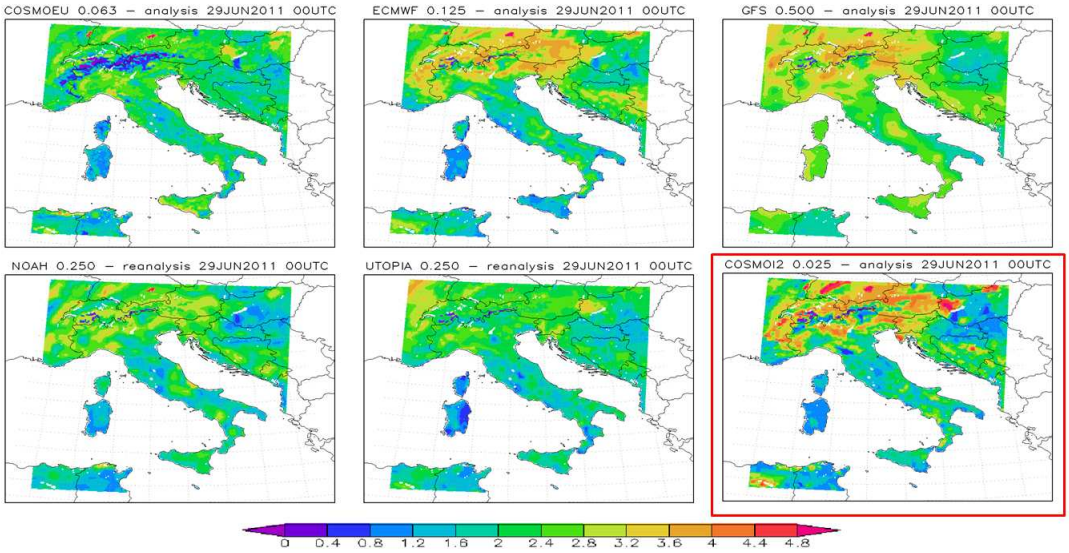

FIGURE 2: Soil moisture fields ($kg\,m^{-2}$) used to initialize the COSMO run for the case study 29-06-2011 at 00UTC. The fields are relative to the first soil layer (1 cm depth). The red box shows the control run.

Figure 3 shows the boxplot of the distribution of the soil moisture fields related to the first soil layer (1 cm depth) for all the 4 case studies considered, whereas figure 4 illustrates the maps of the standard deviation of the surface soil moisture fields at initial time, representative of the spread.

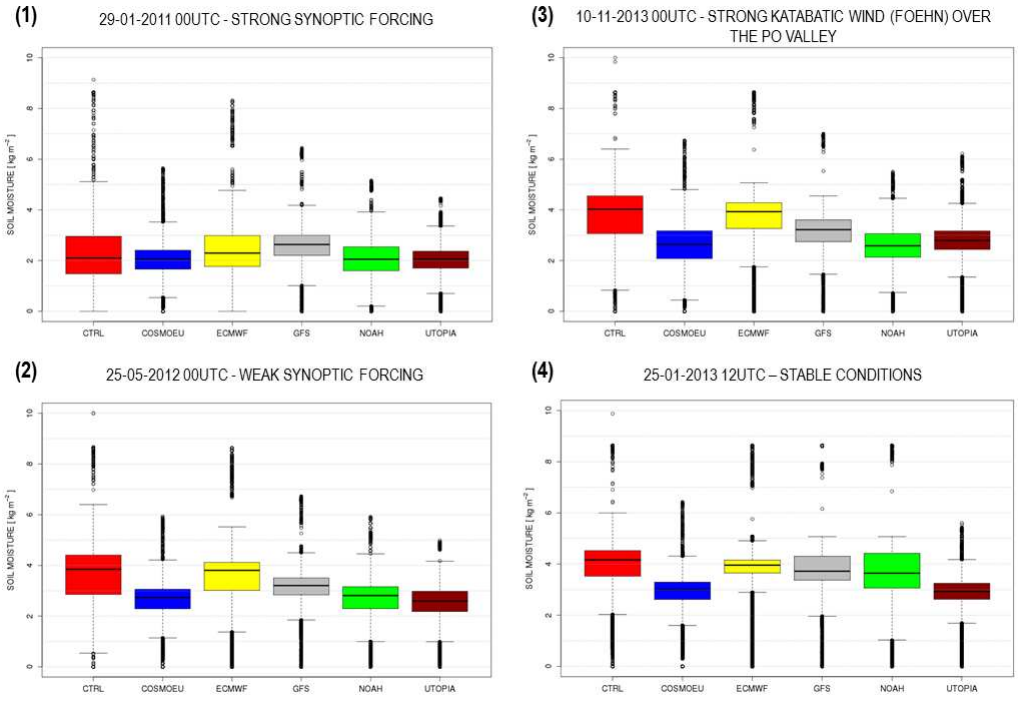

FIGURE 3: Boxplot of the distributions of the soil moisture fields (1 cm depth) for all the 4 case studies.

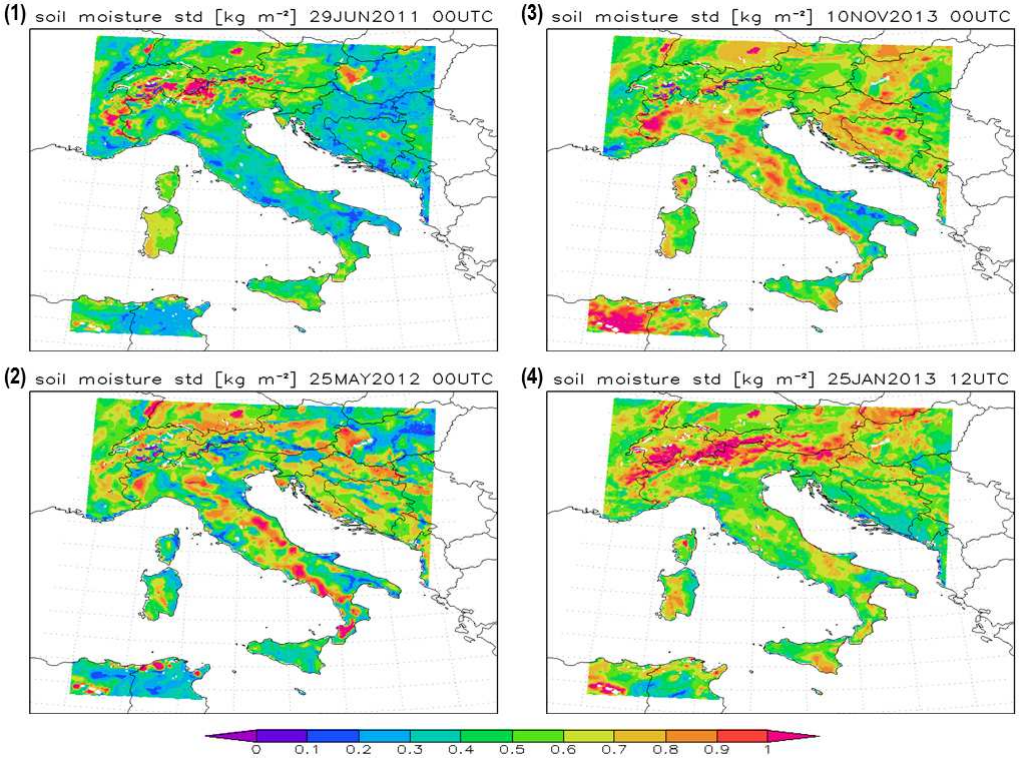

FIGURE 4: Maps of standard deviation (spread) of the initial soil moisture fields (1 cm depth) used to initialize the COSMO runs for all the 4 different case studies.

Examining the boxplot in figure 3, it can be seen that the first case study shows, on average, the lowest soil moisture values and the lowest variability among the distributions compared to other cases. The variability of soil moisture fields can be noticed both in terms of mean values and of width of the distributions.

Considering the spatial distribution (figure 4), the first case study shows, on average, also the lowest spread compared to other cases, according to the considerations coming from the boxplot analysis. Moreover, always in the first but also in the fourth case study, the spread maxima are not homogenously distributed all over the domain but are mostly concentrated over the alpine region.

Considering again the boxplot (figure 3), and in particular the CTRL and the ECMWF boxplot, the effect of the different methodology adopted for the soil moisture interpolation can be inferred. In fact, in both cases, the original model is the same, but the two different interpolation techniques (SMI and S) give different results in term of soil moisture fields values. In particular, the SMI used to interpolate the soil moisture from ECMWF in the operational suite gives a distribution of soil moisture values with a similar average, but wider compared to the one obtained with the technique of the degree of saturation S. As result, the SMI technique gives more "extreme" values of soil moisture as it can be also noticed comparing the ECMWF soil moisture field and the COSMOI2 one (red box) in the example reported in figure 2.

4 Simulations

Once soil fields were available and ready to initialize COSMO model, a number of simulations were carried out to study the response of the model itself to different soil moisture initialization. Being 4 the case studies considered and 5 the different soil moisture analyses (+ 1 of control), we obtained 24 different COSMO runs.

For the model runs, COSMO model version 5.0 was used with an horizontal resolution of 0.025^o (about 2.8 km).

The variables that we opted to analyze for each case study to assess the increase in spread due to different initializations were: 2 meters temperature and dew point, 10 meters wind speed (module), vertical velocity (w) at an altitude of about 1000 m, total precipitation, cloud cover, soil temperature and moisture.

Considering figure 5, showing the spatial average of the spread for all the atmospheric and soil variables considered in this study, a considerable increase in spread can be noticed for the summer, spring and autumn cases, whereas in the winter one the increase is less appreciable. Moreover, the diurnal cycle in some variables is evident (temperatures, wind speed and cloudiness), more pronounced in summer and spring condition (1, 2) and almost absent in winter stable case (4). To be noticed in particular is the fact that the summer case, showing the highest values in spread and the most pronounced diurnal cycle, is also the one with the lowest initial mean spread. These results can be justified by the fact that during spring and summer seasons the fluxes, namely the exchanges of moisture and energy between soil and atmosphere, are stronger compared to autumn or winter conditions, especially during daytime. For this mechanism, variations in soil moisture may deeply affect the boundary layer and influence atmospheric processes leading to a considerable variability among the COSMO runs. This assumption is also confirmed by the behavior of the soil moisture spread of the first soil layer. For the winter stable case study (4) soil moisture spread remains nearly constant, because of small fluxes leading to a limited exchange of moisture between soil and atmosphere. In the other cases where the fluxes are stronger, the initial spread in soil moisture tends to decrease, especially in the first day of the run.

As regard the spread in precipitation, the highest values are reached in the summer case study with strong synoptic forcing (1) when events of heavy rainfall occur. In general for this variable and for all the cases considered, a diurnal cycle is less evident or absent. In fact, for the two convective cases, thunderstorm events may occur also in the late evening and in the nighttime where the cold front (case 1) or the upper level trough (case 2) interests some region of the domain. In the autumn case (3), finally, less convective precipitation due to the deepening of a low pressure system in the Tyrrhenian sea leads to a more uniform increase in spread. For the winter case (4) no spread appears because of stable synoptic conditions.

Also as regards the wind speed and the vertical velocity, the different behavior in spread between spring-summer (1, 2) case studies and the autumn one (3) can be noticed. Whereas for the cases 1 and 2 an evident diurnal cycle appears, for the autumn case a continuous and constant increase in spread can be observed due to the intensification of the winds caused by the deepening of the low pressure system over the Tyrrhenian sea in the second day of the run.

Figure 6 and 7 report maps of spatial distribution of the spread at a chosen time of the run. An example with the 2m temperature and the 48h cumulated precipitation for all 4 case studies considered is shown. It can be seen that locally the value of the spread of these two variables can be really appreciable. Values greater than 3^oC and more than 20 mm as regard the temperature and precipitation respectively can be observed in some

part of the domain for the strong synoptic forcing case (1). For the other case studies the values are smaller, but anyway relevant (about 1-2°C for temperature and 10-20 mm for precipitation). To be noted the foehn effect over the Po valley on the 2m temperature in the 3^{rd} case study and the spread nearly absent for the stable winter case (4).

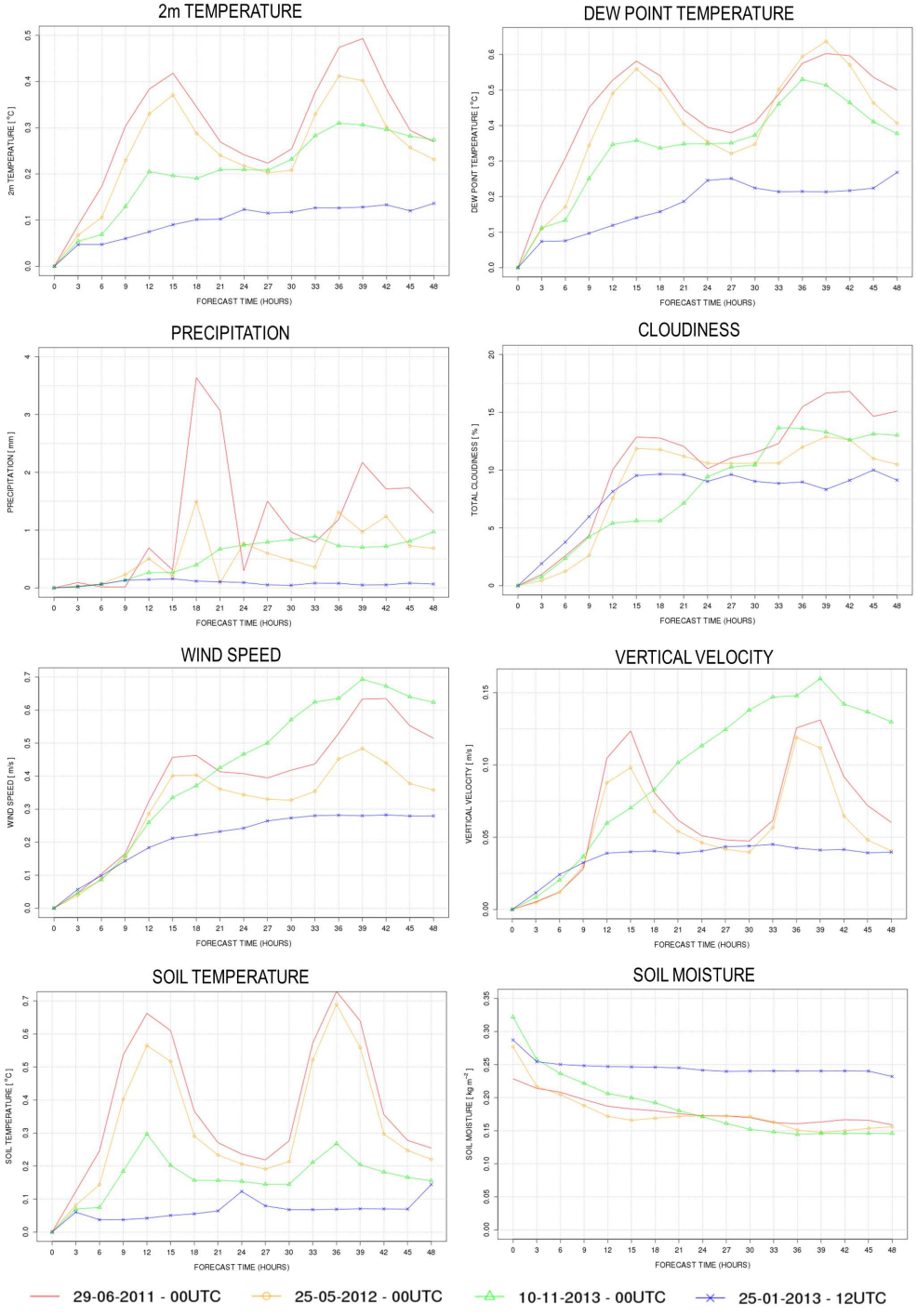

FIGURE 5: spatial average of the spread of different atmospheric and soil variable for the 4 different case studies.

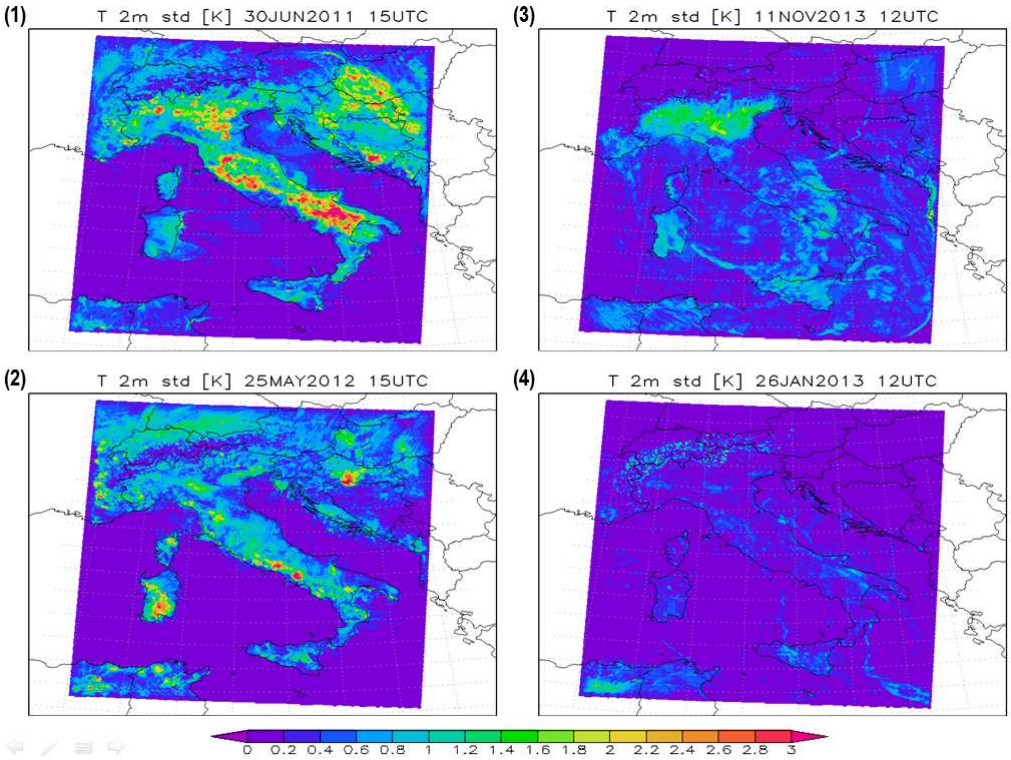

FIGURE 6: 2m temperature spread for the 4 different case studies.

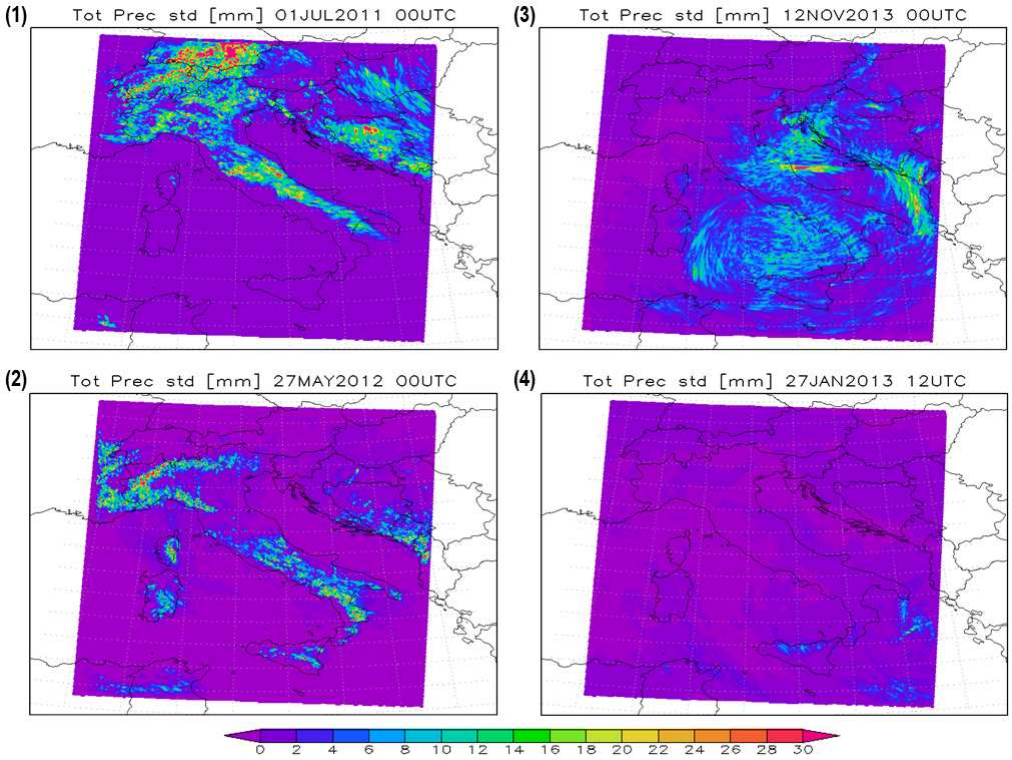

FIGURE 7: 48 h cumulated precipitation spread for the 4 different case studies.

5 Conclusions

In this study we performed a sensitivity test to assess the impact of different soil moisture initializations on short range ensemble variability in COSMO model. For our purpose, five different soil moisture analyses coming from global, regional and land surface models were used.

When examining some variables as 2m temperature and dew point, precipitation, cloudiness, wind speed, vertical velocity, soil moisture and temperature, the results show that the change of the soil moisture initial condition generated some spread, stronger in the spring/summer case studies with convective conditions, weaker in autumn season and nearly absent in stable winter conditions.

To assess if the spread obtained in our test is appreciable with respect to the uncertainty associate to the forecast sufficient it would be wise to compare these values with those coming from an ensemble obtained perturbing the initial atmospheric (and boundary) conditions.

Another point to stress is related to numerical instability. In fact, in our experiments, a simulation of case study similar to the 3^{rd} one presented here failed. Also this case study consisted in a foehn condition in the northwestern Italian Alps with strong winds. This fact remind us how important is to take into account the numerical stability of the model when perturbing soil moisture with a certain technique.

6 Proposal for a perturbation technique for soil moisture initial conditions

A simple technique proposed by Lavaysse et al. (2013) consists in perturbing the spectral coefficients of an expansion on spherical harmonics (in the horizontal) and Fourier harmonics (in the vertical). A three-dimensional random function on the sphere $f(\lambda, \phi, \eta, t)$, correlated in space and time, with a probability density function symmetric around the mean, can be defined as:

$$f(\lambda, \phi, \eta, t) = \mu + \sum_{l=1}^{L} \sum_{m=-l}^{l} \sum_{k=-K}^{K} a_{lmk}(t) Y_{lm}(\lambda, \phi) e^{ik\eta} \tag{4}$$

where μ is the global mean of the random function, and the variables λ, ϕ, η and t are longitude, latitude, vertical coordinate, and time, respectively. The Y_{lm} are spherical harmonics, with l being the total horizontal wavenumber, m the zonal wavenumber and k the vertical wavenumber. L and K are the horizontal and vertical truncations of the random function, and their inverse can be interpreted in terms of spatial decorrelation length scales (or horizontal/vertical wavelength). See Lavaysse et al. (2013) and Li et al. (2008) for further details.

As in our case we have a perturbation in the initial condition of a two-dimensional field, the dependence on the vertical coordinate and time is lost and the function $f(\lambda, \phi)$ now is defined as:

$$f(\lambda, \phi) = \mu + \sum_{l=1}^{L} \sum_{m=-l}^{l} a_{lm} Y_{lm}(\lambda, \phi) \tag{5}$$

In this case a_{lm} becomes a simple random coefficient following a normal distribution with zero mean and unit variance. A stretching function is finally used to regulate the intensity of the perturbation and thus to bound the function f between f_{min} and f_{max}:

$$S(f, \mu) = 2 - \frac{1 - exp\left[\beta \left(\frac{f-\mu}{f_{max}-\mu}\right)^2\right]}{1 - exp(\beta)} \tag{6}$$

with $\beta \approx -1.27$. To better explain the meaning of L, in figure 8 two example of initial spatial correlated random field are shown. Both are obtained with a perturbation intensity of 0.06 m^3/m^3, but the first one corresponds to a value of $L = 80$ (namely, to an horizontal wavelength $\lambda_L \approx 2\pi R_{earth}/L \approx 500km$), whereas the second one is obtained with $L = 160$ ($\lambda_L \approx 250km$).

As regards the perturbation intensity, values of 0.06 $m^3 m^{-3}$ for the surface layer and 0.04 $m^3 m^{-3}$ for root layers are proposed by Lavaysse et al., (2013). These values are comparable of smaller than errors of the operational soil moisture analysis at ECMWF (bias = -0.081 $m^3\,m^{-3}$, RMSE = 0.113 $m^3\,m^{-3}$ over the period 2008-2010, Albergel et al. (2012)). Considering instead the horizontal truncation L, some values corresponding to a horizontal wavelength λ_L between 500 and 1000 km are used by the same authors.

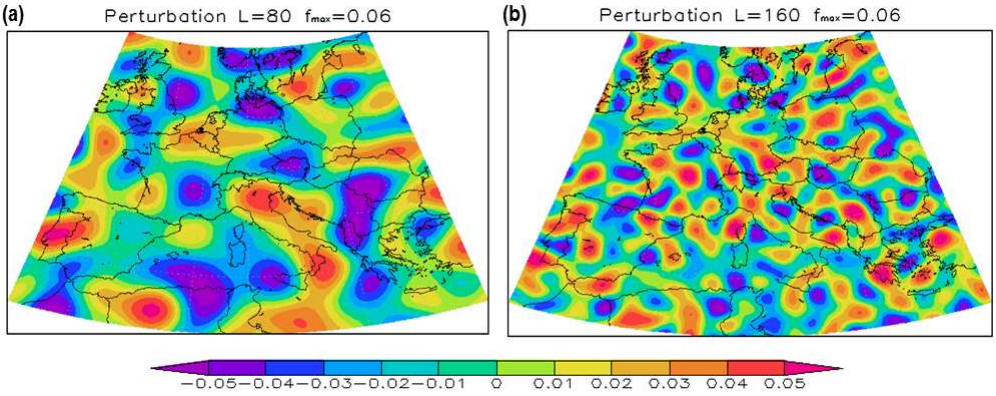

FIGURE 8: Examples of spatial correlated random fields obtained using the function in equation (5) with $L = 80$ ($\lambda_L \approx 500km$, left panel) and $L = 160$ ($\lambda_L \approx 250km$, right panel).

7 Future developments

A test of the perturbation technique proposed here is scheduled with one or more case studies and with different settings of the characteristics of the perturbation fields. In particular, as regards the sensitivity on the spatial scales, values of L corresponding to horizontal wavelength λ_L of about 250, 500, and 750 km may be considered. Also the sensitivity on the intensity of perturbation should be analyzed with a range of values comparable with the typical errors of the soil moisture analysis. Eventually, in case of unsatisfactory results of the test with the technique above mentioned, some more sophisticated approach should be considered, as the one proposed in CONSENS Priority Project or others briefly cited in the introduction.

References

[1] Albergel, C., de Rosnay, P., G. Balsamo, G., Isaksen, L., Munoz-Sabater, J., 2012: Soil Moisture Analyses at ECMWF: Evaluation Using Global Ground-Based In Situ Observations. *J. Hydrometeor*, 13, **1442-1460**.

[2] Aligo, E. A., Gallus, W. A. and Segal, M., 2007: Summer Rainfall Forecast Spread in an Ensemble Initialized with Different Soil Moisture Analyses. *Wea. Forecasting*, 22, **299-314**.

[3] Cloke, H. L., Weisheimer, A., and Pappenberger, F., 2011: Representing uncertainty in land surface hydrology: fully coupled simulations with the ECMWF land surface scheme, in Proceedings of the ECMWF/WMO/WCRP workshop on "Representing Model Uncertainty and Error in Numerical Weather and Climate Prediction Models", 20-24 June 2011 at ECMWF, Reading, UK.

[4] COSMO Technical Report No. 22: C. Marsigli, T. Diomede, A. Montani, T. Paccagnella, P. Louka, F. Gofa, A. Corigliano, The CONSENS Priority Project, 2013. Available at http://www.cosmo-model.org/content/model/documentation/techReports/default.htm.

[5] Hacker, J. P., 2010: Spatial and Temporal Scales of Boundary Layer Wind Predictability in Response to Small-Amplitude Land Surface Uncertainty, *Journal of Atmospheric Sciences*, 67, **217-233**

[6] Huffman, G. J., and Coauthors, 2007: The TRMM Multisatellite Precipitation Analysis (TMPA): Quasi-Global, Multiyear, Combined-Sensor Precipitation Estimates at Fine Scales. *J. Hydrometeor*, 8, **38-55**.

[7] Klupfel, V.,Kalthoff, N.,Gantner, L. and Kottmeier, C., 2011: Evaluation of soil moisture ensemble runs to estimate precipitation variability in convection-permitting model simulations for West Africa.*Atmospheric Research*, 101:1-2, **178-193**.

[8] Lavaysse, C., Carrera, M., Belair, S., Gagnon, N., Frenette, R., Charron, M. and Yau, M. K., 2013: Impact of Surface Parameter Uncertainties within the Canadian Regional Ensemble Prediction System.*Mon. Wea. Rev.*, 141, **1506-1526**.

[9] Li, X., Charron, M., Spacek, L. and Candille, G., 2008: A Regional Ensemble Prediction System Based on Moist Targeted Singular Vectors and Stochastic Parameter Perturbations.*Mon. Wea. Rev.*, 136, **443-462**.

[10] Quintanar,A. I. and Mahmood, R., 2012: Ensemble forecast spread induced by soil moisture changes over mid-south and neighbouring mid-western region of the USA. *Tellus A*, 64:0,

[11] Rodell, M., Houser, P. R., Jambor, U., Gottschalck, J., Mitchell, K., Meng, C.-J., Arsenault, K., Cosgrove, B. , Radakovich, J. , Bosilovich, M. , Entin, J. K. , Walker, J. P. , Lohmann, D. and Toll, D., 2004. The Global Land Data Assimilation System, Bulletin of the *American Meteorological Society*, 85(3): **381-394**.

[12] Sutton, C., Hamill, T.M. and Warner. T. T., 2006: Will Perturbing Soil Moisture Improve Warm-Season Ensemble Forecasts? A Proof of Concept.*Mon. Wea. Rev.*, 134, **3174-3189**.

[13] Sutton, C. J., Hamill, T. M.and Warner, T. T., 2004: Impacts of perturbed soil moisture conditions on short-range ensemble variability, *16th NWP 20th W&F Conference*, Seattle, American Meteorological Society.

[14] Wang, Y., Kann, A., Bellus, M., Pailleux, J., and Wittmann, C., 2010: A strategy for perturbing surface conditions in LAMEPS, *Atmos. Sci. Lett.*, 11, **108-113**

COTEKINO Priority Project – Results of Sensitivity Tests

Grzegorz Duniec, Andrzej Mazur

Department for Numerical Weather Forecasts. Institute of Meteorology and Water Management - National Research Institute. PL-01-673 Warsaw, 61 Podlesna str

grzegorz.duniec@imgw.pl; andrzej.mazur@imgw.pl

Summary

Results of preliminary and detailed sensitivity tests of model output sensitivity to changes in soil-related parameters are presented in the paper. Conclusions and propositions regarding construction of "soil-parameters-based" ensemble(s) as a part of more general, lower-boundary-conditions-based EPS are an outcome of this case study.

1 Introduction

Moist atmospheric processes are clearly sensitive to soil conditions, as it was shown in many studies (see e.g. Sutton et al. 2006 or Cloke et al., 2012). At the Institute of Meteorology and Water Management – National Research Institute (IMWM-NRI) a simple method was proposed to assess a possibility to produce reasonable number of valid ensemble members, taking into consideration predefined soil parameters. The first phase is based on tentative analysis of the influence on a reference results from various model set-ups (e.g. parameter configurations, numerical schemes, physical parameterizations etc.) combined with rough changes of the selected soil-related model parameters (like surface-area index or bottom of the last hydrological active soil layer). This analysis provides an answer about "importance" of mentioned soil parameters and a possibility to neglect "less significant" ones. The proposed tests should answer, how small perturbations of selected parameter(s) are sufficient to induce most significant changes in the forecast of the state of atmosphere, and, thus, to provide qualitative selection of a "proper" member of an ensemble.

So far, the first two phases were applied in the analysis - a predefined group of different model configurations/set-ups was tested providing the first selection of soil-related parameters which will be used in our further ensemble experiments. Then detailed sensitivity test was carried out in order to establish test-bed environment used to assess validity of the selection of ensemble member(s) in a quasi-operational mode. Finally, these experiments should result in preparing a well-defined ensemble based on the soil parameters perturbation to be introduced in the COSMO model operational work.

2 Basic Methodology

COTEKINO sensitivity test setup

Due to convection-permitting grid resolution used in the simulations, shallow convection scheme was chosen as a basic (and invariant) setup to subsequent studies. Other physical parameterizations and numerical schemes selected for the test were as follows (see Schattler et al. 2008, for details):

- The various formulations of the advection:
  - Leapfrog: 3–timelevel HE-VI (Horizontally Explicit – Vertically Implicit) Integration. This scheme is used as a default setup in Poland for 7km resolution operational model instance, as well as for the COSMO-EU in DWD.
  - Runge - Kutta: 2-timelevel HE-VI Integration (irunge_kutta=1). This scheme is used for the COSMO-DE.
  - Runge - Kutta: 2-timelevel HE-VI Integration (irunge_kutta=2) - variant scheme with Total Variation Diminishing.
- Vertical turbulent diffusion:

  - 1-D diagnostic closure (used in combination with leapfrog scheme only).
  - 1-D TKE-based diagnostic closure(used in COSMO-EU and in COSMO-DE).

- Parameter to select the type of parameterization for transpiration by vegetation:
  - Bucket version.
  - BATS version.

All the above gives total of 9 basic (reference) set-ups. Then soil-related parameters to be evaluated in the sensitivity test were chosen as follows:

- c_soil (with relation to c_lnd) – surface-area index of evaporating fraction from 0 to c_lnd (surface-area index of gridpoints over land, default 1.0),
- crsmin – minimum value of stomatal resistance (used in connection with BATS version only) from 50 to 200 (default 150.0),
- pat_len – length scale of subscale sfc parameters over land from 0 to 10000 (500 m),

all the above in TUNING namelist and

- czbot_w_so – depth of bottom of last hydrological active soil layer, from 0.0 to last soil level depth (default 2.0 meters) in PHYCTL namelist.

General assumption for the preliminary assessment was to choose three to four values from a given parameter range, including minimum and maximum ones.

Output fields selected for comparison were:

- Soil – soil temperature at 0 cm down (surface temp.).
- T2m – air temperature at 2m above ground level.
- Water – water + ice content of soil layers 1cm down the surface.
- U10m – zonal wind component, 10m above ground level.
- V10m – meridional wind component, 10m above ground level.

Statistical characteristics selected for sensitivity analysis were as follows:

- point-to-point difference pattern (field) with center of mass of field of differences, defined as

$$\vec{r}_d = \frac{\sum_{r_x} t_x \cdot r_x}{\sum_{r_x}} \tag{1}$$

  with t_x being value of field at point r_x.
- average difference (over entire domain)
- RMS of difference (over entire domain)
- maximum difference of values (MDV) defined as

$$MDV = \max|t_r(i,j) - t_c(i,j)| \ \mathrm{sign}|t_r(i,j) - t_c(i,j)| \tag{2}$$

  where, r and c – reference and changes, respectively)
- normalized difference of values (NDV)

$$NDV = \frac{\langle T_c \rangle - \langle T_r \rangle}{\langle T_r \rangle} 100 \tag{3}$$

  where $\langle T_x \rangle$ being

$$\langle T_x \rangle = \frac{\sum_{i=1}^{i_{max}} \sum_{j=1}^{j_{max}} t_x(i,j)}{i_{max} \cdot j_{max}} \tag{4}$$

  and

- R (Pearson) correlation coefficient (over entire domain)

$$R = \frac{\sum_{i=1}^{i_{max}} \sum_{j=1}^{j_{max}} (t_c(i,j) - \langle T_c \rangle) \cdot (t_r(i,j) - \langle T_r \rangle)}{\sqrt{\sum_{i=1}^{i_{max}} \sum_{j=1}^{j_{max}} (t_c(i,j) - \langle T_c \rangle)^2} \sqrt{\sum_{i=1}^{i_{max}} \sum_{j=1}^{j_{max}} (t_r(i,j) - \langle T_r \rangle)^2}} \quad (5)$$

As a case study basis eleven different synoptic situations were chosen (for Poland area); six of them tested before during COLOBOC priority project, and five new ones:

- 2009.02.01 (00 UTC) - low temperature, the ground was frozen solid
- 2009.02.22 (12 UTC) - sunny/fair day
- 2009.10.16 (00 UTC, 06 UTC) - ground covered with snow
- 2009.11.04 (12 UTC) - windy day with precipitation
- 2009.11.21 (06 UTC) - foggy day
- 2012.02.03 (00 UTC) - very cold day with air temperature below -20^oC, ground frozen solid after two weeks of low air temperatures
- 2012.05.18 (00 UTC) - sunny/fair day, ground temperatures below 0^oC
- 2012.07.01 (00 UTC) - sunny/fair/hot day
- 2020.12.14 (12 UTC) - again, very cold day with air temperature below -10^oC
- 2020.12.16 (12 UTC) - right after previous, some warming in the air (higher temperature)

3 First outcomes, preliminary conclusions

After completed model runs for mentioned terms and subsequent statistical computations following conclusions were drawn:

- There were no significant differences (sensitivities) with changes of numerical schemes (HE-VI, RK1 and/or RK2). Hence it was suggested in further study to limit to operational configuration of COSMO (which is 3-order standard Runge-Kutta scheme, 2-timelevel HE-VI integration with irunge_kutta=1, similar to COSMO-DE).
- "czbot_w_so" has a noteworthy impact on values of water and ice content down to 1458 cm below ground level.
- Parameter "c_soil" has a noteworthy impact on values of air temperature at 2m agl., dew point temperature and relative humidity at 2m agl., wind speed and direction at 10m agl. and surface specific humidity
- Other parameters have rather insignificant impact on tested values against reference ones.

Concerning all the above results, we decided to proceed with sensitivity tests with following assumptions:

1 Due to the (convection-permitting) scale of problem and space resolution of model domain shallow convection scheme is accepted as basic.

2 Basic numerical scheme would be 3-order standard Runge-Kutta scheme (see above).

3 All eleven test cases (different synoptic situations) as listed above were consequently used to study the variability of the "c_soil" parameter within the range from 0 to 2.0 with step of 0.1 and of "czbot_w_so" parameter, within the range of 0.0 to 5.0m with step of 0.25m.

4 Results

Following figures show selected results of sensitivity tests. All of results are described in terms of spatial distribution of "spread" – i.e. standard deviation of result against reference (default value) of selected parameter - and presented as the "spread" of the temperature (a; upper left), dew point (b; upper right), wind speed (c; lower left) and precipitation (d; lower right chart).

1 "c_soil" sensitivity test results (Figures 1–4).

2 "cz_bot_w_so" sensitivity test results (Figures 5–8).

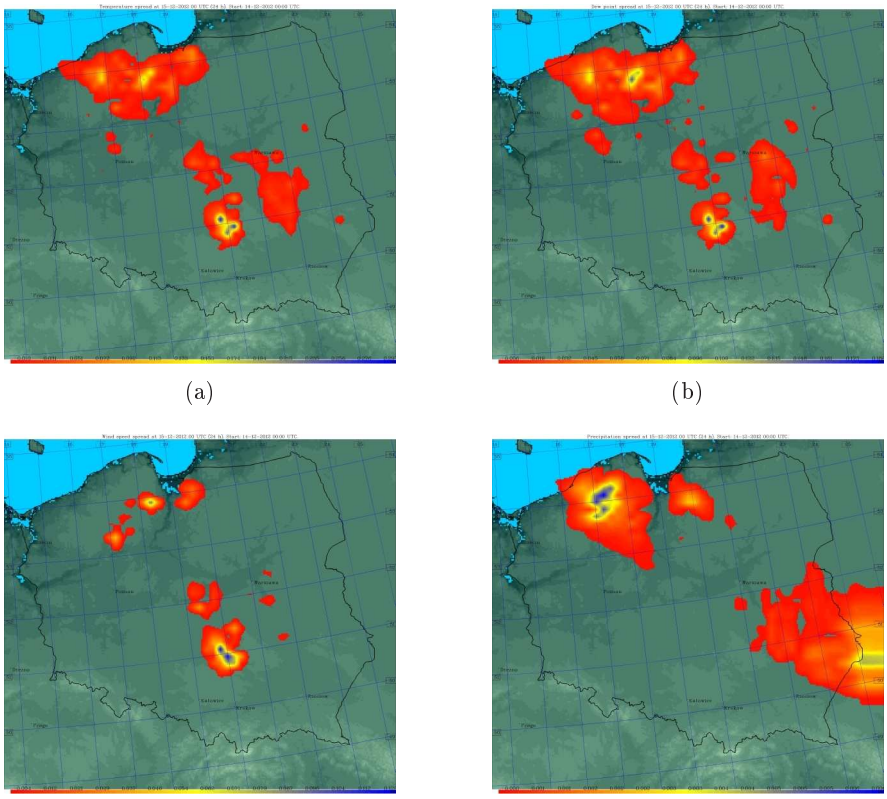

(a) (b)

(c) (d)

FIGURE 1: Winter case (December 14th, 2012)

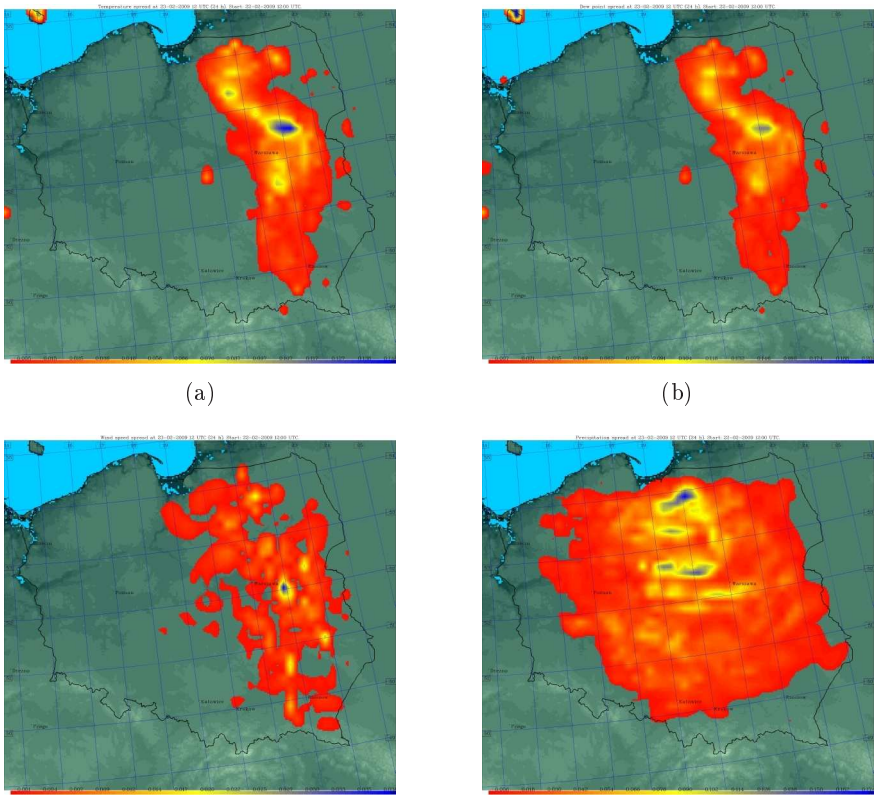

(a) (b)

(c) (d)

FIGURE 2: Spring case (February 22nd, 2009)

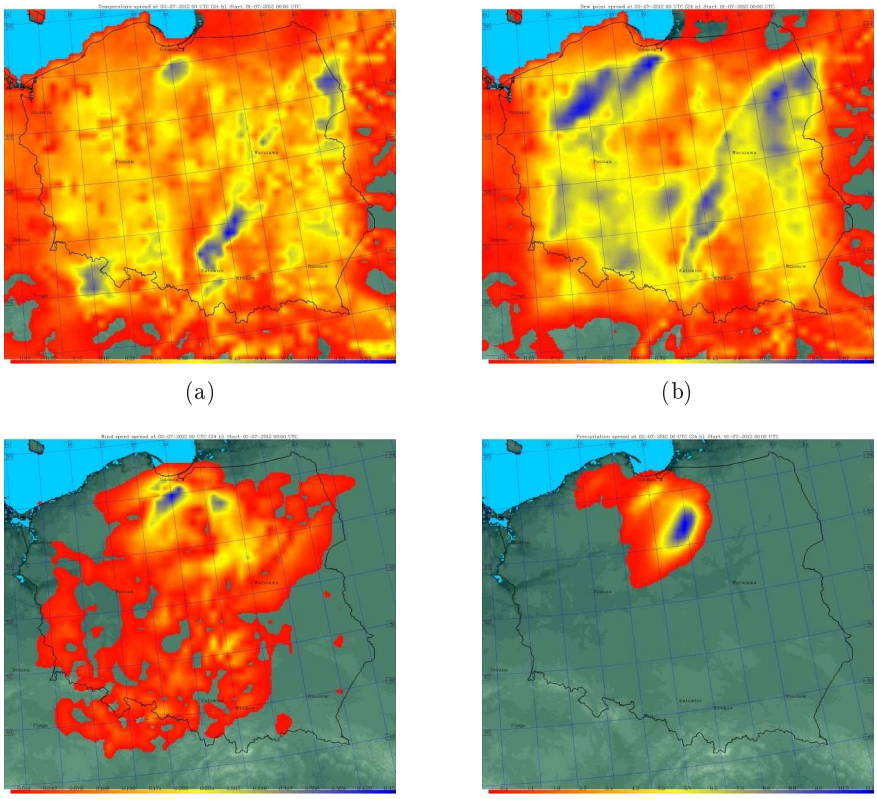

(a) (b)

(c) (d)

FIGURE 3: Summer case (July 1st, 2012)

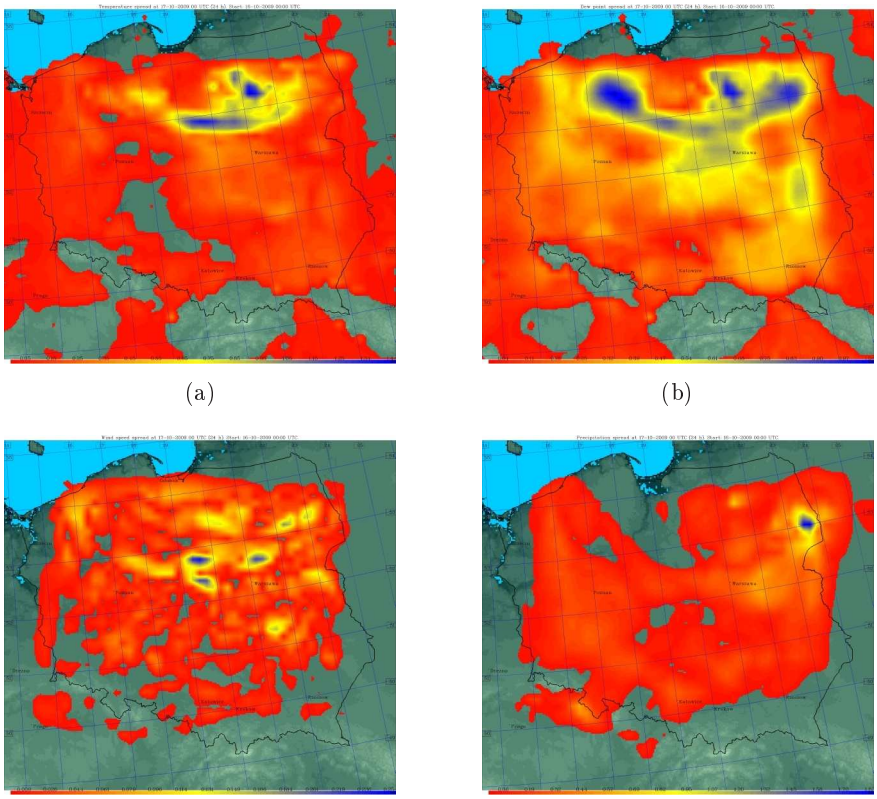

(a) (b)

(c) (d)

FIGURE 4: Fall case (October 16th, 2009)

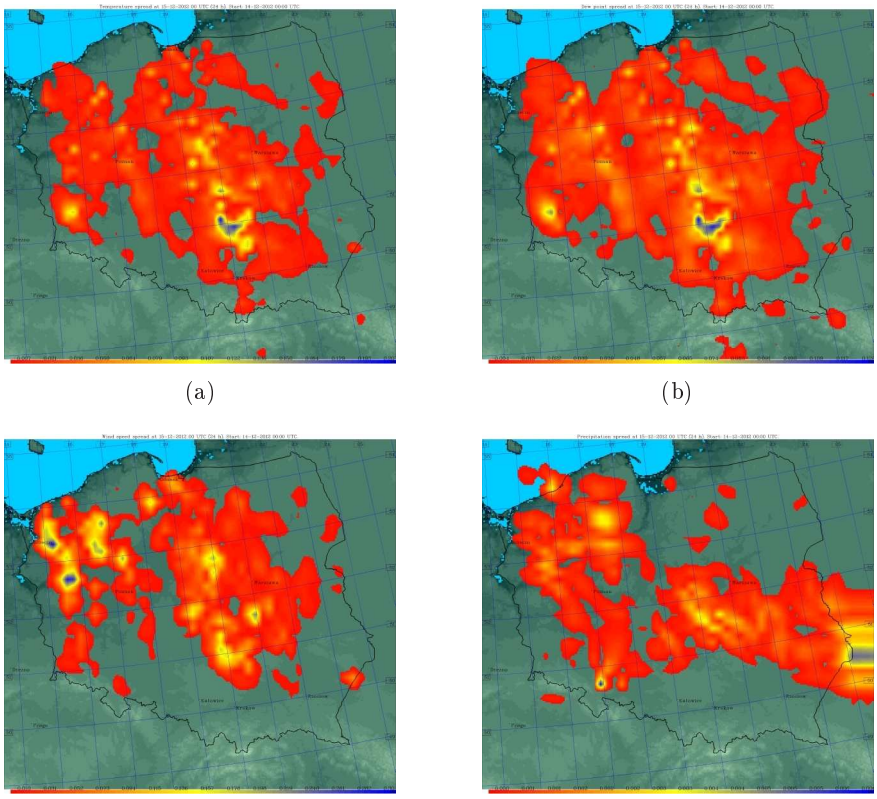

(a) (b)

(c) (d)

FIGURE 5: Winter case (December 14th, 2012)

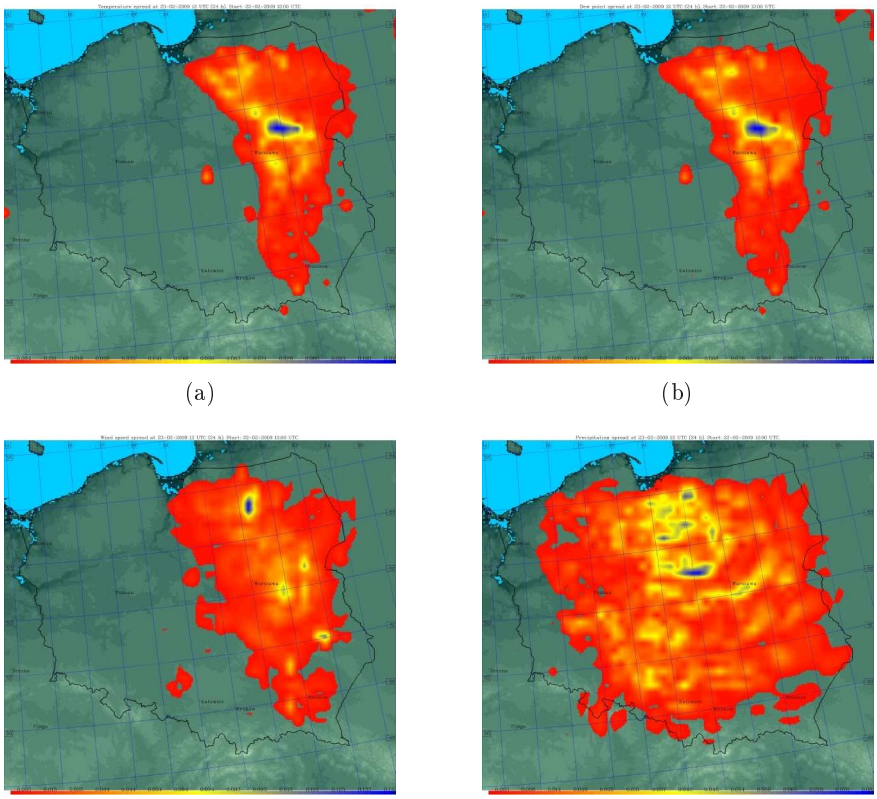

(a) (b)

(c) (d)

FIGURE 6: Spring case (February 22nd, 2009)

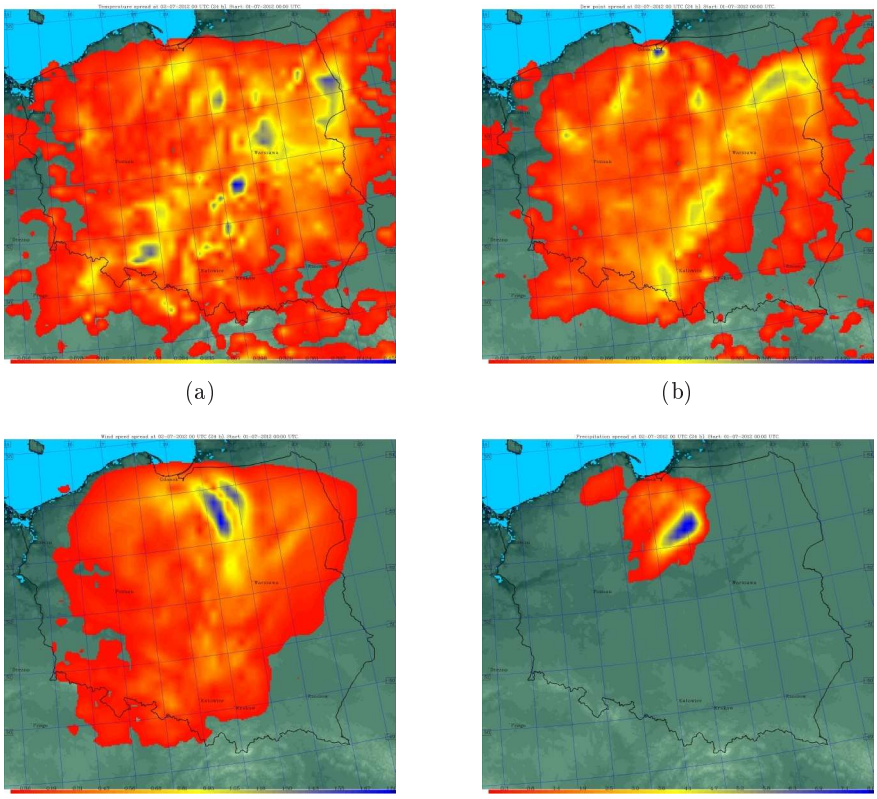

(a) (b)

(c) (d)

FIGURE 7: Summer case (July 1st, 2012)

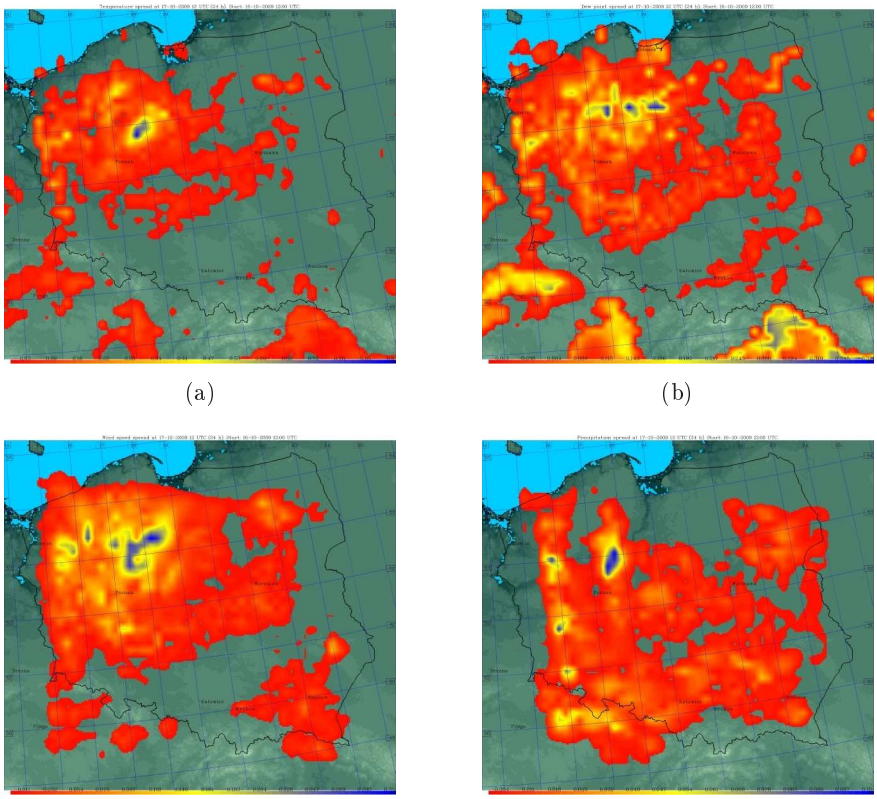

(a) (b)

(c) (d)

FIGURE 8: Fall case (October 16th, 2009)

5 Discussion

As in preliminary computations it should be stressed that changes of "czbot_w_so" had a noteworthy impact on values of "deep soil" parameters, like water/ice and water content, temperature of soil layers etc. down to 1458 cm. This influence varied from 10 to 25 percent of original (reference) value, and seemed to enlarge with increase of czbot_w_so Impact on values of lower-atmosphere parameters like air temperature, dew point, precipitation amount or wind speed most likely to be neglected. On the opposite, changes of "c_soil" seem to induce significant changes of values of air temperature, dew point temperature and relative humidity at 2m agl., wind speed/direction at 10m agl. and surface specific humidity forecast against reference ones. The maximum "spread" (standard deviation of values against reference one) – is as big as 2^oC (in case of temperature or dew point) or 1.5 m/s (wind-speed). Mean difference (over the entire domain) between maximum and minimum values was about 0.1^oC and 0.07 m/s, respectively. This order of changes pertained mostly to "warm" cases (late spring, summer, early fall), since for obvious reasons soil is at this time much more "subtle" to "stimuli" from a boundary layer. Thus, all the changes seemed to be much more visible during warm season as above defined. Impact on values of soil parameters like water/ice and water content, or soil layers temperature is rather irrelevant.

In the frame of COTEKINO priority project it is planned to study a possibility to prepare sufficiently representative ensemble in two different ways. It would be a random setting of a one value of c_soil/czbot_w_so globally/uniformly for the entire domain, which is easier to perform (required change(s) in namelist only), and there's no need for modification of the source code. This approach is, in general, a logical consequence of research described in this paper. The second approach proposed to assess is a more "stochastic" one: a valid ensemble could be prepared via modification of the source code to modify values of c_soil/czbot_w_so from gridpoint to gridpoint over the domain in a random way. Subsequent activities are planned to gain ensemble(s) in both ways and to compare results of these approaches.

References

[1] Cloke,H., Weisheimer,A., Pappenberger,F., 2011; Representing uncertainty in land surface hydrology: fully coupled simulations with the ECMWF land surface scheme. *Workshop on Model Uncertainty*, 20-24 June 2011, ECMWF, Reading (UK).

[2] Doms,G., Schattler,U., 2002; A Description of the Nonhydrostatic Regional Model LM, Part I: Dynamics and Numerics, DWD.

[3] Doms,G., Forstner,J., Heise,E., Herzog,H.-J., Raschendorfer,M., Reinhardt,T., Ritter,B., Schrodin,R., Schulz,J.-P., Vogel,G., 2007; A Description of the Nonhydrostatic Regional Model LM, Part II: Physical Parameterization, DWD.

[4] Rewut,B., 1980; Soil physics (in Polish: Fizyka gleby), PWRiL.

[5] Schattler,U., Doms,G., Schraff,C., 2009; A Description of the Nonhydrostatic Regional Model LM, Part VII: User's Guide, DWD.

[6] Sutton, Hamill,T., Warner,T., 2006; Will perturbing soil moisture improve warm-season ensemble forecasts? A proof of concept. *Mon. Weather Rev.* 134, **3174-3189**.

List of COSMO Newsletters and Technical Reports

(available for download from the COSMO Website: `www.cosmo-model.org`)

COSMO Newsletters

No. 1: February 2001.

No. 2: February 2002.

No. 3: February 2003.

No. 4: February 2004.

No. 5: April 2005.

No. 6: July 2006; Proceedings from the COSMO General Meeting 2005.

No. 7: May 2008; Proceedings from the COSMO General Meeting 2006.

No. 8: August 2008; Proceedings from the COSMO General Meeting 2007.

No. 9: December 2008; Proceedings from the COSMO General Meeting 2008.

No.10: January 2010; Proceedings from the COSMO General Meeting 2009.

No.11: February 2011; Proceedings from the COSMO General Meeting 2010.

No.12: March 2012; Proceedings from the COSMO General Meeting 2011.

No.13: April 2013; Proceedings from the COSMO General Meeting 2012.

No.14: April 2014; Proceedings from the COSMO General Meeting 2013.

COSMO Technical Reports

No. 1: Dmitrii Mironov and Matthias Raschendorfer (2001):
Evaluation of Empirical Parameters of the New LM Surface-Layer Parameterization Scheme. Results from Numerical Experiments Including the Soil Moisture Analysis.

No. 2: Reinhold Schrodin and Erdmann Heise (2001):
The Multi-Layer Version of the DWD Soil Model TERRA_LM.

No. 3: Günther Doms (2001):
A Scheme for Monotonic Numerical Diffusion in the LM.

No. 4: Hans-Joachim Herzog, Ursula Schubert, Gerd Vogel, Adelheid Fiedler and Roswitha Kirchner (2002):
LLM — the High-Resolving Nonhydrostatic Simulation Model in the DWD-Project LITFASS.
Part I: Modelling Technique and Simulation Method.

No. 5: Jean-Marie Bettems (2002):
EUCOS Impact Study Using the Limited-Area Non-Hydrostatic NWP Model in Operational Use at MeteoSwiss.

No. 6: Heinz-Werner Bitzer and Jürgen Steppeler (2004):
Description of the Z-Coordinate Dynamical Core of LM.

No. 7: Hans-Joachim Herzog, Almut Gassmann (2005):
Lorenz- and Charney-Phillips vertical grid experimentation using a compressible nonhydrostatic toy-model relevant to the fast-mode part of the 'Lokal-Modell'

No. 8: Chiara Marsigli, Andrea Montani, Tiziana Paccagnella, Davide Sacchetti, André Walser, Marco Arpagaus, Thomas Schumann (2005):
Evaluation of the Performance of the COSMO-LEPS System

No. 9: Erdmann Heise, Bodo Ritter, Reinhold Schrodin (2006):
Operational Implementation of the Multilayer Soil Model

No. 10: M.D. Tsyrulnikov (2007):
Is the particle filtering approach appropriate for meso-scale data assimilation?

No. 11: Dmitrii V. Mironov (2008):
Parameterization of Lakes in Numerical Weather Prediction. Description of a Lake Model.

No. 12: Adriano Raspanti (2009):
Final report on priority project VERSUS (VERification System Unified Survey).

No. 13: Chiara Mirsigli (2009):
Final report on priority project SREPS (Short Range Ensemble Prediction System).

No. 14: Michael Baldauf (2009):
COSMO Priority Project "Further Developments of the Runge-Kutta Time Integration Scheme" (RK); Final Report.

No. 15: Silke Dierer (2009):
COSMO Priority Project "Further Developments of the Runge-Kutta Time Integration Scheme" (RK); Final Report.

No. 16: Pierre Eckert (2009):
COSMO Priority Project "INTERP"; Final Report.

No. 17: D. Leuenberger, M. Stoll, A. Roches (2010):
Description of some convective indices, implemented in the COSMO model.

No. 18: Daniel Leuenberger (2010):
Statistical Analysis of high-resolution COSMO Ensemble forecasts, in view of Data Assimilation.

No. 19: A. Montani, D. Cesari, C. Marsigli, T. Paccagnella (2010):
Seven years of activity in the field of mesoscale ensemble forecasting by the COSMO-LEPS system: main achievements and open challenges.

No. 20: A. Roches, O. Fuhrer (2012):
Tracer module in the COSMO model.

No. 21: M. Baldauf (2013):
A new fast-waves solver for the Runge-Kutta dynamical core.

No. 22: C. Marsigli, T. Diomede, A. Montani, T. Paccagnella, P. Louka, F. Gofa, A. Corigliano (2013):
The CONSENS Priority Project.

No. 23: M. Baldauf, O. Fuhrer, M. J. Kurowski, G. de Morsier, M. Muellner, Z. P. Piotrowski, B. Rosa, P. L. Vitagliano, D. Wojcik, M. Ziemianski (2013):
The COSMO Priority Project 'Conservative Dynamical Core' Final Report.